CHEMICAL BIOLOGY OF BACTERIAL METAL ACQUISITION AND HOMEOSTASIS

by

Brendan F. Dutter

Dissertation

Submitted to the Faculty of the

Graduate School of Vanderbilt University

in partial fulfillment of the requirements

for the degree of

DOCTOR OF PHILOSOPHY

in

Chemical and Physical Biology

August, 2016

Nashville, Tennessee

Approved:

Craig W. Lindsley, Ph.D.

Brian O. Bachmann, Ph.D.

Timothy L. Cover, M.D.

Dana B. Lacy, Ph.D.

Eric P. Skaar, Ph.D.

Gary A. Sulikowski, Ph.D.

For Mom and Dad,

Grandma and Grandpa

ACKNOWLEDGEMENTS

TABLE OF CONTENTS

LIST OF FIGURES

LIST OF SCHEMES

LIST OF TABLES

LIST OF ABBREVIATIONS

ABC	ATP-binding cassette
Ac	acetyl
Ac2O	acetic anhydride
AcOH	acetic acid
app	apparent
AMP	adenosine monophosphate
ATP	adenosine triphosphate
BCA	bicinchoninic acid
Bn	benzyl
BnBr	benzyl bromide
Boc	*tert*-butoxycarbonyl
Boc$_2$O	di-*tert*-butyl dicarbonate
br	broad
Bz	benzoyl
BzCl	benzoyl chloride
°C	degrees Celsius
Cbz	carboxybenzyl
CoA	coenzyme A
COSY	correlation spectroscopy
d	doublet
DBU	1,8-diazabicyclo[5.4.0]undec-7-ene
DCC	*N,N'*-dicyclohexylcarbodiimide
DEAD	diethylazodicarboxylate
Δ	heat
δ	chemical shift in ppm
DIBAL	diisobutylaluminum hydride
DIEA/DIPEA	diisopropylethyl amine
DMAP	4-dimethylaminopyridine
DMF	dimethylformamide
DMP	Dess-Martin periodinane, 2,2-dimethoxypropane
DMSO	dimethylsulfoxide
DPPA	diphenylphosphoryl azide
EC$_{50}$	half maximal efficacious concentration
EDCI	1-ethyl-3-(3-dimethylaminopropyl)carbodiimide
EEDQ	*N*-ethoxycarbonyl-2-ethoxy-1,2-dihydroquinoline
eq	equivalent

ESI	electrospray ionization
Et$_2$O	diethyl ether
Et$_3$N	triethylamine
EtOH	ethanol
EtOAc	ethyl acetate
FAH	formic acetic anhydride
Fmoc	fluorenylmethyloxycarbonyl
Fur	ferric uptake regulator
g	gram
h	hour
HATU	1-[Bis(dimethylamino)methylene]-1H-1,2,3-triazolo[4,5-b]pyridinium 3-oxid hexafluorophosphate
HMBC	heteronuclear multiple bond correlation spectroscopy
HOBt	1-hydroxybenzotriazole
HPLC	high-performance liquid chromatography
HRMS	high-resolution mass spectrum
Hz	hertz
IBX	2-iodoxybenzoic acid
IC$_{50}$	half maximal inhibitory concentration
i-PrOH	isopropanol
IR	infrared spectroscopy
ISC	intersystem crossing
J	coupling constant
KHMDS	potassium bis(trimethylsilyl)amide
L	liter
LAH	lithium aluminum hydride
LHMDS	lithium bis(trimethylsilyl)amide
M	molar concentration
m	milli, multiplet
*m*CPBA	meta-chloroperoxybenzoic acid
Me	methyl
MeCN	acetonitrile
MeIm	*N*-methylimidazole
MeOH	methanol
MHz	megahertz
min	minute
μ	micro
Mnt	monomethoxytrityl

mol	mole
mp	melting point
MSNT	1-(mesitylene-2-sulfonyl)-3-nitro-1,2,4-triazole
N	normal concentration
n	nano
*n*BuLi	*n*-butyllithium
NHS	*N*-hydroxysuccinimide
NMR	nuclear magnetic resonance
NRP	nonribosomal peptide
NPRS	nonribosomal peptide synthetase
PCC	pyridinium chlorochromate
Ph	phenyl
PhMe	toluene
ppm	parts per million
PyAOP	(7-Azabenzotriazol-1-yloxy)tripyrrolidinophosphonium hexafluorophosphate
PyBOP	(Benzotriazol-1-yloxy)tripyrrolidinophosphonium hexafluorophosphate
PyClU	chlorodipyrrolidinocarbenium hexafluorophosphate
pyr	pyridine
q	quartet
rt	room temperature
s	singlet
SA	streptavidin
SAR	structure-activity relationships
SDS	sodium dodecyl sulfate
SPPS	solid phase peptide synthesis
t	triplet
TBAF	tetrabutylammonium fluoride
TBTA	tris[(1-benzyl-1H-1,2,3-triazol-4-yl)methyl]amine
*t*Bu	*tert*-butyl
TCEP	tris(2-carboxyethyl)phosphine hydrochloride
TE	thioesterase
TFA	trifluoroacetic acid
TFAA	trifluoroacetic anhydride
THF	tetrahydrofuran
TMS	trimethylsilyl
TMSOTf	trimethylsilyl trifuoromethanesulfonate

Troc	2,2,2-trichloroethyloxycarbonyl
Trt	trityl
Ts	*para*-toluenesulfonyl
TsOH	*para*-toluenesulfonic acid
UV	ultraviolet
Zur	zinc uptake regulator

CHAPTER 1

INTRODUCTION

Parts of this chapter are reprinted with permission from Dutter, B. F., Mike, L. A., Reid, P. R., Chong, K. M., Ramos-Hunter, S. J., Skaar, E. P., and Sulikowski, G. A. (2016) Decoupling Activation of Heme Biosynthesis from Anaerobic Toxicity in a Molecule Active in *Staphylococcus aureus*. *ACS Chem. Biol. 11*, 1354–1361. Copyright 2016 American Chemical Society.

1.1 Background

Metals play a crucial role in virtually all biological systems. Owing to their unique reactivity due to the accessibility of d-orbitals, metals are critical components of enzyme catalysis, energy transfer pathways, and of various structural motifs.[1,2] The ability of bacteria to acquire and manage nutrient metals in the niche they inhabit is of utmost importance to survival and bacteria have evolved systems to accomplish these tasks tailored to the environments they inhabit.

1.2 Metal acquisition

Iron

The main obstacle to iron acquisition in the majority of systems is the low solubility of Fe(III).[1,3] Ferric iron predominates under aerobic conditions and its low solubility means it exists in generally inaccessible forms. For example, in neutral or alkaline soils, iron exists primarily as polymeric iron oxides.[4] In the human host, Fe is predominately bound to heme in

hemoproteins, but is also found in Fe storage proteins such as transferrin and lactoferrin (extracellular) and ferritin (intracellular).[2,3]

Siderophores

One of the primary methods of iron acquisition by bacteria is the production of siderophores. Siderophores are low molecular weight molecules that tightly bind ferric iron. Bacteria typically secrete siderophores into their environment, whether inside a host or in soil, where the molecule will bind/solubilize ferric iron and be reabsorbed by the organism to provide it with nutrient iron.[1,3,4]

Siderophores are generally produced by nonribosomal peptide synthesis, which will be discussed in further detail in Chapter 2.[3] Certain functional groups with high affinity for Fe(III) predominate in siderophore. These include catechols, hydroxamic acids, α-hydroxycarboxylic acids, and hydroxyphenyl oxazolines or thiazolines (Figure 1.1).[1,3] Siderophores typically contain three of these functional groups, in various combinations, to result in a very strong hexadentate complex with Fe(III). Despite this, many siderophores exist with fewer metal binding groups resulting in tetra- and bi-dentate complexes. These are thought to solubilize Fe(III) in the environment for transfer to stronger chelators.[1]

catechol   hydroxamic acid   alpha-hydroxy
                                    carboxylic acid   thiazoline X=S
                                                         oxazoline X=O
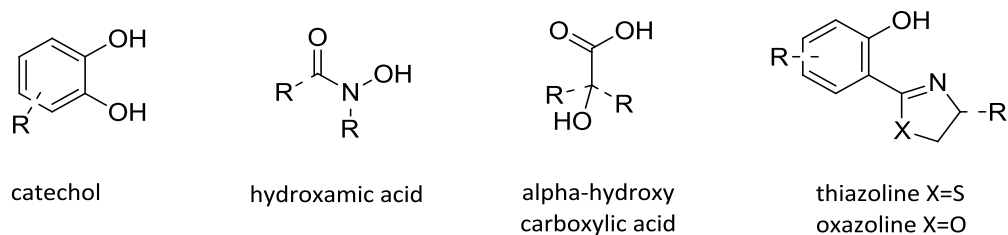
Figure 1.1. Common iron chelating motifs found in siderophores.

In Gram negative bacteria, siderophores are transported into the cell in several stages. First, receptors on the outer membrane recognize and bind the siderophore-Fe(III) complex and use the energy of the TonB-ExbB-ExbD system to transport the molecule across the outer membrane and into the periplasm. ABC-transporters in the cell membrane then recognize the siderophore-Fe(III) complex and transport it into the cytoplasm.[1,2] The siderophore-Fe(III) uptake process in Gram positive bacteria generally involves recognition of the molecule by lipoproteins receptors in the cell wall and transfer to ABC-transporters which pump the molecule into the cytoplasm.[1]

Once internalized, the bacterium must liberate Fe from the siderophore complex. This is primarily accomplished by reduction of Fe(III) to Fe(II). Hexadentate siderophores have a much lower affinity for Fe(II) than Fe(III) permitting the Fe to be released and utilized for cellular processes. This also allows recycling of the siderophore.[1,2,3]

1.2
yersiniabactin

1.1
enterobactin

1.3
acenitoferin

1.4
exochelin MS

1.5
mycobactin
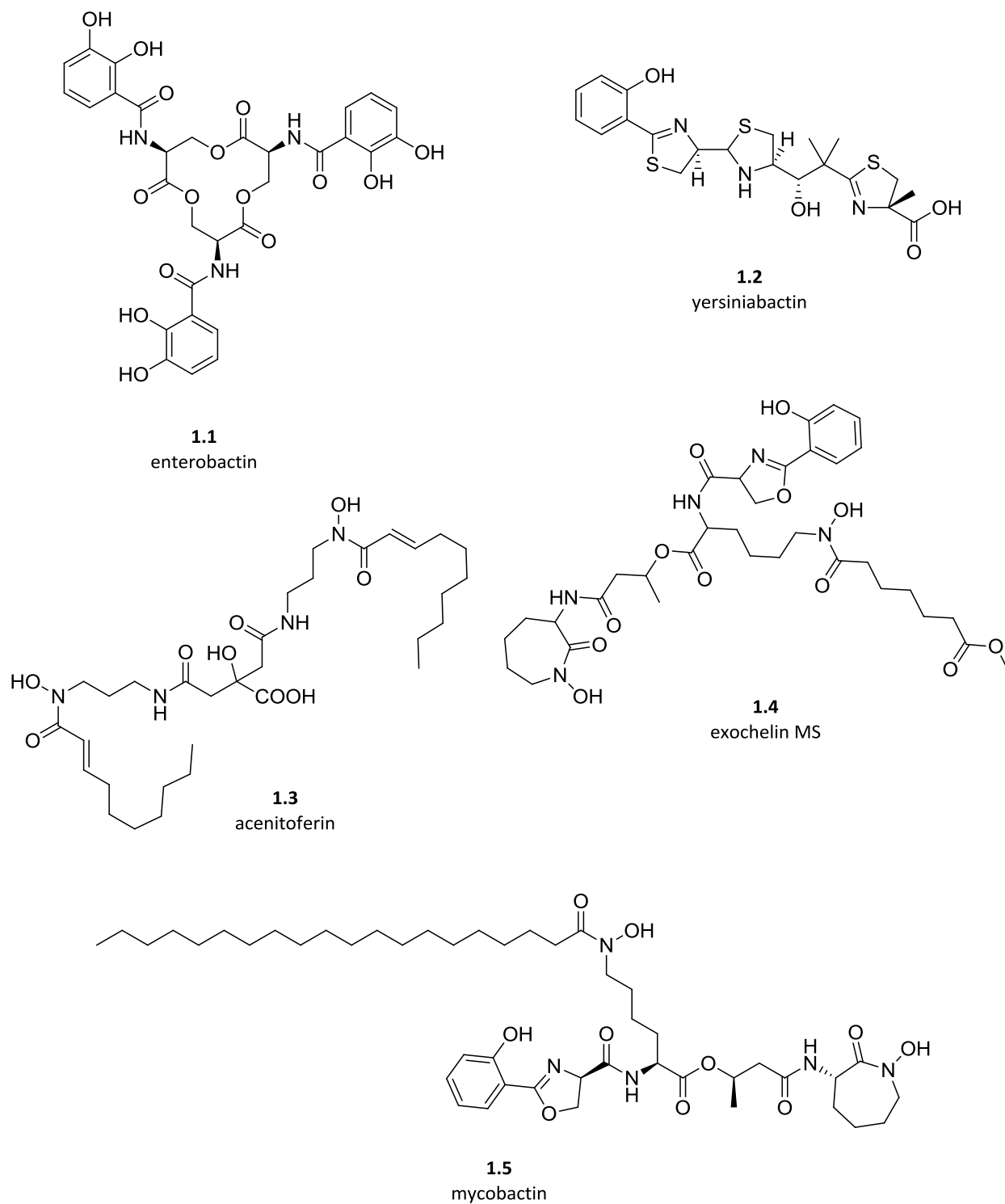
Figure 1.2. Siderophores produced by pathogenic bacteria.

4

Siderophores are produced by bacteria in numerous niches. The best studied are siderophores of pathogens and in general, production of siderophores by pathogenic bacteria is associated with increased virulence.[3] Enterobactin (**1.1**) is a triscatecholate siderophore produced by several Gram negative enteric pathogens including *Escherichia coli* and *Salmonella enterica* subsp. Typhinurium. Enterobactin was one of the first pathogenic siderophores identified.[1,3] Yersiniabactin (**1.2**) is produced by species including *Yersinia pestis*, the causative agent of the bubonic plague. Loss of genes encoding yersiniabactin is associated with decreased virulence in mouse infection models.[3] Acenitoferrin (**1.3**) is an amphiphilic siderphore produced by *Acenitobacter haemolyticus*. Studies have suggested that its ability to pass through membranes allows the bacterium to steal iron from host ferritin during infection.[5] Mycobacteria, including the pathogenic *Mycobacterium tuberculosis,* express several siderophores with various roles. Exochelins (**1.4**) are secreted into the extracellular environment to scavenge for iron.[1,6] In contrast, lipophilic mycobactin (**1.5**) is membrane associated and typically not secreted though evidence suggests a role in iron acquisition through vesicle secretion.[7]

Soil bacteria also rely on siderophores to solubilize iron as well as sequester it from competing organisms. The saprophyte *Streptomyces coelicolor* produces several siderophores including desferrioxamines B and E and coelichelin, which will be the subject of Chapter 2.[4,8] *S. coelicolor* and many other soil bacteria encode multiple siderophore uptake systems, several of which can recognize and transport siderophores produced by other organisms in a process commonly referred to as siderophore piracy.[9]

Non-siderophore mediated iron acquisition

Many pathogens are able to acquire iron in the form of heme from host hemoproteins.[2] This will be discussed below in the section on *Staphylococcus aureus* heme acquisition.

Divalent metal acquisition

While much is known about bacterial iron acquisition, the specific processes involved in Zn(II) and Mn(II) acquisition have not been as extensively studied and are focused mostly on pathogens. In the host environment, extracellular Zn(II) is mostly bound to albumin leaving very little in solution. During infections, immune cells secrete proteins of the S100 class, such as calprotectin, which bind and sequester Zn(II) and other divalent metals. Despite this, many pathogens are able to scavenge sufficient quantities of Zn(II) to promote infection. The ZnuD protein of many Gram negative pathogens is an outer membrane protein that scavenges Zn(II) and passes it to the periplasm via a TonB dependent mechanism.[10]

There also exist many porins in the outer membrane of Gram negative pathogens that allow metals such as Mn(II) to passively diffuse into the periplasm where they are recognized by substrate binding proteins (SBPs) and transported across the cell membrane via ABC-transporters.[11]

Some evidence exists for the production of zinc chelators by bacteria. In particular, *S. coelicolor* is hypothesized to produce coelibactin, a compound believed to be involved in zinc uptake given that its expression is under the control of the zinc uptake regulator (Zur). Coelibactin has never been isolated in culture and the exact structure is not known given the uncertainty surrounding its release from its NRPS.[8]

1.3 Metal homeostasis

Bacterial metal homeostasis is generally controlled by protein metal sensors which bind specific metals at given concentrations and induce some effect at the gene level in response.[11] Some sensors induce relatively small changes specific to that metal while others induce global changes in gene expression including genes tangentially associated with metal acquisition. The best example of this is the ferric uptake regulator (Fur) protein. Fur binds Fe(II) in iron replete conditions. This complex binds to control regions, called Fur boxes, of genes under its control which suppresses their expression. Examples include genes for siderophore biosynthesis, but also extend into other areas such as cell metabolism and virulence factor expression.[1] Under Fe deplete conditions, Fur will dissociate from the Fur boxes inducing expression of the genes of this regulon.

1.4 Iron acquisition and homeostasis in *Staphylococcus aureus*

Staphylococcus aureus is a Gram positive pathogen of humans primarily causing skin and soft tissue infections, but can also be responsible for more severe diseases including toxic shock syndrome and necrotizing pneumonias.[12] *S. aureus* requires iron for normal cellular function and evasion of the immune system during infection. In addition, the availability of iron controls the expression of numerous virulence factors.[13] While *S. aureus* is capable of acquiring iron by secretion of siderophores, heme is its preferred iron source during infection.[14]

Heme acquisition through the Isd system

During an infection, heme is made available to the bacterium by secretion of hemolysins which lyse red blood cells causing a release of hemoglobin. Once hemoglobin is liberated, *S.*

aureus utilizes the the Isd (iron surface determinant) system to scavange heme from hemoglobin and pass it through the cell wall and membrane and into the cytoplasm where it can be degraded to release free iron or stored associated with the membrane for incorporation into hemoproteins.[15] This system consists of several proteins each occupying a step along the path from extracellular hemoglobin to release of intracellular iron.[15]
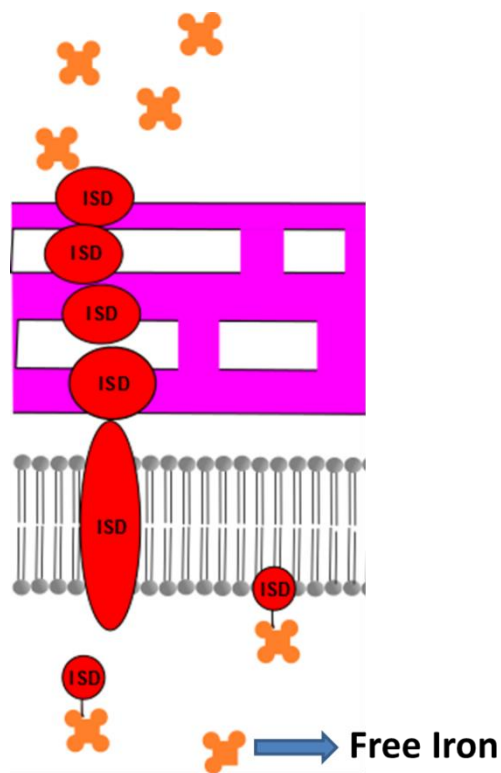
Figure 1.3. Schematic of Isd system shuttling heme into the bacterial cytoplasm.

Heme toxicity and heme sensing

Despite the value of heme as a nutrient iron source, heme is toxic to the bacterium in high concentrations.[16] In order to overcome heme toxicity, *S. aureus* employs a two component system called the heme sensor system (HssRS) to sense heme and activate a response to alleviate heme toxicity. HssS is a transmembrane histidine kinase that senses toxic levels of

heme through an undetermined mechanism. Upon activation, HssS autophosphorylates and transfers the phosphate to an aspartate residue of its cognate response regulator, HssR. HssR is a cytoplasmic protein which, upon phosphorylation by HssS, binds the direct repeat of the promoter for the heme regulated transporter (*hrtAB*), a gene encoding an efflux pump that alleviates heme toxicity.[17,18,19] The mechanism by which HrtAB alleviates heme toxicity is not well understood.
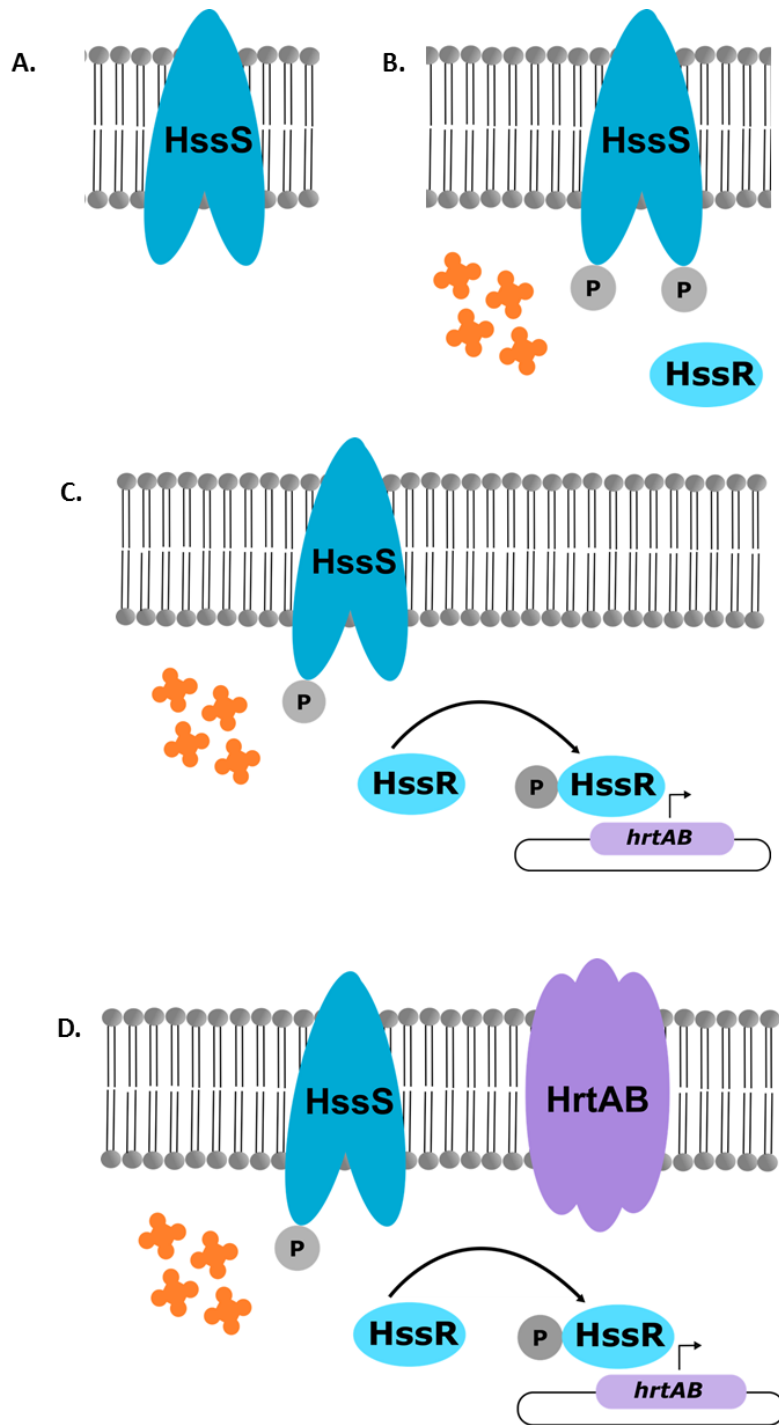
Figure 1.4. Activation of HssRS by heme. HssS is a transmembrane histidine kinase (A) which in the presence of toxic concentrations of heme autophosphorylates (B). HssS can then phosphorylate its cognate response regulator HssR and when phosphorylated, HssR can bind the promoter of *hrt* (C) Inducing expression of HrtAB, an efflux pump which alleviates heme toxicity (D).

High throughput screen for activators of HssRS in *S. aureus*

Since heme toxicity in *S. aureus* is not well understood, the Skaar lab conducted a high throughput screen for activators of the heme stress response to identify potentially useful chemical probes to study this system. To accomplish this, a strain of *S. aureus* harboring a plasmid with the *hrt* promoter fused to a luciferase reporter was constructed. This strain was used to screen the Vanderbilt Small Molecule Library. Molecules that produced a luminescent response were run through a secondary screen using a catechol oxidase reporter and a tertiary screen for the ability of the molecule to preadapt *S. aureus* to toxic concentrations of heme. The top two hits which will be the subject of several chapters of this dissertation are shown in Figure 1.5.

'8882   '3981
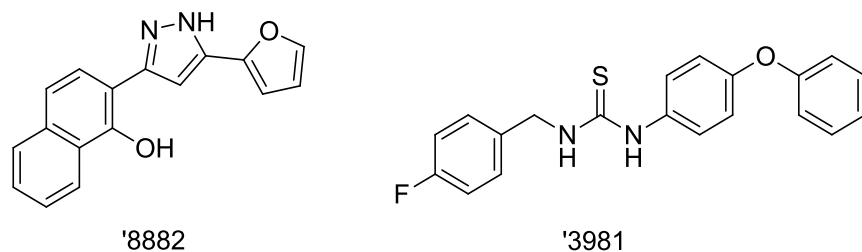
1.5 Statement of Dissertation

The work presented herein involves the application of chemical synthesis to study two distinct questions in the realm of bacterial metal acquisition and homeostasis. The first aims at developing a concise total synthesis of the *Streptomyces coelicolor* produced siderophore coelichelin. While this molecule can be obtained from culture, a synthetic route would enable more flexibility in using it as a chemical probe. The second project focuses on studying the activities of the two molecules identified in the screen for HssRS activators. In both cases, libraries around these scaffolds were prepared and screened for activity to establish structure-activity relationships. These data were utilized in later work to develop chemical probes for target identification to help elucidate their mechanism of action and better define heme toxicity in *S. aureus*.

References

(1)   Hider, R. C.; Kong, X. Chemistry and Biology of Siderophores. *Nat. Prod. Rep.* **2010**, *27* (5), 637–657.

(2)   Hood, M. I.; Skaar, E. P. Nutritional Immunity: Transition Metals at the Pathogen-Host Interface. *Nat. Rev. Microbiol.* **2012**, *10* (8), 525–537.

(3)   Crosa, J. H.; Walsh, C. T. Genetics and Assembly Line Enzymology of Siderophore Biosynthesis in Bacteria. *Microbiol. Mol. Biol. Rev.* **2002**, *66* (2), 223–249.

(4)   Barona-Gómez, F.; Lautru, S.; Francou, F.-X.; Leblond, P.; Pernodet, J.-L.; Challis, G. L. Multiple Biosynthetic and Uptake Systems Mediate Siderophore-Dependent Iron Acquisition in Streptomyces Coelicolor A3(2) and Streptomyces Ambofaciens ATCC 23877. *Microbiology* **2006**, *152* (Pt 11), 3355–3366.

(5)   Luo, M.; Fadeev, E. A.; Groves, J. T. Membrane Dynamics of the Amphiphilic Siderophore, Acinetoferrin. *J. Am. Chem. Soc.* **2005**, *127* (6), 1726–1736.

(6)   Sharman, G. J.; Williams, D. H.; Ewing, D. F.; Ratledge, C. Isolation, Purification and Structure of Exochelin MS, the Extracellular Siderophore from Mycobacterium Smegmatis. *Biochem. J.* **1995**, *305* (1), 187–196.

(7)   Prados-Rosales, R.; Weinrick, B. C.; Piqué, D. G.; Jacobs, W. R.; Casadevall, A.; Rodriguez, G. M. Role for Mycobacterium Tuberculosis Membrane Vesicles in Iron Acquisition. *J. Bacteriol.* **2014**, *196* (6), 1250–1256.

(8)   Bentley, S. D.; Chater, K. F.; Cerdeño-Tárraga, A.-M.; Challis, G. L.; Thomson, N. R.; James,

K. D.; Harris, D. E.; Quail, M. A.; Kieser, H.; Harper, D.; et al. Complete Genome Sequence of the Model Actinomycete Streptomyces Coelicolor A3(2). *Nature* **2002**, *417* (6885), 141–147.

(9)   Traxler, M. F.; Seyedsayamdost, M. R.; Clardy, J.; Kolter, R. Interspecies Modulation of Bacterial Development through Iron Competition and Siderophore Piracy. *Mol. Microbiol.* **2012**, *86* (3), 628–644.

(10)   Calmettes, C.; Ing, C.; Buckwalter, C. M.; El Bakkouri, M.; Chieh-Lin Lai, C.; Pogoutse, A.; Gray-Owen, S. D.; Pomès, R.; Moraes, T. F. The Molecular Mechanism of Zinc Acquisition by the Neisserial Outer-Membrane Transporter ZnuD. *Nat. Commun.* **2015**, *6*, 7996.

(11)   Ma, Z.; Jacobsen, F. E.; Giedroc, D. P. Coordination Chemistry of Bacterial Metal Transport and Sensing. *Chem. Rev.* **2009**, *109* (10), 4644–4681.

(12)   DeLeo, F. R.; Otto, M.; Kreiswirth, B. N.; Chambers, H. F. Community-Associated Meticillin-Resistant Staphylococcus Aureus. *Lancet* **2010**, *375* (9725), 1557–1568.

(13)   Somerville, G. A.; Proctor, R. A. At the Crossroads of Bacterial Metabolism and Virulence Factor Synthesis in Staphylococci. *Microbiol. Mol. Biol. Rev.* **2009**, *73* (2), 233–248.

(14)   Skaar, E. P.; Humayun, M.; Bae, T.; DeBord, K. L.; Schneewind, O. Iron-Source Preference of Staphylococcus Aureus Infections. *Science* **2004**, *305* (5690), 1626–1628.

(15)   Hammer, N. D.; Skaar, E. P. Molecular Mechanisms of Staphylococcus Aureus Iron Acquisition. *Annu. Rev. Microbiol.* **2011**, *65*, 129–147.

(16)   Anzaldi, L. L.; Skaar, E. P. Overcoming the Heme Paradox: Heme Toxicity and Tolerance in Bacterial Pathogens. *Infect. Immun.* **2010**, *78* (12), 4977–4989.

(17)   Friedman, D. B.; Stauff, D. L.; Pishchany, G.; Whitwell, C. W.; Torres, V. J.; Skaar, E. P. Staphylococcus Aureus Redirects Central Metabolism to Increase Iron Availability. *PLoS Pathog.* **2006**, *2* (8), 0777–0789.

(18)   Torres, V. J.; Stauff, D. L.; Pishchany, G.; Bezbradica, J. S.; Gordy, L. E.; Iturregui, J.; Anderson, K. L.; Dunman, P. M.; Joyce, S.; Skaar, E. P. A Staphylococcus Aureus Regulatory System That Responds to Host Heme and Modulates Virulence. *Cell Host Microbe* **2007**, *1* (2), 109–119.

(19)   Stauff, D. L.; Torres, V. J.; Skaar, E. P. Signaling and DNA-Binding Activities of the Staphylococcus Aureus HssR-HssS Two-Component System Required for Heme Sensing. *J. Biol. Chem.* **2007**, *282* (36), 26111–26121.

CHAPTER 2

PROGRESS TOWARD THE TOTAL SYNTHESIS OF COELICHELIN

2.1 Introduction

Coelichelin is a nonribosomal peptide produced by the bacterium *Streptomyces coelicolor*.[1] The goal of this work is to develop a laboratory synthesis of the molecule for confirmation of the proposed structure and to establish a convenient and flexible route to provide significant quantities of the material and derivatives for biological studies. Coelichelin could potentially be a useful chemical tool to study metal acquisition pathways and bacterial responses to iron depletion. For these kinds of experiments, synthetic chemicals such as 2,2'-bipyridine, are often used as iron chelators to sequester iron in growth media.[2,3,4] Natural product siderophores may be superior to synthetic chelators in such experiments as they are likely more selective for ferric iron. However, the use of many natural product siderophores is limited by their availability since most are only accessible by isolation from the producing organism. A convenient synthetic route to a natural product siderophore would provide ample material to conduct these experiments as well as study the basic biology of the siderophore itself. Coelichelin is an attractive target because it is structurally interesting but accessible using chemistry developed for the synthesis of similar siderophores. In addition, no chemical synthesis of coelichelin has been reported to date.

2.2 Background

Traditionally, discovery of bioactive natural products involves screening of biological extracts for activity against systems of interest, fractionation of active extracts using chromatographic methods to identify active components, and structure determination.[5] Many medically and industrially important compounds have been identified through these methods including antibiotics, antifungals, antineoplastics, cardiovascular drugs, and pain medications.[6] While this process has been fruitful, it can be tedious and self-limiting depending on the conditions of isolation and stability of the natural products being isolated.[5] The inception of the genomic age has introduced the possibility of predicting natural products from genomic information[7] allowing these limitations to be circumvented.

Many antimicrobial drugs are either derived from or are themselves metabolites of microorganisms, and of these natural product based drugs, approximately half come from actinomycetes.[8] Considerable work to characterize the numerous biosynthetic pathways in actinomycetes as well as homologous pathways in other organisms, has provided invaluable information that can be applied to search for sequence similarities in whole genomes to identify gene clusters encoding biosynthetic pathways.[7]

Nonribosomal peptide synthesis

Nonribosomal peptides (NRPs) constitute a rich class of bacterial (and fungal) metabolites, many of which are used clinically including bacitracin, cyclosporine, and daptomycin. They are synthesized by modular mulitenzyme complexes called nonribosomal peptide synthetases (NRPSs) which function similarly to polyketide and fatty acid synthetases.[9]

17

Each module is minimally composed of an adenylation domain (A-domain) and a thiolation domain (T-domain, also referred to as a peptidyl carrier protein or PCP). The A-domain activates the amino acid to be added to the growing peptide by reaction with ATP to transfer AMP to the amino acid and release pyrophosphate. The A-domain recognizes a specific amino acid to be activated for each module and this can be discerned from the amino acid sequence of the domain and thus, predicted from genomic data.[10,11] Since the NRP is synthesized from module to module, the sequence of A-domains determines the primary sequence of the NRP.[9]

The T-domain consists of a 4'-phosphopantethenyl (4'-PP) cofactor bound to the protein through a conserved serine residue. After amino acid activation by the A-domain, the thiol of the 4'-PP reacts with the activated carboxylate forming a thioester linkage and displacing AMP. The amino acid is now bound to the module and can be acted upon by modifying domains such as epimerases and *N*-methyltransferases. The chain is elongated by condensation domains (C-domians) which catalyze the attack of the amino group of a module on the thioester carbonyl of the substrate of the previous module bound to the T-domain. Many NRPSs have a terminal thioesterase domain which will hydrolyze the completed peptide from the NRPS though some lack this function and rely instead on nonenzymatic reactions to achieve hydrolysis of the thioester.[9]

Identification of coelichelin from genome mining

Utilizing genome sequences from an ordered cosmid library from *S. coelicolor*[12], Challis and coworkers identified a region on cosmid SCF-34 with sequence homology to NRPSs. This region codes for a 3643 amino acid protein with a predicted molecular weight of 390 kDa. The

gene was determined to be part of a large gene cluster consisting of ~20 genes spanning ~29 kbp. The functions of these genes were hypothesized based on sequence homology and the cluster determined to provide the components and biosynthetic machinery for siderophore synthesis as well as proteins involved in siderophore secretion and reuptake (Figure 2.1.A).[13]
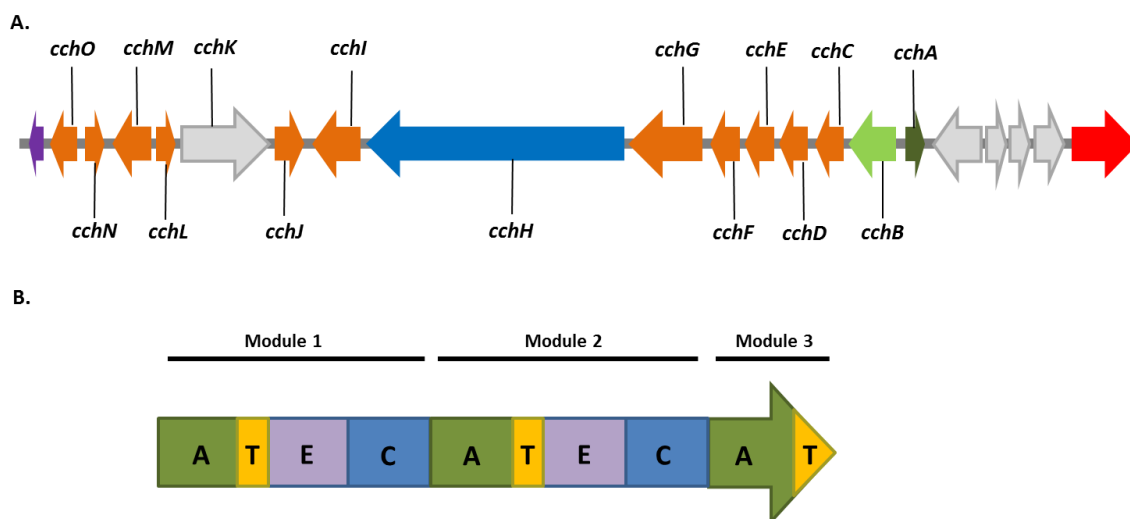
Figure 2.1. Coelichelin gene cluster and NRPS. A. Organization of coelichelin gene cluster: blue = NRPS (*cchH*), light green = ornithine $^{\delta}N$-oxidase (*cchB*), dark green = $^{\delta}N$-hydroxy-L-ornithine formyl transferase (*cchA*), orange = genes involved in siderophore secretion and reuptake, red = RNA helicase, purple = chitinase, grey = unknown function. B. Organization of coelichelin NRPS: A = adenylation domain, T = thiolation domain, E = epimerase, C = condensation domain.

The functions of each module were determined based on conserved sequence similarity to known NRPS modules and the order is depicted in Figure 2.1.B. A notable feature of this NRPS is the lack of a terminal thioesterase domain responsible for releasing the final product from the synthetase. Taking this into account, analysis of the module sequence in *cchH* led to the two hypothesized structures **2.1** and **2.2** (Figure 2.2). Challis and coworkers favored **2.2** arguing that a thioesterase domain would be required for **2.1** while **2.2** could be released by attack of the δ-amino group on the thiosester in a favored 6-exo-trig closure.[13]

Figure 2.2. Proposed structures of coelichelin based on genomic information.

Isolation of coelichelin from culture

Challis and coworkers next attempted to isolate coelichelin from culture utilizing methods for the isolation and structure determination of similar siderophores.[14] They compared HPLC traces of growth media of wild type *S. coelicolor* and a *cchH* knockout grown in iron deplete conditions and identified a fraction present in the growth media of wild type, but not the knockout. A strong absorbance at 435 nm in this fraction suggested a trishydroxamate bound to iron. This peak was isolated and subjected to various analyses to identify the structure including mass spectrometry, hydrolysis to the constituent amino acids followed by derivatization and chiral gas chromatography, and removal of iron by a competing siderophore to isolate apo-coelichelin followed by formation of the Ga^{3+} bound species for NMR analysis. These studies led to the revised structure **2.3** shown unbound and **2.4** bound to Fe^{3+} (Figure 2.3 A and B).

Figure 2.3. A. Revised structure of coelichelin (**2.3**). **B.** Coelichelin depicted bound to ferric iron (**2.4**).
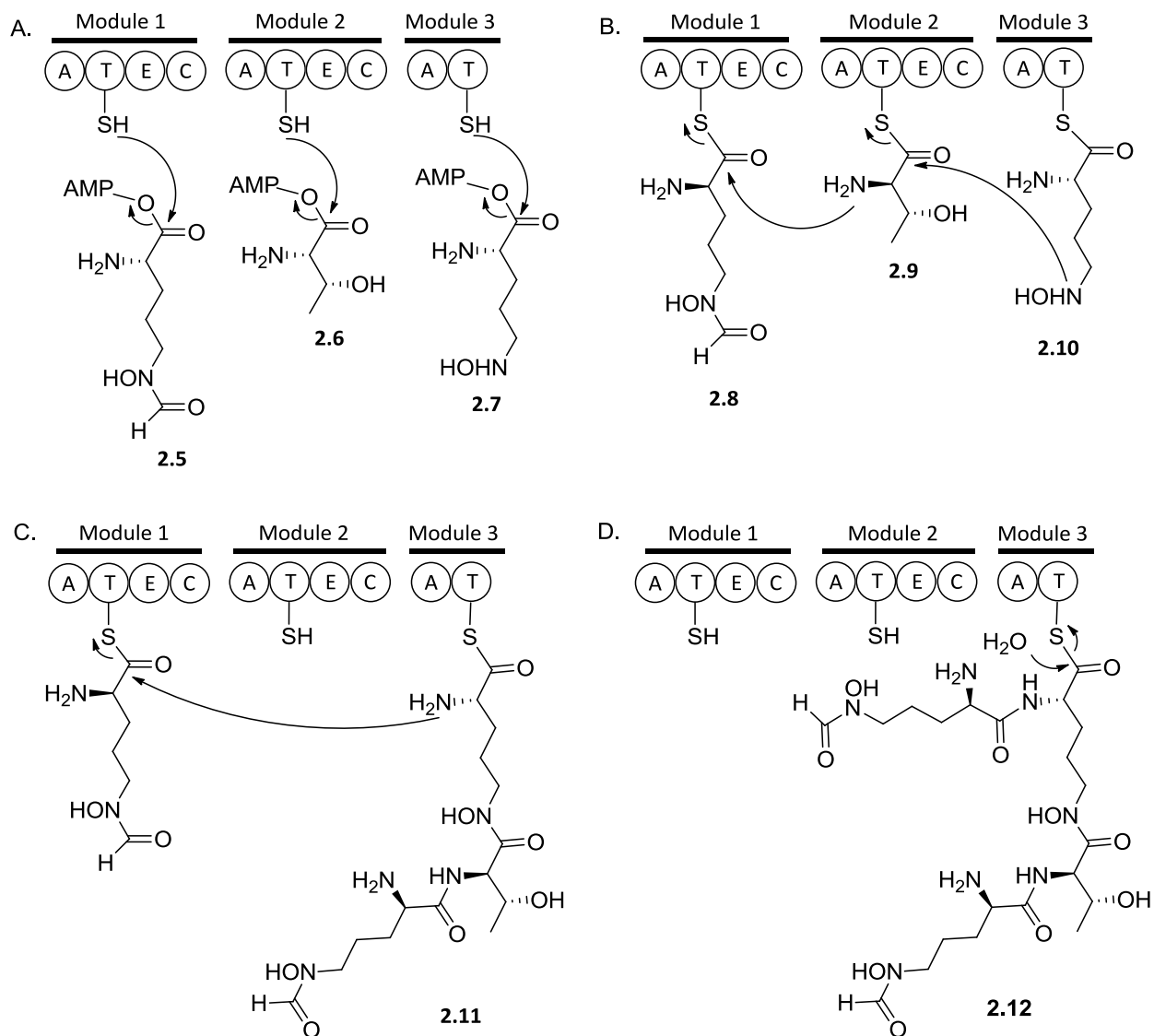
Figure 2.4. Proposed biosynthesis of coelichelin.

This tetrapeptide is hypothesized to be biosynthesized as depicted in Figure 2.4. In this model, the first A-domain recognizes and activates $^\delta N$-formyl-$^\delta N$-hydroxy-L-ornithine, the second, L-threonine, and the third, $^\delta N$-hydroxy-L-ornithine, to provide **2.5**, **2.6**, and **2.7** respectively, which are then loaded on to their respective T-domains (Figure 2.4.A). The first and second epimerase modules invert the stereochemistry at the α-carbons and then the

condensation domains catalyze the formation of the elaborated tripeptide **2.11** (Figure 2.4.B). A second $^\delta N$-formyl-$^\delta N$-hydroxy-L-ornithine is then loaded on to the first module where it is epimerized and condensed with **2.11** to give tetrapeptide **2.12** bound to the T-domain of the third modules (Figure 2.4.C). Finally, this is hydrolysed nonenzymatically to give **2.3** (Figure 2.4.D).

2.3 Previous synthetic studies towards siderophores

Syntheses of $^\delta N$-acyl-$^\delta N$-hydroyornithine and derivatives

Interest in the synthesis of $^\delta N$-hydroyornithine and acylated derivatives began in the 1960s with identification of these as components of siderophores and microbial natural products.[15] Nielands reported the first synthesis of $^\delta N$-hydroxyornithine. Starting from DL-glutamic acid, the amino acid moiety was protected as the hydantoin and the terminal carboxylic acid was converted to bromide **2.13** in 3 steps. From **2.13**, $^\delta N$-hydroxy-DL-ornithine (**2.14**) was obtained by conversion to the nitro compound, semi-reduction with zinc dust, and subsequent acid hydrolysis of the hydantoin to provide **2.14** in 17 % yield. The authors noted that significant quantities of optically active **2.14** could be obtained from natural sources.[16]

Isowa reported the first synthesis of optically active **2.14** and $^\delta N$-acetyl-$^\delta N$-hydroxyornithine (**2.18**). This procedure began with monoalkyation of 1,3-dibromopropane with *N*-tosyl-*O*-benzylhydroxylamine to provide **2.15**. The resulting bromide was alkylated with the sodium salt of diethyl acetamidomalonate followed by decarboxylation to provide **2.16** as a racemate. The enantiomers were resolved enzymatically by reaction with aniline using papain, providing the L-isomer as the anilide. Both enantiomers were converted to the amino acid by

heating with concentrated HCl in AcOH. The tosyl group was removed by reaction with HBr in AcOH for 50 h to provide **2.17** (or its enantiomer).[17] **2.18** was obtained by acetylation of the hydrobromide salt with acetic anhydride followed by catalytic hydrogenolysis to remove the benzyl ethers.[18] Fujii expanded on this method by reacting the intermediate 3-bromopropyl diethylacetamidomalonate with *O*-benzylhydroxylamine under basic conditions to install the $^\delta$*N*-hydroxylamine group, though poly-*N*-alkyation was problematic.[19] Emery reported an analogous approach where α-protected 5-hydroxy-2-aminopentanoic acid was converted to the bromide and this intermediate reacted with *N*-acetyl-*O*-benzylhydroxylamine under basic conditions.[20]

Maehr and coworkers reported a route to **2.14** utilizing *N*-alkylation of methyl 2-acetamido-5-iodovalerate with the thallium(I) salt of *trans*-benzaldoxime in DMF to provide the nitrone which was then hydrolyzed under acidic conditions to provide the hydroxylamine with subsequent ester and acetamide hydrolysis to provide **2.14**.[21] A similar route utilizing nitrone hydrolysis was employed by Keller-Schierlein starting from α-protected L-ornithine **2.21**, the δ-nitrogen was reacted with *p*-methoxybenzaldehyde to form the imine followed by oxidation to provide oxaziridine **2.22** which was hydrolyzed to **2.29**.[15] Using a direct *N*-oxidation approach, Chimiak reported the oxidation of the δ-nitrogen of α-protected L-ornithine with benzoyl peroxide followed by same-pot acetylation.[22]

Neilands, 1963

HO—O
H₂N
HO—O

→

Br

2.13

1. NaNO₂
2. Zn dust, H₂O
3. 6 N HCl, 125 °C

17 %

NHOH
H₂N
COOH

2.14

Isowa, 1972

Ts—NOBn
Br

2.15

1.
EtOOC—COOEt
NHAc

→

Ts—NOBn
AcHN
COOH

2.16

2. Enzymatic resolution
3. HCl, AcOH
4. HBr, AcOH

→

NOHBn
Br⁻ H₃N⁺
COOH

2.17

5. Ac₂O, H₂O
6. H₂, Pd/C

→

O
NOH
H₂N
COOH

2.18

Maehr, 1974

I
AcHN
COOR

2.19

Ph
N—OTl
Ph—
DMF

→

Ph
N⁺—O⁻
AcHN
COOR

2.20

H⁺, H₂O

→

HN—OH
H₂N
COOH
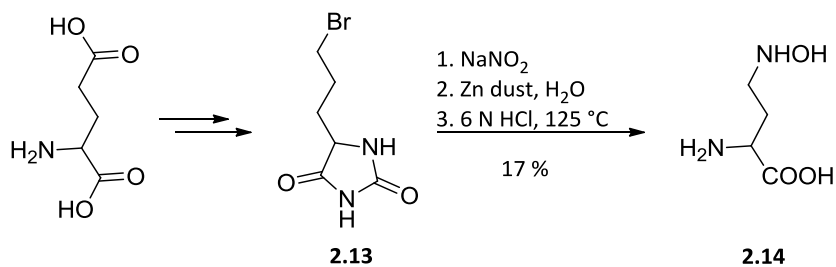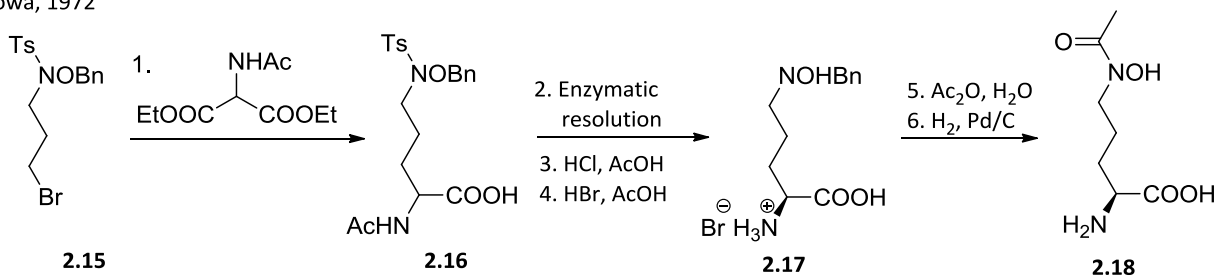
2.14

Keller-Scheirlein, 1978

NH₂
R₁HN
COOR₂

2.21

1. MeO-C₆H₄-CHO
2. mCPBA

→

O
N
OMe
R₁HN
COOR₂

2.22

3. H⁺, H₂O

→

OH
NH
R₁HN
COOR₂

2.23

Chimiak, 1990

NH₂
CbzHN
COOt-Bu

2.24

1. (BzO)₂, Na₂CO₃, DCM.
2. AcCl/H₂O

61 %

→

O
NOBz
CbzHN
COOt-Bu

2.25

3. NH₃, MeOH
4. TFA
5. H₂, Pd/C

75 %

→

O
NOH
H₂N
COOH

2.18

25
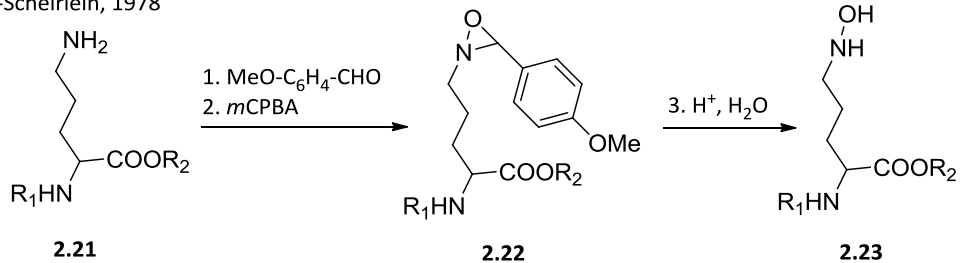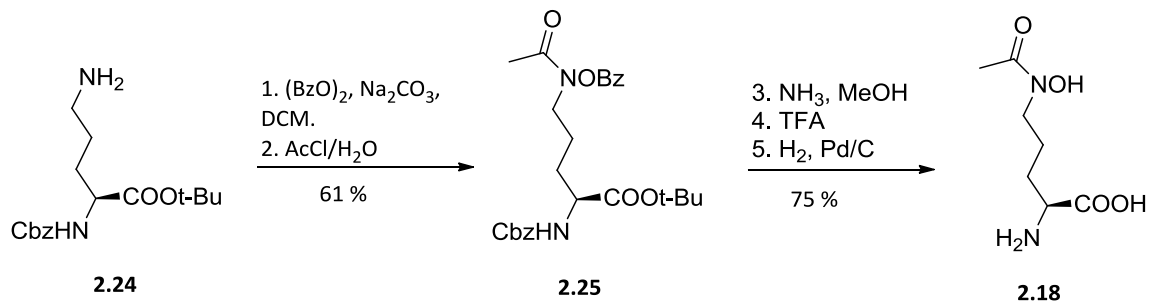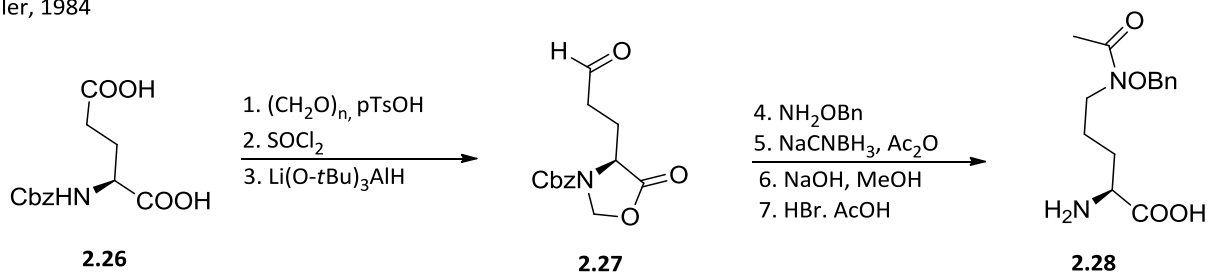
Figure 2.5. Methods for synthesizing $^{\delta}$N-acyl-$^{\delta}$N-hydroyornithines.

Miller and coworkers have devised several methodologies to synthesize $^{\delta}$N-acyl-$^{\delta}$N-hydroxyornithine precursors for siderophore syntheses. Their first route to optically active $^{\delta}$N-hydroxyornithine started from carboxybenzyl protected L-glutamic acid (**2.24**) with the amino acid function further protected by reaction with paraformaldehyde. The δ-carboxylic acid was converted to the acid chloride with thionyl chloride followed by reduction to aldehyde **2.25** with lithium tri-*t*-butoxyaluminum hydride. The aldehyde was converted to a mixture of oximes by reacting with *O*-benzylhydroxylamine followed by reduction with sodium cyanoborohydride and acetylation in the same pot. The amino acid was deprotected to provide **2.26** with the hydroxamic acid protected as the benzyl ether. **2.26** could be used in siderophore synthesis with late stage hydrogenolysis to remove the benzyl ether.[23] Alternately, they reacted α-protected 5-hydroxy-2-aminopentanoic acid with *N*-Cbz or *N*–troc-*O*-benzylhydroxylamine under Mitsonobu conditions followed by deprotection of the δ-nitrogen to provide derivatives of **2.14**.[24]

Syntheses of $^{\delta}N$-acyl-$^{\delta}N$-hydroxyornithine containing siderophores

By modern standards, the synthesis of peptide derived siderophores is not overly complex. The primary concerns when synthesizing hydroxamate containing siderophores in the laboratory are minimizing racemization during peptide coupling and strategic and orthogonal deprotection of functional groups. To a lesser extent, minimizing metal contamination of glassware in the final steps of the synthesis is important to obtain pure, unbound samples of the final product for characterization.

Much of the work towards efficient syntheses of $^{\delta}N$-acyl-$^{\delta}N$-hydroxyornithine was a component of larger syntheses of siderophores containing these functionalities. Several examples of siderophore syntheses will be presented to highlight the synthetic challenges and methods used to overcome them, as well as the guiding principles for our synthetic approach to coelichelin.

Ferrichrome is a cyclic hexapeptide consisting of three contiguous glycines followed by three contiguous $^{\delta}N$-acetyl-$^{\delta}N$-hydroxy-L-ornithines. The first synthesis of ferrichrome was accomplished by Keller-Schierlein utilizing the nitro reduction chemistry pioneered by Neilands. They assembled a hexapeptide (**2.30**) containing the requisite three glycines and three L-5-nitro-2-aminopentanoic acids (**2.29**), cyclized, and then reduced the nitro groups to provide δ-hydroxylamines. This molecule was acetylated to give ferrichrome (**2.31**).[15,25] Isowa's group used a similar approach but employed their N-tosyl-O-benzylhydroxylamine compound **2.32** in the coupling process. Cyclization of **2.33** followed by global removal of tosyl groups with HBr in AcOH, acetylation, and global hydrogenolysis of benzyl ethers gave **2.31**.[26]
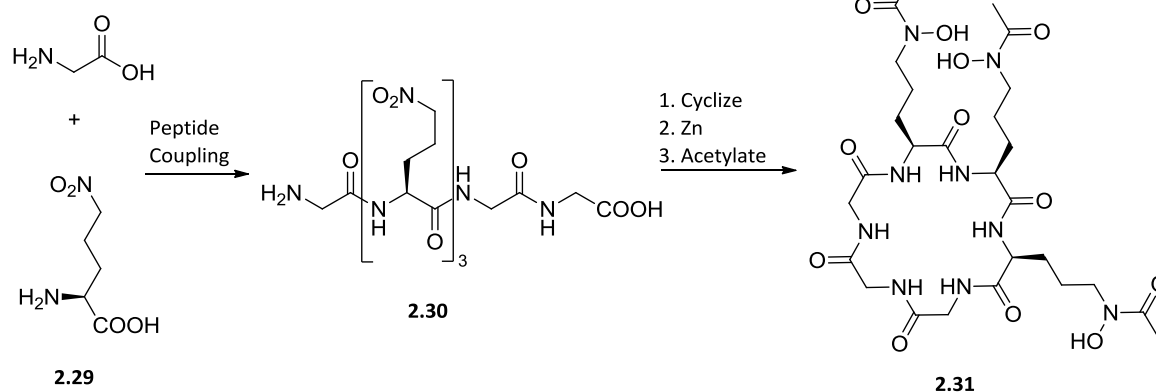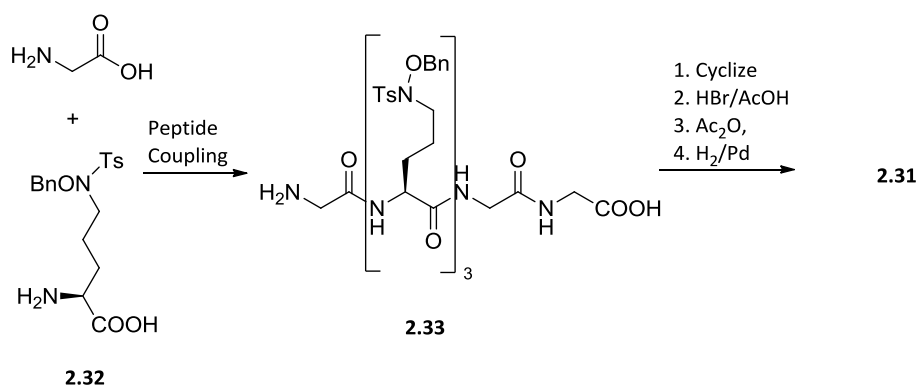
Figure 2.6. Syntheses of ferrichrome.

Another early target of siderophore synthesis was rhodotrulic acid (**2.40**). This compound is a diketopiperazine formed from the condensation of two $^\delta N$-acetyl-$^\delta N$-hydroxyornithines. Isowa and coworkers first synthesized **2.40** using their *N*-tosyl-*O*-benzylhydroxylamine alkylation chemistry. Keller-Schierlein adapted their nitro reduction chemistry to this molecule as well with a late stage global reduction followed by acetylation to give the natural product.[15] Miller and coworkers used a contrasting route by installing the *O*-benzyl protected hydroxamic acid into their monomer before coupling. Starting from protected glutamic acid **2.34**, they converted the δ-carboxylate into the anhydride with ethyl

chloroformate and reduced to the alcohol with sodium borohydride to give **2.35**. This was then reacted with *N*-troc-*O*-benzylhydroxylamine under Mitsonobu conditions, the troc group was selectively removed under reductive conditions, and the δ-nitrogen acetylated to provide **2.36**. After several protecting group manipulations, they arrived at intermediates **2.37** and **2.38** which were coupled with EEDQ to give **2.39**. The Boc group and methyl ester were removed leading to cyclization and the benzyl ethers were removed by hydrogenolysis to give **2.40**.[24]
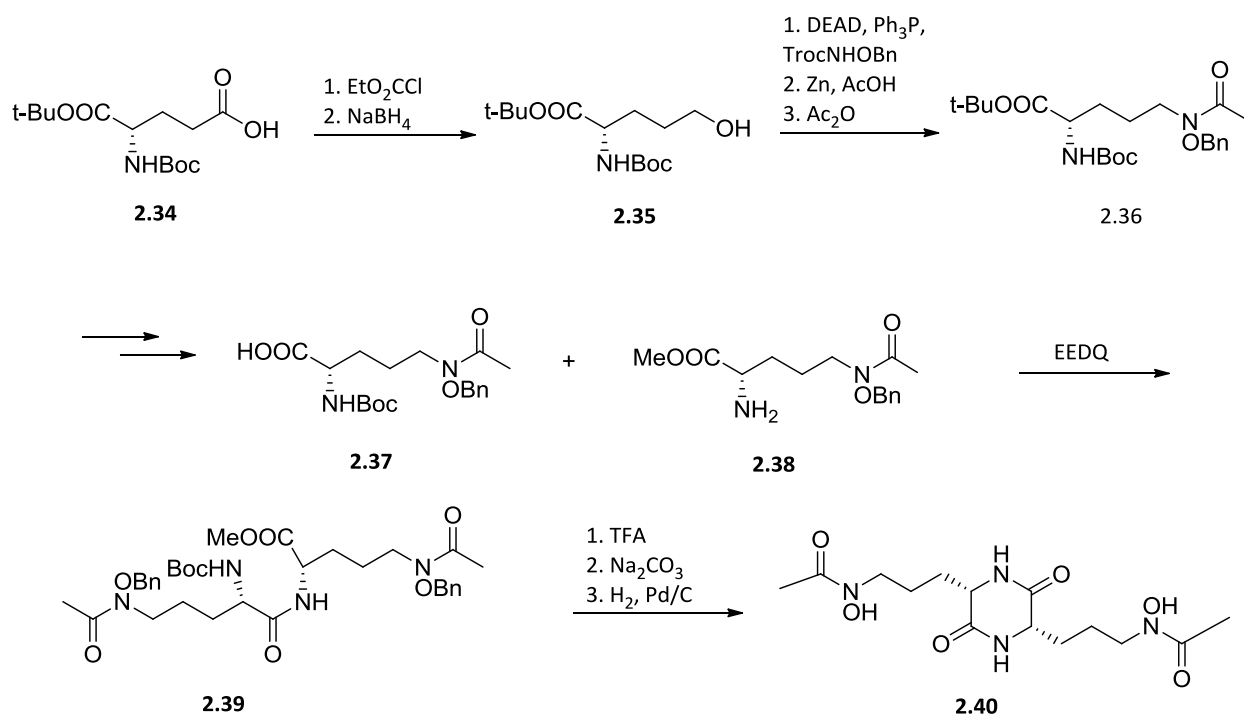
Scheme 2.1. Miller's synthesis of rhodotrullic acid.

Foroxymithine, **2.48**, is structurally similar to rhodotrullic acid. Miller's lab synthesized this using a convergent approach applying their Mitsonobu chemistry. They prepared mono-*N*-troc protected diketopiperazine **2.43** and coupled this with the succinimide ester of dipeptide

2.45. Tetrapeptide **2.46** was then subjected to sequential removal of protecting groups and *N*-formylation. The Cbz group was removed by HBr in acetic acid and the free amine was acetylated by acetic anhydride and triethylamine which also consequently *O*-acylated serine to provide **2.47**. Treatment of this tetrapeptide with zinc dust and acetic formic anhydride in THF removed the Troc groups with subsequent *N*-formylation. The *O*-acetyl was removed under mildly basic conditions and the final product was provided by hydrogenolysis of the benzyl ethers.[27]
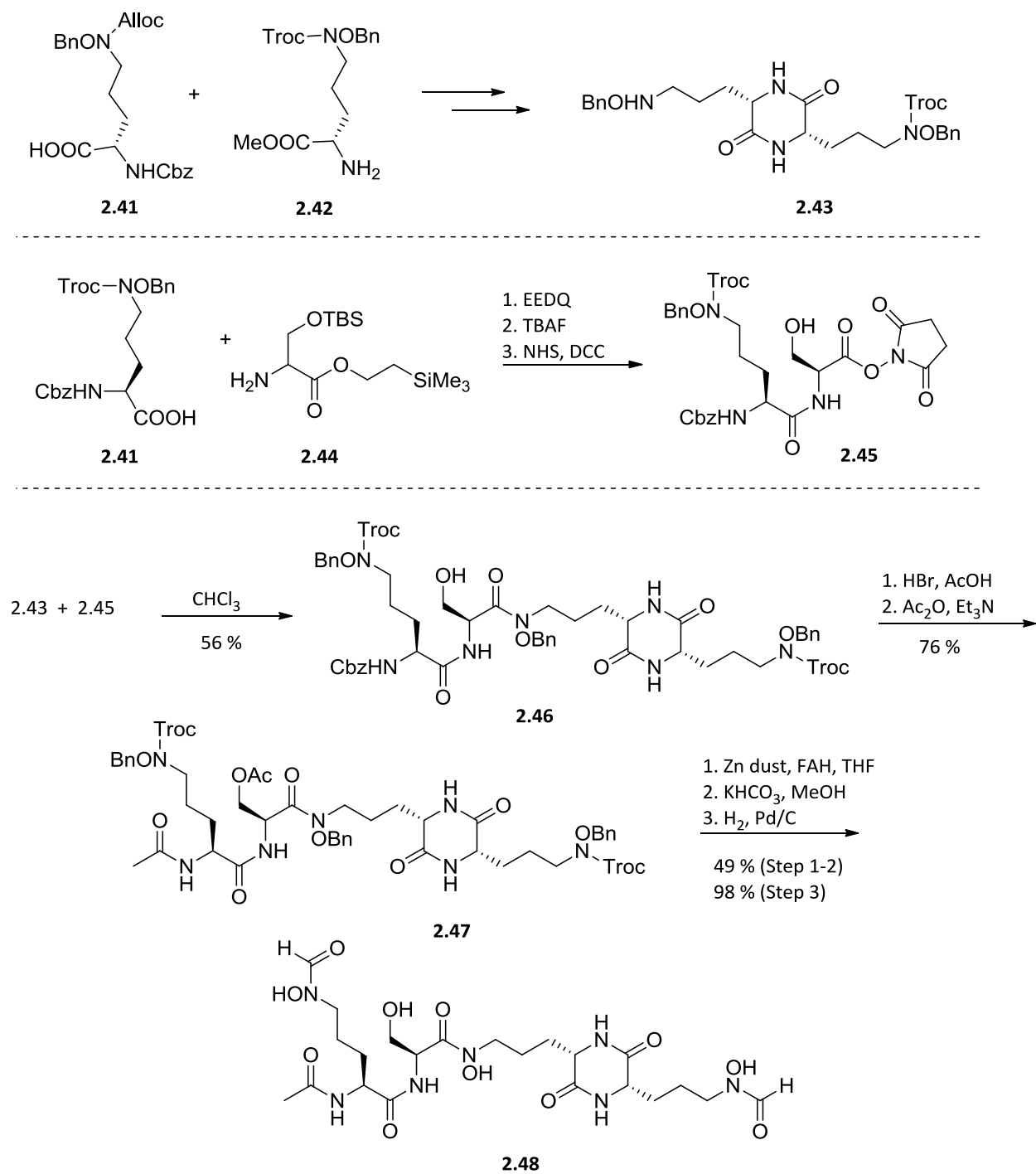
Scheme 2.2. Miller's synthesis of foroxymithine.

A more modern synthesis (2013) of a $^{\delta}N$-formyl-$^{\delta}N$-hydroxyornithine containing siderophore was reported by Meijler with their synthesis of pyoverdin D (**2.58**), a complex molecule secreted by *Pseudomonas aeruginosa*. It consists of a partially cyclic octapeptide where the macrolide portion includes a lysine side chain at the N-terminus cyclized through four backbone amino acids to the lysine α-carboxylate. The macrolide is connected through the lysine α-amino group to a linear tripeptide bound at its N-terminus to a dihydroxyquinolone derived chromophore. Pyoverdin D contains two $^{\delta}N$-formyl-$^{\delta}N$-hydroxy-L-ornithine residues, one in the macrolide and one in the linear side chain.[28]

Meijler utilized solid phase peptide synthesis (SPPS) to construct the octapeptide. They synthesized the $^{\delta}N$-formyl-$^{\delta}N$-hydroxy-L-ornithine component for SPPS by direct oxidation of the δ-nitrogen of protected ornithine **2.49** with benzoyl peroxide. The δ-nitrogen was then formylated by treatment with formic acid and EDC, the benzoate ester removed under basic conditions with added benzyl bromide to reprotect the hydroxamate oxygen as the benzyl ether. Protecting group manipulations provided the Fmoc protected compound **2.52** for SPPS. The octapeptide **2.56** was synthesized as depicted in Scheme 2.3.[28]

The chromophore component **2.55** was prepared separately from **2.53** and **2.54**. The carboxylic acid of the chromophore was coupled to the resin bound octapeptide **2.56** with PyBOP and released from the resin with concomitant trityl and Mmt deprotection by treatment with acid. The macrolide was formed by coupling the C-terminus with the ε-nitrogen of lysine by treatment with HATU and *N,N*-diisopropylethylamine to provide **2.57**. The remaining protecting groups were removed by hydrogenolysis and the succinimide hydrolyzed with base to afford **2.58**.

1. H$_2$, Pd/C
2. 1 M NaOH, H$_2$O

48 %

2.59
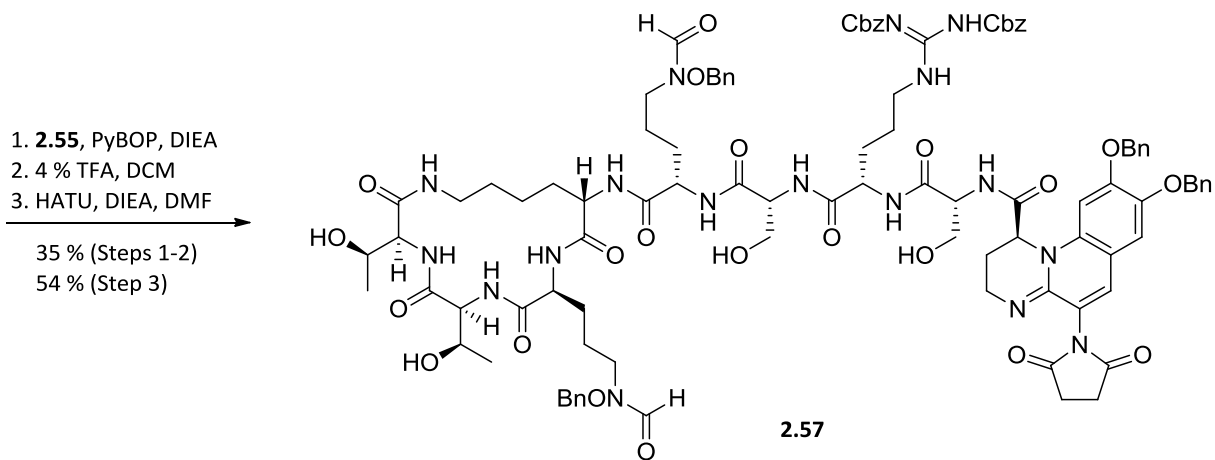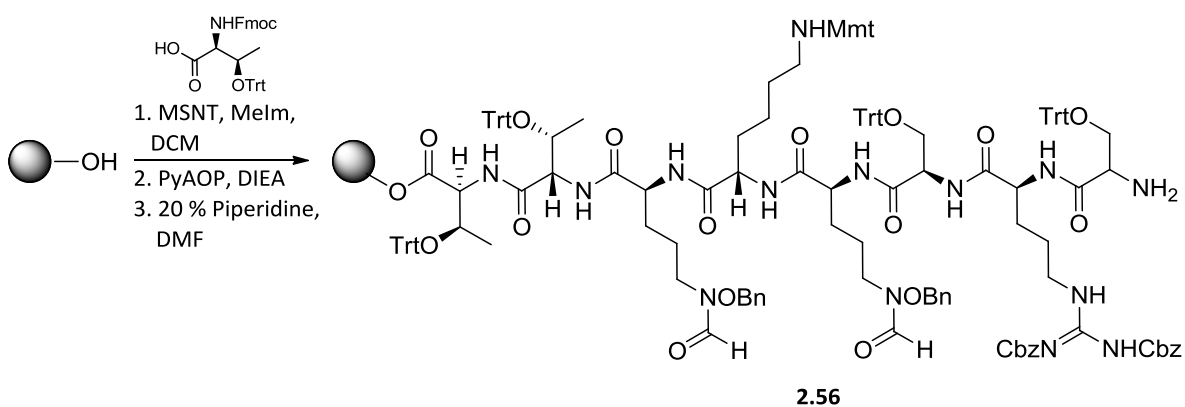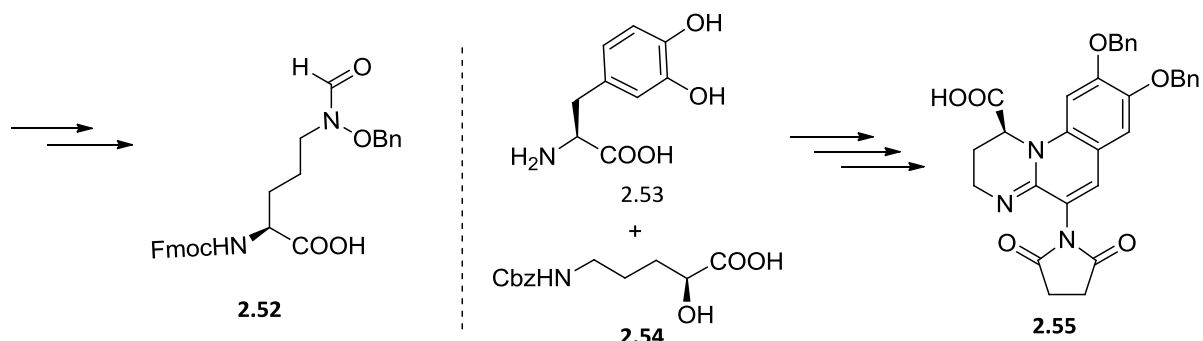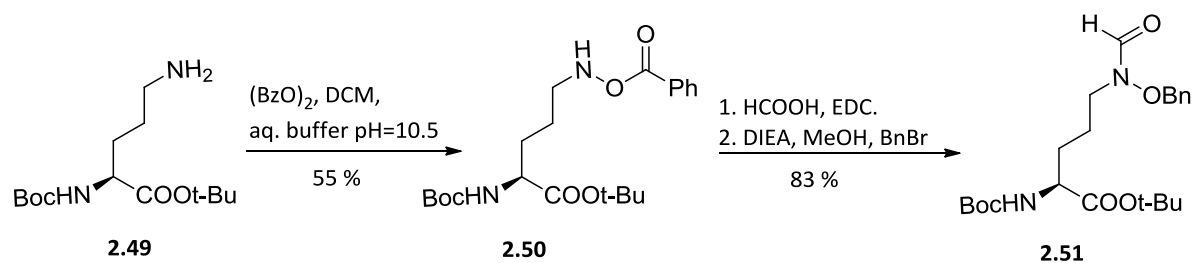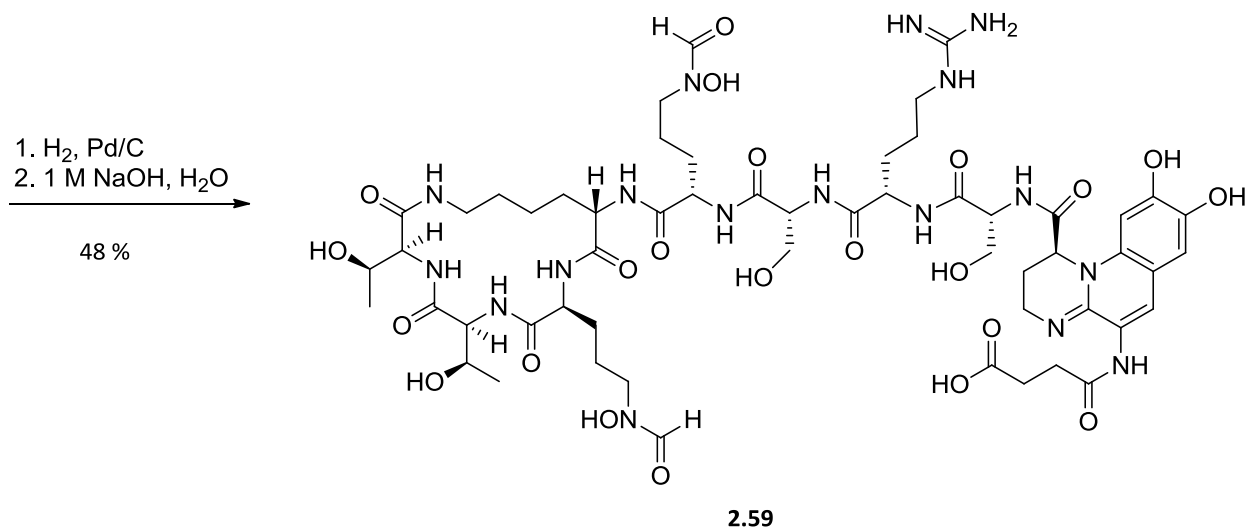
Scheme 2.3. Meijler synthesis of pyoverdin D.

2.4 Studies towards the synthesis of coelichelin

Coelichelin retrosynthetic analysis

Using a similar approach as the previously described syntheses, we envisioned assembling coelichelin through peptide couplings of suitably protected amino acid precursors and globally deprotecting the assembled polypeptide to provide the natural product. The molecule can be disconnected through the peptide bonds to three precursor amino acids; the Boc and acetonide protected D-*allo*-threonine **2.59**, protected $^{\delta}N$-hydroxy-L-ornithine **2.60**, and protected $^{\delta}N$-formyl- $^{\delta}N$-hydroxy-D-ornithine **2.61** (Scheme 2.4). **2.59** can be prepared from D-*allo*-threonine by a reported route.[29] D-*allo*-threonine is prohibitively expensive but can be prepared from D-threonine in several steps and acceptable yield.[30] **2.60** and **2.61** can be prepared by a similar route differing only by the stereochemistry at the α-carbon and formylation of the D-isomer. Protected 5-hydroxy-2-aminopentanoic acid **2.62** is an excellent substrate for synthesis of **2.60** and **2.61** since a variety of the previously described chemistry to

34

install the *N*-hydroxy functionality can be utilized including the oxidation/reductive amination and conversion to a leaving group/displacement strategies. This material can be prepared from commercially available D- and L-pyroglutamic acids. Starting with this material allows simple incorporation of the correct stereochemistry and additionally allows easy modification of protecting groups should the need arise.
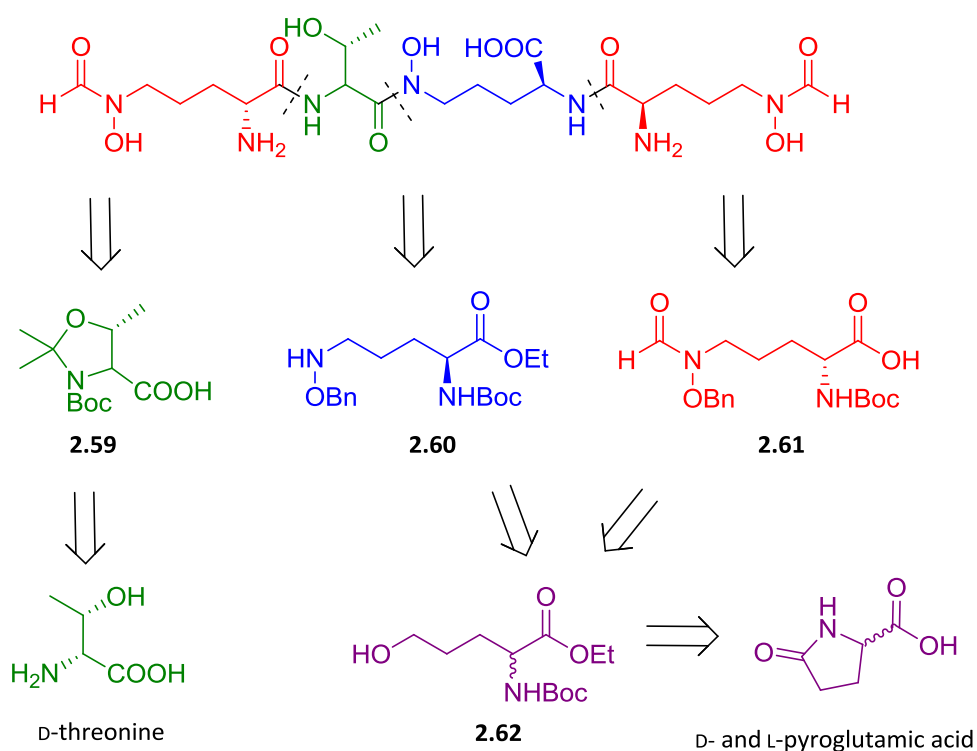
Scheme 2.4. Retrosynthetic analysis of coelichelin.

Synthesis of protected threonine 2.59

Using a literature procedure[30], D-allo-threonine was prepared by converting D-threonine to methyl ester **2.63** by treatment with thionyl chloride in methanol. **2.63** was then treated with benzoyl chloride and triethylamine in methanol to provide benzamide **2.64**. This was

reacted with thionyl chloride for 5 days at 0 °C leading to formation of oxazoline **2.65** and inversion of the stereocenter at the β-carbon. The oxazoline and methyl ester of **2.65** were then hydrolyzed in 6 N HCl to provide D-allo-threonine as the hydrochloride salt. The nitrogen was Boc protected by treatment with di-tert-butyl-dicarbonate in methanol-aqueous sodium bicarbonate. Under these conditions, methyl ester formation occurred to some extent. To resolve this, the crude product after work up was dissolved in THF and treated with 1 M LiOH to saponify the ester and provide **2.66** in 80 % yield. The Boc protected D-allo-threonine was converted to the acetonide by treating with 2,2-dimethoxypropane and catalytic TsOH in DCM to give **2.59** in 83 % yield.[29]
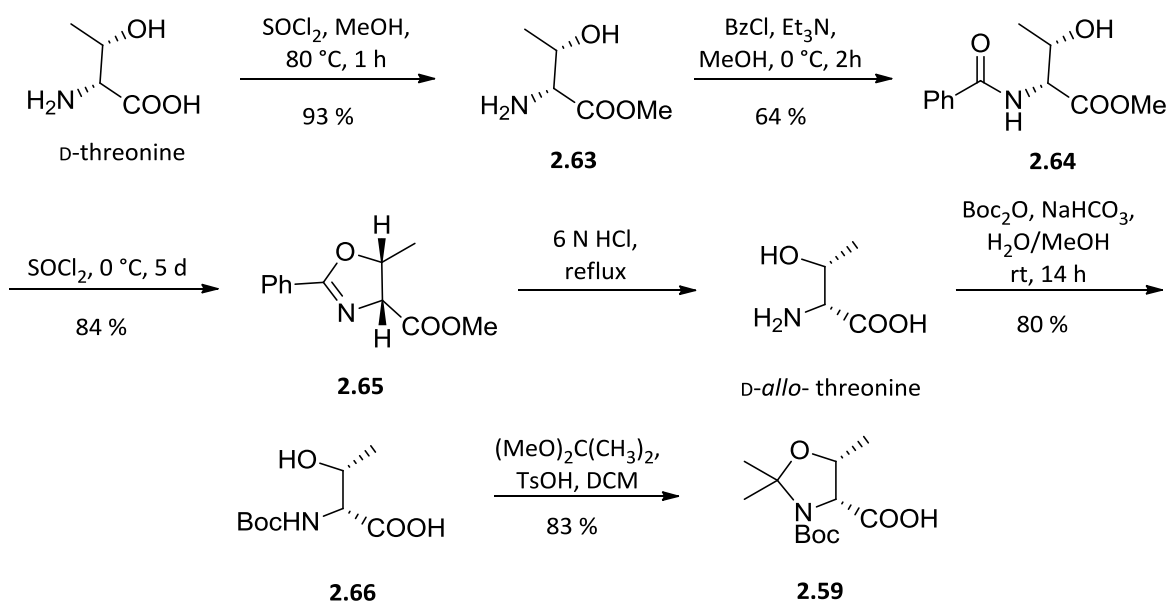
Scheme 2.5. Synthesis of threonine precursor **2.59**.

Synthesis of intermediate 2.60 and 2.61

We began investigating a route to **2.61** reasoning that the same chemistry could be applied to arrive at **2.60** but starting from the opposite enantiomer. Intermediate **2.62** was prepared from commercially available D-pyroglutamic acid ethyl ester in two steps. The nitrogen was Boc protected to provide **2.67** which was then treated with sodium borohydride in 5:1 THF/water to provide **2.68** in 42 - 68 % yield over two steps.[31] The sodium borohydride reduction did not give consistent yields and efforts to optimize were unsuccessful. While an alternate strategy to go from **2.67** to **2.68** by lactam hydrolysis with base followed by conversion to the anhydride and subsequent reduction has been reported[31], the added steps and possibility of ester saponification rendered this route undesirable and we deemed potential material losses at this step to be acceptable.
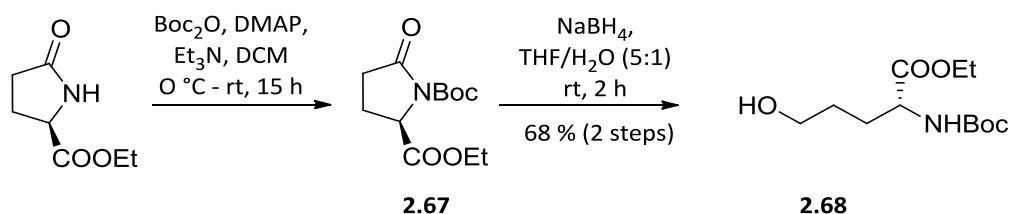
Scheme 2.6. Preparation of intermediate **2.68**.

We initially explored a route to **2.60/2.61** via conversion of the alcohol of **2.68** to a leaving group and direct displacement by *O*-benzylhydroxylamine similar to the previously described method of Fujii. **2.68** was easily converted to tosylate **2.69** by treatment with tosyl chloride in pyridine at 0 °C overnight. **2.69** was reacted with *O*-benzylhydroxylamine and a base under various conditions, but generally, only starting material was recovered. A small amount

of product was obtained when the reaction was carried out in DMF at 150 °C under microwave

irradiation. In an attempt to see if an alternate leaving group would provide higher yields, we

attempted to convert **2.68** to the bromide with triphenylphosphine and carbon tetrabromide

but observed a complex mixture of products. Given the lack of success with this route, we

decided to pursue an alternate strategy.
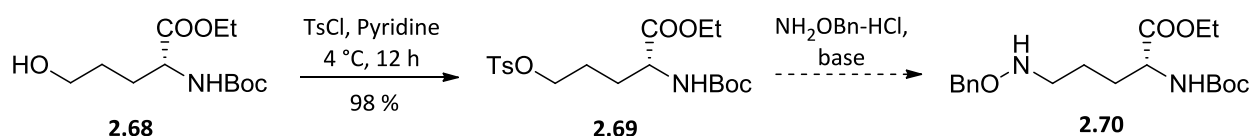
Base	Solvent	Temperature	Result
DIEA	MeOH	rt	No reaction
DIEA	DMF	rt	No reaction
DIEA(TBAI added)	DMF	rt	No reaction
K$_2$CO$_3$	DMF	rt	No reaction
K$_2$CO$_3$	DMF	150 °C (mw)	10 % yield

Figure 2.7. Investigation of S$_N$2 approach to **2.60/2.61**.

The next method we attempted to employ was an oxidation/reductive amination

approach. Initial efforts to oxidize **2.68** to the aldehyde were problematic. Pyridinium

chlorochromate (PCC) was initially used as a similar reaction was previously reported by Miller.

However, the aldehyde was not isolated in good yield and purification was not productive as it

appeared the aldehyde was not entirely stable and thus could not be stored. Attempts to form

the oxime from the crude product of PCC oxidation were also not productive. In addition to

PCC, oxidations with IBX and Dess-Martin periodinane were also attempted with little success.

Ultimately, the Parikh-Doering oxidation was successful at producing the aldehyde in sufficient quantities to move forward. Oxidation under these conditions and subsequent oxime formation with *O*-benzylhydroxylamine hydrochloride and sodium acetate in ethanol provided oximes **2.72** as a mixture of geometric isomers.

Reduction of oximes **2.72** was rendered needlessly time consuming by the insistence that sodium cyanoborohydride, the reagent of choice for this transformation, not be used. Instead, many alternate reagents and conditions including sodium triacetoxyborohydride, tetramethylammonium triacetyoxyborohydride, sodium borohydride, and triethylsilane were explored. While there was literature precedence for oxime reduction by all of these reagents, none reproducibly resulted in formation of **2.73**. After much wasted time, treatment of **2.72** with sodium cyanoborohydride and 0.1 M HCl in ethanol resulted in formation of **2.73** in excellent yield, naturally.

Formylation of **2.73** was accomplished by treatment with formic acetic anhydride[32] to provide **2.74**. Saponification of the ester to provide advanced intermediate **2.61** was attempted with 1 M LiOH in THF. Unfortunately, in addition to saponification this also resulted in loss of the formyl group. This result suggested that treatment of this compound and any advanced material with formyl groups would be problematic. Since component **2.60** also contains an ethyl ester, a late stage saponification in the presence of two formyl amides would be necessary. Given these limitations, we decided to change the type of ester to make deprotection more compatible with other functional groups in the molecule.
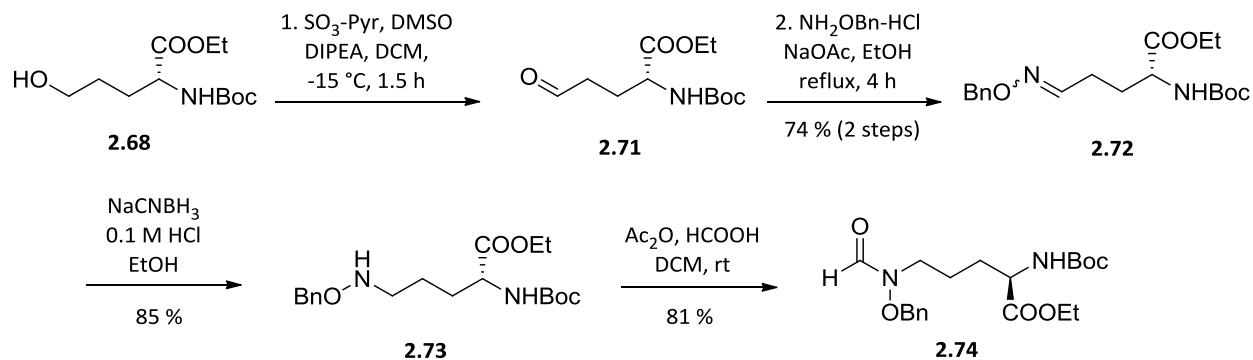
Scheme 2.7. Preliminary route to 2.61.

To synthesize **2.61**, the ethyl ester was swapped for an allyl ester since this could be removed by treatment with catalytic Pd(0) and a π-allyl cation scavenger which should not affect any other functional groups. The allyl ester **2.75** was formed by treatment of commercially available D-pyroglutamic acid with allyl alcohol and TsOH in toluene. **2.75** was Boc protected and carried through the route previously described for the ethyl ester. While this route was mostly compatible with the allyl ester, the yields for the reductive ring opening were lower using this substrate. The sequential Parihk-Doering oxidation-oxime formation was also problematic generally providing the oximes **2.78** in yields ~40 % over the two steps. This low yield was likely the result of the instability of the aldehyde. To overcome this, a one-pot oxidation-oxime formation was employed which significantly increased the yields of the sequence reliably to 80 – 90 %. The oximes **2.78** were reduced with sodium cyanoborohydride and the allyl ester removed with catalytic Pd(PPh$_3$)$_4$ and morpholine in THF to provide **2.61**.
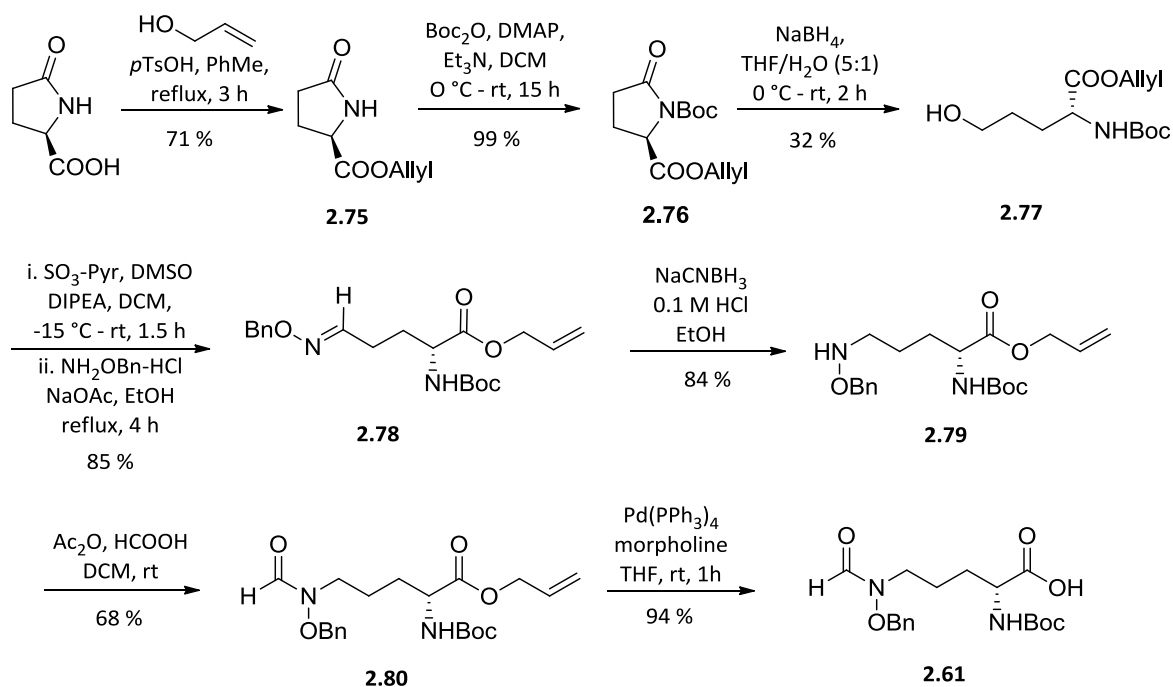
Scheme 2.8. Revised route to **2.61**.

Replacing the ethyl ester of **2.60** with a benzyl ester seemed prudent given that this could be removed under the same conditions as the benzyl ethers in the anticipated final global deprotection step. This component was prepared similarly to **2.78**. Starting from L-pyroglutamic acid, benzyl ester formation by treatment with benzyl alcohol and thionyl chloride followed by Boc protection provides **2.81**. This is reduced to alcohol **2.83** and the oximes prepared in the one pot reaction previously described. Reduction with sodium cyanoborohydride provides **2.85**.
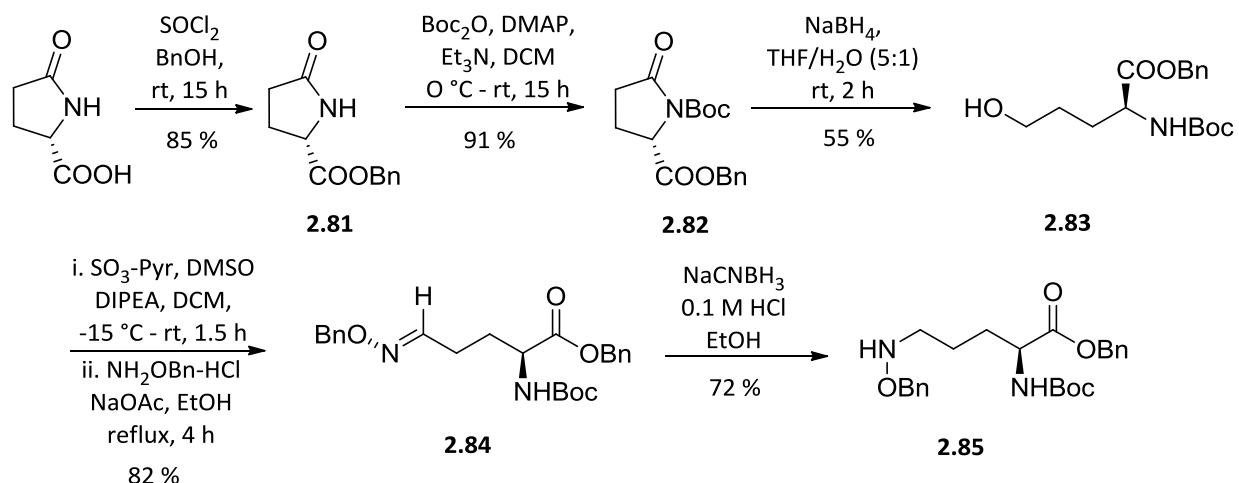
Scheme 2.9. Synthesis of advanced intermediate **2.85**.

Coupling strategy

With the three advanced coupling components **2.59**, **2.85** (in place of **2.60**), and **2.61** in hand, we envisioned a coupling strategy where **2.59** and **2.85** would be coupled and the resulting dipeptide Boc-deprotected to provide dipeptide **2.86**. This could be treated with 2 eq of **2.61** to acylate both primary amines of **2.86** simultaneously to give protected tetrapeptide **2.87**.
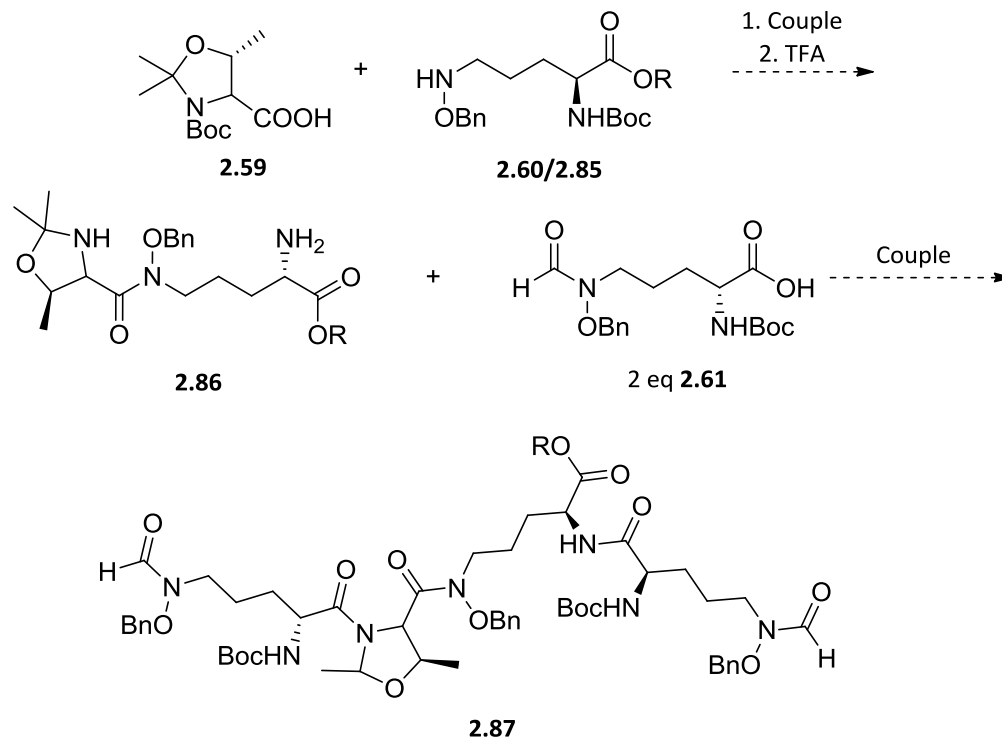
Scheme 2.10. Coupling strategy.
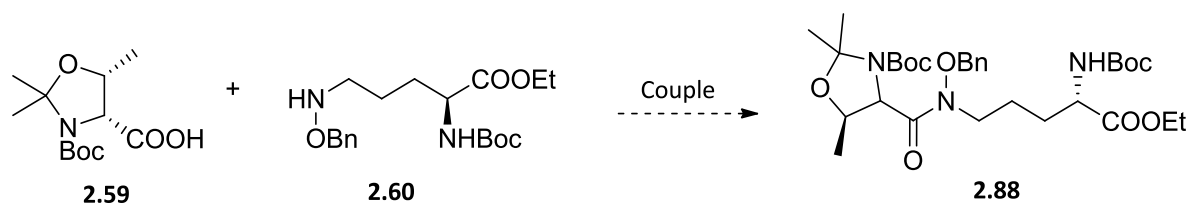
Coupling Conditions	Result
EDC, HOBt, DCM	HOBt ester formation/No coupling
EDC, HOBt, DMAP, DCM	HOBt ester formation/No coupling
PyBOP, DIEA, DCM	HOBt ester formation/No coupling
PyClU, Et3N, THF	No coupling
HATU, DIEA, DMF	HOAt ester formation/No coupling

Figure 2.8. Attempted synthesis of *2.88*.

We initially explored the first coupling with **2.60** which had been prepared through the established route. Attempts to couple **2.59** with **2.60** were wholly unsuccessful. Several coupling reagents were investigated for this transformation including EDC (with HOBt as an additive), PyBOP, HATU, and PyClU. In the first three cases, no coupling reaction occurred but **2.59** was converted to its respective activated ester. We hypothesized that the five membered acetonide was locked in a very rigid conformation and attack of a nucleophile on the carbonyl would be sterically hindered because of interactions with the bulky *t*-butyl carbamate and cis-methyl. Since HOBt and HOAt are relatively small and flat, attack on the carbonyl is possible and thus, the activated esters can be formed. In contrast, **2.60** is a rather bulky nucleophile and the *O*-benzyl and aliphatic side chains would certainly clash with the substituents of the ring during any attack on the carbonyl.

The primary motivation for acetonide protection of the threonine component was to prevent *O*-acylation during this and the subsequent coupling reaction. We hypothesized that foregoing the acetonide protection of threonine and instead using Boc protected D-*allo*-threonine (**2.66**) would allow for a conformation where attack on the carbonyl by **2.85** was possible. We further hypothesized that *O*-acylation would not be a significant concern since acyl migration to the adjacent nitrogen was favored. Reaction of **2.66** and **2.85** with HATU and DIEA in DMF led to formation of dipeptide **2.89** in 56 % yield after purification. Removal of the Boc groups of **2.89** was accomplished by treatment with 20 % TFA in DCM. This reaction is not entirely clean and product **2.90** (as the trifluoroacetate salt) was purified by HPLC leading to a lower yield for this transformation.
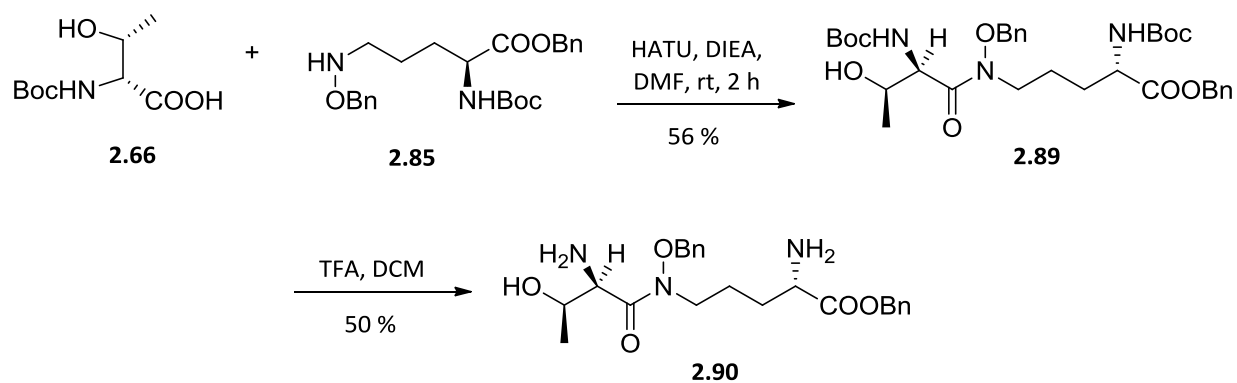
Scheme 2.11. Synthesis of dipeptide **2.90**.

2.5 Conclusion

With dipeptide **2.90** in hand, we can now investigate the double acylation reaction to the fully protected tetrapeptide. Once assembled, the Boc groups will be removed by treatment with acid and the benzyl ethers and ester removed by treatment with hydrogen gas and palladium on carbon to provide the final product.

We will characterize the final product as the unbound and Ga^{3+} bound compounds by NMR and mass spectrometry and compare to the originally reported spectra. Assuming the spectra match, we will move the material on to biological testing. If the spectra do not match, we will evaluate where the discrepancies may be and rework the synthesis to address this.

Once synthetic coelichelin is available, we will test its activity against *Staphylococcus aureus*. First we will generate a dose response curve to determine an IC50 value for coelichelin. We anticipate this will be similar to other iron chelators. We will also supplement growth media with iron to see if this reverses any growth inhibition by coelichelin. Finally, we will treat a strain of *S. aureus* bearing a Fur reporter construct for activity.

Experimental section

Note: The following experimental procedures were jointly written by Hunter Imlay and me.

General Procedure: All non-aqueous reactions were performed in flame-dried flasks under an atmosphere of argon. Stainless steel syringes were used to transfer air- and moisture-sensitive liquids. Reaction temperatures were controlled using a thermocouple thermometer and analog hotplate stirrer. Reactions were conducted at room temperature (rt, approximately 23 °C) unless otherwise noted. Flash column chromatography was conducted using silica gel 230-400 mesh. Analytical thin-layer chromatography (TLC) was performed on E. Merck silica gel 60 F254 plates and visualized using UV and iodine stain.

Materials: All solvents and chemicals were purchased from Sigma-Aldrich except D-pyroglutamic acid and O-benzylhydroxylamine hydrochloride (Combi-Blocks) and di-tert-butyldicarbonate, sodium borohydride, sodium triacetoxyborohydride, sodium cyanoborohydride, and HATU (Oakwood Chemicals). Dry dichloromethane was collected from an MBraun MB-SPS solvent system. Triethylamine, N,N-dimethylformamide (DMF) and dimethyl sulfoxide were used as received in a bottle with a Sure/Seal. N,N-diisopropylethylamine was distilled from calcium hydride and stored over KOH. Deuterated solvents were purchased from Cambridge Isotope Laboratories.

Instrumentation: ^{1}H NMR spectra were recorded on Bruker 400, 500, or 600 MHz spectrometers and are reported relative to deuterated solvent signals. Data for ^{1}H NMR spectra are reported as follows: chemical shift (δ ppm), multiplicity (s = singlet, d = doublet, t = triplet, q = quartet, p = pentet, m = multiplet, br = broad, app = apparent), coupling constants (Hz), and integration. ^{13}C NMR spectra were recorded on Bruker 100, 125, or 150 MHz spectrometers and

are reported relative to deuterated solvent signals. Low resolution mass spectrometry (LRMS) was conducted and recorded on an Agilent Technologies 6130 Quadrupole instrument.

Compound data:
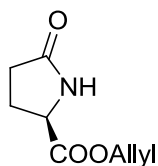
Allyl (*R*)-5-oxopyrrolidine-2-carboxylate (**2.75**): To a stirred susupension of D-pyroglutamic acid (6.00 g, 46.5 mmol) in toluene (185 mL) was added allyl alcohol (12.6 mL, 185 mmol) and *p*-toluenesulfonic acid hydrate (441 mg, 2.31 mmol). The reaction was refluxed 3 h at which point the reaction was judged complete by TLC. The reaction was allowed to cool to room temperature and aqueous sodium bicarbonate was added to quench the acid. The reaction was concentrated *in vacuo*, extracted dichloromethane (3x), washed with brine (2x), dried (MgSO$_4$), filtered, and concentrated to yield 5.56 g (71 %) of **2.75** as a white solid. Compound characterization data was consistent with previous reports.[33]
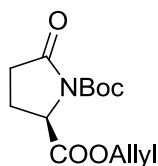
2-allyl 1-(*tert*-butyl) (*R*)-5-oxopyrrolidine-1,2-dicarboxylate (**2.76**): To a stirred solution of **2.75** (5.56 g, 32.9 mmol) in dichloromethane (140 mL) was added 4-dimethylaminopyridine (401 mg, 3.29 mmol), and triethylamine (5.05 mL, 36.2 mmol). The solution was cooled to 0 °C and di-*t*-butyl dicarbonate (7.83 g, 36.2 mmol) at 0 °C was added. The reaction was allowed to warm to room temperature and stirred overnight at which point the reaction was judged complete by TLC. The reaction was washed with saturated aqueous ammonium chloride and brine, dried (MgSO$_4$), and concentrated *in vacuo* to afford 8.83 (99 %) of **2.76** as a yellow solid: [α]$^{23}_D$ 35.25; IR (neat) 3550.8, 2981.0, 1790.1, 1751.9, 1458.8, 1367.7, 1313.1, 1158.7, 1028.7, 985.2, 844.2, 779.3, 600.0, 421.3 cm^{-1}; ^{1}H NMR (400 MHz) δ 5.94-5.81 (m, 1H), 5.38-5.12 (m, 2H), 4.69-4.56 (m, 3H), 2.66-2.53 (m, 1H), 2.52-2.41 (m, 1H), 2.38-2.23 (m, 1H), 2.07-1.96 (m, 1H), 1.45 (s, 9H); ^{13}C NMR (100 MHz) δ 173.1, 170.2,

159.1, 130.9, 119.5, 83.7, 78.2, 78.0, 77.8, 66.0, 59.2, 30.7, 28.5, 21.1; HRMS (ESI-TOF MS) calculated for $C_{13}H_{19}NO_5$ (M+Na)$^+$ *m/z*: 292.1155, measured 292.1171.
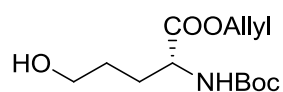
Allyl (*R*)-2-((*tert*-butoxycarbonyl)amino)-5-hydroxypentanoate (2.77): To a stirred solution of **2.76** (8.06 g, 29.9 mmol) in THF (39 mL) and water (7.7 mL) at 0 °C was added sodium borohydride (1.59 mg, 41.9 mmol). The reaction was stirred for 1 h at 0 °C and then allowed to warm to room temperature and stirred for 45 min, at which point the reaction was judged complete by TLC. The reaction was diluted with diethyl ether (20 mL) and washed with water. The aqueous layer was extracted with diethyl ether (2), and the organic layers were combined and washed with water (1x) and brine (2x), dried (MgSO$_4$), and concentrated. The resulting residue was purified by flash chromatography with a 40 – 60 % ethyl acetate in hexanes gradient to afford 2.60 g (32 %) of **2.77** as a colorless oil: [α]$^{23}_D$ -3.59; IR (neat) 3370.00, 2969.5, 2358.0, 1706.2, 1519.0, 1451.8, 1369.4, 1252.7, 1168.9, 1054.2, 932.8, 863.4, 781.0 cm^{-1}; ^{1}H NMR (400 MHz, CDCl$_3$) δ 5.95-5.813 (m, 1H), 5.35-5.18 (m, 3H), 4.66-4.55 (m, 2H), 4.39-4.25 (br, 1H), 3.637 (tr, J = 6.142 Hz, 2H), 2.18 (s, 1H), 1.96-1.82 (m, 1H), 1.791-1.667 (m, 1H), 1.66-1.54 (m, 2H), 1.41 (s, 9H); ^{13}C NMR (100 MHz) δ 172.60, 155.65, 131.71, 118.91, 77.48, 77.16, 76.84, 65.96, 62.06, 53.32, 29.52, 28.40; HRMS (ESI-TOF MS) calculated for $C_{13}H_{23}NO_5$ (M+H)$^+$ *m/z*: 274.1649, measured 274.1666.
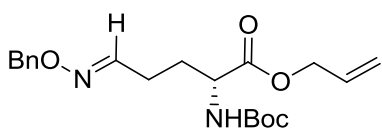
Allyl (*R*)-5-((benzyloxy)imino)-2-((*tert*-butoxycarbonyl)amino)pentanoate (2.78): To a stirred solution of **2.77** (500 mg, 1.82 mmol) in dichloromethane (8.0 mL) under an Ar atmosphere was added diisopropylethylamine (958 μL, 5.46 mmol) and dimethylsulfoxide (4.0 mL), and the resulting solution was cooled to -15 °C using a dry ice and acetone bath. Sulfur trioxide-pyridine

complex (871 mg, 5.46 mmol) was dissolved in dimethylsulfoxide (4.0 mL) and the resulting solution was added dropwise to the solution of **2.77**. The reaction was stirred in the acetone bath until the temperature rose to -5 °C at which point the cooling bath was removed and the reaction allowed to warm to room temperature (20 min). TLC indicated complete consumption of starting materials. To the reaction was added ethanol (4.0 mL) and the reaction was stirred for 5 min followed by addition of diisopropylethylamine (476 µL, 2.73 mmol) and *O*-benzylhydroxylamine hydrochloride (436 mg, 2.73 mmol). The reaction was stirred for room temperature for 1.5 h at which point it was judged complete by TLC. The reaction was diluted with diethyl ether and water, washed with 1 N HCl, saturated $NaHCO_3$ (aq), and brine, dried ($MgSO_4$), filtered, and concentrated *in vacuo* to afford 584 mg (85 %) of **2.78** as a colorless oil. ^{1}H-NMR shows a mixture of geometric isomers. The mixture was not separated and carried through to the next step without further characterization.
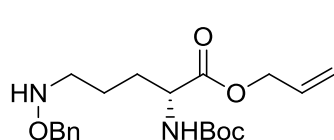
Allyl (R)-5-((benzyloxy)amino)-2-((*tert*-butoxycarbonyl)amino)pentanoate (2.79): To a stirred solution of oximes **2.78** (1.28 mg, 3.40 mmol) in methanol (128 mL) and concentrated hydrochloric acid (1.10 mL) at room temperature was added sodium cyanoborohydride (321 mg, 5.10 mmol). The reaction was maintained at room temperature for 1.5 h when the reaction was judged complete by TLC. Solvent was concentrated *in vacuo* to half volume and diluted with EtOAc (50 mL) and H_2O (40 mL). The organic layer was washed with brine (2 x 400 mL), dried ($MgSO_4$), and concentrated *in vacuo* to afford 1.08 g (84%, crude) of **2.79** as a colorless oil: $[\alpha]^{23}_D$ -4.00; IR (neat) 3355.9, 2932.9, 1713.0, 1508.5, 1452.8, 1366.5, 1250.4, 1167.4, 993.17, 863.0, 744.1, 698.3 cm^{-1}; ^{1}H NMR (400 MHz) δ 7.38-7.27 (m, 5H), 5.97-5.83 (m, 1H), 5.37-5.09 (m, 3H), 4.72-

4.58 (m, 4H), 4.36-4.27 (br, 1H), 2.93 (t, J = 6.76, 2H), 1.94-1.79 (br, 1H), 1.76-1.64 (m, 1H), 1.63-1.52 (m, 2H), 1.44 (s, 9H); ^{13}C NMR (100 MHz) δ 172.34, 155.31, 137.78, 131.57, 128.36, 128.31, 127.77, 118.68, 79.75, 77.28, 76.96, 76.64, 76.21, 65.74, 53.27, 51.36, 30.29, 28.25, 23.20; HRMS (ESI-TOF MS) calculated for $C_{20}H_{30}N_2O_5$ (M+H)$^+$ *m/z*: 379.2227, measured 379.2228.
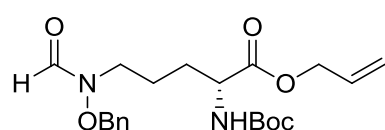
Allyl **(*R*)-5-(*N*-(benzyloxy)formamido)-2-((*tert*-butoxycarbonyl)amino)pentanoate** (**2.80**): To a stirred solution of **2.79** (285 mg, 0.75 mmol) in dichloromethane (4 mL) was added formic acetic anhydride (0.5 mL) previously prepared by heating acetic anhydride (0.8 mL) and formic acid (0.4 mL) at 65 °C for 45 min under Ar atmosphere. The reaction was stirred for 1 h until judged complete by TLC. The reaction was diluted with DCM and washed with saturated NaHCO$_3$ (aq) and then brine, dried (MgSO$_4$), filtered, and concentrated *in vacuo*. The residue was purified by flash chromatography (2:1 hexane:ethyl acetate) to provide 208 mg (68 %) of **2.80** as a colorless oil: [α]$^{23}_D$ -8.13; IR (neat) 3341.7, 2972.1, 1683.0, 1513.8, 1452.6, 1364.5, 1251.4, 1167.5, 1055.4, 987.9, 749.5, 700.1 cm^{-1}; ^{1}H NMR (500 MHz) δ 8.16 (s, 1H), 7.47-7.33 (m, 5H), 6.91 (s, 1H), 5.95-5.84 (m, 1H), 5.34-5.16 (m, 2H), 4.91 (s, 2H), 4.63-4.51 (m, 2H), 4.02 (s, 1H), 3.52 (d, J = 5.75, 2H), 3.05 (s, 1H), 2.50 (s, 1H), 1.80-1.55 (m, 4H), 1.39 (s, 9H); ^{13}C NMR (125 MHz) δ 172.11, 135.39, 132.69 129.44, 128.78, 128.59, 117.86, 78.60, 76.65, 64.90, 53.81, 40.69, 40.52, 40.35, 40.19, 40.02, 39.85, 39.69, 28.43, 28.39, 23.70.
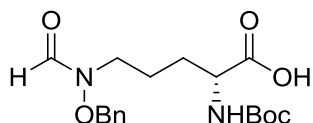
(*R*)-5-(*N*-(benzyloxy)formamido)-2-((*tert*-butoxycarbonyl)amino)pentanoic acid (**2.61**): To a stirred solution of **2.80** (110 mg, 0.271 mmol) in tetrahydrofuran (1 mL) was added morpholine (234 μL, 2.71 mmol) and palladium tetrakistriphenylphosphine (31 mg, 0.0271 mmol) under an Ar

atmosphere. The reaction was stirred overnight at which point it was judged complete by TLC. The reaction was diluted with ethyl acetate (5 mL) and washed was 1 N hydrochloric acid (1 x 3 mL). The acid layer was extracted with ethyl acetate (2 x 2 mL), and the organic layers were combined, washed with brine (1 x 5 mL), dried (MgSO₄), and concentrated *in vacuo* to afford 93 mg (94 %) of **2.61**, as a pale yellow solid: characterization: $[\alpha]^{23}_D$ -10.93; IR (neat) 2974.0, 2357.4, 1705.0, 1512.6, 1365.5, 1166.3, 751.6 cm^{-1}; HRMS (ESI-TOF MS) calculated for $C_{18}H_{26}N_2O_6$ (M+H)$^+$ *m/z*: 367.1864, measured 367.1854.
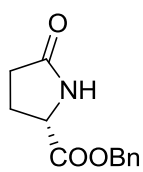
Benzyl (*S*)-5-oxopyrrolidine-2-carboxylate (**2.81**) To a stirred solution of 2.00 g (15.5 mmol, 1.0 eq) of L-pyroglutamic acid dissolved in 15.0 mL (136 mmol, 8.8 eq) benzyl alcohol cooled in an ice bath was added 2.25 mL (31.0 mmol, 2.0 eq) of thionyl chloride dropwise. The mixture was allowed to warm to room temperature and stirred overnight. The reaction was quenched by addition of saturated NaHCO₃ (aq) and extracted 3x with EtOAc, washed with brine, dried (MgSO₄), and concentrated. The residual benzyl alcohol was removed by distillation under reduced pressure to give 2.90 g (85 %) of **1**. Compound characterization data was consistent with previous reports [34]
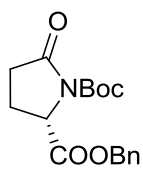
2-benzyl 1-(*tert*-butyl) (*S*)-5-oxopyrrolidine-1,2-dicarboxylate (**2.82**) To a stirred solution of dichloromethane (180 mL) and **2.81** (7.41 g, 33.80 mmol) was added 4-dimethylaminopyridine (413 mg, 3.38 mmol), triethylamine (4.71 mL, 33.80 mmol), and di-*t*-butyl dicarbonate (8.85 g, 40.56 mmol) at 0 °C under inert atmosphere. The reaction was warmed to room temperature after 1 h and stirred overnight, at which point the reaction was judged complete by TLC. The reaction was diluted with DCM (100 mL), washed with saturated ammonium chloride solution (2 x 70 mL) and brine (1 x 70 mL), dried (MgSO₄), and

concentrated *in vacuo* to afford 9.84 g (91%, crude) of **2.82** as a yellow solid. Compound

characterization data was consistent with previous reports.[35]

Benzyl (S)-2-((tert-butoxycarbonyl)amino)-5-hydroxypentanoate (2.83)
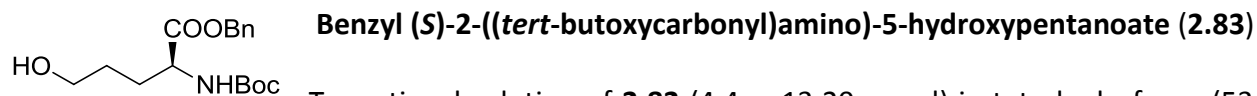
To a stirred solution of **2.82** (4.4 g, 13.20 mmol) in tetrahydrofuran (53

mL), and water (10.5 mL) was added sodium borohydride (1.05 g, 27.72 mmol) at 0 °C. The

reaction was stirred for 1 h then warmed to room temperature and stirred for 45 min, at which

point the reaction was judged complete by TLC. The reaction was diluted with diethyl ether (50

mL) and washed with water (1 x 60 mL). The aqueous layer was extracted with diethyl ether (2 x

25 mL), and the organic layers were combined and washed with water (1 x 25 mL) and brine (2

x 20 mL), dried (MgSO₄), and concentrated in vacuo. The resulting residue was purified by flash

chromatography (60/40, 50/50, 40/60 hexane/EtOAc) to afford 2.35 g (55%) of **2.83** as a

colorless oil. Compound characterization data was consistent with previous reports [36]

Benzyl (S)-5-((benzyloxy)imino)-2-((tert-butoxycarbonyl)amino)pentanoate (2.84) To a stirred solution of

2.83 (1.05 g, 3.25 mmol) in dichloromethane (10 mL) was added *N,N*-diisopropylethylamine

(1.29 mL, 7.39 mmol) and dimethylsulfoxide (5.0 mL) and the resulting solution was cooled to -

15 °C using a dry ice/acetone bath. Sulfur trioxide-pyridine complex (1.18 g, 7.39 mmol) was

dissolved in dimethylsulfoxide (5.0 mL), and the resulting solution was added dropwise to the

solution of **2.83**. The reaction was stirred in the cooling bath until the temperature rose to -5 °C

at which point the cooling bath was removed and the reaction allowed to warm to room

temperature (~30 min). TLC indicated complete consumption of starting materials. To the

reaction was added ethanol (4.0 mL) and the reaction was stirred for 5 min followed by addition

of *N,N*-diisopropylethylamine (642 µL, 3.68 mmol) and *O*-benzylhydroxylamine hydrochloride (588 mg, 3.68 mmol). The reaction was stirred at room temperature for 1.5 h at which point it was judged complete by TLC. The reaction was diluted with diethyl ether and water, washed with 1 N HCl, saturated NaHCO$_3$ (aq), and brine, dried (MgSO$_4$), filtered, and concentrated *in vacuo* to afford 1.14 g (82 %) of **2.78** as a colorless oil. ^{1}H-NMR shows a mixture of geometric isomers. The mixture was not separated and carried through to the next step without further characterization.
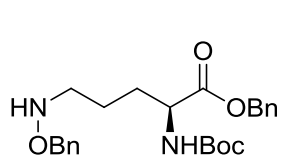
(S)-benzyl 5-((benzyloxy)amino)-2-((tert-butoxycarbonyl)amino)pentanoate (**2.85**): To a stirred solution of oximes **2.84** (1.14 g, 2.67 mmol) in ethanol (25 mL) and concentrated hydrochloric acid (408 µL) at room temperature was added sodium cyanoborohydride (336 mg, 5.34 mmol). The reaction was maintained at room temperature for 1.5 h when the reaction was judged complete by TLC. The reaction was diluted with EtOAc (90 mL) and H$_2$O (50 mL). The organic layer was washed with brine (2 x 30 mL), dried (MgSO$_4$), and concentrated *in vacuo*. The residue was purified by flash chromatography to afford 819 mg (72 %) of **2.85** as a colorless oil: $[\alpha]^{23}_D$ -12.32; IR (neat) 3354.80, 3030.86, 2968.28, 1713.64, 1507.03, 1454.15, 1364.20, 1250.85, 1168.09, 1009.56, 915.19, 863.23, 744.08, 699.25, 605.26 cm^{-1}; ^{1}H NMR (400 MHz, CDCl$_3$) δ 7.37-7.27 (m, 10H), 5.28 (s, 2H), 5.23-5.10 (app q, 3H), 4.67 (s, 2H), 4.39-4.31 (br, 1H), 2.90 (t, J = 6.82 Hz, 2H), 1.92-1.79 (m, 1H), 1.75-1.63 (m, 1H), 1.61-1.49 (m, 2H), 1.44 (s, 9H); ^{13}C NMR (150 MHz, CDCl$_3$) δ 172.6, 155.4, 137.9, 135.4, 128.6, 128.4, 128.4, 128.2, 127.8, 79.8, 77.3, 77.1, 76.9, 76.2, 66.9, 53.4, 51.4, 30.2, 28.3, 23.2; HRMS (ESI-TOF MS) calculated for C$_{24}$H$_{32}$N$_2$O$_5$ (M+H)$^+$ *m/z*: 429.2384, measured 429.2360.
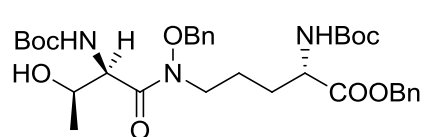
Benzyl (S)-5-((2R,3R)-N-(benzyloxy)-2-((*tert*-butoxycarbonyl)amino)-3-hydroxybutanamido)-2-((*tert*-butoxycarbonyl)amino)pentanoate (2.89) To a stirred solution of **2.85** (123 mg, 0.287 mmol) and **2.66** (60 mg, 0.274 mmol) in dimethylformamide (1 mL) was added diisopropylethylamine (48 µL, 0.274 mmol) and HATU (156 mg, 0.411 mmol) at 30 °C under inert atmosphere. The reaction was maintained at 30 °C for 1.75 h, when TLC indicated the reaction was complete. The reaction was diluted with EtOAc (5 mL) washed with 1 N HCl (1 x 5 mL) and brine (1 x 5 mL), dried (MgSO$_4$), and concentrated *in vacuo*. The residue was purified using flash chromatography with a hexane/ethyl acetate solvent gradient (70/30, 60/40, 50/50) to afford 96 mg (56%) of **2.89** as a white solid: [α]$^{23}_D$ -9.23; IR (neat) 3348.21, 2974.05, 1707.87, 1648.93, 1505.79, 1452.80, 1368.42, 1248.35, 1166.99, 1015.70, 741.54, 698.87 cm^{-1}; ^{1}H NMR (400 MHz) δ 7.47-7.17 (m, 10H), 5.53 (d, J = 6.04 Hz, 1H), 5.17-5.04 (m, 3H), 4.97 (d, J = 9.66 Hz, 1H), 4.91-4.79 (m, 2H), 4.41-4.30 (br, 1H), 4.02-3.88 (br, 2H), 3.40-3.28 (br, 1H), 3.09-2.94 (br, 1H), 1.88-1.77 (br, 1H), 1.75-1.58 (m, 4H), 1.43 (d, J = 19.80 Hz, 18H), 1.10 (d, J = 5.76 Hz, 3H); ^{13}C NMR (150 MHz) δ 172.6, 171.8, 155.6, 135.5, 134.1, 129.8, 129.4, 129.0, 128.9, 128.7, 128.6, 80.3, 80.2, 77.5, 77.3, 77.2, 77.1, 69.5, 67.4, 55.0, 53.2, 44.8, 30.1, 28.6, 28.5, 22.9, 19.6.
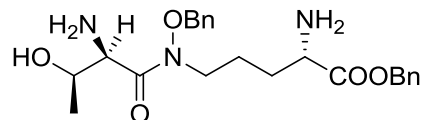
Benzyl (S)-2-amino-5-((2R,3R)-2-amino-N-(benzyloxy)-3-hydroxybutanamido)pentanoate (2.90): To a stirred solution of **2.89** (25 mg, 0.0397 mmol) in dichloromethane (2 mL) at room temperature was added trifluoroacetic acid (100 µL). The reaction was stirred for 2 h at which point it was judged complete by TLC. The reaction was concentrated *in vacuo* and purified by reverse phase HPLC to provide **2.90** as the TFA salt: ^{1}H-NMR (600 MHz, MeOD) δ 7.47 - 7.41 (m, 5H), 7.38 – 7.31 (m,

5H), 5.26 (d, J=12.06 Hz, 1H), 5.22 (d, J=12.00 Hz, 1H), 5.02 (d, J=10.26 Hz, 1H), 4.91 (d, J=10.26

Hz, 1H), 4.38 – 4.33 (m, 2H), 4.12 (t, J=6.21 Hz, 1H), 4.07 – 4.00 (m, 1H), 3.59 – 3.52 (m, 1H),

2.00 – 1.79 (m, 3H), 1.03 (d, J=7.32 Hz, 3H); ^{13}C-NMR (150 MHz, MeOD) δ 170.2, 168.3, 136.3,

135.2, 130.7, 130.5, 130.0, 129.9, 129.8, 77.89, 69.2, 64.7, 58.2, 53.6, 45.4, 28.8, 23.4, 17.6;

HRMS (ESI-TOF MS) calculated for $C_{23}H_{31}N_3O_5$ (M+Na)$^+$ *m/z*: 452.2156, measured 452.2187.

References

(1)   Lautru, S.; Deeth, R. J.; Bailey, L. M.; Challis, G. L. Discovery of a New Peptide Natural Product by Streptomyces Coelicolor Genome Mining. *Nat. Chem. Biol.* **2005**, *1* (5), 265–269.

(2)   Paustian, M. L.; May, B. J.; Kapur, V. Pasteurella Multocida Gene Expression in Response to Iron Limitation. *Infect. Immun.* **2001**, *69* (6), 4109–4115.

(3)   Acosta, N.; Pukatzki, S.; Raivio, T. L. The Vibrio Cholerae Cpx Envelope Stress Response Senses and Mediates Adaptation to Low Iron. *J. Bacteriol.* **2015**, *197* (2), 262–276.

(4)   Stentzel, S.; Vu, H. C.; Weyrich, A. M.; Jehmlich, N.; Schmidt, F.; Salazar, M. G.; Steil, L.; Völker, U.; Bröker, B. M. Altered Immune Proteome of *Staphylococcus Aureus* under Iron-Restricted Growth Conditions. *Proteomics* **2014**, *14* (16), 1857–1867.

(5)   Koehn, F. E.; Carter, G. T. The Evolving Role of Natural Products in Drug Discovery. *Nat. Rev. Drug Discov.* **2005**, *4* (3), 206–220.

(6)   Newman, D. J.; Cragg, G. M.; Snader, K. M. The Influence of Natural Products upon Drug Discovery (Antiquity to Late 1999). *Nat. Prod. Rep.* **2000**, *17* (3), 215–234.

(7)   Challis, G. L. Genome Mining for Novel Natural Product Discovery. *J. Med. Chem.* **2008**, *51* (9), 2618–2628.

(8)   Demain, A. L. Pharmaceutically Active Secondary Metabolites of Microorganisms. *Appl. Microbiol. Biotechnol.* **1999**, *52* (4), 455–463.

(9)   Marahiel, M. A.; Stachelhaus, T.; Mootz, H. D. Modular Peptide Synthetases Involved in

Nonribosomal Peptide Synthesis. *Chem. Rev.* **1997**, *97* (7), 2651–2674.

(10) Stachelhaus, T.; Mootz, H. D.; Marahiel, M. A. The Specificity-Conferring Code of Adenylation Domains in Nonribosomal Peptide Synthetases. *Chem. Biol.* **1999**, *6* (8), 493–505.

(11) Podgornaia, A. I.; Casino, P.; Marina, A.; Laub, M. T. Structural Basis of a Rationally Rewired Protein-Protein Interface Critical to Bacterial Signaling. *Structure* **2013**, *21* (9), 1636–1647.

(12) Redenbach, M.; Kieser, H. M.; Denapaite, D.; Eichner, A.; Cullum, J.; Kinashi, H.; Hopwood, D. A. A Set of Ordered Cosmids and a Detailed Genetic and Physical Map for the 8 Mb Streptomyces Coelicolor A3(2) Chromosome. *Mol. Microbiol.* **1996**, *21* (1), 77–96.

(13) Challis, G. Coelichelin, a New Peptide Siderophore Encoded by the Streptomyces Coelicolor Genome: Structure Prediction from the Sequence of Its Non-Ribosomal Peptide Synthetase. *FEMS Microbiol. Lett.* **2000**, *187* (2), 111–114.

(14) Sharman, G. J.; Williams, D. H.; Ewing, D. F.; Ratledge, C. Isolation, Purification and Structure of Exochelin MS, the Extracellular Siderophore from Mycobacterium Smegmatis. *Biochem. J.* **1995**, *305* (1), 187–196.

(15) Miller, M. J. Syntheses and Therapeutic Potential of Hydroxamic Acid Based Siderophores and Analogs. *Chem. Rev.* **1989**, *89* (7), 1563–1579.

(16) Rogers, S.; Neilands, J. B. The α-Amino-ʟ-Hydroxamino Acids *. *Biochemistry* **1963**, *2* (1),

6–9.

(17) Isowa, Y.; Takashima, T.; Ohmori, M.; Kurita, H.; Sato, M.; Mori, K. Synthesis of Nδ-Hydroxyornithine. *Bull. Chem. Soc. Jpn.* **1972**, *45* (5), 1461–1464.

(18) Isowa, Y.; Takashima, T.; Ohmori, M.; Kurita, H.; Sato, M.; Mori, K. Acylation of Nδ-Benzyloxyornithine. *Bull. Chem. Soc. Jpn.* **1972**, *45* (5), 1464–1466.

(19) Fujii, T.; Hatanaka, Y. A Synthesis of Rhodotorulic Acid. *Tetrahedron* **1973**, *29* (23), 3825–3831.

(20) Olsen, R. K.; Ramasamy, K.; Emery, T. Synthesis of N.alpha.,N.delta.-Protected N.delta.-Hydroxy-L-Ornithine from L-Glutamic Acid. *J. Org. Chem.* **1984**, *49* (19), 3527–3534.

(21) Maehr, H.; Leach, M. Antimetabolites Produced by Microorganisms. IX. Chemical Synthesis of N5-Hydroxyornithine and N5-Hydroxyarginine. *J. Org. Chem.* **1974**, *39* (8), 1166–1168.

(22) Milewska, M. J.; Chimiak, A. An Alternative Synthesis of N 5 -Acetyl- N 5 -Hydroxy-L-Ornithine from L-Ornithine. *Synthesis (Stuttg).* **1990**, *1990* (03), 233–234.

(23) Hyun Lee, B.; Miller, M. J. Constituents of Microbial Iron Chelators. The Synthesis of Optically Active Derivatives of δ-N-Hydroxy-L-Ornithine. *Tetrahedron Lett.* **1984**, *25* (9), 927–930.

(24) Lee, B. H.; Gerfen, G. J.; Miller, M. J. Constituents of Microbial Iron Chelators. Alternate Syntheses of .delta.-N-Hydroxy-L-Ornithine Derivatives and Applications to the Synthesis of Rhodotorulic Acid. *J. Org. Chem.* **1984**, *49* (13), 2418–2423.

(25) Keller-Schierlein, W.; Maurer, B. Stoffwechselprodukte von Mikroorganismen. 75. Mitteilung [1]. Synthese Des Ferrichroms; 2. Teil. *Helv. Chim. Acta* **1969**, *52* (3), 603–610.

(26) Isowa, Y.; Ohmori, M.; Kurita, H. Total Synthesis of Ferrichrome. *Bull. Chem. Soc. Jpn.* **1974**, *47* (1), 215–220.

(27) Dolence, E. K.; Miller, M. J. Synthesis of Foroxymithine, a Microbial Fermentation Product and Angiotensin 1 Converting Enzyme Inhibitor. *J. Org. Chem.* **1991**, *56* (2), 492–499.

(28) Mashiach, R.; Meijler, M. M. Total Synthesis of Pyoverdin D. *Org. Lett.* **2013**, *15* (7), 1702–1705.

(29) Duranti, A.; Tontini, A.; Antonietti, F.; Vacondio, F.; Fioni, A.; Silva, C.; Lodola, A.; Rivara, S.; Solorzano, C.; Piomelli, D.; et al. N-(2-Oxo-3-Oxetanyl)carbamic Acid Esters as N-Acylethanolamine Acid Amidase Inhibitors: Synthesis and Structure-Activity and Structure-Property Relationships. *J. Med. Chem.* **2012**, *55* (10), 4824–4836.

(30) Liang, X.; Lee, C.-J.; Chen, X.; Chung, H. S.; Zeng, D.; Raetz, C. R. H.; Li, Y.; Zhou, P.; Toone, E. J. Syntheses, Structures and Antibiotic Activities of LpxC Inhibitors Based on the Diacetylene Scaffold. *Bioorg. Med. Chem.* **2011**, *19* (2), 852–860.

(31) Dolence, E. K.; Lin, C. E.; Miller, M. J.; Payne, S. M. Synthesis and Siderophore Activity of Albomycin-like Peptides Derived from N5-Acetyl-N5-Hydroxy-L-Ornithine. *J. Med. Chem.* **1991**, *34* (3), 956–968.

(32) Reisman, S. E.; Ready, J. M.; Hasuoka, A.; Smith, C. J.; Wood, J. L. Total Synthesis of (±)-Welwitindolinone A Isonitrile. *J. Am. Chem. Soc.* **2006**, *128* (5), 1448–1449.

(33) Rigo, B.; Lespagnol, C.; Pauly, M. Studies on Pyrrolidinones. Synthesis of N-Acylpyroglutamic Esters with Bactericide and Fungicide Properties. *J. Heterocycl. Chem.* **1988**, *25* (1), 49–57.

(34) Johnson, A. L.; Price, W. A.; Wong, P. C.; Vavala, R. F.; Stump, J. M. Synthesis and Pharmacology of the Potent Angiotensin-Converting Enzyme Inhibitor N-[1(S)-(Ethoxycarbonyl)-3-Phenylpropyl]-(S)-Alanyl-(S)-Pyroglutamic Acid. *J. Med. Chem.* **1985**, *28* (11), 1596–1602.

(35) Aggarwal, V. K.; Astle, C. J.; Rogers-Evans, M. A Concise Asymmetric Route to the Bridged Bicyclic Tropane Alkaloid Ferruginine Using Enyne Ring-Closing Metathesis. *Org. Lett.* **2004**, *6* (9), 1469–1471.

(36) Jackson, R. F. W.; Moore, R. J.; Dexter, C. S.; Elliott, J.; Mowbray, C. E. Concise Synthesis of Enantiomerically Pure Phenylalanine, Homophenylalanine, and Bishomophenylalanine Derivatives Using Organozinc Chemistry: NMR Studies of Amino Acid-Derived Organozinc Reagents. *J. Org. Chem.* **1998**, *63* (22), 7875–7884.

APPENDIX Spectra relevant to Chapter 2
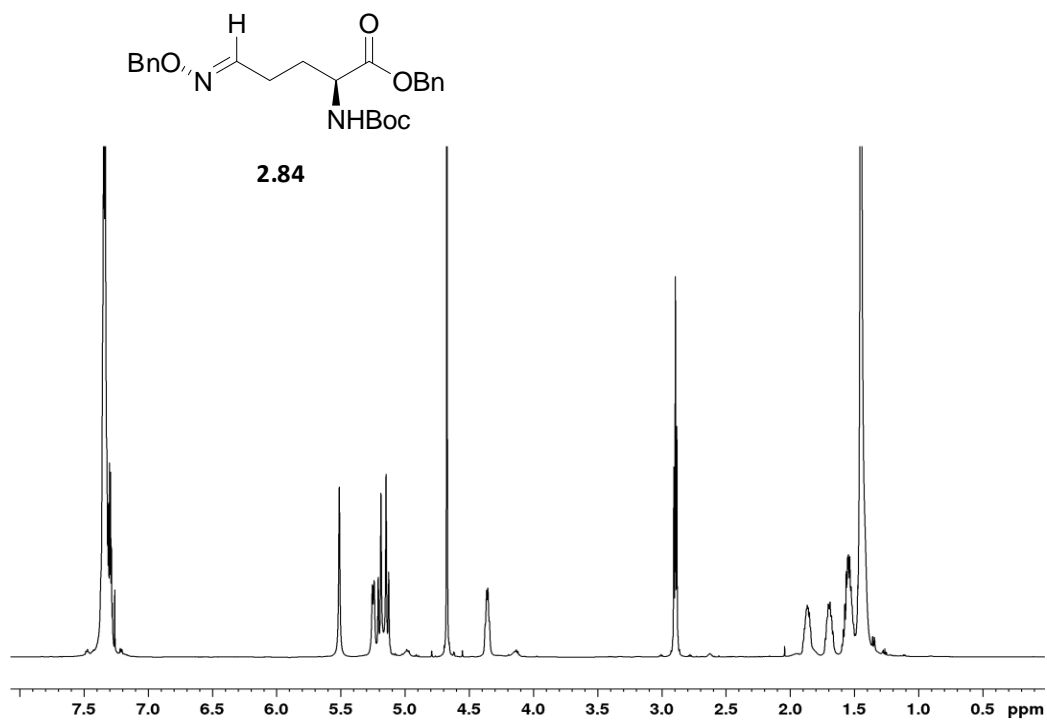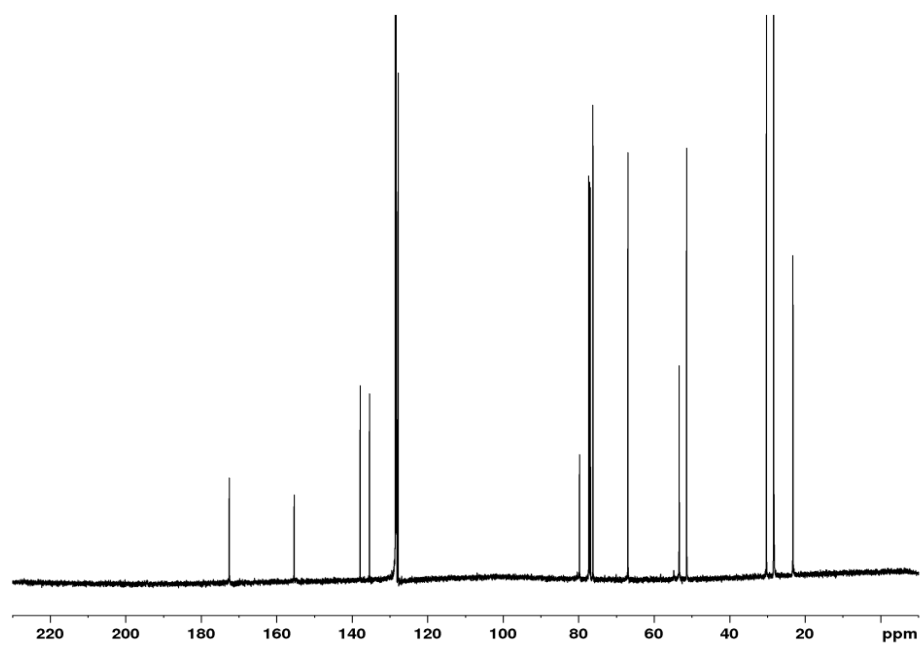
Figure A2.1. 1H-NMR spectrum (600 MHz, CDCl3) and 13C-NMR spectrum (150 MHz, CDCl3) of 2.84.
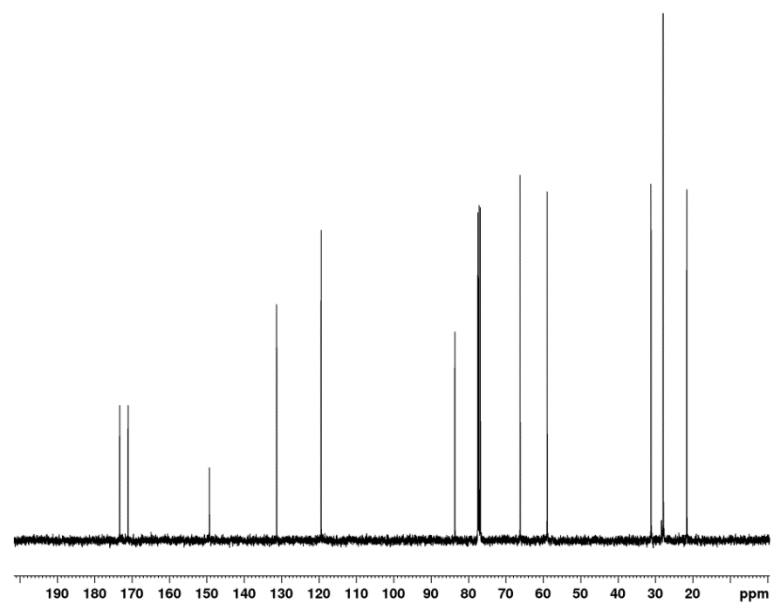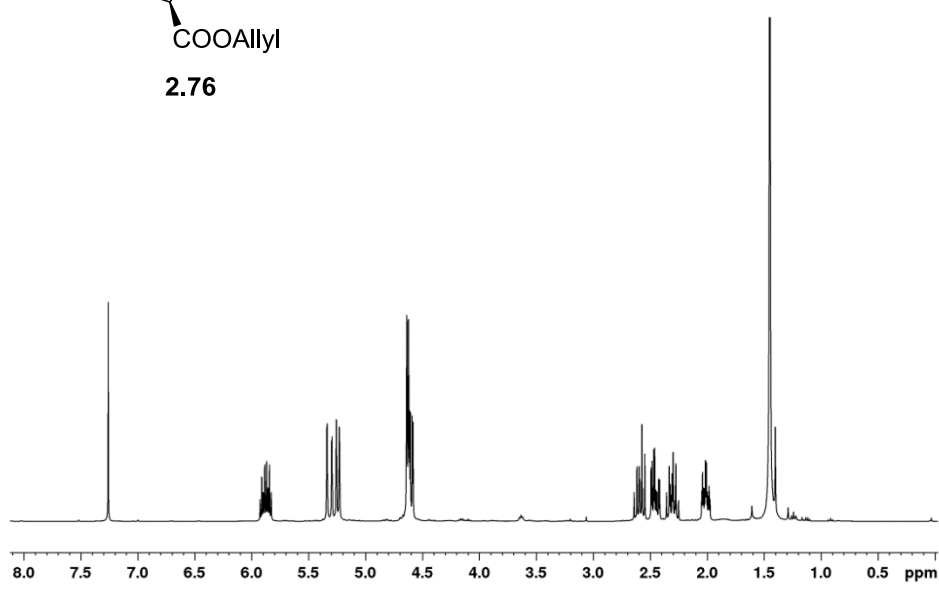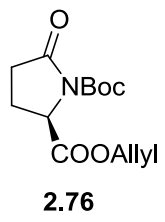
Figure A2.2. ^{1}H-NMR spectrum (400 MHz, CDCl$_3$) and ^{13}C-NMR spectrum (100 MHz, CDCl3) of **2.76**.
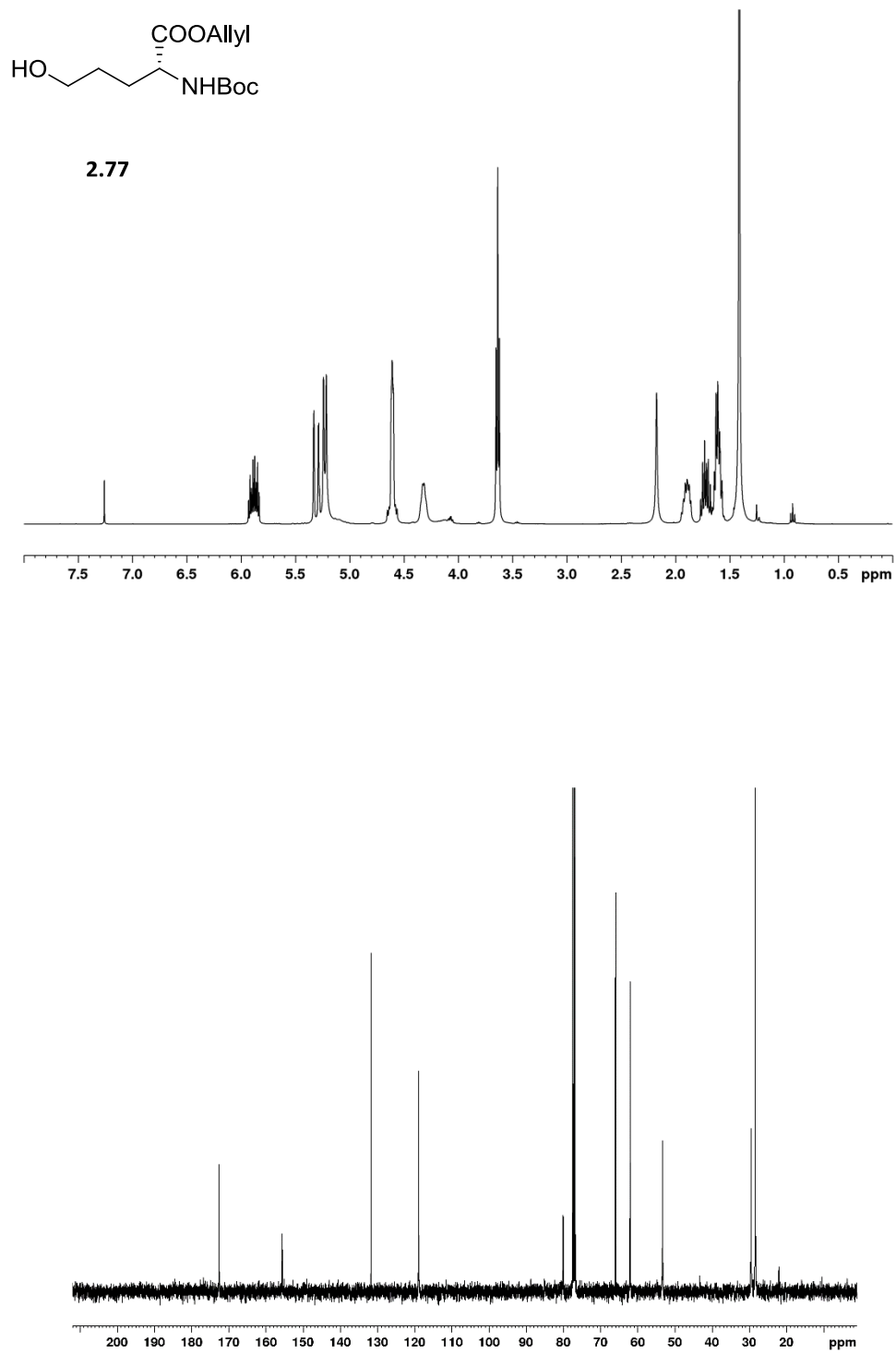
Figure A2.3. ^{1}H-NMR spectrum (400 MHz, CDCl$_3$) and ^{13}C-NMR spectrum (100 MHz, CDCl3) of **2.77**.
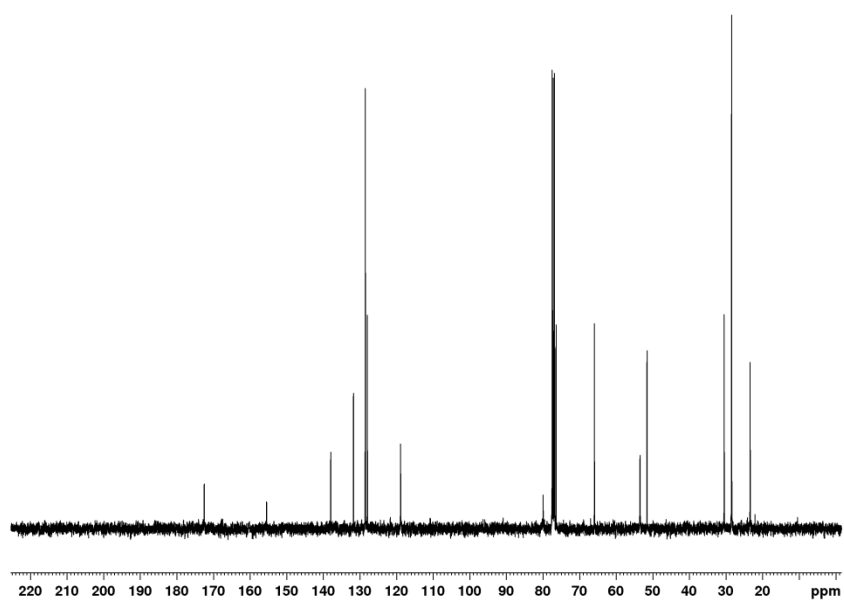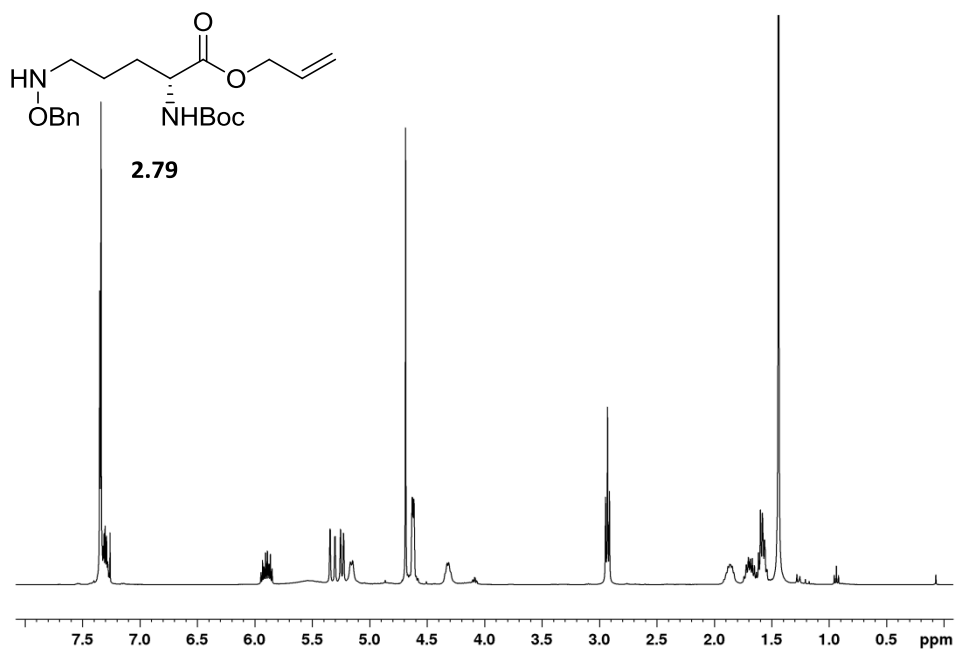
Figure A2.4. ^{1}H-NMR spectrum (400 MHz, CDCl$_3$) and ^{13}C-NMR spectrum (100 MHz, CDCl3) of **2.79.**
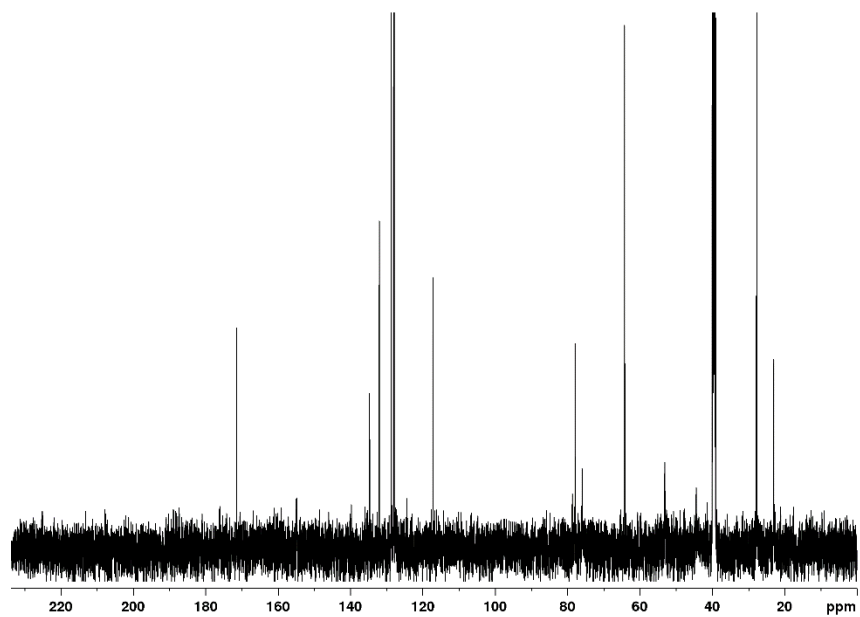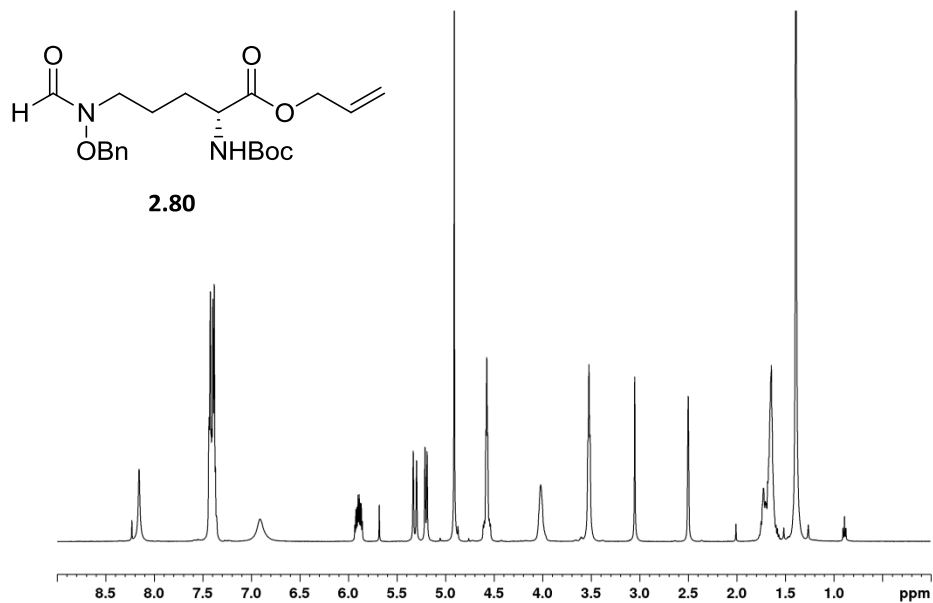
Figure A2.5. ^{1}H-NMR spectrum (500 MHz, DMSO-d6, 80 °C) and ^{13}C-NMR spectrum (125 MHz, DMSO-d6, 80 °C) of **2.79.**
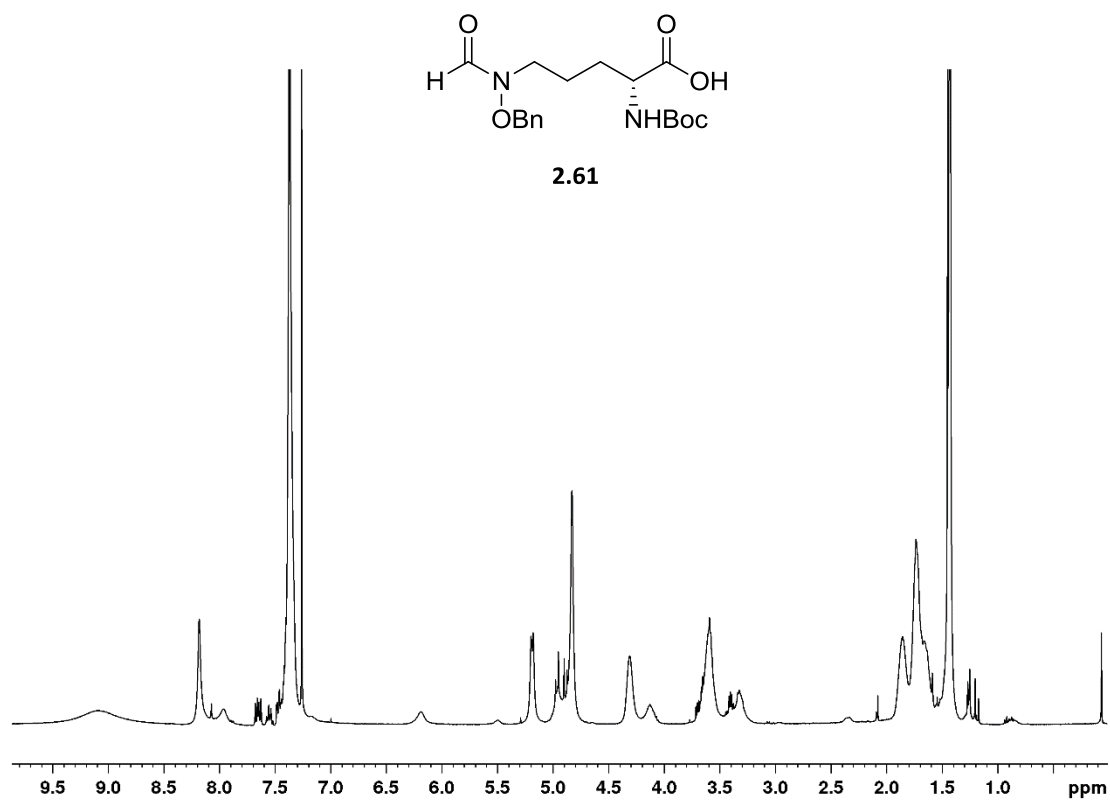
Figure A2.6 ^{1}H-NMR spectrum (400 MHz, CDCl$_3$) of **2.61**.
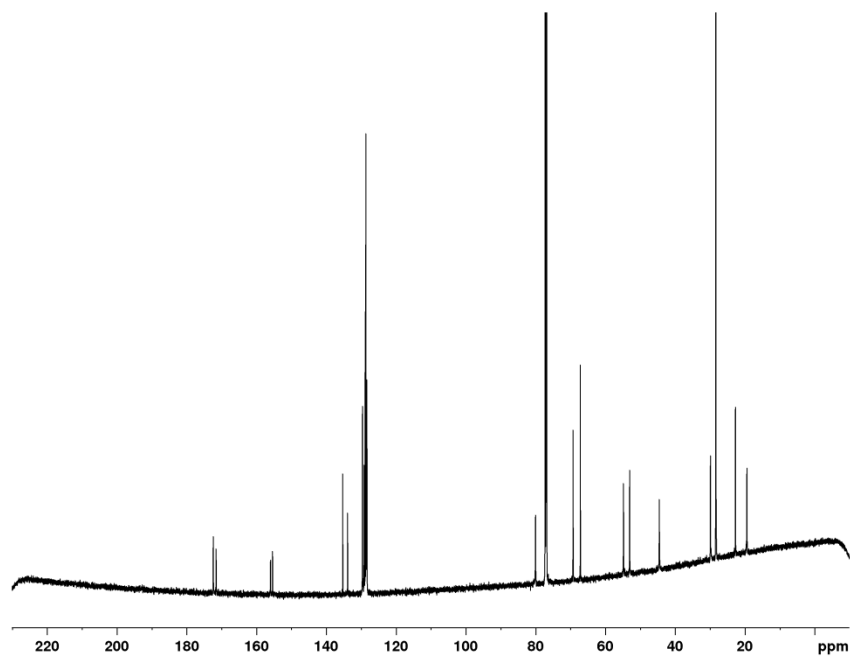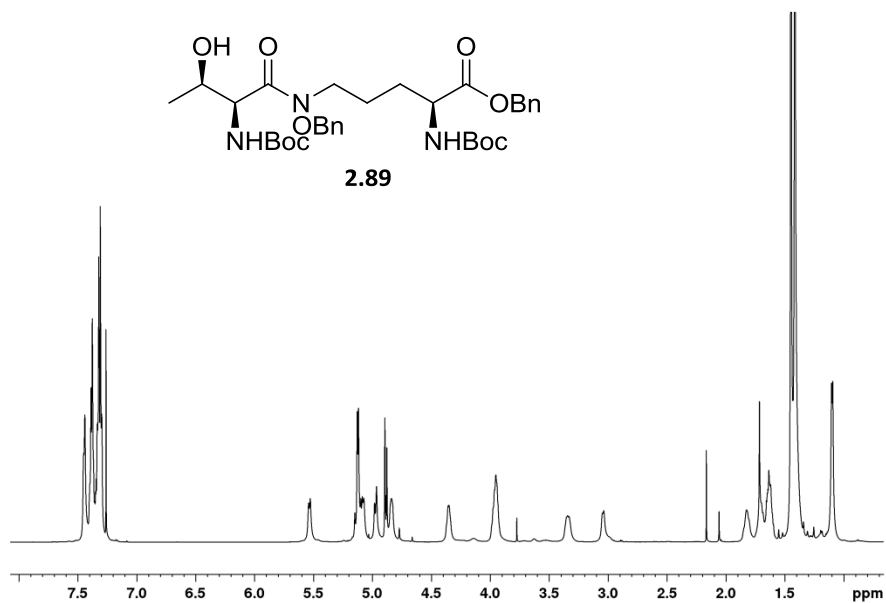
Figure A2.7. ^{1}H-NMR spectrum (600 MHz, CDCl$_3$) and ^{13}C-NMR spectrum (100 MHz, CDCl$_3$) of **2.89.**
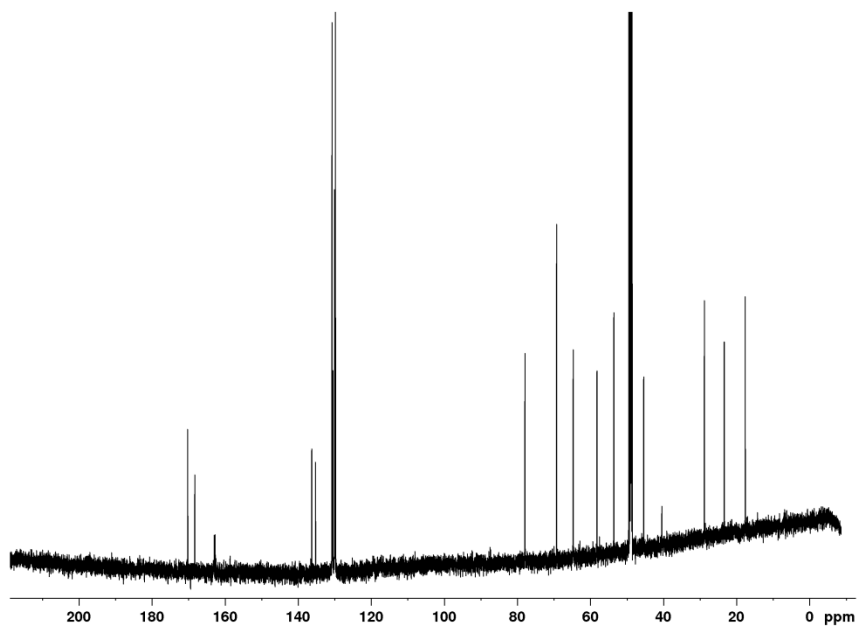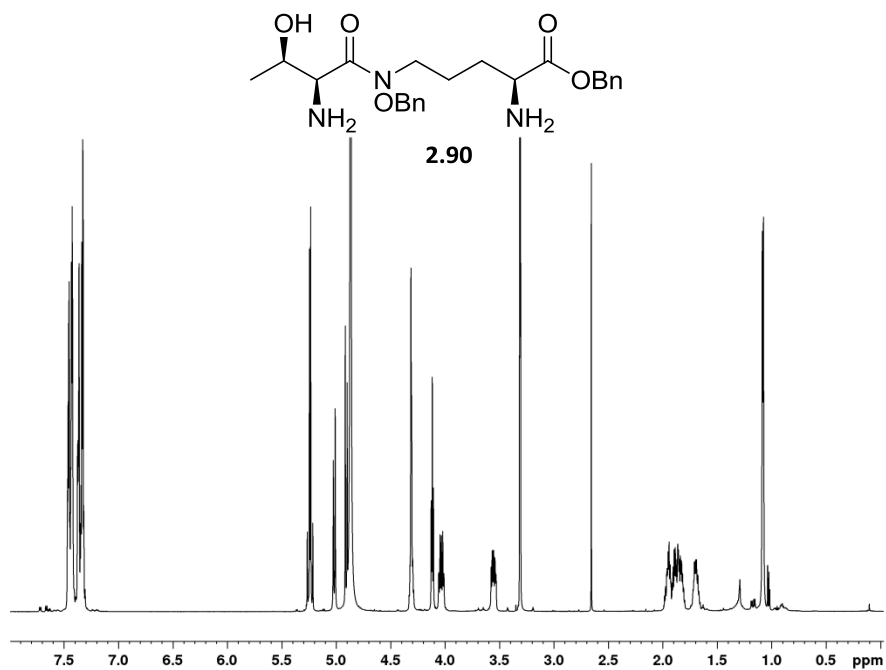
Figure A2.8. ^{1}H-NMR spectrum (600 MHz, MeOD) and ^{13}C-NMR spectrum (150 MHz, MeOD) of **2.90.**

CHAPTER 3

STRUCTURE-ACTIVITY RELATIONSHIP STUDIES OF '8882

Reprinted with permission from Dutter, B. F., Mike, L. A., Reid, P. R., Chong, K. M., Ramos-Hunter, S. J., Skaar, E. P., and Sulikowski, G. A. (2016) Decoupling Activation of Heme Biosynthesis from Anaerobic Toxicity in a Molecule Active in *Staphylococcus aureus*. *ACS Chem. Biol. 11*, 1354–1361. Copyright 2016 American Chemical Society.

3.1 Introduction

Initial studies of '8882 determined that it activate HssRS by increasing endogenous heme biosynthesis leading to intracellular accumulation of heme sufficient to activate HssRS but not affect overall growth.[1] In addition, while studying the mechanism of action of '8882, we observed that **it** was toxic to *S. aureus* growing anaerobically, potentially through the inhibition of a process essential during fermentation. *S. aureus* is a facultative anaerobe capable of generating energy through respiration or fermentation depending on the availability of terminal electron acceptors. Fermentative growth of *S. aureus* is significantly inhibited by '8882 compared to an untreated control or *S. aureus* treated with '8882 under aerobic conditions.[1]
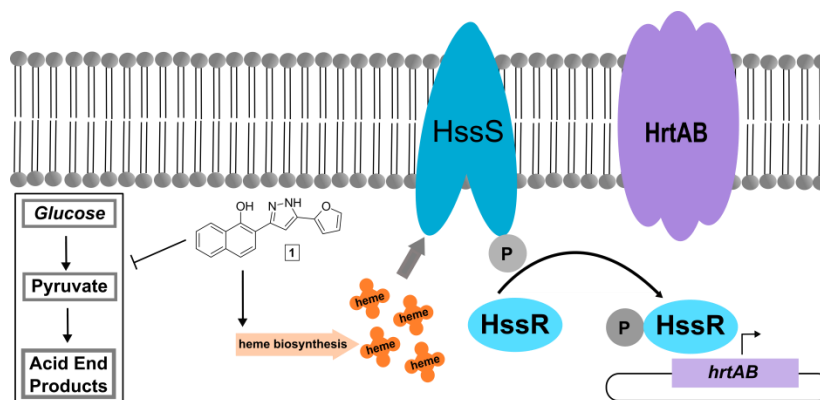
Figure 3.1. Schematic of '8882 activity.

Activators of heme biosynthesis are potentially useful chemical tools to study the regulation of heme biosynthesis in bacteria as little is known regarding the regulation of heme import and biosynthesis. Small molecules toxic to fermenting bacteria may serve as the basis for a new class of therapeutics. During certain types of infections, *S. aureus* relies heavily on fermentation to generate energy. In addition, phenotypic variants of *S. aureus* known as small colony variants (SCVs) are often obligate fermenters and are generally more resistant to current antimicrobial therapies.[2,3,4]

While we initially concluded these two activities were linked through a single target, given the promiscuous nature of molecules identified through high throughput screens, it is possible that these phenotypes are the result of interactions of the same molecule with distinct targets in the bacterium.

We synthesized a library of compounds around the scaffold of '8882 and screened for HssRS activation and anaerobic toxicity to determine how chemical modifications affect the two activities. Using this approach, we have effectively decoupled the two activities of '8882 and established that it likely has two or more targets. Furthermore, we have identified the

71

structural features of '8882 that promote one activity over the other and identified derivatives

that maintain each activity while introducing higher specificity.

3.2 Library synthesis
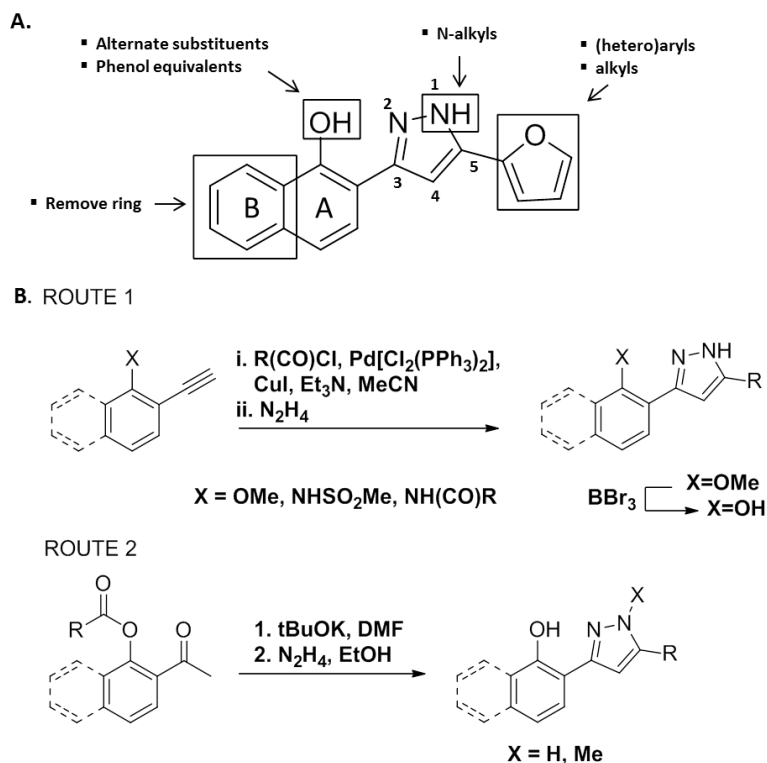
Figure 3.2. Synthetic strategy for '8882 library development.

	3.2 - 3.13		3.14 - 3.28		
Cmpd	Aryl Group	Cmpd	R Group	Cmpd	R Group
3.2		3.14		3.26	
3.3		3.15		3.27	
3.4		3.16		3.28	
3.5		3.17			

3.29 - 3.30

Cmpd	Aryl Group
3.6		3.18		Cmpd	Aryl Group
3.7		3.19		3.29	
3.8		3.20		3.30	
3.9	NHSO₂Me	3.21			
3.10		3.22			

3.31 - 3.32

Cmpd	Structure
3.11		3.23	H		
3.12		3.24	Me	3.31	
3.13		3.25		3.32	

Figure 3.3. Derivatives of '8882 synthesized for this work.

Our initial efforts towards varying the structure of '8882 focused on four regions of the molecule (Figure 2.2A); removal of the B ring of the naphthol moiety; modification of the phenol by walking to the *m-* and *p*-positions (with B ring removed), *O*-methylation, and replacement with phenol equivalents (amides and sulfonamide); *N*-methylation of the pyrazole; and replacement of the furan with aromatic, heteroaromatic, and alkyl groups.

Many routes to 3,5-substituted pyrazoles have been reported.[5] We utilized two routes, 1) cyclocondensation of hydrazine with an alkynone and 2) cyclocondensation of hydrazine with a 1,3-diketone (Figure 2.2B). The alkynone can be installed by palladium-mediated coupling with the acid chloride containing the corresponding 5-position substituent. This route requires methyl ether protection of the phenol. As such, synthesis of free phenol containing compounds involves subsequent deprotection with boron tribromide. For this reason, this sequence was primarily utilized to synthesize the amide, sulfonamide, and *O*-methylated derivatives of **1** (Figure 3; **3.4, 3.5, 3.9 − 3.13, 3.29, and 3.30**). The amide derivatives were quite labile in the presence of acid, particularly when substituted with small R groups (Me), and underwent further dehydration to generate 2,5-substituted pyrazolo[1,5-c]quinazolines. These compounds will not be discussed due to their divergence from the optimization plan.

Using route 2, the 5-position was diversified by acylating the 2'-phenol of the corresponding acetophenone to generate the ester substrate for an intramolecular Claisen condensation to provide the 1,3-diketone. Compounds **3.14 − 3.17, 3.15–3.22, and 3.24 − 3.28** were afforded by cyclocondensation with hydrazine. **3.17** was prepared by acylating 2'-hydroxyacetophone with 2-methoxybenzoyl chloride, carrying the ester through this reaction sequence, and subsequently removing the methyl group using boron tribromide. **3.23** was

synthesized by reacting hydrazine with the corresponding chromone under the same conditions as the cyclocondensation. Using an analogous reaction sequence but acylating 3'- and 4'-hydroxyacetophenone allowed synthesis of **3.6** and **3.7**. Compound **3.8** was prepared by intermolecular Claisen condensation of the lithium enolate of acetophenone, prepared by reaction with LHMDS in toluene, with furoyl chloride to provide the 1,3-diketone. Methylation of the pyrazole nitrogen was achieved by reaction of the intermediate 1,3-diketone with methylhydrazine followed by HPLC separation of the resulting isomeric pyrazoles **3.31** and **3.32**.

3.3 Activity

HssRS activation
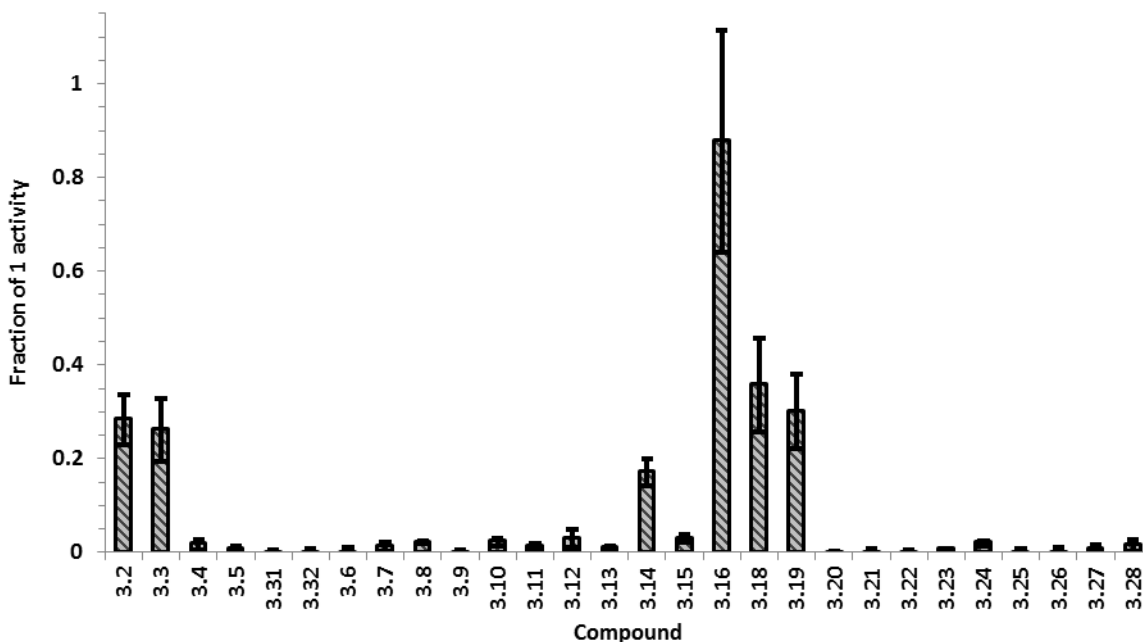
Figure 3.4. HssRS activity at 50 µM relative to '8882.

The library was screened for activation of the heme stress response as an indicator for activation of heme biosynthesis in *S. aureus*. We began by screening at the single point

75

concentration of 50 μM using a previously described reporter assay (Figure 4).[6] In this assay, Newman harboring a plasmid with the *hrt* promoter fused to *xylE,* a gene encoding a catechol oxidase, is treated with compound for six hours, the bacteria lysed, and the oxidation of catechol by XylE quantified by spectrophotometry. An increase in absorbance due to the oxidation of catechol indicates elevated levels of xylE transcription and hrt promoter activity. Results are expressed as the fraction of activation of HssRS by the compound compared to '8882. An arbitrary cut-off of 0.05 was chosen to define active vs. inactive compounds.

Replacement of the naphthol substituent with phenol (**3.2**) or 4-methoxyphenol (**3.3**) resulted in a modest loss of activity compared to '8882, but still retained significant ability to activate HssRS. *O*- and *N*-methylation of '8882 (**3.4, 3.31** and **3.32**) resulted in complete loss of activity. These data suggest that disruption of the hydrogen bonding properties of '8882 has a significant effect on its ability to activate heme biosynthesis. To test this further, several modifications to the phenol of **3.2** were made. *O*-methylation (**3.5**), movement to *m*- or *p*-positions (**3.6** and **3.7**), removal (**3.8**)**,** and replacement with a methyl sulfonamide (**3.9**) or various aryl or heteroaryl amides (**3.10 – 3.14**) resulted in a loss of HssRS activation compared to '8882 and **3.2**. This suggests that the *ortho*-OH is required for activity.

To explore modification at the 5-position, we chose the *o*-hydroxyphenyl substituent at the 3-position instead of the *o*-hydroxynaphthyl of the parent molecule for convenience. Replacement of the furan with hydrogen (**3.23**), alkyl (**3.24 – 3.28**) or pyridyl (**3.20 – 3.22**) substituents eliminates activity compared to '8882 and **3.2**. The furan can be replaced with several aromatic or heteroaromatic groups and retain considerable activity. In particular, replacement of the furan with an unsubstituted phenyl group, **3.16**, seems to restore activity

comparable to '8882 without the presence of the naphthol B-ring. However, fluorination of **3.16** decreases activity though **3.18** and **3.19** are comparable to **3.2** in activity. Substitution with hydroxyl at the *ortho* position of the phenyl ring of **3.16** to provide **3.17** renders the molecule toxic under the single point assay conditions and is therefore not included in Figure 4. However, **3.17** activates HssRS at lower concentrations and its activity was explored further.

Concentration response curves for the top six activators from the single point screen (**3.2**, **3.3**, **3.14**, **3.16**, **3.18**, and **3.19**) and **3.17** were generated to determine EC_{50} values as a measure of compound potency. (Table 3.1). Compound efficacy is presented as percent activation compared to '8882 as displayed in Figure 4 since most compounds reach their E_{max} at or below 50 µM. Exceptions to this are **3.14,** which did not reach a plateau below its solubility limit (~80 µM), **3.3** which plateaus around 100 µM, and **3.17** which is toxic in the XylE assay at 50 µM. For the most part, compound potency does not significantly deviate from that of '8882. In addition, **3.18** and **3.19** maintain comparable potency to '8882 while exhibiting a ~70 % drop in efficacy indicating potency and efficacy do not correlate well. These data suggest that efficacy is a more important quantitative descriptor of compound activity.
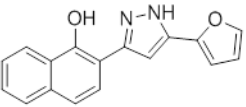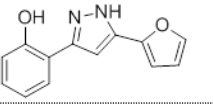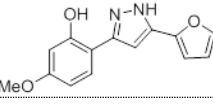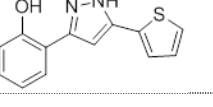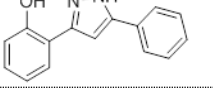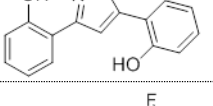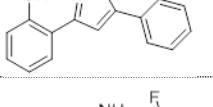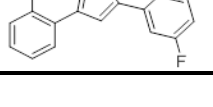
Cmpd	Structure	EC50 (µM)	pEC50	Efficacy (%)
8882		11.6	4.90 ± 0.37	100
3.2		30.4	4.49 ± 0.083	28.2 ± 5.4
3.3		50.2	4.30 ± 0.20	26.2 ± 6.7
3.14		ND	ND	17.0 ± 2.9
3.16		14.6	4.66 ± 0.016	87.8 ± 23.7
3.17		5.81	5.24 ± 0.076	ND
3.18		10.7	4.97 ± 0.033	35.7 ± 10.1
3.19		13.6	4.90 ± 1.1	30.1 ± 8.0

Table 3.1. Compound potency data.

Finally, the top activators were assayed for their ability to preadapt *S. aureus* to heme as an indication that they can activate HssRS outside the context of a reporter assay. Pretreatment of cultures with a compound that induces HrtAB expression through activation of HssRS at subtoxic concentrations allows the bacteria to survive and grow when subcultured into a toxic concentration of heme. We compared pretreatment with 4 µM heme, 40 µM '8882, and vehicle with 40 µM of each of the top activators (excluding **3.17** because of toxicity). All derivatives

were able to preadapt *S. aureus* to a toxic concentration of heme (20 μM) as well as 4 μM heme

and 40 μM '8882 (Figure 3.5). The discrepancy between XylE assay and heme adaptation

activity is likely due to the length of treatment with compound (6 h vs. 15 h). Pretreatment with

3.17 at the nontoxic concentration of 20 μM also induced excellent preadaptation to heme

toxicity.. Four inactive derivatives from the single point screen, **3.10**, **3.22**, **3.28**, and **3.29**, were

also assayed for preadaptation to heme toxicity. Growth of bacteria subcultured into 20 μM

heme after pretreatment with 40 μM compound was indistinguishable from vehicle confirming

that these compounds do not activate HssRS.
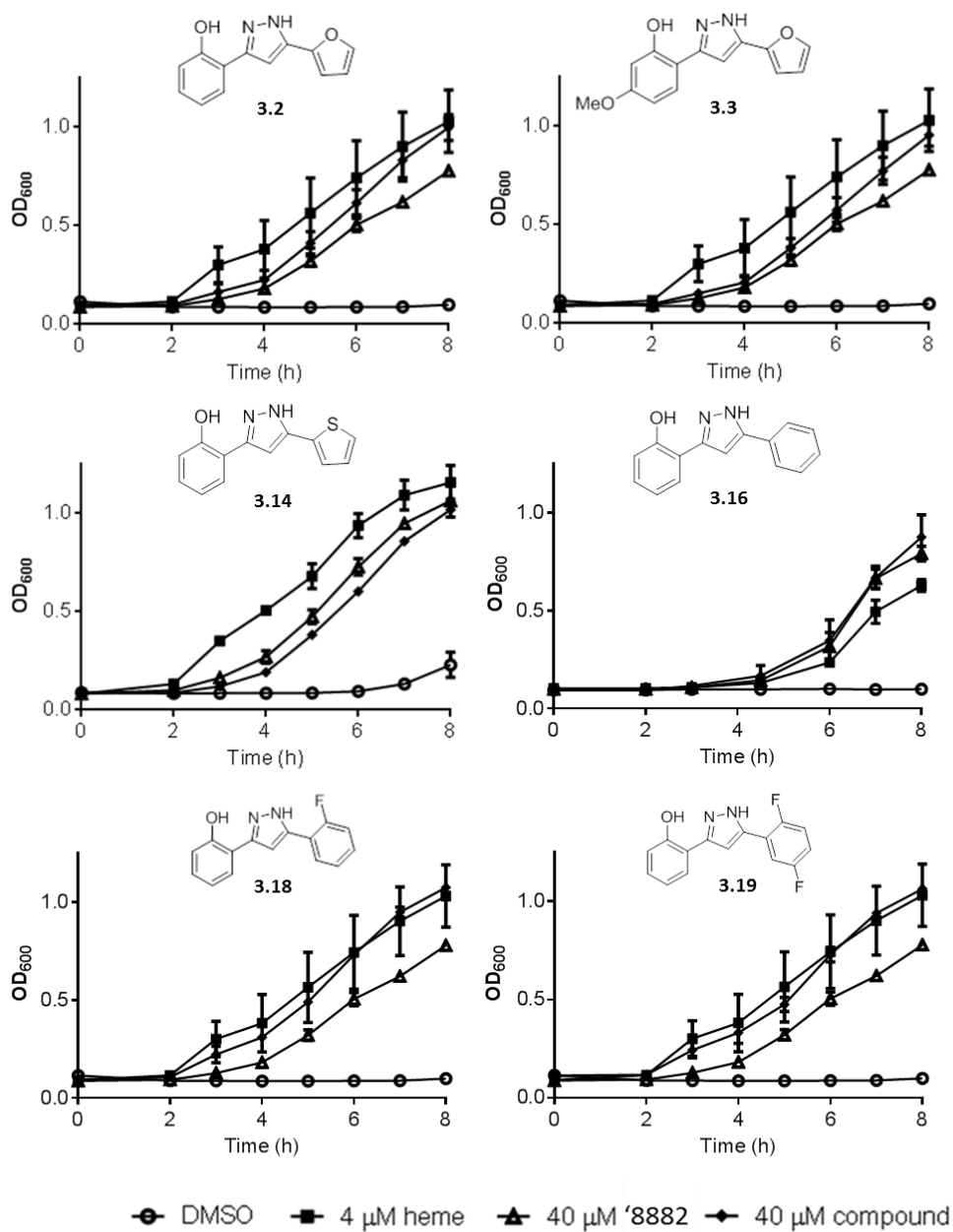
Figure 3.5. Heme adaptation by derivatives of '8882.

The results of the HssRS activation screen suggest that any disruption to the hydrogen bonding ability of the molecule eliminates this activity. While this may be important for binding to a protein target, it may also interfere with the potential for the molecule to bind to metals of biological significance. The hydrogen bond donor-acceptor orientation is potentially capable of

binding iron.[7] Since its primary activity is associated with heme-iron metabolism, the ability of

'8882 to bind iron was determined using the Chromazural-S (CAS) assay.[8] When compared to

the known iron chelator deferasirox, '8882 does not strongly bind iron Figure 3.6. Therefore, it

is unlikely that iron chelation is involved in the activity of these molecules.
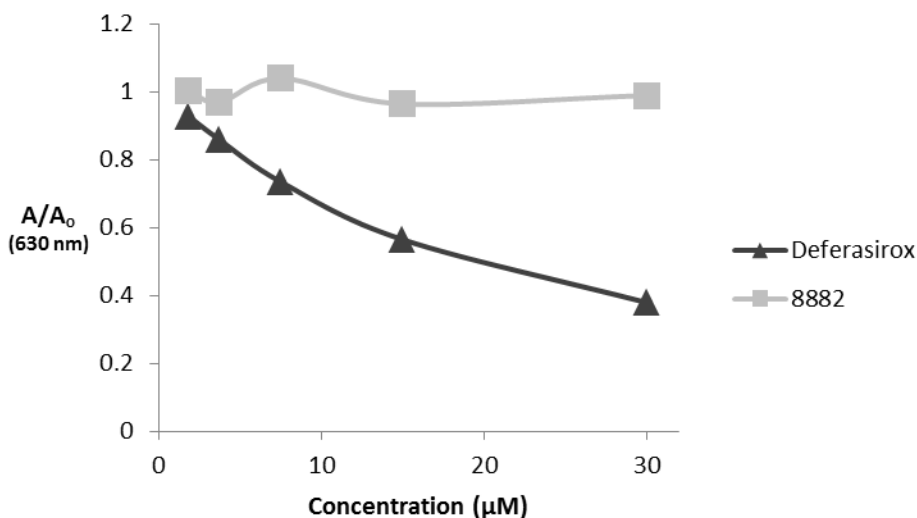
Figure 3.6. Assay for the ability of '8882 to chelate iron.

Anaerobic toxicity

Next, the compound library was screened for anaerobic toxicity by generating

concentration response curves for 9 h of growth and determining IC_{50} values (Table 3.2). Wild

type *S. aureus* strain Newman was grown in an anaerobic chamber in appropriate media to

ensure exclusion of terminal electron acceptors sufficient to force the bacteria to ferment. In

addition, an isogenic *menB* mutant was used as a positive control as this strain lacks the

electron carrier menaquinone, rendering the bacterium incapable of generating energy through

respiration in the presence of any terminal electron acceptor.[3] In parallel, the IC_{50} values were

determined in *S. aureus* grown aerobically to identify derivatives that exhibit toxicity

independent of respiration. The arbitrary cut off point for toxicity of 60 μM was chosen as many

of the compounds were not entirely soluble above this concentration.

Cmpd	Newman aerobic	Newman anaerobic	ΔmenB
8882	>60	13.5 (8.42-21.7)	1.66 (0.491-5.63)
3.2	>60	>60	35.6 (31.0-41.5)
3.3	>60	>60	>60
3.4	>60	>60	>60
3.5	>60	>60	>60
3.31	>60	26.5 (21.9-32.1)	15.7 (11.5-21.5)
3.32	>60	4.27 (3.39-4.65)	3.3 (1.28-8.55)
3.6	>60	>60	>60
3.7	>60	>60	>60
3.8	>60	>60	>60
3.9	>60	>60	>60
3.10	>60	19.6 (16.9-22.8)	8.69 (7.65-9.88)
3.11	>60	11.6 (10.2-13.0)	6.63 (5.02-8.76)
3.12	>60*	28.8 (22.0-37.7)	21.4 (13.9-32.8)
3.13	>60	13.4 (12.3-14.7)	5.89
3.14	>60	>60	>60
3.15	>60	>60	>60
3.16	>60	24.0 (20.0-28.7)	25.2 (7.84-81.2)
3.17	42.5 (40.2-44.9)	15.8 (15.3 - 16.4)	9.33 (4.89-20.1)
3.18	>60	>60	>60
3.19	>60	>60	>60
3.20	>60	>60	>60
3.21	>60	>60	>60
3.22	>60	>60	>60
3.23	>60	>60	>60
3.24	>60	>60	>60
3.25	>60	>60	>60
3.26	>60	>60	>60
3.27	>60	25.3 (23.4-27.2)	29.7 (24.6-35.9)
3.28	48.6 (37.9-62.3)	11.6 (10.3-13.1)	13.2 (10.4-16.6)
3.29	>60	20.8 (17.9-24.2)	24.9 (10.2-60.4)
3.30	>60	>60	>60

Table 3.2. Toxicity data for '8882 derivatives. Values are IC_{50}s (µM) for 9 h of growth under the indicated conditions.

The majority of compounds were essentially nontoxic to aerobically growing Newman with the exceptions of **3.17** and **3.24** with IC$_{50}$'s of 42.2 and 48.6 μM, respectively. These data indicate that the majority of derivatives do not exhibit general toxicity.

Compounds **3.2** and **3.3** were relatively nontoxic to fermenting *S. aureus* suggesting that the B-ring of '8882 is important for toxicity. *O*-methylation (**3.4**) also eliminates toxicity. However, pyrazole *N*-methylation does not decrease the toxicity of the molecules. In addition, the regiochemistry of *N*-methylation appears to exert a significant effect on toxicity. **3.31** is approximately five times less toxic to fermenting wildtype *S. aureus* and Δ*menB* than **3.32** while the toxicity of '8882 is intermediate between the two.

Substitution of the *o*-hydroxyl of **3.2** with aromatic amides (**3.10 – 3.14**) seems to impart toxicity to fermenting *S. aureus* comparable to '8882. However, substitution with a sulfonamide renders the compound nontoxic under fermentative conditions. This may be a consequence of the differing properties of amides and sulfonamides (pK$_a$, hydrogen bonding, etc) or may be related to the added aromatic bulk of the amides while the methyl group of **3.9** is innocuous. We were unable to test this due to the propensity of amides with smaller R-groups to dehydrate to pyrazolo[1,5-c]quinazolines.

Replacement of the furan with most aromatic or heteroaromatic groups resulted in nontoxic molecules under most conditions, the notable exceptions being **3.16** and **3.17**, with the furan replaced by phenyl and *o*-hydroxyphenyl, respectively. These compounds exhibit anaerobic toxicity similar to '8882. Substitution of the phenyl ring with fluorine(s) (**3.18**, **3.19**) eliminates this toxicity. Replacement of the furan with large (>4C) alkyl groups also produced

molecules with anaerobic toxicity. **3.27** and **3.28** were comparably toxic to '8882 while **3.23**, **3.24**, **3.25**, and **3.26**, with hydrogen or smaller alkyl groups were nontoxic under all conditions.

While *O*-methylation of '8882 eliminates toxicity, *O*-methylation of **3.16** (**3.29**), maintains toxicity comparable to the parent molecule. This suggests that *O*-alkylation is not a major contributor to the toxic character of these molecules.

Compound **3.18** was previously reported to exhibit anaerobic toxicity and efficacy in a mouse model of *S. aureus* infection.[1] The difference in these toxicity results is likely due to the method of IC_{50} determination. The previous method relied on a significant back-dilution of overnight cultures prior to compound addition to account for the time needed for the apparatus to become anaerobic. Bacteria grown at this low cell density could experience greater toxicity from the compound than the higher cell density used in this work. Although, **3.18** is not bacteriostatic under the conditions tested here, the ability of the compound to activate HssRS was corroborated (Figure 4). This suggests that derivatives that either activate HssRS or inhibit growth under anaerobiosis may both be valid antibacterial approaches. This is supported by previous studies that have reported that HssRS activation affects virulence during infection.[6]

Relationship between HssRS activation and anaerobic toxicity

Any disruption to the hydrogen bond donating ability of the molecule through *O*- or *N*-methylation or replacement with alternate hydrogen bond donor groups removes its ability to activate heme biosynthesis and is absolutely required for this activity. In contrast, the hydrogen bonding character seems to be less important for toxicity as several *O*- and *N*-methylated derivatives maintain toxicity levels comparable to '8882. Comparing the methylated derivatives

of '8882; **3.5, 3.31,** and **3.32**, *O*-methylation eliminates toxicity while the regiochemistry of *N*-methylation has a significant impact on the magnitude of toxicity.

Modification at the 5-position significantly affects which activity is favored. Aromatic or heteroaromatic groups are required to activate heme biosynthesis while large alkyl groups favor toxicity. Despite this, some overlap between HssRS activation and toxicity is evident. Replacement of the furan with a phenyl ring (**3.2** to **3.16**) restores toxicity comparable to '8882 and maintains HssRS activity. *O*-methylation of this derivative (**3.29**) removes HssRS activity as expected while maintaining toxicity. Fluorination of **3.16** to **3.18** maintains HssRS activity, but removes toxicity. In addition, fluorination of **3.29** to **3.30** eliminates toxicity. Interestingly, **2.17** which is highly symmetric, exhibits both activities.
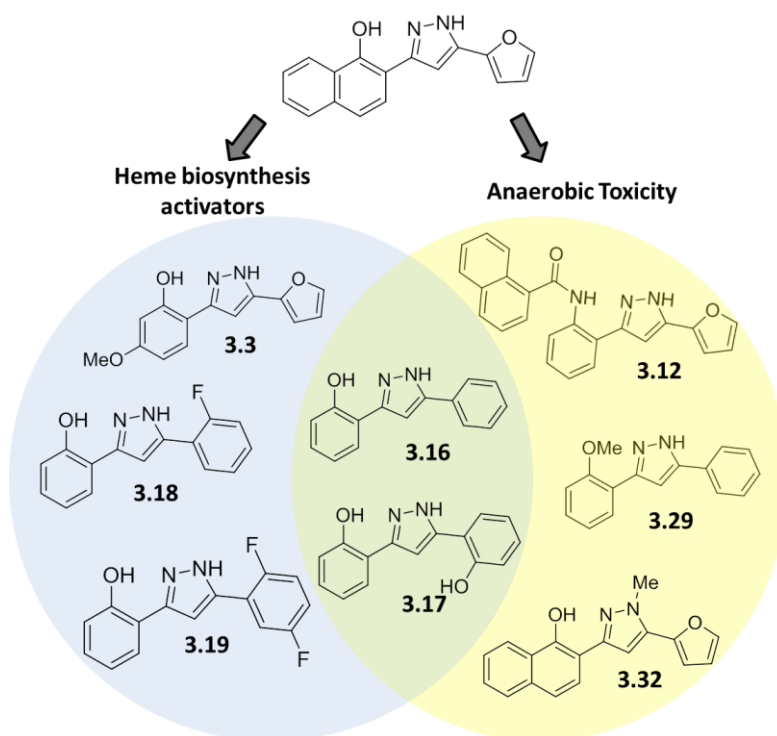
Figure 3.7. Summary of SAR results.

Relationship between XylE activity and HemY activity

Ultimately, the target of '8882 responsible for activation of heme biosynthesis was determined to be HemY, an enzyme in the late stages of heme biosynthesis (unpublished data). '8882 has been established as an activator of this enzyme. Given this specific target, it was possible to screen the molecules prepared for this work in a biochemical assay to determine their ability to activate HemY relative to '8882 as had been done in the *in vivo* XylE assay. Several of the molecules appearing in this chapter (though not all due to lack of material) were tested in the HemY assay by Matthew Surdel and Audra Fullen (Skaar lab) and their activity was represented as the percent activation of HemY compared to '8882. This data is presented in Figure 3.8 in decending order of HemY activity and is side by side with data from the XylE assay. It is clear from these data that *in vivo* activity and *in vitro* activity do not correlate well. **3.5** was the most active compound in the HemY assay exhibiting almost 1.5x the activity of '8882. However, this compound is O-methylated which was established to eliminate HssRS activity *in vivo*. This signifies that much of the requirements for activity as determined from *in vivo* data is likely not related to binding to HemY, but possibly some other component of in vivo activity such as ability to access the target.
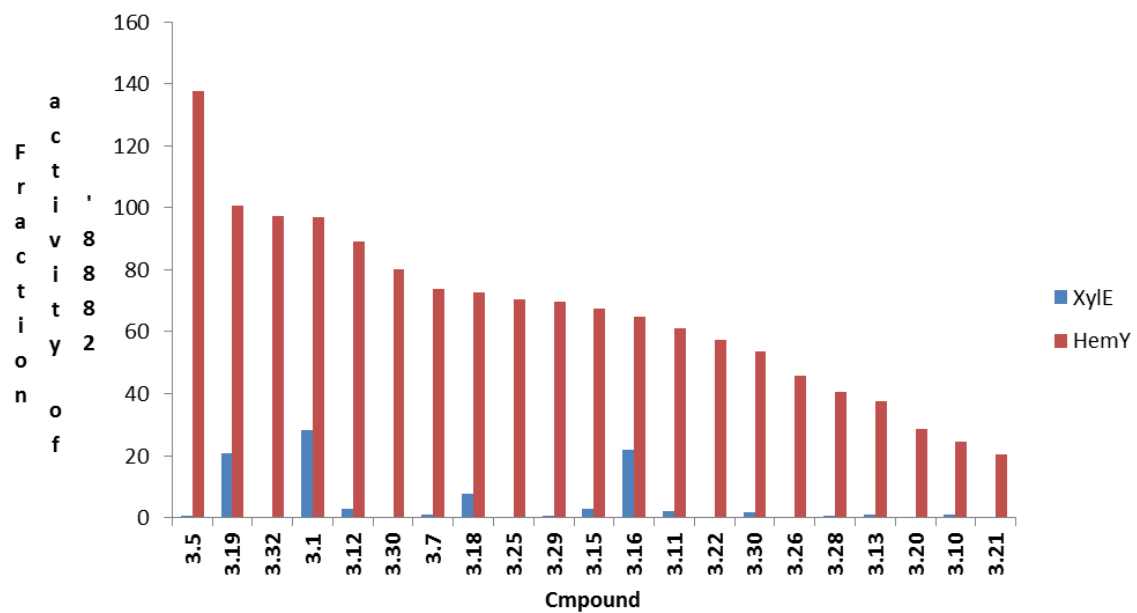
Figure 3.8. Activity of each compound in the XylE assay compared to the HemY assay.

Experimental Section

XylE assay. Previously reported strains were used.[6] Cultures grown overnight in 5 ml TSB with 10 µg mL^{-1} chloramphenicol for 15-18 h were subcultured 1:100 into 0.5 mL TSB with 10 µg mL^{-1} chloramphenicol containing compound and incubated at 37 °C, 180 rpm for 6 h. Cells were washed and lysed as previously described. 200 µL of a 200 µM catechol solution in 100 mM potassium phosphate (pH 8.0) was added to 20 µL of lysate and the oxidation of catechol was followed by monitoring absorbance at 375 nm for 10 min. Samples were normalized to protein concentration as determined by BCA assay (Pierce).

HssRS activation dose response curves and EC$_{50}$ determination. The above XylE procedure was followed using different concentrations of compound. The data were then entered into Graphpad Prism 6 and fit to a curve to determine EC$_{50}$ values.

IC$_{50}$ determination. Cultures of wild type *S. aureus* strain Newman and Δ*menB*[1] were grown in aeration tubes aerobically at 37 °C with shaking for 15 – 18 h. Anaerobic cultures were prepared by growing bacteria at 37 °C without shaking in an anaerobic chamber for 15 -18 h. Bacteria from each condition were subcultured 1:100 into TSB containing various concentrations of compound in a 96 well plate. Aerobic wild type and Δ*menB* plates are incubated aerobically at 37 °C with shaking while anaerobic plates were grown in an anaerobic chamber (Coy) at 37 °C without shaking. The absorbance at 600 nm (OD$_{600}$) was determined after 9 h of growth and the fraction of growth at each compound concentration is determined by dividing the OD$_{600}$ by the vehicle control (DMSO) value. IC$_{50}$s were calculated using Graphpad Prism 6 and errors are reported as 95 % confidence intervals.

Heme adaptation assays. Overnight cultures of *S. aureus* were subcultured into 500 μL TSB containing compound in 1.5 mL tubes and incubated at 37 °C with shaking for 15 h. Bacteria from the compound treated cultures were then subcultured 1:100 into 100 μL TSB containing heme and incubated at 37 °C with shaking for 8 h. Growth was monitored by reading the OD_{600} on a Biotek microplate reader at the defined time intervals.

Iron chelation assay. Iron chelation by **1** was characterized using the CAS assay. Solutions were prepared as described.[8] The clinical iron chelator deferasirox (AK Scientific) was used as a control. Samples were incubated in 1 mL cuvettes at room temperature for 30 min after addition of compound. The maximum concentration of compound used was 30 μM which is a 4:1 stoichiometry of **1** to Chromeazural-S. Absorbance at 630 nm was measured on a Varian UV/Vis spectrophotometer.

Chemical Synthesis

General Procedure: All non-aqueous reactions were performed in flame-dried flasks under an atmosphere of argon. Stainless steel syringes were used to transfer air- and moisture-sensitive liquids. Reaction temperatures were controlled using a thermocouple thermometer and analog hotplate stirrer. Reactions were conducted at room temperature (rt, approximately 23 °C) unless otherwise noted. Flash column chromatography was conducted using silica gel 230-400 mesh. Analytical thin-layer chromatography (TLC) was performed on E. Merck silica gel 60 F254 plates and visualized using UV and iodine stain.

Materials: All solvents and chemicals were purchased from Sigma-Aldrich unless otherwise noted. Dry dichloromethane was collected from an MBraun MB-SPS solvent system. N,N-dimethylformamide (DMF), tetrahydrofuran (THF), and acetonitrile (MeCN) were used as

received in a bottle with a Sure/Seal. Triethylamine was distilled from calcium hydride and stored over KOH. Deuterated solvents were purchased from Cambridge Isotope Laboratories.

Instrumentation: ^{1}H NMR spectra were recorded on Bruker 400, 500, or 600 MHz spectrometers and are reported relative to deuterated solvent signals. Data for ^{1}H NMR spectra are reported as follows: chemical shift (δ ppm), multiplicity (s = singlet, d = doublet, t = triplet, q = quartet, p = pentet, m = multiplet, br = broad, app = apparent), coupling constants (Hz), and integration. ^{13}C NMR spectra were recorded on Bruker 100, 125, or 150 MHz spectrometers and are reported relative to deuterated solvent signals. Low resolution mass spectrometry (LRMS) was conducted and recorded on an Agilent Technologies 6130 Quadrupole instrument.

Synthetic procedures and compound characterization data:

X = SO₂Me, or C(O)R
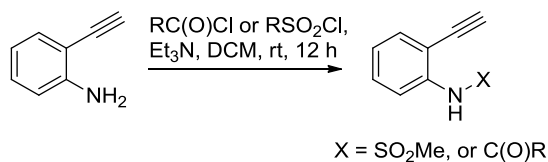
2-ethynyl-N-acylbenzamides: To a stirred solution of 2-ethynylaniline (1.0 eq) dissolved in dichloromethane (0.3 M) at room temperature was added acyl or sulfonyl chloride (1.0 eq). Tiriethylamine was slowly added to the reaction and once addition was complete, the reaction was stirred at room temperature overnight. Solvents were removed *in vacuo* and the residue was partitioned between ethyl acetate and saturated $NaHCO_3$ (aq), the organic layer dried ($MgSO_4$), and concentrated *in vacuo*. The crude product was purified by flash chromatography.

 N-(2-ethynylphenyl)methanesulfonamide (S1). Light brown solid; ^{1}H-NMR (400 MHz, $CDCl_3$) δ 7.61 (d, J=8.20 Hz, 1H) 7.50 (dd, J=7.72 Hz, J=1.40 Hz, 1H), 7.39 (br t,

J=7.90 Hz, 1H), 7.13 (t, J=7.67 Hz, 1H), 7.02 (br, 1H), 3.49 (s, 1H), 3.02 (s, 3H); ^{13}C-NMR (100

MHz, CDCl$_3$) δ 139.6, 133.0, 130.7, 124.8, 119.6, 113.0, 84.9, 78.8, 39.8; LRMS calculated for

C$_9$H$_9$NO$_2$S (M+H)$^+$ *m/z*: 196.0, measured 196.1.
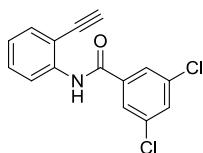
N-(2-ethynylphenyl)-4-methoxybenzamide (S2). Off-white solid; ^{1}H-NMR (400

MHz, CDCl$_3$) δ 8.64 (br, 1H), 8.51 (d, J=8.28 Hz, 1H), 7.77 (d, J=1.84 Hz, 2H),

7.57 (t, J=1.86 Hz, 1H), 7.44 (t, J=7.95 Hz, 1H), 7.12 (td, J=7.57 Hz, 1.05 Hz, 1H),

3.64 (s, 1H); ^{13}C-NMR (100 MHz, CDCl$_3$) δ 162.7, 139.2, 137.8, 136.0, 132.4, 132.1, 130.6, 125.9,

124.3, 119.6, 111.5, 85.3, 79.4; LRMS calculated for C$_{15}$H$_9$Cl$_2$NO (M+H)$^+$ *m/z*: 290.0, measured

290.0.
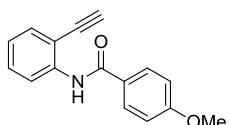
3,5-dichloro-N-(2-ethynylphenyl)benzamide (S3). White solid; ^{1}H-NMR (400

MHz, CDCl$_3$) δ 8.72 (br, 1H), 8.59 (d, J=8.20 Hz, 1H), 7.89 (d, J=6.78 Hz, 2H),

7.50 (dd, J=7.68 Hz, 1.48 Hz, 1H), 7.42 (t, J=7.95 Hz, 1H), 7.06 (td, J=7.54 Hz, 1.08 Hz, 1H), 7.00

(d, J=8.84 Hz, 2H), 3.88 (s, 3H), 3.59 (s, 1H); ^{13}C-NMR (100 MHz, CDCl$_3$) δ 164.9, 162.8, 140.2,

132.3, 130.5, 129.1, 127.2, 123.3, 119.3, 114.3, 110.9, 84.7, 79.7, 55.6; LRMS calculated for

C$_{16}$H$_{13}$NO$_2$ (M+H)$^+$ *m/z*: 252.1, measured 252.1.
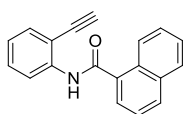
N-(2-ethynylphenyl)-1-naphthamide (S4). White solid; ^{1}H-NMR (400 MHz,

CDCl$_3$) δ 8.71 (d, J=8.20 Hz, 1H), 8.57 (br s, 1H), 8.50 (d, J=8.24 Hz, 1H), 8.00 (d,

J=8.00 Hz, 1H), 7.92 (d, J=7.64 Hz, 1H), 7.83 (d, J=7.04 Hz, 1H), 7.63-7.45 (m, 5H), 7.12 (t, J=7.52

Hz, 1H), 3.42 (s, 1H); ^{13}C-NMR (100 MHz, CDCl$_3$) δ 167.5, 140.1, 134.3, 134.0, 132.4, 131.6,

130.5, 130.3, 128.6, 127.6, 126.8, 125.6, 125.5, 124.9, 123.8, 119.7, 111.3, 84.9, 79.3 ; LRMS

calculated for C$_{19}$H$_{13}$NO (M+H)$^+$ *m/z*: 272.1, measured 272.1.
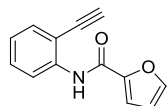
N-(2-ethynylphenyl)furan-2-carboxamide (S5). Brown solid; ^{1}H-NMR (400 MHz, CDCl$_3$) δ 8.99 (br, 1H), 8.55 (d, J=8.24 Hz, 1H), 7.53 (s, 1H), 7.49 (dd, J=7.68 Hz, 1.48 Hz, 1H), 7.40 (t, J=7.94 Hz, 1H), 7.25 (d, J=3.54 Hz, 1H), 7.06 (t, J=7.71 Hz, 1H), 6.56 (dd, J=3.50 Hz, 1.72 Hz, 1H), 3.60 (s, 1H); ^{13}C-NMR (100 MHz, CDCl$_3$) δ 156.1, 148.0, 144.7, 139.4, 132.3, 130.4, 123.6, 119.4, 115.6, 112.7, 111.1, 84.8, 79.1 ; LRMS calculated for C$_{13}$H$_9$NO$_2$ (M+H)$^+$ *m/z*: 212.1, measured 212.1.
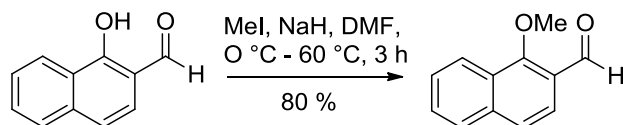
1-methoxy-2-naphthaldehyde (S6). To a stirred solution of 193 mg (1.12 mmol, 1.0 eq) 1-hydroxy-2-naphthaldehyde (TCI America) dissolved in 5 mL N,N-dimethylformamide at 0 °C was added 49.0 mg (1.23 mmol, 1.2 eq) sodium hydride. The mixture was stirred at 0 °C for 5 min and 140 µL (2.24 mmol, 2.0 eq) methyl iodide was added. The reaction was heated to 60 °C and stirred for 3 h. The reaction was partitioned between ethyl acetate and water, the organic layer washed with water (1x), brine (2x), and dried (MgSO$_4$). The organic layer was concentrated and the residue purified by flash chromatography with a 0-20 % ethyl acetate in hexane gradient to provide 165 mg (80 %) of product as a light brown solid. ^{1}H-NMR (400 MHz, CDCl$_3$) δ 10.59 (d, J=0.76 Hz, 1H), 8.23 (d, J=8.16 Hz, 1H), 7.86 – 7.82 (m, 2H), 7.64 - 7.54 (m, 3H), 4.12 (s, 3H); ^{13}C-NMR (100 MHz) δ 189.6, 162.6, 138.1, 129.4, 128.4, 127.9, 126.9, 124.9, 124.7, 123.2, 122.7, 65.7; LRMS calculated for C$_{12}$H$_{10}$O$_2$ (M+H)$^+$ *m/z*: 187.1, measured 187.1.
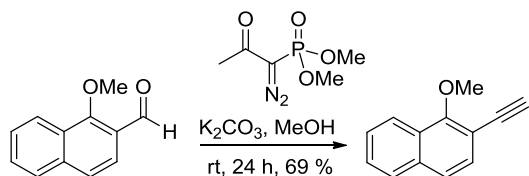
2-ethynyl-1-methoxynaphthalene (S7). To a stirred solution of 106 mg (0.570 mmol, 1.0 eq) 1-methoxy-2-naphthaldehyde in 5 mL methanol was added 158 mg (1.14 mmol, 2.0 eq) potassium carbonate followed by 131 mg (0.682 mmol, 1.2 eq) dimethyl (1-diazo-2-oxopropyl)phosphonate. The suspension was stirred for 24 h. The reaction was partitioned between ethyl acetate and water, the aqueous layer extracted with ethyl acetate (2x), the organics combined and washed with brine (1x), dried (MgSO$_4$), and flash filtered through silica with 5:1 hexane/ethyl acetate to provide 72 mg (69 %) 2-ethynyl-1-methoxynaphthaldehyde. ^{1}H-NMR (400 MHz, CDCl$_3$) δ 8.01 – 7.97 (m, 1H), 7.62 – 7.58 (m, 1H), 7.35 – 7.27 (m, 4H), 3.97 (s, 3H), 3.22 (s, 1H); ^{13}C-NMR (100 MHz, CDCl$_3$) δ 159.3, 144.2, 134.9, 129.8, 127.9, 127.4, 126.5, 123.5, 122.5, 110.3, 82.5, 80.8, 61.9; LRMS calculated for C$_{13}$H$_{10}$O (M+H)$^+$ *m/z*: 183.1, measured 183.1.

The alkyne precursor for **3.29** and **3.30** was prepared from *o*-anisaldehyde as previously described.[9]

2'-acyloxyacetophenone synthesis. To a stirred solution of 2'-hydroxyacetophenone in dichloromethane (0.2 M) was added triethylamine (1.1 eq) and 4-dimethylaminopyridine (0.05 eq). The solution was cooled to 0 °C in an ice bath and acid chloride (1.1 eq) was added. The reaction was allowed to warm to room temperature and monitored by TLC and LCMS. When starting material was completely consumed and product observed by LC-MS, the reaction was partitioned between dichloromethane and saturated NaHCO$_3$ (aq). The organic layer was washed with brine and dried (MgSO$_4$), filtered, and concentrated. The products generally did

not require further purification but may be crystallized from hexane/ethyl acetate or purified by flash chromatography as needed. Products were generally carried on uncharacterized.
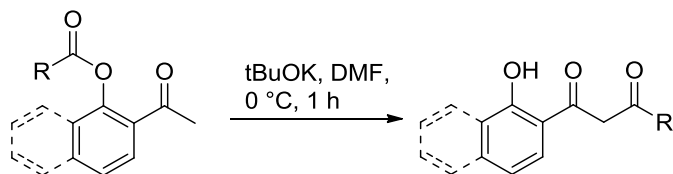
1,3-diketone synthesis. A suspension of potassium *tert*-butoxide (2.0 eq) in dimethylformamide (0.2 M) was cooled to 0 °C under Ar. A solution of 2'-acyloxyacetophenone (1.0 eq) in DMF was added dropwise to the *t*BuOK suspension and stirred at 0 °C until consumption of starting material was observed by TLC (~1 h). The reaction was quenched with 1 N HCl and the resulting suspension extracted with diethyl ether (3x), washed with H_2O, brine, dried ($MgSO_4$) and solvents removed *in vacuo*. Products were carried on crude and uncharacterized.

'8882 and **3.18** were previously reported.[1]

Pyrazole synthesis. ROUTE 1: To a stirred solution of terminal alkyne (1 eq) in THF (0.2 M) was added triethylamine (3 eq), bistriphenylphosphine palladium dichloride (0.05 eq), copper(I) iodide (0.1 eq), and acid chloride (1.5 eq) at room temperature. The reaction was stirred until conversion of starting material was observed by TLC. The reaction was diluted 1:1 with acetonitrile followed by addition of hydrazine hydrate (4 eq). The reaction was stirred until complete as determined by TLC. The reaction was filtered through celite, concentrated, and purified by preparative scale reverse phase HPLC.

ROUTE 2: To a solution of crude diketone in ethanol (0.25 M) in a microwave vial was added hydrazine hydrate (2 eq). The vial was sealed and heated to 150 °C in a microwave reactor for 5

min. The reaction was concentrated and the product was purified by preparative scale reverse phase HPLC.

General procedure for demethylation of aryl ethers. To a solution of reactant in dichloromethane (0.20 M) was added 6.0 eq BBr_3 (1.0 M in dichloromethane) in a microwave vial. The vial was sealed and maintained at 90 °C under microwave irradiation for 20 min. The reaction was quenched with saturated $NaHCO_3$ and extracted with dichloromethane. The organic layer was washed with brine, dried ($MgSO_4$), and concentrated. Products were purified by flash chromatography or HPLC.
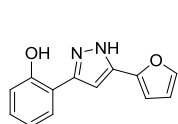
2-(5-(furan-2-yl)-1H-pyrazol-3-yl)phenol (3.2) ^{1}H-NMR (400 MHz, acetone-d6) δ 7.76 (d, J=7.78 Hz, 1H), 7.72 (s, 1H), 7.22 (t, J=7.73 Hz, 1H), 7.12 (s, 1H), 6.96-6.90 (m, 3H), 6.63 (dd, J=3.39 Hz, 1.86 Hz, 1H); ^{13}C-NMR (150 MHz, acetone-d6) δ 158.3, 154.6, 144.1, 130.0, 127.6, 120.1, 117.6, 117.5, 112.7, 108.5, 99.2; LRMS calculated for $C_{13}H_{11}N_2O_2$ (M+H)[+] *m/z*: 227.1, measure, 227.1.
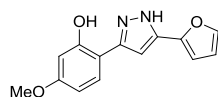
2-(5-(furan-2-yl)-1H-pyrazol-3-yl)-5-methoxyphenol (3.3) ^{1}H-NMR (400 MHz, acetone-d6) δ 12.75 (br, 1H), 10.95 (br; 1H), 7.70 (s, 1H), 7.65 (d, J=8.44 Hz, 1H), 7.00 (s, 1H), 6.91 (s, 1H), 6.62 (br, 1H), 6.54-6.48 (m, 2H), 3.80 (s, 3H); ^{13}C-NMR (100 MHz, acetone-d6) δ 161.9, 158.4, 144.0, 128.5, 112.6, 110.7, 108.3, 106.8, 102.4, 98.5, 55.4; .LRMS calculated for $C_{14}H_{12}N_2O_3$ (M+H)[+] *m/z*: 257.1, measured 257.1.
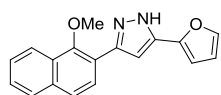
5-(furan-2-yl)-3-(1-methoxynaphthalen-2-yl)-1H-pyrazole (3.4) ^{1}H-NMR (400 MHz, CDCl₃) δ]8.18 (d, J=8.20 Hz, 1H), 7.86 (d, J=7.80 Hz, 1H), 7.76 (d, J=8.60 Hz, 1H), 7.70 (d, J=8.64 Hz, 1H), 7.61 − 7.50 (m, 2H), 6.99 (s, 1H), 6.81 (d, J=3.28 Hz, 1H), 6.52 (dd, J=3.28 Hz, J=1.80, 1H), 3.92 (s, 3H); ^{13}C-NMR (100 MHz, CDCl₃) δ 152.8,148.8, 142.0,

134.9, 128.3, 128.2, 127.0, 126.9, 125.3, 122.4, 117.7, 111.5, 106.0, 101.1, 62.0; LRMS calculated for $C_{18}H_{14}N_2O_2$ (M+H)$^+$ m/z: 291.1, measured 291.1.
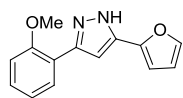
5-(furan-2-yl)-3-(2-methoxyphenyl)-1H-pyrazole (3.5) ^{1}H-NMR (400 MHz, CD$_3$OD) δ 7.73 (d, J=7.20 Hz, 1H), 7.57 (s, 1H), 7.38 (t, J=6.8 Hz, 1H), 7.17 (d, J=8.4 Hz, 1H), 7.06 (t, J=7.60 Hz, 1H), 6.94 (s, 1H), 6.76 (d, J=3.20 Hz, 1H), 6.54 (m, 1H), 3.99 (s, 3H); ^{13}C-NMR (100 MHz, acetone-d6) δ 157.1, 150.3, 142.7, 142.5, 130.2, 128.7, 121.8, 119.3, 112.6, 112.1, 105.9, 101.5, 56.0; LRMS calculated for $C_{14}H_{12}N_2O_2$ (M+H)$^+$ m/z: 241.1, measured 241.1.
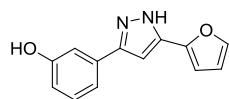
3-(5-(furan-2-yl)-1H-pyrazol-3-yl)phenol (3.6) ^{1}H-NMR (400 MHz, acetone-d6) δ 7.62 (s, 1H), 7.36 - 7.31 (m, 2H), 7.26 (t, J=7.77 Hz, 1H), 6.89 (s, 1H), 6.83 (d, J=8.18 Hz, 1H), 6.77 (d, J=3.19 Hz, 1H), 6.56 (dd, J=3.35 Hz, 1.41 Hz, 1H); ^{13}C-NMR (100 MHz, acetone-d6) δ 158.7, 143.0, 130.7, 117.6, 115.9, 113.2, 112.3, 106.6, 99.9; LRMS calculated for $C_{13}H_{10}N_2O_2$ (M+H)$^+$ m/z: 227.1, measured 227.2.
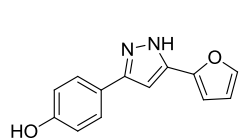
3-(5-(furan-2-yl)-1H-pyrazol-3-yl)phenol (3.7) ^{1}H-NMR (400 MHz, acetone-d6) δ 7.70 (d, J=8.57 Hz, 2H), 7.61 (d, J=1.24 Hz, 1H), 6.92 (d, J=8.57 Hz, 2H), 6.81 (s, 1H), 6.75 (d, J=3.24 Hz, 1H), 6.54 (dd, J=3.24 Hz, 1.24 Hz, 1H); ^{13}C-NMR (150 MHz, acetone-d6) δ 158.4, 157.3, 149.1, 148.0, 142.8, 127.7, 123.8, 116.5, 112.2, 106.2, 99.0; LRMS calculated for $C_{13}H_{10}N_2O_2$ (M+H)$^+$ m/z: 227.1, measured 227.1.
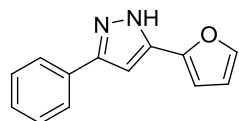
5-(furan-2-yl)-3-phenyl-1H-pyrazole (3.8) ^{1}H-NMR (400 MHz, acetone-d6) δ 7.77 (d, J=7.57 Hz, 2H), 7.57 (s, 1H), 7.44 (t, J=7.32 Hz, 2H), 7.35 (t, J=7.28

Hz, 1H), 6.87 (s, 1H), 8.77 (d, J=3.28 Hz, 1H), 6.54 (dd, J=3.28 Hz, 1.48 Hz, 1H); ^{13}C-NMR (150

MHz, acetone-d6) δ 143.1, 129.7, 128.8, 126.2, 112.3, 106.7, 9.8; LRMS calculated for $C_{13}H_{10}N_2O$

(M+H)$^+$ *m/z*: 211.1, measured 211.1.
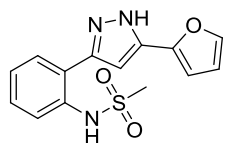
N-(2-(5-(furan-2-yl)-1H-pyrazol-3-yl)phenyl)methanesulfonamide (3.9) ^{1}H-NMR (400 MHz, acetone-d6) δ 7.91 (d, J=7.94 Hz, 1H), 7.74 (s, 1H), 7.71 (d, J=7.72 Hz, 1H), 7.22 (t, J=7.60 Hz, 1H), 7.16 (s, 1H), 6.95 (d, J=3.40 Hz, 1H),

6.64 (dd, J=3.40 Hz, 1.80 Hz, 1H), 2.97-2.95 (m, 3H); ^{13}C-NMR (100 MHz, acetone-d6) δ 152.6,

145.4, 144.2, 137.0, 136.5, 129.6, 129.1, 124.5, 121.5, 120.3, 112.7, 108.5, 100.7, 39.6; LRMS

calculated for $C_{14}H_{13}N_3O_3S$ (M+H)$^+$ *m/z*: 304.1, measured 304.0.
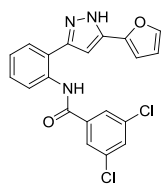
3,5-dichloro-N-(2-(5-(furan-2-yl)-1H-pyrazol-3-yl)phenyl)benzamide (3.10) ^{1}H-NMR (400 MHz, acetone-d6) δ 8.82 (d, J=8.20 Hz, 1H), 8.01 (d, J=1.92 Hz, 2H), 7.93 (dd, J=7.82 Hz, 1.46 Hz, 1H), 7.72 (br s, 2H), 7.39 (br t, J=7.84 Hz, 1H), 7.23

(br t, J=7.58 Hz, 1H), 7.19 (s, 1H), 6.94 (d, J=3.28 Hz, 1H), 6.63 (dd, J=3.40 Hz, 1.84 Hz, 1H); ^{13}C-

NMR (125 MHz, acetone-d6) 163.2, 145.4, 144.2, 140.0, 137.4, 136.2, 132.0, 129.4, 128.9,

127.0, 124.7, 121.4, 121.3. 112.7, 108.7, 101.2; LRMS calculated for $C_{20}H_{13}Cl_2N_3O_2$ (M+H)$^+$ *m/z*:

398.1, measured 398.0.
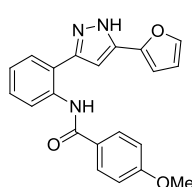
N-(2-(5-(furan-2-yl)-1H-pyrazol-3-yl)phenyl)-4-methoxybenzamide (3.11) ^{1}H-NMR (400 MHz, acetone-d6) δ 8.95 (d, J=7.84 Hz, 1H), 8.16 (d, J=8.88 Hz, 2H), 7.90 (d, J=7.84 Hz, 1H), 7.71 (s, 1H), 7.36 (t, J=7.89 Hz, 1H), 7.19 - 7.14 (m, 2H),

7.05 (d, J=8.89 Hz, 2H), 6.94 (d, J=3.36 Hz, 1H), 6.62 (dd, J=3.38 Hz, 1.82 Hz, 1H), 3.88 (s, 3H);

^{13}C-NMR (100 MHz, acetone-d6) δ 165.5, 163.4, 144.1, 138.3, 130.2, 129.3, 128.7, 123.6, 121.1,

114.7, 112.7, 108.5, 101.0, 55.9; LRMS calculated for $C_{21}H_{17}N_3O_3$ (M+H)$^+$ *m/z*: 360.1, measured 360.1.
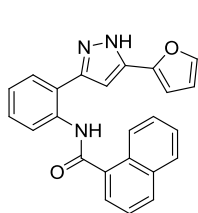
N-(2-(5-(furan-2-yl)-1H-pyrazol-3-yl)phenyl)-1-naphthamide (3.12) ^{1}H-NMR (600 MHz, acetone-d6) δ 9.00 (d, J=8.28 Hz, 1H), 8.58 - 8.53 (m, 1H), 8.10 (d, J=8.24 Hz, 1H), 8.02 - 7.99 (m, 1H), 7.97 (d, J=7.97 Hz, 1H), 7.92 (dd, J=7.84 Hz, 1.48 Hz, 1H), 7.68 (d, J=1.44 Hz, 1H), 7.64 - 7.56 (m, 2H), 7.44 (td, J=7.88 Hz, 1.48 Hz, 1H), 7.24 (td, J=7.63 Hz, 0.96 Hz, 1H), 7.14 (s, 1H), 6.90 (d, J=3.36 Hz, 1H), 6.60 (dd, J=3.40 Hz, 1.80 Hz, 1H); ^{13}C-NMR (150 MHz, acetone-d6) δ 168.1, 153.0, 145.5, 144.1, 142.3, 138.0, 136.3, 134.9, 131.3, 131.4, 129.3, 129.2, 128.8, 127.7, 127.3, 126.6, 126.4, 126.0, 124.3, 121.3, 112.6, 108.3, 101.1; LRMS calculated for $C_{24}H_{17}N_3O_2$ (M+H)$^+$ *m/z*: 380.1, measured 380.1.
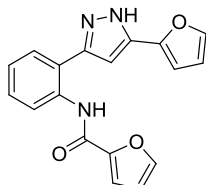
N-(2-(5-(furan-2-yl)-1H-pyrazol-3-yl)phenyl)furan-2-carboxamide (3.13) ^{1}H-NMR (400 MHz, acetone-d6) δ 8.83 (d, J=4.31 Hz, 1H), 7.89 (dd, J=7.82 Hz, 1.50 Hz, 1H), 7.73 (ddd, J=4.60 Hz, 1.70 Hz, 0.78 Hz, 2H), 7.36 (app t, 1H), 7.26 (dd, J=3.48 Hz, 0.76 Hz, 1H), 7.19 (app t, 1H), 7.15 (s, 1H), 6.95 (dd, J=3.40 Hz, 0.50 Hz, 1H), 6.65 (dd, J=3.48 Hz, 1.76 Hz, 1H), 6.63 (dd, J=3.42 Hz, 1.82 Hz, 1H); ^{13}C-NMR (100 MHz, acetone-d6) δ 157.1, 149.8, 145.9, 145.6, 144.0, 137.4, 136.5, 129.2, 128.8, 124.2, 121.3, 121.1, 115.0, 113.0, 112.7, 108.4, 100.9; LRMS calculated for $C_{18}H_{13}N_3O_3$ (M+H)$^+$ *m/z*: 320.1, measured 320.1.
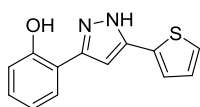
2-(5-(thiophen-2-yl)-1H-pyrazol-3-yl)phenol (3.14) ^{1}H-NMR (400 MHz, acetone-d6) δ 7.77 (dd, J=7.74 Hz, 1.54 Hz, 1H), 7.56 (br s, 1H), 7.24 - 7.15 (m, 2H), 7.11 (s, 1H), 6.93 (app q, 2H) ^{13}C-NMR (150 MHz, acetone-d6) δ 157.3, 153.5, 139.2, 130.0, 128.9, 127.4, 127.0, 119.3, 117.5, 116.8, 99.5; LRMS calculated for $C_{13}H_{10}N_2OS$ (M+H)$^+$ *m/z*: 243.1, measured 243.1.
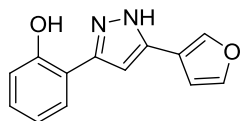
2-(5-(furan-3-yl)-1H-pyrazol-3-yl)phenol (3.15) ^{1}H-NMR (400 MHz, acetone-d6) δ 8.13 (s, 1H), 7.73 – 7.69 (m, 2H), 7.20 (app tr, 1H), 7.07 (s, 1H), 6.96 – 6.87 (m, 3H); ^{13}C-NMR (100 MHz, acetone-d6) δ 157.1, 145.2, 141.0, 129.9, 127.5, 120.0, 117.7, 117.5, 109.4, 100.0; LRMS calculated for $C_{13}H_{10}N_2O_2$ (M+H)$^+$ *m/z*: 227.1, measured 227.1.
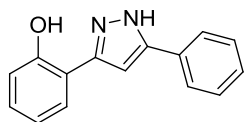
2-(5-phenyl-1H-pyrazol-3-yl)phenol (3.16) ^{1}H-NMR (400 MHz, acetone-d6) δ 7.91 - 7.87 (m, 2H), 7.78 (dd, J=7.74 Hz, 1.62 Hz, 1H), 7.52 (t, J=7.54 Hz, 2H), 7.43 (t, J=7.38 Hz, 1H), 7.27 (s, 1H), 7.21 (app t, 1H), 6.97 - 6.90 (m, 2H); ^{13}C-NMR (150 MHz, acetone-d6) δ 157.2, 153.8, 144.7, 130.0, 129.9, 129.7, 127.6, 126.5, 120.0, 117.7, 117.5, 100.1; LRMS calculated for $C_{15}H_{12}N_2O$ (M+H)$^+$ *m/z*: 237.1, measured 237.1.
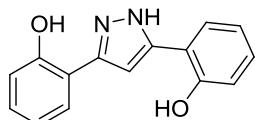
2,2'-(1H-pyrazole-3,5-diyl)diphenol (3.17) ^{1}H-NMR (400 MHz, CD₃OD) δ 7.71 (d, J=7.52 Hz, 2H), 7.19 (t, J=7.58 Hz, 2H), 7.14 (s, 1H), 6.97 – 6.89 (m, 4H); ^{13}C-NMR (100 MHz, CD₃OD) δ 156.4, 130.2, 128.3, 120.7, 117.8, 117.4, 100.4; LRMS calculated for $C_{15}H_{12}N_2O_2$ (M+H)$^+$ *m/z*: 253.1, measured 253.2.
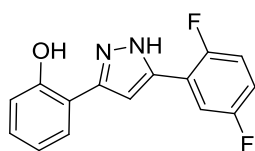
2-(5-(2,5-difluorophenyl)-1H-pyrazol-3-yl)phenol (3.19) ^{1}H-NMR (600 MHz, acetone-d6) δ 9.12 (br s, 1H), 8.62 (br s, 1H), 8.24 (dd, J=7.89 Hz, 1.88 Hz, 1H), 7.79 (dd, J=7.74 Hz, 1.56 Hz, 1H), 7.51 (dd, J=7.59 Hz, 4.83 Hz, 1H), 7.38 (s, 1H), 7.23 (app t, 1H), 6.97 (d, J=8.10 Hz, 1H), 6.94 (t, J=7.30 Hz, 1H); ^{13}C-NMR (150 MHz, acetone-d6) δ 156.9, 150.5, 147.8, 133.5, 130.1, 129.9, 128.1, 127.8, 124.7, 120.2, 118.5, 117.6,117.5, 100.8; LRMS calculated for $C_{15}H_{10}F_2N_2O$ (M+H)$^+$ *m/z*: 273.1, measured 273.1.
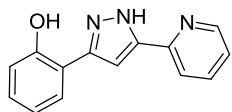
2-(5-(pyridin-2-yl)-1H-pyrazol-3-yl)phenol (3.20) ^{1}H-NMR (400 MHz, acetone-d6) δ 10.93 (br s, 1H), 8.66 (d, J=4.64 Hz, 1H), 8.00 (m, 2H), 7.78

(dd, J=7.72 Hz, 1.56 Hz, 1H), 7.47 (s, 1H), 7.39 (app t, 1H), 7.22 (app t, 1H), 6.97 − 6.90 (m, 2H); ^{13}C-NMR (150 MHz, acetone-d6) δ 150.5, 138.2, 129.9, 127.5, 124.4, 121.3, 120.0, 117.7, 117.6,100.8; LRMS calculated for C$_{1e}$H$_{11}$N$_3$O (M+H)$^+$ m/z: 238.1, measured 238.1.
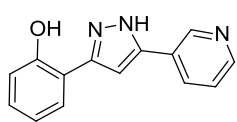
2-(5-(pyridin-3-yl)-1H-pyrazol-3-yl)phenol (3.21) ^{1}H-NMR (400 MHz, acetone-d6) δ 9.12 (s, 1H), 8.62 (br s, 1H), 8.24 (dt, J= 7.96 Hz, 1.92 Hz, 1H), 7.80 (dd, J=7.76 Hz, 1.60 Hz, 1H), 7.51 (br, 1H), 7.38 (br s, 1H), 7.25 − 7.20 (m, 1H), 7.01 − 6.91 (m, 2H); ^{13}C-NMR (150 MHz, DMSO-d6) δ 148.3, 146.4, 132.2, 129.2, 127.5, 123.9, 116.3, 101.4; LRMS calculated for C$_{1e}$H$_{11}$N$_3$O (M+H)$^+$ m/z: 238.1, measured 238.1.
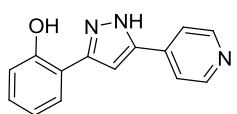
2-(5-(pyridin-4-yl)-1H-pyrazol-3-yl)phenol (3.22) ^{1}H-NMR (600 MHz, DMSO-d6) δ 8.62 (d, J=4.80 Hz, 2H), 7.81 (app d, 2H), 7.72 (d, J=7.32 Hz, 1H), 7.39 (br, 1H), 7.20 (app t, 1H), 6.99 (d, J=7.80 Hz, 1H), 6.92 (app t, 1H); ^{13}C-NMR (150 MHz, DMSO-d6) δ 154.5, 150.2, 129.3,127.3, 119.5, 119.4, 116.4, 102.2; LRMS calculated for C$_{1e}$H$_{11}$N$_3$O (M+H)$^+$ m/z: 238.1, measured 238.1.
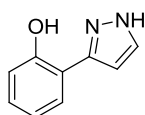
2-(1H-pyrazol-3-yl)phenol (3.23) ^{1}H-NMR (400 MHz, acetone-d6) δ 11.01 (s, 1H), 7.90 (d, J=2.36 Hz, 1H), 7.72 (d, J=7.64 Hz, 1H), 7.19 (t, J=7.64 Hz, 1H), 6.96 − 6.85 (m, 3H); ^{13}C-NMR (100 MHz, acetone-d6) δ 157.0, 130.7, 129.7, 127.4, 127.2, 119.9, 117.9, 117.5, 102.3; LR7MS calculated for C$_9$H$_8$N$_2$O (M+H)$^+$ m/z: 161.1, measured 161.2.
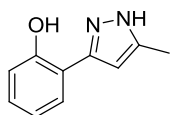
2-(5-methyl-1H-pyrazol-3-yl)phenol (3.24) ^{1}H-NMR (600 MHz, acetone-d6) δ 11.07 (s, 1H), 7.63 (dd, J=7.74 Hz, J=1.50 Hz, 1H), 7.16 (t, J=7.50 Hz, 1H), 6.89 (d, J=8.16 Hz, 1H), 6.86 (t, J=7.50 Hz, 1H), 6.58 (s, 1H), 2.39 (s, 3H); ^{13}C-NMR (150 MHz, acetone-d6) δ 157.2, 129.5, 127.3, 119.8, 118.0, 117.4, 101.6, 10.6; LRMS calculated for C$_{10}$H$_{10}$N$_2$O (M+H)$^+$ m/z: 175.1, measured 175.2.
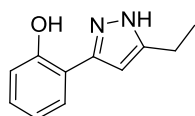
2-(5-ethyl-1H-pyrazol-3-yl)phenol (3.25) ^{1}H-NMR (600 MHz, acetone-d6) δ 12.13 (br s, 1H), 11.09 (br s, 1H), 7.56 (J=7.70 Hz, 1.58 Hz, 1H), 7.16 (app tr, 1H), 6.87 (app q, 1H), 6.62 (s, 1H), 2.79 (q, J=7.60 Hz, 2H), 1.32 (t, J=7.60 Hz, 3H); ^{13}C-NMR (150 MHz, acetone-d6) δ 157.2, 152.8, 147.4, 129.5, 127.3, 119.8, 118.1, 117.4, 117.3, 100.1, 19.3, 13.7; LRMS calculated for $C_{11}H_{12}N_2O$ (M+H)$^+$ *m/z*: 189.1, measured 189.2.
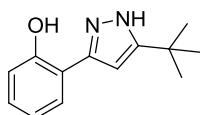
2-(5-(tert-butyl)-1H-pyrazol-3-yl)phenol (3.26) ^{1}H-NMR (600 MHz, acetone-d6) δ 7.68 (dd, J=7.72 Hz, 1.60 Hz, 1H), 7.16 (app t, 1H), 6.91 - 6.84 (m, 1H), 6.65 (s, 1H), 1.42 (s, 9H); ^{13}C-NMR (150 MHz, acetone-d6) δ 157.2, 155.0, 152.4, 129.4, 127.3, 119.6, 118.1, 117.4, 117.3, 98. 6, 31.7, 30.4; LRMS calculated for $C_{13}H_{16}N_2O$ (M+H)$^+$ *m/z*: 217.1, measured 217.1.
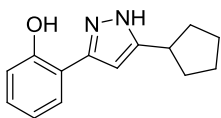
2-(5-cyclopentyl-1H-pyrazol-3-yl)phenol (3.27) ^{1}H-NMR (400 MHz, acetone-d6) δ 12.13 (br, 1H), 11.09 (s, 1H), 7.66 (dd, J=7.72 Hz, 1.60 Hz, 1H), 7.16 (app t, 1H), 6.91 – 6.83 (m, 1H), 6.64 (s, 1H), 3.22 (p, J=7.98 Hz, 1H), 2.19 – 2.10 (m, 2H), 1.85 – 1.66 (m, 6H); ^{13}C-NMR (150 MHz, acetone-d6) δ 157.4, 152.7, 150.2, 129.5, 127.4, 119.6, 118.2, 117.8, 99.5, 33.8, 26.3, 25.7; LRMS calculated for $C_{14}H_{16}N_2O$ (M+H)$^+$ *m/z*: 229.1, measured 229.2.
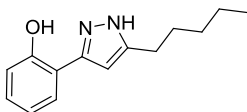
2-(5-pentyl-1H-pyrazol-3-yl)phenol (3.28) ^{1}H-NMR (400 MHz, acetone-d6) δ 7.65 (dd, J=7.70 Hz, 1.56 Hz, 1H), 7.17 (app t, 1H), 6.91 – 6.84 (m, 1H), 6.62 (m, 1H), 2.76 (t, J=7.66 Hz, 2H), 1.74 (br p, 2H), 1.40 – 1.33 (m, 4H), 0.90 (t, J=7.06 Hz, 3H) ^{13}C-NMR (150 MHz, acetone-d6) δ 157.2, 152.9, 146.0, 129.5, 127.3, 119.8, 118.1, 117.4, 100.6, 41.4, 32.1, 25.9, 23.0, 14.2; LRMS calculated for $C_{14}H_{18}N_2O$ (M+H)$^+$ *m/z*: 231.2, measured 231.2.
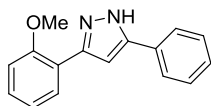
3-(2-methoxyphenyl)-5-phenyl-1H-pyrazole (3.29) ^{1}H-NMR (400 MHz, acetone-d6) δ 7.92 (app d, 2H), 7.87 (app d, 1H), 7.41 (t, J=7.64 Hz, 2H), 7.38 – 7.27 (m, 2H), 7.20 – 7.15 (m, 2H), 7.06 (app t, 1H), 4.04 (s, 3H); ^{13}C-NMR (150 MHz, acetone-d6) δ 157.1, 130.1, 129.4, 128.7, 128.2, 126.2, 121.8, 112.6, 101.6, 56.0; LRMS calculated for $C_{16}H_{14}N_2O$ (M+H)$^+$ *m/z*: 251.1, measured 251.2.
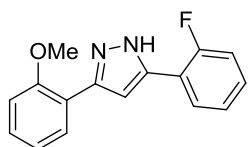
5-(2-fluorophenyl)-3-(2-methoxyphenyl)-1H-pyrazole (3.30) ^{1}H-NMR (400 MHz, acetone-d6) δ 8.09 (br, 1H), 7.85 (d, J=6.84 Hz, 1H), 7.39 – 7.33 (m, 2H), 7.28 – 7.17 (m, 3H), 7.16 (d, J=3.60 Hz, 1H), 7.07 (t, J=7.47 Hz, 1H), 4.04 (s, 3H); ^{13}C-NMR (150 MHz, acetone-d6); δ 157.1, 130.2, 130.0, 129.8, 129.2, 129.1, 128.7, 125.2, 121.9, 116.9, 112.6, 104.7, 56.0; LRMS calculated for $C_{16}H_{13}FN_2O$ (M+H)$^+$ *m/z*: 269.1, measured 269.1.
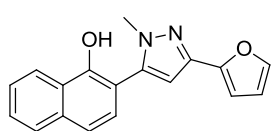
2-(3-(furan-2-yl)-1-methyl-1H-pyrazol-5-yl)naphthalen-1-ol (3.31) ^{1}H-NMR (400 MHz, acetone-d6) δ 8.66 (br, 1H), 8.40 – 8.36 (m, 1H), 7.95 – 7.90 (m, 1H), 7.62 – 7.52 (m, 4H), 7.34 (d, J=8.44 Hz, 1H), 6.70 (d, J=3.80 Hz, 1H), 6.58 (s, 1H), 6.54 (dd, J=3.28 Hz, 1.80 Hz, 1H), 3.77 (s, 3H); ^{13}C-NMR (150 MHz, acetone-d6) δ 151.6, 150.6, 143.7, 142.5,141.4, 136.1, 128.8, 128.6, 127.9, 126.5, 126.2, 123.4, 120.6, 112.1, 111.9, 105.6, 104.9, 37.5; LRMS calculated for $C_{18}H_{15}N_2O_2$ (M+H)$^+$ *m/z*: 291.1, measured 291.2.
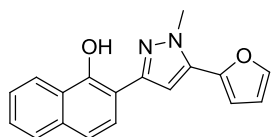
2-(5-(furan-2-yl)-1-methyl-1H-pyrazol-3-yl)naphthalen-1-ol (3.32) ^{1}H-NMR (600 MHz, acetone-d6) δ 8.36 – 8.33 (m, 1H), 7.84 – 7.80 (m, 2H), 7.50 (dt, J=9.72 Hz, 3.36 Hz, 2H), 7.45 (d, J=8.52 Hz, 1H), 7.17 (s, 1H), 6.98 (d, J=3.78 Hz, 1H), 6.69 (dd, J=3.42 Hz, 1.80 Hz, 1H), 4.21 (s, 3H); ^{13}C-NMR (150 MHz, acetone-d6) δ 152.6, 151.4, 145.0, 144.6, 136.2, 135.1, 128.3, 127.4, 126.3,126.0, 124.9, 123.5,

119.7, 112.7, 110.7, 110.4, 102.1, 39.2; LRMS calculated for $C_{18}H_{15}N_2O_2$ $(M+H)^+$ *m/z*: 291.1, measured 291.2.

References

(1) Mike, L. A.; Dutter, B. F.; Stauff, D. L.; Moore, J. L.; Vitko, N. P.; Aranmolate, O.; Kehl-Fie, T. E.; Sullivan, S.; Reid, P. R.; DuBois, J. L.; et al. Activation of Heme Biosynthesis by a Small Molecule That Is Toxic to Fermenting Staphylococcus Aureus. *Proc. Natl. Acad. Sci. U. S. A.* **2013**, *110* (20), 8206–8211.

(2) Allison, K. R.; Brynildsen, M. P.; Collins, J. J. Metabolite-Enabled Eradication of Bacterial Persisters by Aminoglycosides. *Nature* **2011**, *473* (7346), 216–220.

(3) Kohler, C.; von Eiff, C.; Liebeke, M.; McNamara, P. J.; Lalk, M.; Proctor, R. A.; Hecker, M.; Engelmann, S. A Defect in Menadione Biosynthesis Induces Global Changes in Gene Expression in Staphylococcus Aureus. *J. Bacteriol.* **2008**, *190* (19), 6351–6364.

(4) Proctor, R. A.; von Eiff, C.; Kahl, B. C.; Becker, K.; McNamara, P.; Herrmann, M.; Peters, G. Small Colony Variants: A Pathogenic Form of Bacteria That Facilitates Persistent and Recurrent Infections. *Nat. Rev. Microbiol.* **2006**, *4* (4), 295–305.

(5) Fustero, S.; Sánchez-Roselló, M.; Barrio, P.; Simón-Fuentes, A. From 2000 to Mid-2010: A Fruitful Decade for the Synthesis of Pyrazoles. *Chem. Rev.* **2011**, *111* (11), 6984–7034.

(6) Torres, V. J.; Stauff, D. L.; Pishchany, G.; Bezbradica, J. S.; Gordy, L. E.; Iturregui, J.; Anderson, K. L.; Dunman, P. M.; Joyce, S.; Skaar, E. P. A Staphylococcus Aureus Regulatory System That Responds to Host Heme and Modulates Virulence. *Cell Host Microbe* **2007**, *1* (2), 109–119.

(7) Richardson, D. R.; Bernhardt, P. V. Crystal and Molecular Structure of 2-Hydroxy-1-Naphthaldehyde Isonicotinoyl Hydrazone (NIH) and Its iron(III) Complex: An Iron Chelator with Anti-Tumour Activity. *J. Biol. Inorg. Chem.* **1999**, *4* (3), 266–273.

(8)   Schwyn, B.; Neilands, J. B. Universal Chemical Assay for the Detection and Determination of Siderophores. *Anal. Biochem.* **1987**, *160* (1), 47–56.

(9)   Kallander, L. S.; Lu, Q.; Chen, W.; Tomaszek, T.; Yang, G.; Tew, D.; Meek, T. D.; Hofmann, G. A.; Schulz-Pritchard, C. K.; Smith, W. W.; et al. 4-Aryl-1,2,3-Triazole: A Novel Template for a Reversible Methionine Aminopeptidase 2 Inhibitor, Optimized to Inhibit Angiogenesis in Vivo. *J. Med. Chem.* **2005**, *48* (18), 5644–5647.

CHAPTER 4

STRUCTURE-ACTIVITY RELATIONSHIP STUDIES OF '3981

4.1 Introduction

Another molecule identified in the screens for HssRS activators was the thiourea '3981. The chemical structure of '3981 differs significantly from '8882. Preliminary efforts to elucidate the mechanism of activation of HssRS by '3981 were conducted by Matthew Surdel (Skaar lab). These studies revealed that, unlike '8882, '3981 does not require endogenous heme biosynthesis to activate HssRS. It also does not induce an increase in intracellular heme accumulation. In addition, '3981 is not active in anaerobically grown *S. aureus*. '3981 also exhibited considerable toxicity under both aerobic and anaerobic conditions. These results indicate a very different mechanism of HssRS activation from '8882 and that '3981 could be a useful probe to study the mechanism(s) of heme toxicity in *S. aureus* . A library of '3981 derivatives was prepared to determine structure-activity relationships and identify compounds with better activity and toxicity profiles.
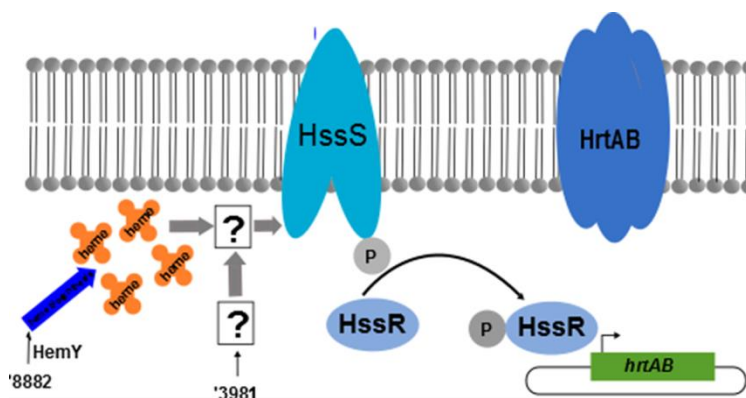
Figure 4.1. Hypothesis of '3981 activation of HssRS.

4.2 Synthesis of '3981 derivatives

The HssRS activating small molecule '3981 is a thiourea composed of N-benzyl and N'-4-biaryl ether groups flanking the central thiocarbonyl. Thioureas are readily synthesized by preparing the isothiocyanate of one amine and reacting that with the second amine.[1] A library of '3981 derivatives was prepared in this manner. First, one component was reacted with thiophosgene in biphasic saturated sodium bicarbonate-DCM to generate the isothiocyanate. The isocyanate in the reaction mixture was divided several times and the corresponding component was added to each sub-reaction to generate several derivatives. The products were purified by either preparative scale HPLC or recrystallization from either hexanes/ethyl acetate or isopropanol. Using this method, 18 derivatives with modifications to the benzylamine component (Figure 4.2) and eight derivatives with modifications to the biaryl ether component (Figure 4.3) were prepared
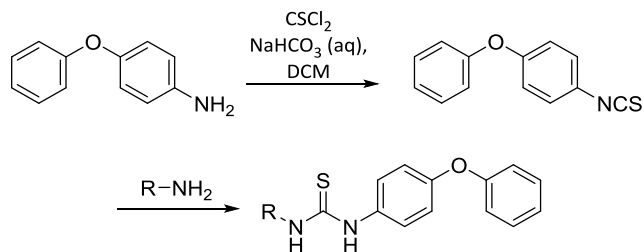
Cmpd	R group	Cmpd	R group
4.2	(4-F phenyl)	4.12	(2-Me phenyl)
4.3	(benzyl)	4.13	(3-Me phenyl)
4.4	(2-F benzyl)	4.14	(4-Me phenyl)
4.5	(3-F benzyl)	4.15	(2-OMe benzyl)
4.6	(2,3-diF benzyl)	4.16	(3-OMe benzyl)
4.7	(2,4-diF benzyl)	4.17	(4-OMe benzyl)
4.8	(2,5-diF benzyl)	4.18	(3-I benzyl)
4.9	(2,6-diF benzyl)	4.19	(4-Cl benzyl)
4.10	(3,4-diF benzyl)		
4.11	(3,5-diF benzyl)		

Figure 4.2. Derivatives of '3981 with modified benzylamine component.

Cmpd	R Group
4.20	phenyl
4.21	4-Me-phenyl
4.22	4-OMe-phenyl
4.23	4-Ph-phenyl
4.24	4-(N-phenylsulfamoyl)phenyl
4.25	2-OPh-phenyl
4.26	3-OPh-phenyl
4.27	adamantyl
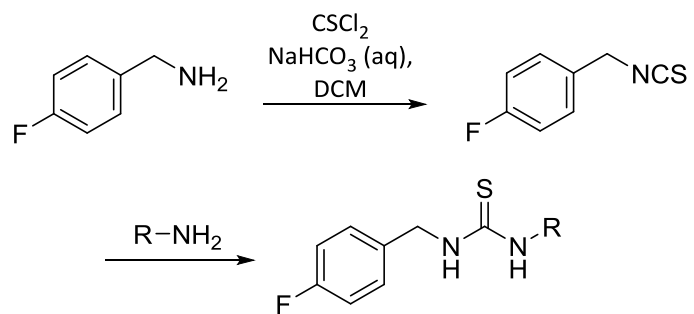
Figure 4.3. Derivatives of '3981 with modified biaryl ether component.

4.3 HssRS activity of '3981 derivatives

Single-point data

The ability of the '3981 derivatives to activate HssRS was determined using the XylE assay. Compounds were screened at the single point concentration of 10 µM due to the toxicity of '3981. The assay was followed as described in chapter 3.
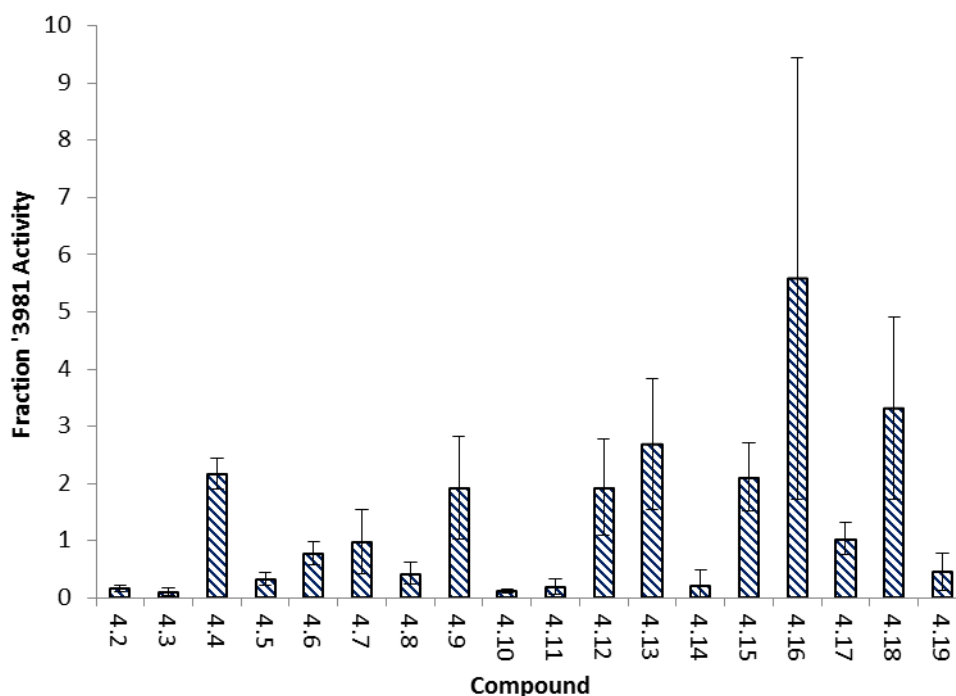
Figure 4.4. Activation of HssRS by **4.2 – 4.19** at 10 µM relative to '3981.

Removal of the benzyl carbon to provide **4.2** resulted in significant loss of activity indicating the benzyl carbon is necessary for activity. Introducing an unsubstituted benzyl group (**4.3**) into the molecule also results in loss of activity indicating that substitution by certain groups is necessary for activity. Movement of the fluorine into the 3-position (**4.5**) is deleterious to activity while movement into the 2-position (**4.4**) increases activity two-fold

compared to '3981 indicating *ortho*-fluorine substitution is favored. The series of di-fluoro substituted compounds (**4.6** – **4.11**) indicates that 3-fluorine substitution is deleterious to activity regardless of the position of the other fluorine. In addition, the di-*ortho* fluorine substituted compound **4.9** exhibited approximately the same level of activity as **4.4** indicating this substitution pattern is not additive or synergistic.

Introduction of methyl or methyl ether groups into the benzyl ring gave different results. In general, 3-substitution resulted in significant increases in activity compared to '3981. The most active of these, **4.16** (which will hereafter be referred to as '7501), routinely exhibited activity 2 – 6x that of '3981. 2-substitution also resulted in compounds more active than '3981 while 4-substitution did not promote activity. In addition, 3-iodo (**4.18**) substitution also resulted in a significant increase in activity.
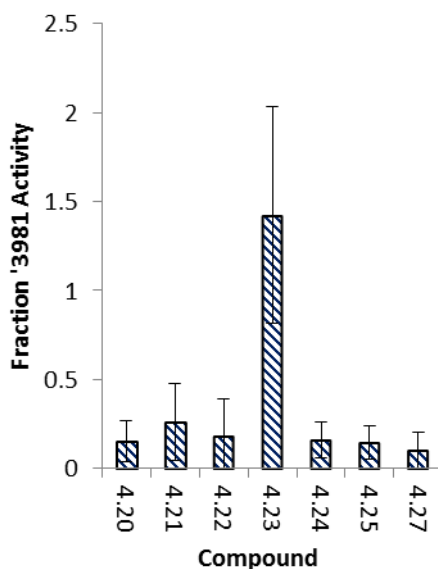
Figure 4.5. Activation of HssRS by **4.20** – **4.27** at 10 μM relative to '3981.

Modification of the biaryl ether component was in general less well tolerated. Replacement with smaller aryl groups including phenyl (**4.20**), 4-methylphenyl (**4.21**), and 4-methoxyphenyl (**4.22**) resulted in significant loss of activity. Movement of the 4-phenoxy moiety to the 2-position (**4.25**) also resulted in loss of activity. Movement to the 3-position (**4.26**) resulted in significant toxicity and as a result, the HssRS activity could not be determined in this screen.   The only modification that was tolerated was replacement of the 4-phenoxyphenyl group with 4-biphenyl. This result suggested that activity is dependent on a large biaryl system in this component of the molecule. Despite this, biaryl sulfonamide **4.23** was not active. Finally, replacement of the biaryl ether system with an adamantlyl group (**4.27**) was also deleterious to activity.

Another modification explored was converting '3981 to a urea by replacing the sulfur with oxygen. This was accomplished by reacting 4-phenoxyaniline with carbonyldiimidazole and reacting the resulting isocyanate with 4-fluorobenzylamine with carbonyldiimidazole.[2] The resulting urea **4.28** demonstrated approximately the same activity as '3981 at 10 µM.
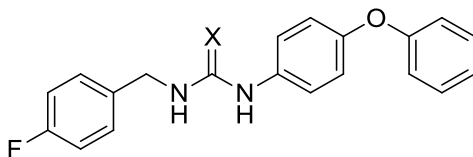
X	Cmpd	Relative HssRS Activity
S	'3981	1
O	**4.28**	0.97

Figure 4.6. Comparison of urea **4.28** activity with '3981.

Concentration response curves

Concentration response curves were generated for '3981 and several of the more active derivatives including **4.9**, **4.12**, **4.13**, **4.15**, '**7501**, **4.18**, and **4.28**. EC$_{50}$s were determined for each of these compounds as a measure of potency. For the most part, these modifications do not significantly affect potency. The only molecule with significantly increased potency was **4.18** with iodine in the 3-position of the benzyl component.

Cmpd	EC$_{50}$ (µM)	pEC$_{50}$ (M)
'3981	3.26	5.49 ± 0.0351
4.9	1.13	5.95
4.12	3.56	5.45 ± 0.196
4.13	6.31	5.20 ± 0.121
4.15	2.91	5.54 ± 0.0911
'7501/**4.16**	4.44	5.35 ± 0.156
4.18	0.78	6.11 ± 0.112
4.28	3.04	5.52

Table 4.1. EC$_{50}$ values for '3981 and derivatives.
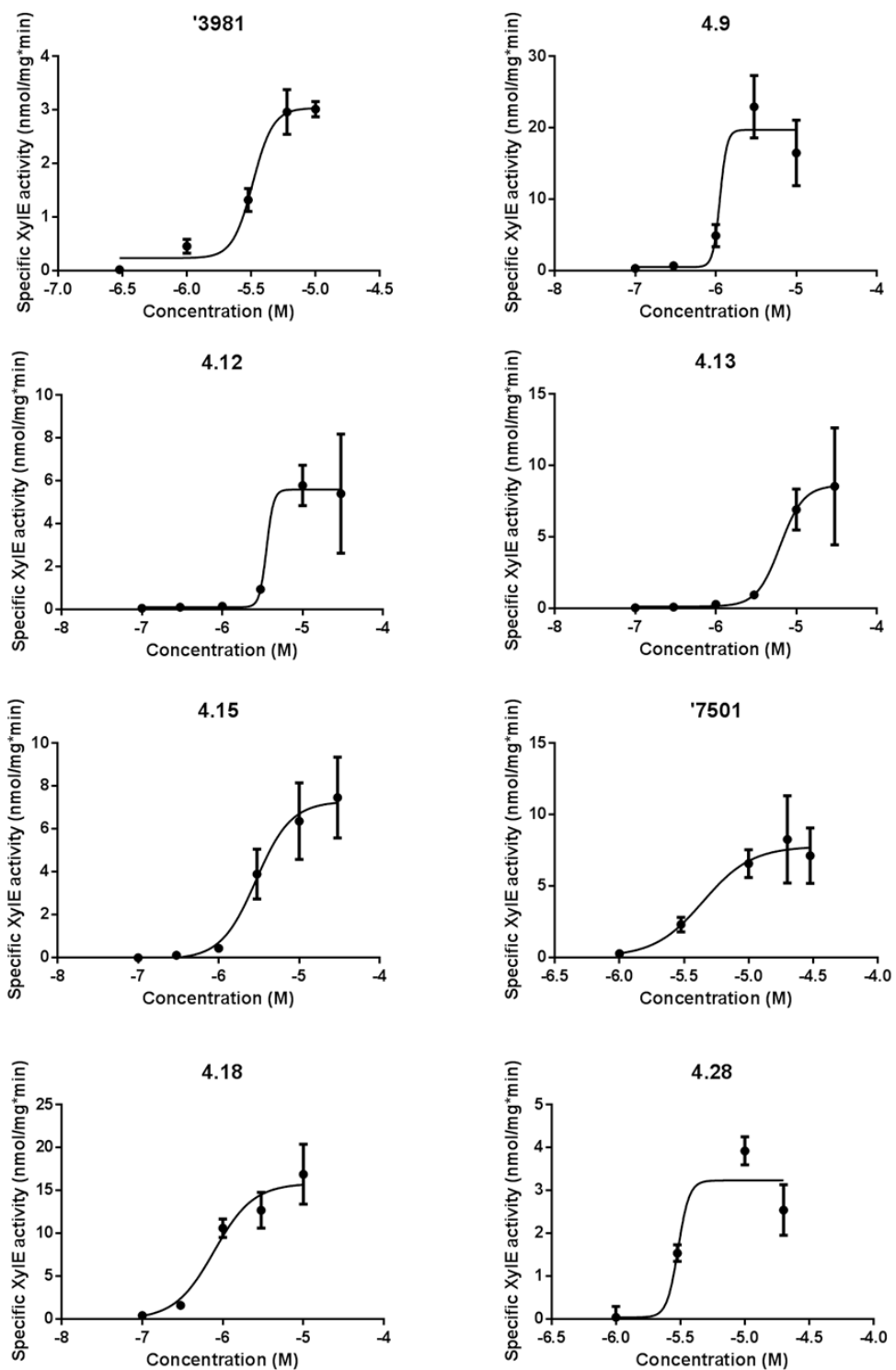
Figure 4.7. Concentration response curves for select '3981 derivatives.

4.4 Conclusions

The results of the SAR study of '3981 indicate that several structural features of the molecule are important for activity. Substituents on the benzyl ring significantly affect activity. Activity is significantly ablated when fluorine is moved to the 3-position. In contrast, moving fluorine to the 2-position increases activity twofold compared to '3981. The series of difluoro compounds further indicates that fluorine in the 3-position is detrimental to activity. Substitution with methyl or methyl ethers in the 2- and 3- positions increases activity compared to '3981 while substitution in the 4-position decreases activity (Me) or does not alter activity (OMe). These results indicate that inductive effects in the benzyl ring are important for activity. This could be important for processes associated with protein binding such as π-cation interactions.

Modification of the 4-biaryl ether was generally not well tolerated. All modification with the exception of substitution with 4-biphenyl resulted in loss of activity compared to '3981. Most modifications were truncation of the biaryl ether, although movement of the phenoxy ether to the 2- and 3- positions also negatively affected activity. These results may suggest that this region of the molecule binds to a hydrophobic pocket of a potential target protein. Altering the 4-biary ether may destabilize this binding leading to a loss of activity.

Experimental Section

General synthesis of thioureas. To a stirred solution of amine A (1.0 eq) in dichloromethane (0.25 M) was added an equal volume of saturated sodium bicarbonate. The resulting biphasic mixture was cooled to 0 °C and stirred vigorously. Thiophosgene (1.0 eq) dissolved in a minimal amount of dichloromethane was added dropwise to the mixture. Once addition was complete, the mixture was stirred vigorously for 30 min at 0 °C. Amine B (1.0 eq) was added to the reaction neat and the reaction was allowed to warm to room temperature. When the reaction was judged complete (TLC or LCMS), it was diluted with dichloromethane, the aqueous layer removed, the organic layer washed with 1 N HCl, brine, and dried (MgSO$_4$). The reaction was concentrated and the residue purified either by preparative scale HPLC or recrystallization from hexanes/ethyl acetate or isopropanol. Yields were generally not determined.

Synthesis of urea 4.28. To a stirred solution of 50.0 mg (0.270 mmol, 1.0 eq) of 4-phenoxyaniline in 1 ml dichloromethane at 0 °C was added 52.5 mg (0.324 mmol, 1.2 eq) of carbonyldiimidazole. The mixture was stirred for 1 h and 35.0 mg (0.270 mmol, 1.0 eq) of 4-fluorobenzylamine was added neat. The reaction was allowed to warm to room temperature and was judged complete by TLC. Volatiles were removed *in vacuo* and the residue purified by preparative scale reverse phase HPLC to provide **4.28**. A yield was not recorded.

References

(1)   Manjula, S. N.; Malleshappa Noolvi, N.; Vipan Parihar, K.; Manohara Reddy, S. A.; Ramani,

        V.; Gadad, A. K.; Singh, G.; Gopalan Kutty, N.; Mallikarjuna Rao, C. Synthesis and

        Antitumor Activity of Optically Active Thiourea and Their 2-Aminobenzothiazole

        Derivatives: A Novel Class of Anticancer Agents. *Eur. J. Med. Chem.* **2009**, *44* (7), 2923–

        2929.

(2)   Padiya, K. J.; Gavade, S.; Kardile, B.; Tiwari, M.; Bajare, S.; Mane, M.; Gaware, V.;

        Varghese, S.; Harel, D.; Kurhade, S. Unprecedented "In Water" imidazole Carbonylation:

        Paradigm Shift for Preparation of Urea and Carbamate. *Org. Lett.* **2012**, *14* (11), 2814–

        2817.

CHAPTER 5

CHEMICAL METHODS OF TARGET IDENTIFICATION

5.1 Background

Modern discovery of bioactive small molecules centers on high throughput screening. The nature of each screen greatly depends on the biological system under study, but in general falls into one of two categories: phenotypic (or cell based forward genetic) screens and biochemical (or reverse genetic) screens.[1] Biochemical screens involve screening molecules against one protein or a system of proteins outside their native environment. The read-out of such a screen is often an assay for enzyme activity or receptor response.[2] This type of screen is useful for identifying molecules that modify the activity of a given protein. However, since the systemic outcome of modification of a protein's activity is difficult to predict, biochemical screens are primarily useful for identifying small molecules whose targets are already well validated in a disease model or whatever biological context is under study. In contrast, phenotypic screens are run with whole cells or organisms and the response of the system is monitored through a reporter that induces a measurable response such as luminescence or fluorescence. This type of screen is advantageous because molecules that induce a specific response can be identified and used as tools to study whole pathways.[1,3]

Despite the potential for phenotypic screens as rich sources of tool compounds and leads for therapeutic development, one major drawback is that the targets of the small molecules, and thus the underlying mechanism of their activity, are frequently unknown. As such, one of the great challenges in chemical biology is to discover the targets of small

molecules identified in phenotypic screens. There are two divergent approaches to small molecule target identification: genetic and chemical. Chemical methods will be discussed in this chapter.

5.2 Chemical methods of target identification

Chemical methods for the identification of targets of bioactive small molecules typically involve the development of a molecule (or set of molecules) called the probe(s). Probes are based on the structure of the original molecule but incorporate additional functional groups that enable target identification. In general, there are two methods that fall under the realm of chemical methods of target identification: affinity purification, which generally relies on noncovalent interaction between the probe and target to purify the target from a complex mixture of proteins; and ligand directed protein labeling, which involves the covalent modification of the target by the probe followed by isolation.[4] These methods and the chemistry frequently utilized to carry them out will be discussed below.
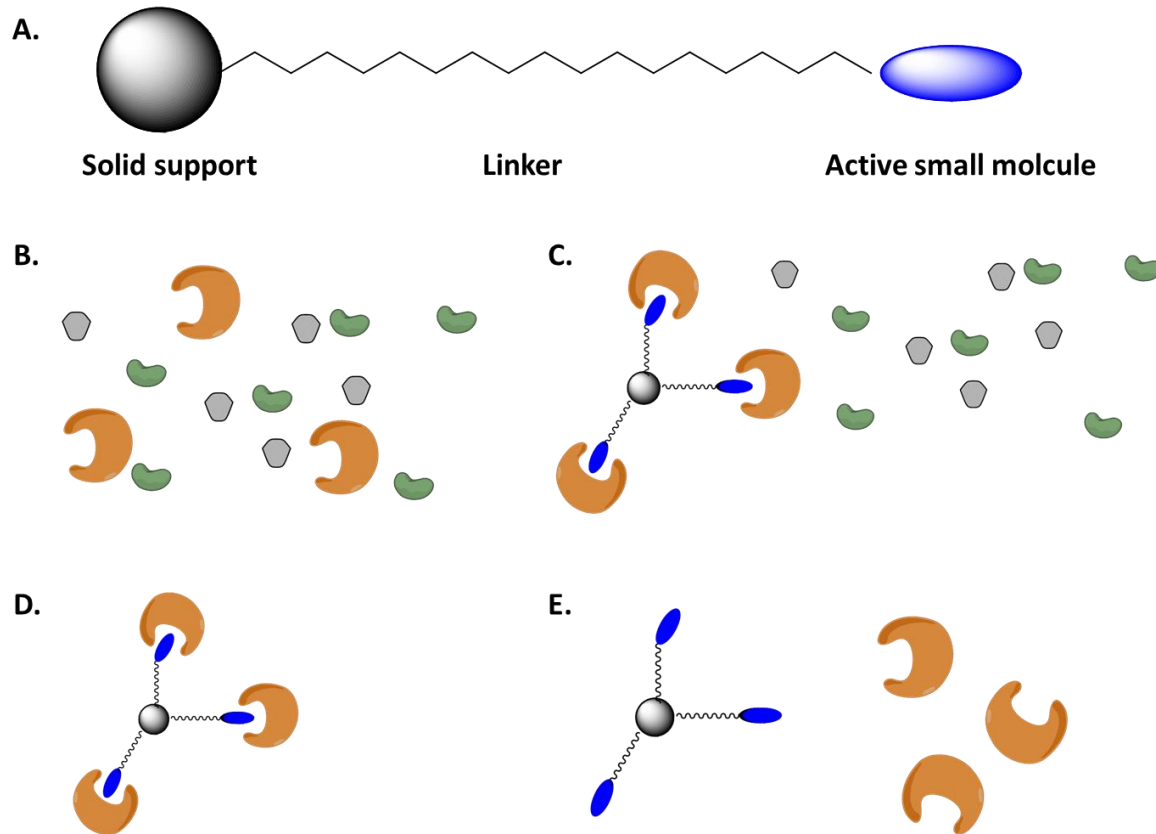
Figure 5.1. Scheme representing the affinity purification process. A. General structure of an affinity purification probe. The process begins with a complex mixture of proteins (B), usually a lysate. The lysate is incubated with the probe and the target proteins (orange) bind (C) while non-target proteins do not and are washed away (D). Finally the target proteins are eluted from probe (E).

Affinity Purification

The general method of affinity purification is depicted in Figure 5.1. The underlying principle of this method is a molecule will have a higher affinity for its target than other non-target proteins. A typical affinity purification experiment involves immobilization of an active molecule on a solid support, passage of a complex mixture of proteins of biological interest over the probe matrix, washing the matrix to remove nonspecifically bound (non-target) proteins, and elution of specifically bound (target) proteins from the solid matrix followed by

visualization and identification.[4,5] In practice, the affinity pulldown experiment is much more nuanced and several factors must be optimized.

Given a bioactive small molecule with an unknown target, the first step in any affinity pulldown experiment is determining structure-activity relationships (SAR) to identify positions in the molecule that can be modified while maintaining activity. This will help determine where a linker for immobilization can be placed.[4] Placement of this linker is important and can significantly affect the results. Heck and coworkers conducted affinity pulldown experiments with two probes of cGMP, each with different points of linker attachment. While their results overlapped to some degree, there were differences in the proteins each probe pulled down.[6]

The type of linker used is also an important consideration. The purpose of a linker is to extend the immobilized small molecule far enough from the solid support so as to not hinder binding of proteins.[4] A variety of linkers have been prepared and utilized for affinity purification experiments. The simplest linker is a long alkyl chain. However, the hydrophobic nature of alkyl chains is thought to promote nonspecific binding of proteins in a lysate. Therefore, more hydrophllic linkers such as polyethylene glycols are frequently used. In addition, more structurally complex linkers such as polyprolines, which form a rod shaped structure, have been used to prevent nonspecific binding.[4,5,7]

Many solid supports are available for conducting affinity purification experiments. Several activated resins are commercially available that can be reacted with a probe to form a covalent linkage. For example, NHS ester activated resins can be reacted with molecule-linker conjugates with terminal amines to covalently link the probe via amide bond formation. A very popular solid support for affinity purification is streptavidin proteins immobilized to a bead. The

small molecule is immobilized through a linkage with biotin. The biotin-streptavidin dissociation constant is very small and represents one of the strongest noncovalent interactions in nature.[4,5] Many probes are constructed with the active compound at one end of the linker and a biotin moiety at the other end for immobilization on streptavidin beads.

A typical affinity purification experiment (Figure 5.1) consists of a binding step, where the protein mixture of interest (usually a lysate) is incubated with the immobilized probe. The solid support is then subjected to several washes to remove nonspecifically bound proteins. Because the binding between probe and target is not covalent, these washes are typically not harsh. After sufficient washing, the bound proteins are eluted from the solid support. This frequently involves heating in a detergent such as SDS. While this method is effective, it will also elute nonspecifically bound proteins that were not removed in the washing step. An alternative elution strategy is to use the active compound itself. For example, the beads can be incubated with free compound which will compete with the probe for binding to the target and effectively remove the protein from the solid support-probe complex.[4,5]

Another strategy for reducing the number of nonspecifically bound proteins during an elution step is the use of selectively cleavable linkers. This method utilizes a functional group usually placed somewhere on the linker between the probe and solid support. The linker can undergo a reaction that will induce cleavage thus separating the probe and any bound proteins from the solid support. The cleavage conditions are generally quite mild and do not interfere with protein-protein interactions. Functional groups that have been used include; disulfide bonds which can be cleaved by reduction or thiol exchange, ortho-nitrobenzyl esters which can be cleaved by irradiation with 365 nm light, and siloxy ethers which can be cleaved under mildly

acidic conditions. The extent to which cleavable linkers decrease the amount of nonspecifically bound proteins in the elution step varies depending on the cleavable functionality. For example, disulfide cleavable linkers can undergo thiol exchange with cysteine residues in proteins during the binding step leading to poor enrichment of target proteins and high background.[8,9]

A critical component of affinity purification experiments are the use of proper controls. A good control will help distinguish specific interaction with the probe from nonspecific interactions. Some controls simply involve capping the linker with a small functional group such as an acetyl group. More elaborate controls commonly consist of attaching molecules deemed inactive by SAR or in the case of chiral molecules, the enantiomer (which is frequently not active).[4,5]

While many successful target identifications have been conducted using the affinity purification strategy, this method does have its limitations. Even with proper solid support and linker choice, a high affinity probe, and excellent controls, nonspecific protein binding is common. In particular, high abundance proteins are difficult to completely remove in a pulldown experiment. This can convolute the target identification process, and is especially problematic when the target is a protein of low abundance.[4,5]
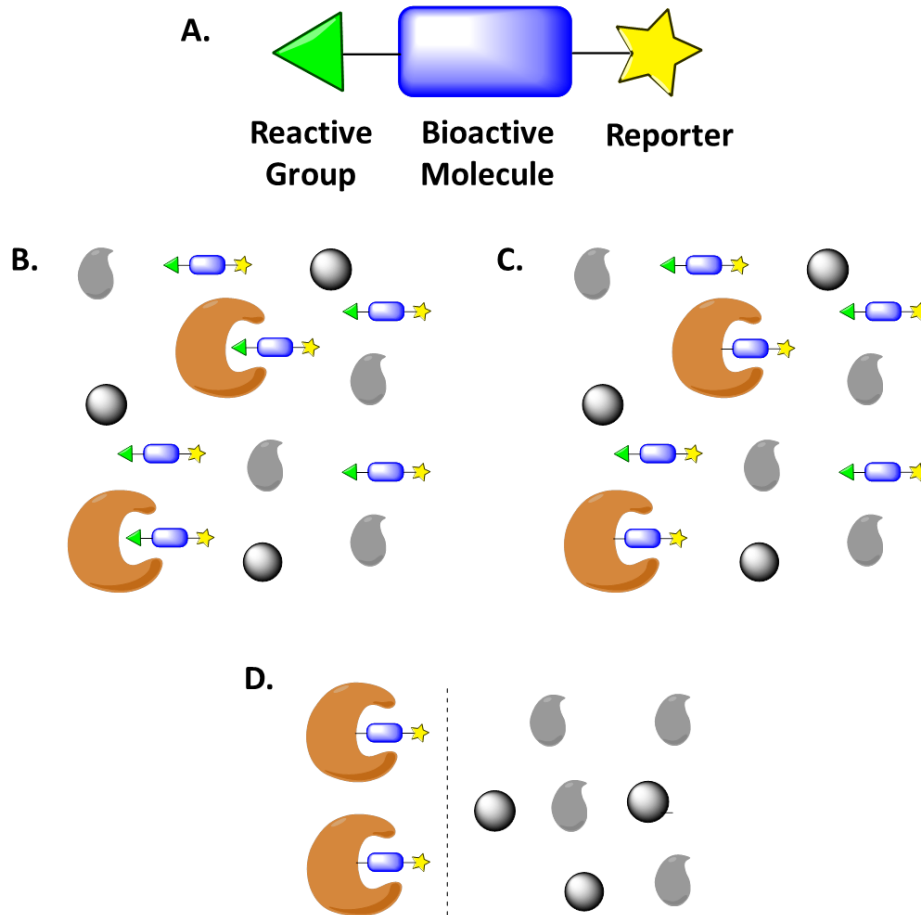
Figure 5.2. General overview of ligand-directed target identification. (A) General structure of a probe for this experiment. (B) A sample, either in vivo or in a lysate, is treated with the probe which associates with target proteins. (C) The reactive group covalently modifies the target and (D) the tagged fractions are isolated from the rest of the sample by use of a reporter group.

Ligand directed target identification

Like affinity purification, probes used for ligand-directed target identification are based on the structure of the molecule of interest, but instead of a site for immobilization, they contain a functional group that is capable of covalently linking to a protein of interest. The underlying theory of this method is that the probe will have a higher affinity for, and will covalently label, a larger population of target proteins over nontarget proteins (Figure 5.2).[4] A critical component of such a probe is a reporter that will allow downstream identification of

labeled proteins. Probes of this sort frequently contain biotin handles or a fluorophore that can be identified by streptavidin binding or in-gel fluorescence, respectively. These handles can be quite large and may affect the activity of the molecule if incorporated into the probe. To overcome this, smaller reporter groups can be utilized. Radiolabels such as ^{3}H, ^{14}C and ^{125}I have proven to be excellent reporters as they can be incorporated into the molecule without significantly modifying the structure. Another common method is incorporation of handles for click chemistry, primarily azides or alkynes, into the molecule. These are relatively small functional groups that are compatible with most biological systems and allow downstream incorporation of larger reporter groups.[10] Click chemistry and its use in target identification experiments will be discussed further in section 5.4.

Many methods of residue selective chemical modification of proteins[11] have been developed and can be used for target identification (Figure 5.3). For example, vinyl sulfones can be incorporated into molecules for adduction to cysteine residues. Their reactivity can also be modulated by varying substituents on the alkene.[12] Despite high selectivity, use of these functional groups in target identification may be undesirable since generally very little is known about the binding site and the residue required for adduction may not be present in the binding site or may be in an undesirable orientation to react with the probe.

An alternate strategy is to incorporate a normally unreactive functional group that can be activated under specific conditions to generate a reactive intermediate. This is most commonly accomplished by use of a photoaffinity label (PAL). A PAL is a functional group that is normally inert toward the biological system, but upon activation by an appropriate wavelength

of light, generates a very reactive intermediate that can covalently modify a protein.[13,14] PALs will be discussed further in section 5.3.

Ligand directed target identification offers several advantages over affinity purification. Because the probe does not need to be immobilized, the labeling step can be conducted *in vivo* which may provide a more biologically relevant result than experiments in a lysate. Functional groups used for labeling and downstream fraction identification are generally much smaller than the linkers needed for immobilization and may prevent significant loss of activity when incorporated into a probe.[4]
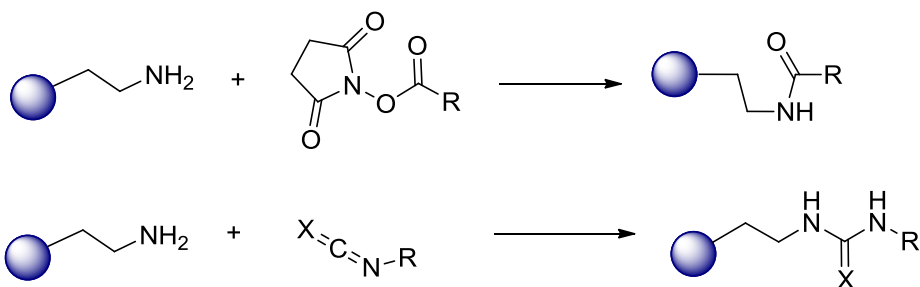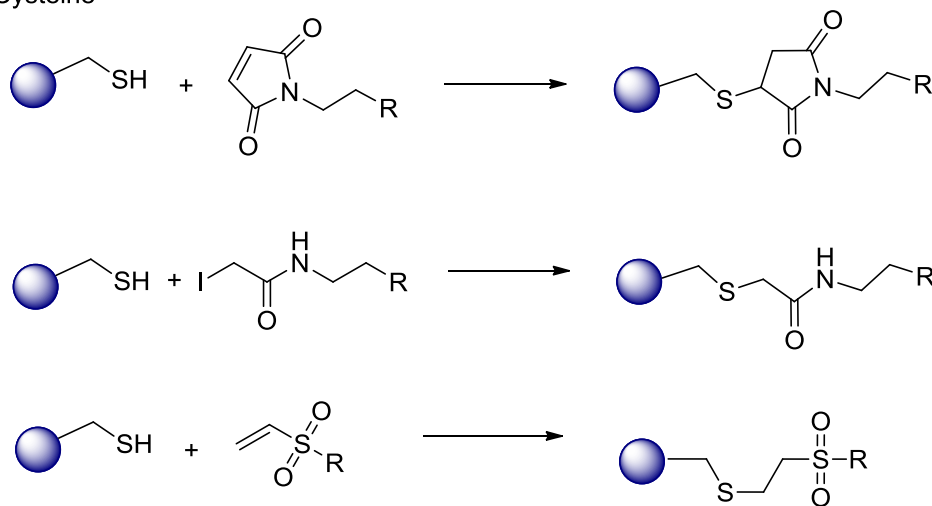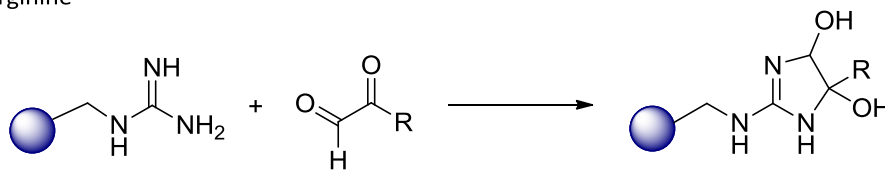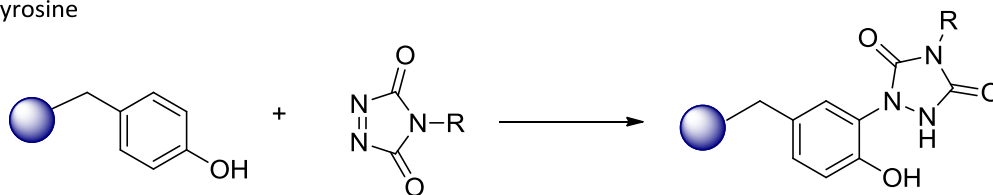
Figure 5.3. Examples of functional groups used for site specific labeling of proteins.

Miscellaneous methods

In addition to the methods described above, several other chemical methods of target identification have been proposed. Emili and coworkers described a method they call target identification by chromatographic coelution (TICC). The premise of this method is that when a protein is bound to a compound, it will have a different HPLC retention time. By comparing an untreated to compound treated lysate, fractions whose retention times differed may be targets of the molecule and later identified using proteomics. The primary advantage of this method is the target can be identified without the need to develop probes.[15]

Another method called drug affinity responsive target stability (DARTS) is based on the idea that when a compound binds to a protein, the protein may be more stable towards processes such as proteolysis or chemical denaturation. In this experiment, a lysate can be treated with a bioactive compound, exposed to proteolytic or denaturing conditions, and the ratio of surviving proteins compared to an untreated control determined to identify targets.[4]

5.3 Photoaffinity probes

The concept of labeling biomolecules by generation of reactive intermediates from photoreactive functional groups was first introduced in the 1960s.[16] Since then, photoaffinity labeling has been extensively used in chemical biology for target identification, the study of protein-protein interactions, and compound binding studies. The three most commonly used functional groups for PAL experiments are aryl azides, the benzophenones, and diazirines. While they differ in several key properties which will be discussed below, they are all stable in

most biological systems (particularly when light is excluded) and they each generate reactive intermediates when exposed to the appropriate wavelength of light.[13,10]

Aryl azides

Aryl azides are convenient photoaffinity reagents due to the ease with which they can be incorporated into molecules. The azide moiety is relatively small and thus generally does not significantly alter the activity of a molecule. When exposed to 250-280 nm light, aryl azides are excited to a singlet state. This can either expel nitrogen and generate a singlet nitrene or undergo intersystem crossing (ISC) to a triplet state which can eliminate nitrogen generating a triplet nitrene. While in theory, the singlet nitrene can undergo insertion reactions; its fate depends on the other substituents of the aryl ring. When hydrogens are *ortho* to the singlet nitrene, insertion reactions are typically not observed. Instead, the molecule either rapidly undergoes a rearrangement to the didehydroazepine or converts to the triplet nitrene through ISC. The didehydroazepine generated is potentially of use in photoaffinity labeling and can react with sufficiently nucleophilic amino acids such as cysteine and histidine. However, oxygen nucleophiles and protonated lysine typically do not react. Kohn and coworkers developed probes for target identification of the anti-epileptic drug lacosamide. One probe contained an arylazide photoaffinity label and the other used an isothiocyanate in the same position as the azide on the aryl ring. Despite the azide probe being significantly more active, the isothiocyanate probe allowed successful target identification. This result underscores the potential complications posed by the ring expansion.[17] When both *ortho* substituents are fluorine, the rearrangement is suppressed and the singlet nitrene can undergo insertion reactions. Triplet nitrene can react with molecules through hydrogen abstraction and resulting

radical chemistry (Scheme 5.1) Aside from the potential inability of nonfluorine substituted aryl azides to undergo insertion reactions, another major drawback of their use is the short wavelengths needed to excite them have the potential to damage biomacromolecules.[13,14,18]
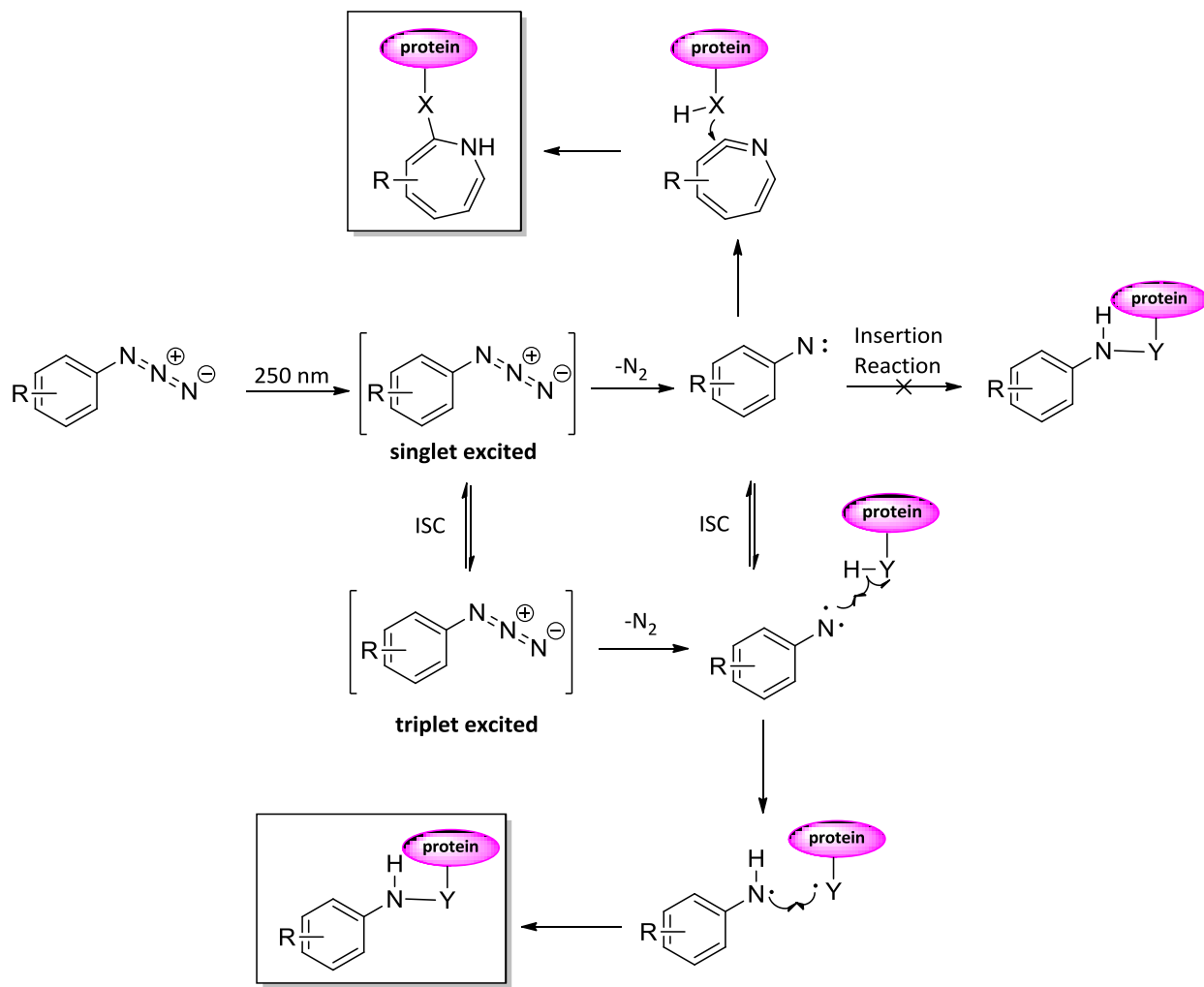
Scheme 5.1. Photoaffinity labeling by aryl azides. (X = N,S; Y = C, N, O, S)

Benzophenones

Benzophenones can be excited to ketyl radicals with ~350 nm light. The excited intermediate can adduct proteins through hydrogen abstraction and resulting radical chemistry

(Scheme 5.2). While they are relatively large, they can be easily incorporated into certain bioactive molecules. One major disadvantage of benzophenones as photoaffinity labels is they require relatively long irradiation times. While 350 nm light typically does not damage biomacromolecules, the long irradiation times tend to lead to nonspecific labeling of proteins.[13]
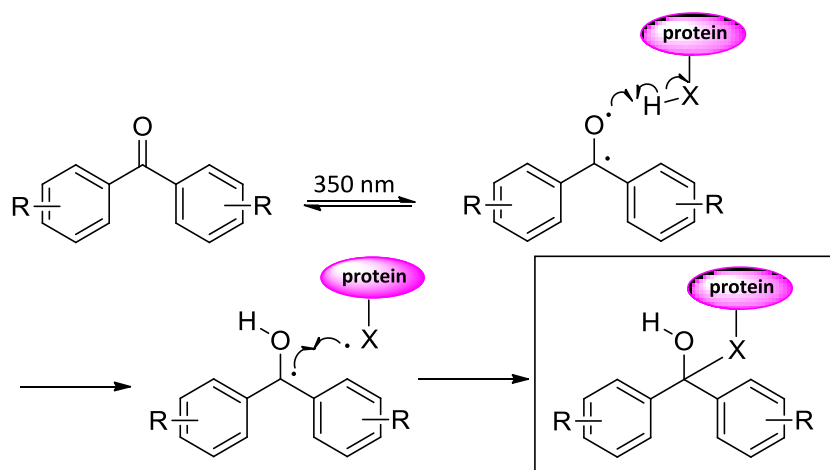
Scheme 5.2. Photoaffinity labeling by benzophenones. (X = C, N, O, S)

Diazirines

Diazirines are three membered heterocycles composed of one carbon atom bonded to two nitrogen atoms that are double bonded to each other. Upon irradiation with ~365 nm light, they either eject nitrogen to generate a reactive carbene or isomerize to the diazo compound (Scheme 5.3). Which pathway predominates and the nature of the carbene generated depends greatly on the substitution of the diazirine carbon. Aryl trifluoromethyl diazirines tend to suppress isomerization pathway and promote carbene formation. For this reason, they are predominantly used in photoaffinity labeling experiments, though aliphatic diazirines have also been successfully used.[13,16]
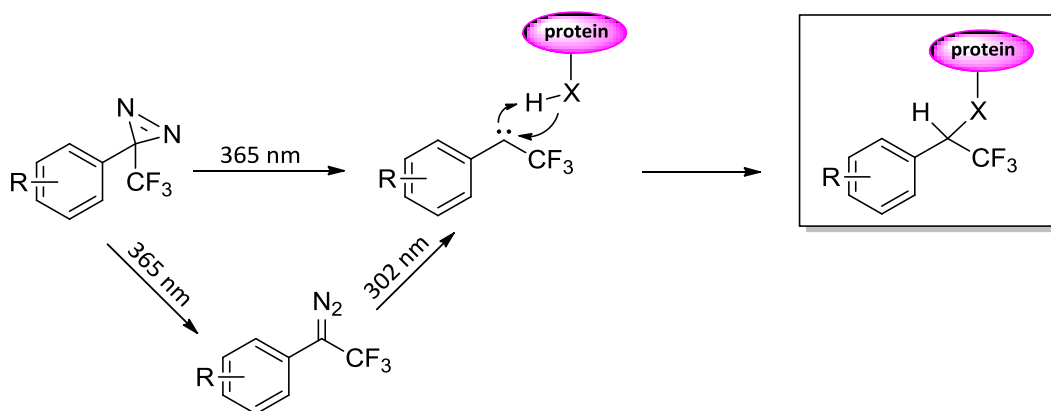
Scheme 5.3. Photoaffinity labeling by aryltrifluoromethyl diazrines. (X = C, N, O, S)

5.4 Click Chemistry and Bioorthogonal Reactions

The concept of click chemistry was introduced by Sharpless as a set of reactions with certain properties such as high yielding, modular, wide in scope, and easy to conduct.[19] The reaction most synonymous with click chemistry is the copper(I) catalyzed Huisgen 1,3 dipolarcycloaddition between an azide and an alkyne. Due to the stability of alkynes and azides in biological systems and the ability to conduct this reaction in aqueous solutions, this reaction has been described as bioorthogonal and has been extensively utilized and expanded on to study biology. In particular, azides and alkynes (and other clickable groups) have been utilized as handles for affinity purification and ligand directed target identification experiments.[20]

Copper catalyzed azide alkyne cycloaddition (CuAAC)

The canonical click reaction, while capable of occurring thermally, occurs best under Cu(I) catalysis. Cu(I) is not particularly stable in aqueous solutions and direct use of its salts without stabilizing ligands is generally not practiced. Instead, Cu(II) salts are used with a co-reductant. Sodium ascorbate is predominantly used for this purpose though other reducing

agents including TCEP and hydrazine have been employed. Despite the use of co-reductants, Cu(I) produces reactive oxygen species in aqueous solutions. This presents certain challenges for bioconjugation reactions because of the potential for damage to biomacromolecules. Several ligands have been developed that stabilize the Cu(I) oxidation state and are essential in biological click reactions. Another complicating factor for click reactions using sodium ascorbate as co-reductant in biological systems is the dehydroascorbate produced from sodium ascorbate reduction of Cu(II) can adduct certain protein residues such as lysine and arginine.[20] Finn and coworkers have extensively studied the click reaction for bioconjugations and have determined generally optimal conditions to suppress the negative aspects of CuAAC including the use of tris-triazole Cu(I) ligands and aminoguanidine as a dehydroascorbate scavenger.[21]

Strain promoted azide alkyne cycloaddition (SPAAC)

Since the majority of issues with CuAAC bioconjugation arise from the presence of Cu(I), researchers have devised methods for metal-free click reactions. The best developed of these is the strain promoted azide alkyne cycloaddition (SPAAC) developed by Bertozzi and co-workers. This method makes use of the reactive nature of alkynes incorporated in eight membered rings. These molecules are highly strained and cycloadditons with dipoles is favored since this will alleviate strain. Several cyclooctyne click reagents have been developed with varying substituents to improve the reactivitiy in the click reaction. Despite not needing metal catalysis, these reactions are 10 – 100 times slower than the Cu(I) catalyzed counterpart. In addition, certain biological nucleophiles such as thiols and sulfenic acids have been reported to react with cyclooctynes.[20]

Alternate click reactions

Several methods mirroring the selective and bioorthogonal nature of the canonical azide-alkyne click have been developed with other functional groups. One such method utilizes Pd-mediated cross couplings for bioconjugations. Several Pd cross coupling reactions have been utilized to this end, including the Heck, Suzuki, and Sonogashira couplings.[22,23,24] These reactions have enabled the use of aryl iodides, terminal alkenes, and boronic acids to be used as click handles. In addition, to Pd cross-coupling chemistry, cross metathesis has also been used for bioconjugation.[20]

Copper-catalyzed azide alkyne click (CuAAC)
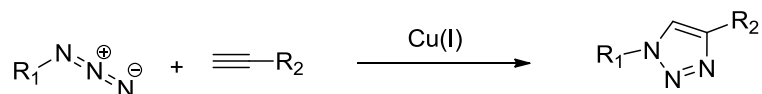
Strain promoted azide alkyne click (SPAAC)
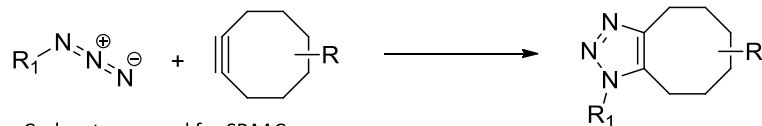
Clicooctynes used for SPAAC
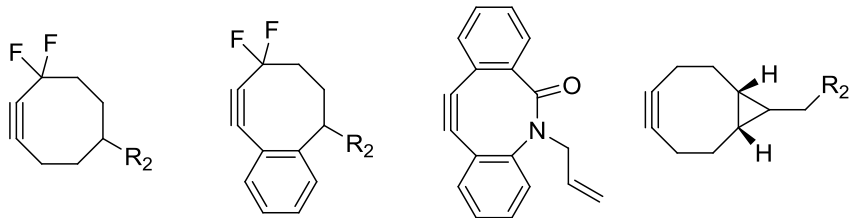
Palladium-catalyzed click reactions

Heck
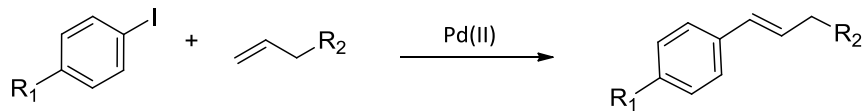
Sonogashira
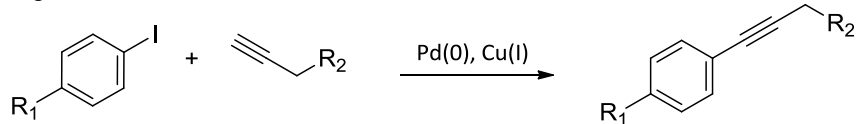
Suzuki
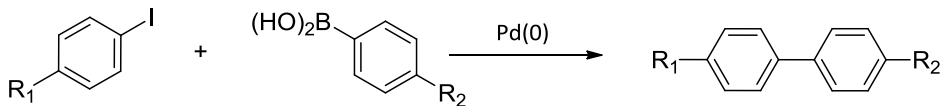
Tetrazine click reactions
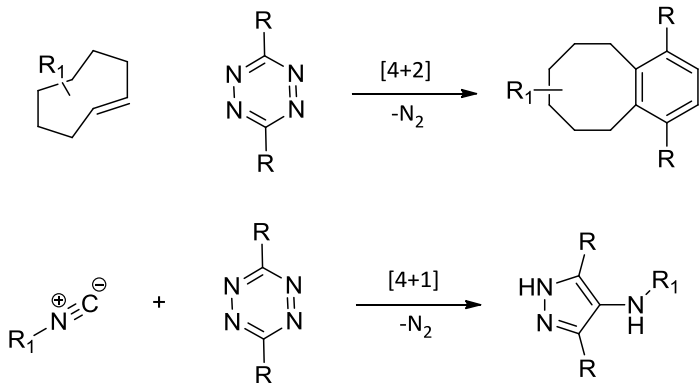
Figure 5.4. Bioorthogonal click reactions

136

In addition to these metal-catalyzed reactions, metal-free click reactions (aside from cyclooctyne reactions) have also been developed with different functional groups as click handles. One class of these reactions utilizes tetrazines which react with a variety of strained alkenes and alkynes in reverse-electron demand-Diels-Alder reactions followed by retro-Diels-Alder to eliminate nitrogen. These reactions occur with considerably high rate constants. In addition to undergoing [4+2] reactions, tetrazines also undergo [4+1] cycloadditons with isonitriles again followed by retro-Diels-Alder reaction to release nitrogen.[20]

5.5 Quantitative proteomic methods for target identification experiments

A crucial component of target identification by chemical methods is proteomic identification and quantification of probe and control samples. This is such an important component of chemical methods of target identification that the process is often referred to as chemical proteomics. Proteins are typically identified by shotgun proteomics and many methods for sample preparation, high resolution tandem mass spectrum acquisition, and data analysis have been developed.[25]

A more challenging aspect is the quantification of proteins obtained in target identification experiments. Accurately discerning enrichment in a probe treated sample vs. control is of paramount importance in target identification. One of the major sources of error in the quantification of proteins in target identification experiments is in the post ligand directed or affinity purification sample handling. Since the samples must be kept separate, any manipulation introduces error and may skew the results and provide misleading data. Several methods have been developed to overcome this by combining the probe and control sample

into one so they are handled together, but introducing conditions that allow the ratios of proteins from each condition to be discerned. Stable isotope labeling by amino acids in cell culture (SILAC) involves incorporation of heavy amino acids into a protein sample by supplementing the media cells are grown in with stable isotope-labeled amino acids. This requires the organism be auxotrophic for the heavy labeled amino acids and require several rounds of cell division to fully incorporate the heavy amino acids into the proteome. A target identification experiment can then be conducted with the heavy proteome used for one condition and an unlabeled "light" proteome used for the second condition. The samples can then be combined, processed, subjected to shotgun proteomics, and quantified by observing the ratio of heavy to light peptides. While SILAC is a very powerful tool in quantitative proteomics, heavy amino acids can be quite expensive and the process is not applicable to all biological systems. Methods to exogenously label protein samples after target identification experiments have been developed. Isotopically coded affinity tags (ICAT) consist of a biotin moiety, a light or heavy labeled linker, and a thiol reactive group. Samples are treated with either the light or heavy labeled ICAT reagents which covalently link to proteins through cysteine residues, the samples processed, and protein ratios determined by observing the ratio of heavy to light tags. In a similar approach, isobaric tags for relative and absolute quantitation (ITRAQ) reagents consist of a reporter group (an isotopically labeled piperazine), a balance group (isotopically labeled carbonyl), and an NHS-ester. Proteins or peptides are treated with the ITRAQ reagent and labeled at the N-terminus by amide bond formation through the NHS ester. Quantification is possible using collision induced dissociation (CID) where the reporter tag will fly off. Up to four samples can be analyzed at once using ITRAQ reagents. In addition to

138

these labeling approaches, label-free techniques such as spectral counting are frequently used to quantify proteins in target identification experiments.[4,26]

5.6 Examples of target identification experiments in bacteria

The following are examples of chemical probes used for the target identification of small molecules active in bacteria. Several of the procedures for affinity pulldowns, photoaffinity labeling, and click chemistry have been applied to my work on target identification that will be described in chapters six and seven.

Identification of the binding site of oxazolidinone antibiotics

Oxazolidinones are a class of synthetic antibiotics represented by linezolid (**5.1**) and eperozilid (**5.2**) that inhibit bacterial growth by interfering with ribosomal protein synthesis. While the ribosome was well established as the target of oxazolidinones, the binding site within the ribosome was not. The ribosome is a large multicomponent complex composed of proteins and nucleic acids that work together to translate mRNA into proteins through several stages. Many early studies of the mechanism of action of oxazolidinone antibiotics relied on either *in vivo* genetic studies or biochemical studies of reconstituted components of the ribosome. These studies gave conflicting results. Colca and coworkers devised an oxazolidinone photoaffinity probe containing an aryl azide as the photoreactive group and a radiolabel as the reporter to identify which component of the ribosome this class of antibiotics binds to. Using SAR data, they designed photoaffinity probe **5.4** with an ^{125}I radiolabel. This probe maintained an MIC < 10 µM against *S. aureus*.[27]
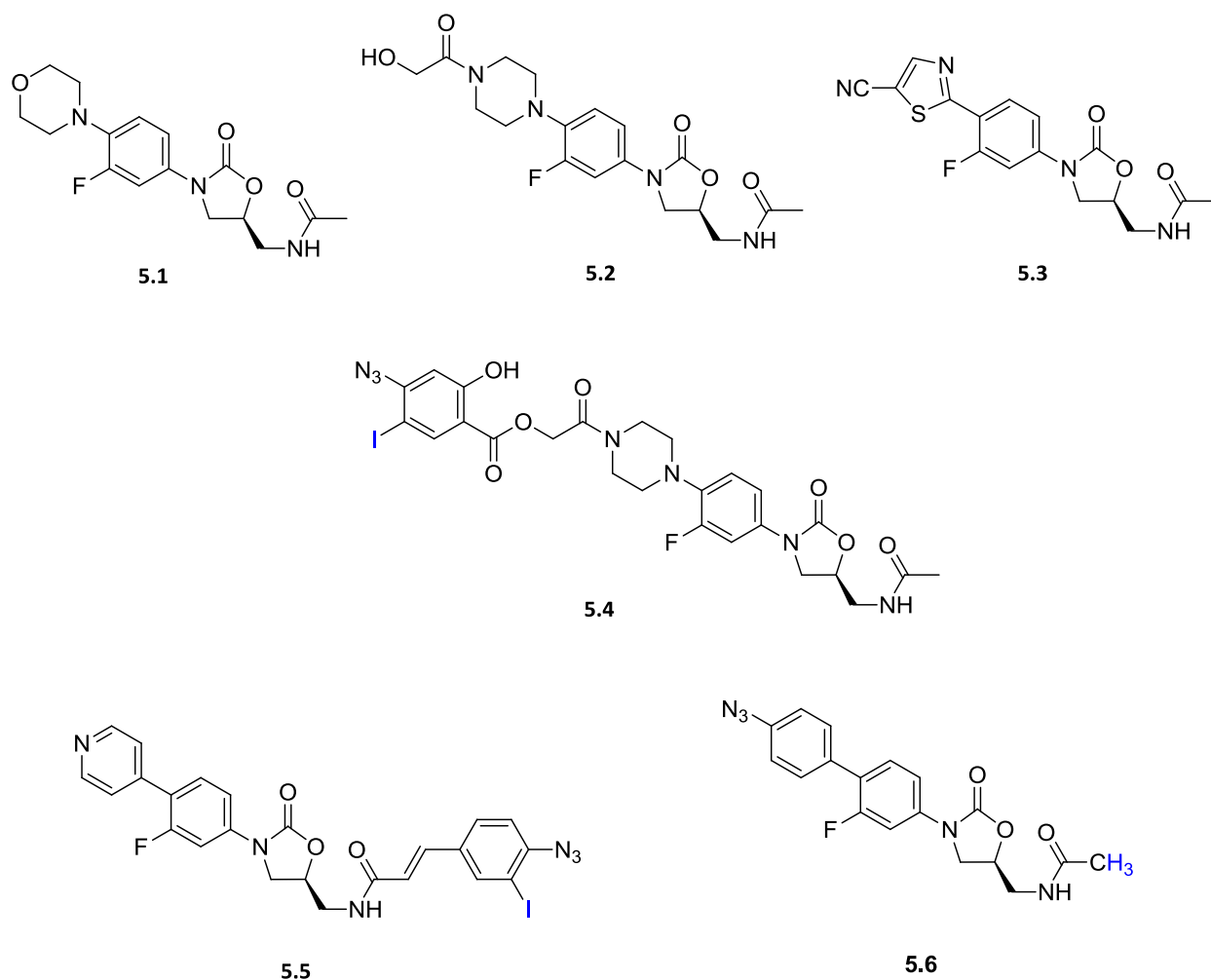
Figure 5.5. Oxazolidinones and derived photoaffinity probes. Radiolabels in blue.

The authors incubated *S. aureus* in exponential phase with 2 μM of **5.4** for 30 minutes either alone, with 40 μM **5.2** as a competitor, or 40 μM of the enantiomer of **5.2** (which is not active against *S. aureus*). The crosslinking was accomplished by irradiation with 254 nm light for 2.1 minutes in a Stratalinker device. The cells were lysed and the RNA and protein fractions were isolated, run on gels, and visualized by autoradiography to identify sites of cross-linking. They observed crosslinking to the 23S rRNA subunit, a tRNA, and two proteins, L27 and LepA.

Labeling of all of these by the probe was competed off by cotreatment with **5.2** but not competed when its enantiomer was present. They concluded from these results that oxazolidinones act on the peptidyl transferase complex (PTC) of the ribosome.[27]

In a follow up study, the authors introduced probes **5.5** and **5.6** with the azides and radiolabels placed in different parts of the molecule to better study the binding site of oxazoldinones in the PTC. Using the same crosslinking conditions as previously described, they used the three probes to map the binding site. From this information, they created a model whereby oxazolidinones occupy the A-site of the PTC which effectively blocks the binding of aminoacyl-tRNAs leading to inhibition of protein synthesis.[28]

Affinity purification to identify the target of salicylidene acylhydrazides

Salicylidene acylhydrazides such as **5.7** and **5.8** were identified as inhibitors of Gram negative bacterial type 3 secretion systems (T3SS) and exhibit *in vitro* and *in vivo* reduction of bacterial virulence. Despite activity related to T3SS inhibition, the mechanism of action of salicylidene acylhydrazide was not known. Elofson, Roe, and coworkers utilized affinity purification probe **5.9** to identify proteins that bind salicylidene acylhydrazides. [29]
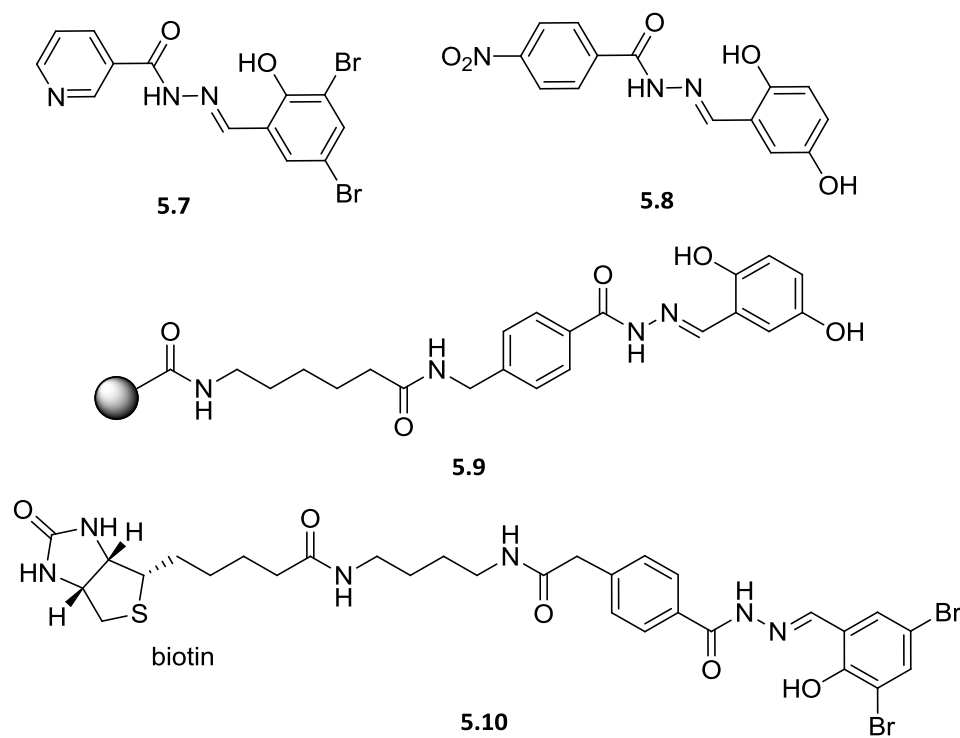
Figure 5.6. Salicylidene acylhydrazide inhibitors of bacterial T3SS and affinity purification probes.

Affinity probe **5.9** was based on the structure of **5.8** with the nitro group replaced by a linker. The solid support used was an NHS ester activated agarose bead (Affi-Gel) and linked to the probe through amide bond formation with the terminal amine of the probe linker. Whole cell lysates of *E. coli* were prepared and incubated with **5.9** overnight at 4 °C. The beads were washed 10 times with PBS. The elution step was performed by incubation with 20 µM **5.7** followed by another elution with 200 µM **5.7**, and finally the beads were treated with 0.1% acetic acid to strip them of proteins. They performed SDS-PAGE on each fraction and identified 16 bands enriched in the compound elution lanes, but less prominent in the acetic acid elution. Of the 16 candidate proteins, the authors were able to express seven and determined their ability to bind salicylidene acylhydrazides using biotinylated protein **5.10** for far western

experiments. Three proteins showed affinity for **5.10** in the far western experiments and homologs in several other Gram negative species also showed affinity for **5.10**.[29]

Work to validate these targets included creation of point mutants and knockout strains of several of the targets identified in the pulldown. The authors observed an increase in T3SS activity in several of the mutants as well as >2-fold changes in transcription of several other genes related to virulence. Treatment of the mutants with **5.7** and **5.8** decreased T3SS activity suggesting they had multiple targets. They conclude that the salicylidene acylhydrazides likely affect T3SS by interaction with several targets resulting in global downregulation of virulence.[29]

A clickable photoaffinity probe used to identify the targets of a compound with anti-tuberculosis activity

Jacobs, Schultz, and coworkers identified benzothiazole **5.11** in a high throughput screen for compounds capable of disrupting *M. tuberculosis* biofilms. Further testing of **5.11** demonstrated *in vivo* activity against *M. tuberculosis* in dormancy models. To establish a mechanism of action, they initially pursued a genetic approach to target identification by analyzing transcriptome changes induced by compound treatment, screening of a *M. smegmatis* cosmid library for mutants insensitive to **5.11**, and generation of spontaneously resistant mutants followed by genome sequencing to identify genes that were mutated. This approach led to the hypothesis that **5.11** targets DprE1, a protein involved in cell wall arabinan synthesis.[30]
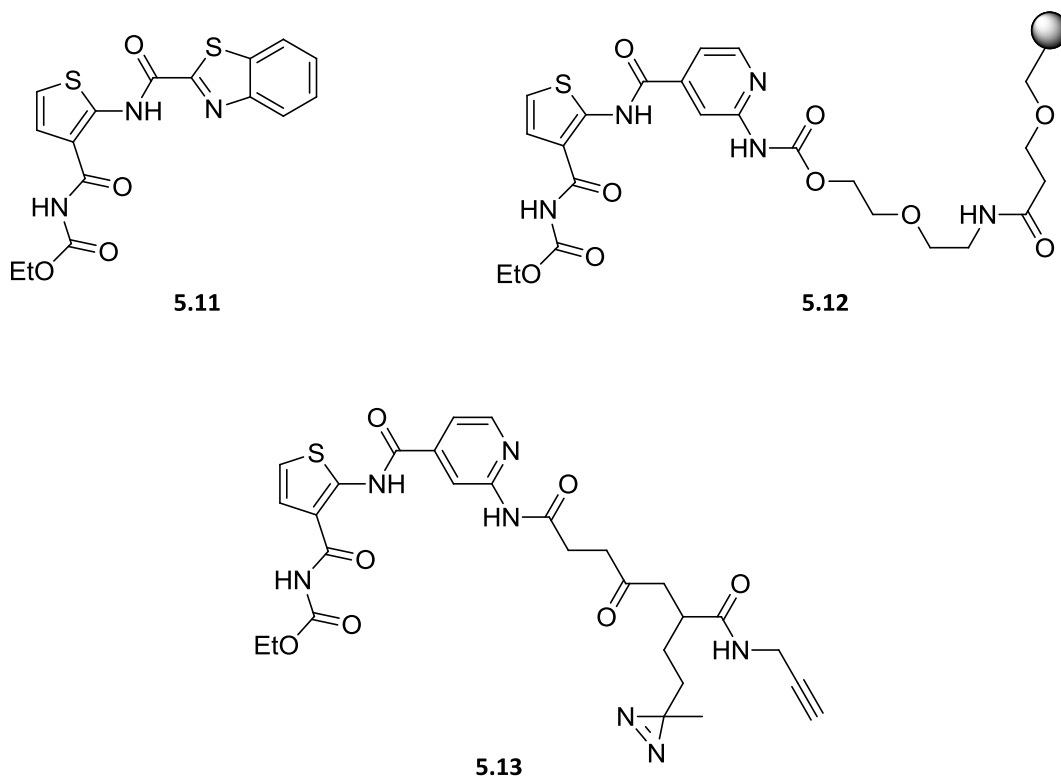
Figure 5.7. Benzothioazole active against dormant *M. tuberculosis* and probes based on its structure.

However, several follow up experiments indicated the probability of secondary targets. In order to identify these targets, they prepared affinity probe **5.12** and photoaffinity probe **5.13**, containing an alkyl diazirine as the photoreactive group and alkyne click handle. A *M. tuberculosis* lysate was treated with **5.12** and **5.12** with 50 µM of **5.11** as a competitor. The beads were washed with loading buffer and eluted by boiling in Laemmli sample buffer. After the elution samples were run on SDS-PAGE and visualized by silver staining, the authors note a band that appears in the **5.12** only lane, but absent in the **5.12** plus competitor lane. They excised this band and identified the protein as MoeW, a protein involved in molybdenum cofactor biosynthesis.[30]

To further validate the interaction of **5.11** with MoeW, the authors created a strain of *E. coli* (which does not express endogenouse MoeW or any homolog) expressing MoeW from *M. tuberculosis* and conducted an *in vivo* crosslinking experiment with photoaffinity probe **5.13**. Using an azido-rhodamine reporter that was clicked on via the alkyne handle, the authors demonstrated that **5.13** labels MoeW. The authors conclude that the activity of **5.11** is based on interactions with both DprE1 and MoeW.[30]

Vancomycin photoaffinity probes identify alternate targets

Vancomycin has been well established as an inhibitor of cell wall biosynthesis through binding to the D-Ala-D-Ala of nascent peptidoglycan and blocking crosslinking. Despite this well-defined mechanism, off target effects that contribute to the antibacterial activity have been proposed. Affinity purification of lysates using immobilized vancomycin identified several proteins capable of binding it. Since interactions in lysates may not reflect actual *in vivo* interactions, Sieber and co-workers developed a series of vancomycin probes using benzophenones as the photoreactive moiety and propargyl groups as click handles. These probes were prepared by utilizing the C-terminal carboxylate and primary amine of the vancosamine moiety of vancomycin. Addition of these functional groups did not significantly affect activity and the probes were active against several strains of S. *aureus* and *E. faecalis*.[31]

Figure 5.8. Clickable photoaffinity probes of vancomycin.
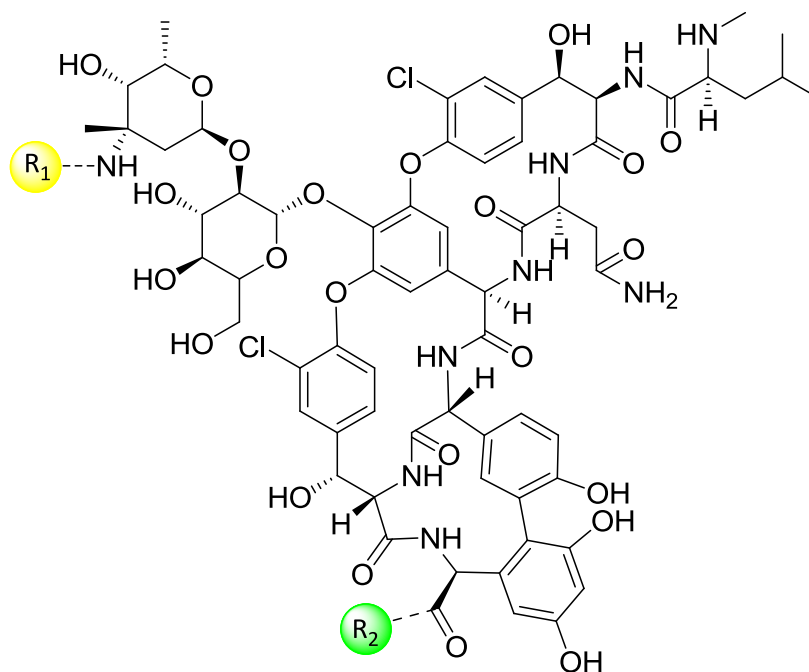
Compound	R$_1$	R$_2$
Vancomycin	- -H	- -H
5.14		
5.15		
5.16	- -H	

With these probes in hand, the authors conducted *in vivo* target identification experiments. They treated stationary phase bacteria with either 10 μM probe or 10 μM with vancomycin competitor and irradiated at 366 nm for two hours. The cells were harvested and lysed, and reporters were introduced via click chemistry. Using this method, the authors identified staphylococcal autolysin as a secondary target of vancomycin. They hypothesized this contributes to disruption of the cell wall. In *E. faecalis*, an ABC transporter was found to interact specifically with the probes. The authors concluded that this contributes to the antibacterial activity by blocking the uptake of essential nutrients.[31]

5.7 Conclusion

It is clear from a survey of the literature that successful target identification by chemical methods requires a robust approach. Multiple probes, whether for affinity purification or ligand directed approaches, should be prepared to increase the chances of successful target engagement and purification. Much chemistry has been developed to enable the production of probes and should be relatively easy to tailor to the scaffold under study. This process must also be followed by rigorous validation using complementary genetic and biochemical approaches.

References

(1)   Eggert, U. S. The Why and How of Phenotypic Small-Molecule Screens. *Nat. Chem. Biol.* **2013**, *9* (4), 206–209.

(2)   Walters, W. P.; Namchuk, M. A Guide to Drug Discovery: Designing Screens: How to Make Your Hits a Hit. *Nat. Rev. Drug Discov.* **2003**, *2* (4), 259–266.

(3)   Schenone, M.; Dančík, V.; Wagner, B. K.; Clemons, P. A. Target Identification and Mechanism of Action in Chemical Biology and Drug Discovery. *Nat. Chem. Biol.* **2013**, *9* (4), 232–240.

(4)   Ziegler, S.; Pries, V.; Hedberg, C.; Waldmann, H. Target Identification for Small Bioactive Molecules: Finding the Needle in the Haystack. *Angew. Chem. Int. Ed. Engl.* **2013**, *52* (10), 2744–2792.

(5)   Sato, S.; Murata, A.; Shirakawa, T.; Uesugi, M. Biochemical Target Isolation for Novices: Affinity-Based Strategies. *Chem. Biol.* **2010**, *17* (6), 616–623.

(6)   Scholten, A.; Poh, M. K.; van Veen, T. A. B.; van Breukelen, B.; Vos, M. A.; Heck, A. J. R. Analysis of the cGMP/cAMP Interactome Using a Chemical Proteomics Approach in Mammalian Heart Tissue Validates Sphingosine Kinase Type 1-Interacting Protein as a Genuine and Highly Abundant AKAP. *J. Proteome Res.* **2006**, *5* (6), 1435–1447.

(7)   Sato, S.-I.; Kwon, Y.; Kamisuki, S.; Srivastava, N.; Mao, Q.; Kawazoe, Y.; Uesugi, M. Polyproline-Rod Approach to Isolating Protein Targets of Bioactive Small Molecules: Isolation of a New Target of Indomethacin. *J. Am. Chem. Soc.* **2007**, *129* (4), 873–880.

(8)   Leriche, G.; Chisholm, L.; Wagner, A. Cleavable Linkers in Chemical Biology. *Bioorg. Med. Chem.* **2012**, *20* (2), 571–582.

(9) Szychowski, J.; Mahdavi, A.; Hodas, J. J. L.; Bagert, J. D.; Ngo, J. T.; Landgraf, P.; Dieterich, D. C.; Schuman, E. M.; Tirrell, D. A. Cleavable Biotin Probes for Labeling of Biomolecules via Azide-Alkyne Cycloaddition. *J. Am. Chem. Soc.* **2010**, *132* (51), 18351–18360.

(10) Lapinsky, D. J. Tandem Photoaffinity Labeling-Bioorthogonal Conjugation in Medicinal Chemistry. *Bioorg. Med. Chem.* **2012**, *20* (21), 6237–6247.

(11) Boutureira, O.; Bernardes, G. J. L. Advances in Chemical Protein Modification. *Chem. Rev.* **2015**, *115* (5), 2174–2195.

(12) Flanagan, M. E.; Abramite, J. A.; Anderson, D. P.; Aulabaugh, A.; Dahal, U. P.; Gilbert, A. M.; Li, C.; Montgomery, J.; Oppenheimer, S. R.; Ryder, T.; et al. Chemical and Computational Methods for the Characterization of Covalent Reactive Groups for the Prospective Design of Irreversible Inhibitors. *J. Med. Chem.* **2014**, *57* (23), 10072–10079.

(13) Sumranjit, J.; Chung, S. J. Recent Advances in Target Characterization and Identification by Photoaffinity Probes. *Molecules* **2013**, *18* (9), 10425–10451.

(14) Kotzyba-Hibert, F.; Kapfer, I.; Goeldner, M. Recent Trends in Photoaffinity Labeling. *Angew. Chemie Int. Ed. English* **1995**, *34* (12), 1296–1312.

(15) Chan, J. N. Y.; Vuckovic, D.; Sleno, L.; Olsen, J. B.; Pogoutse, O.; Havugimana, P.; Hewel, J. A.; Bajaj, N.; Wang, Y.; Musteata, M. F.; et al. Target Identification by Chromatographic Co-Elution: Monitoring of Drug-Protein Interactions without Immobilization or Chemical Derivatization. *Mol. Cell. Proteomics* **2012**, *11* (7), M111.016642.

(16) Dubinsky, L.; Krom, B. P.; Meijler, M. M. Diazirine Based Photoaffinity Labeling. *Bioorg. Med. Chem.* **2012**, *20* (2), 554–570.

(17) Park, K. D.; Stables, J. P.; Liu, R.; Kohn, H. Proteomic Searches Comparing Two (R)-

Lacosamide Affinity Baits: An Electrophilic Arylisothiocyanate and a Photoactivated Arylazide Group. *Org. Biomol. Chem.* **2010**, *8* (12), 2803–2813.

(18)   Karney, W. L.; Borden, W. T. Why Does O -Fluorine Substitution Raise the Barrier to Ring Expansion of Phenylnitrene? *J. Am. Chem. Soc.* **1997**, *119* (14), 3347–3350.

(19)   Kolb, H. C.; Finn, M. G.; Sharpless, K. B. Click Chemistry: Diverse Chemical Function from a Few Good Reactions. *Angew. Chem. Int. Ed. Engl.* **2001**, *40* (11), 2004–2021.

(20)   McKay, C. S.; Finn, M. G. Click Chemistry in Complex Mixtures: Bioorthogonal Bioconjugation. *Chem. Biol.* **2014**, *21* (9), 1075–1101.

(21)   Hong, V.; Presolski, S. I.; Ma, C.; Finn, M. G. Analysis and Optimization of Copper-Catalyzed Azide-Alkyne Cycloaddition for Bioconjugation. *Angew. Chem. Int. Ed. Engl.* **2009**, *48* (52), 9879–9883.

(22)   Kodama, K.; Fukuzawa, S.; Nakayama, H.; Sakamoto, K.; Kigawa, T.; Yabuki, T.; Matsuda, N.; Shirouzu, M.; Takio, K.; Yokoyama, S.; et al. Site-Specific Functionalization of Proteins by Organopalladium Reactions. *Chembiochem* **2007**, *8* (2), 232–238.

(23)   Li, J.; Chen, P. R. Moving Pd-Mediated Protein Cross Coupling to Living Systems. *Chembiochem* **2012**, *13* (12), 1728–1731.

(24)   Li, J.; Lin, S.; Wang, J.; Jia, S.; Yang, M.; Hao, Z.; Zhang, X.; Chen, P. R. Ligand-Free Palladium-Mediated Site-Specific Protein Labeling inside Gram-Negative Bacterial Pathogens. *J. Am. Chem. Soc.* **2013**, *135* (19), 7330–7338.

(25)   Zhang, Y.; Fonslow, B. R.; Shan, B.; Baek, M.-C.; Yates, J. R. Protein Analysis by Shotgun/bottom-up Proteomics. *Chem. Rev.* **2013**, *113* (4), 2343–2394.

(26)   Liu, H.; Sadygov, R. G.; Yates, J. R. A Model for Random Sampling and Estimation of

Relative Protein Abundance in Shotgun Proteomics. *Anal. Chem.* **2004**, *76* (14), 4193–4201.

(27)   Colca, J. R.; McDonald, W. G.; Waldon, D. J.; Thomasco, L. M.; Gadwood, R. C.; Lund, E. T.; Cavey, G. S.; Mathews, W. R.; Adams, L. D.; Cecil, E. T.; et al. Cross-Linking in the Living Cell Locates the Site of Action of Oxazolidinone Antibiotics. *J. Biol. Chem.* **2003**, *278* (24), 21972–21979.

(28)   The Site of Action of Oxazolidinone Antibiotics in Living Bacteria and in Human Mitochondria. *Mol. Cell* **2007**, *26* (3), 393–402.

(29)   Wang, D.; Zetterström, C. E.; Gabrielsen, M.; Beckham, K. S. H.; Tree, J. J.; Macdonald, S. E.; Byron, O.; Mitchell, T. J.; Gally, D. L.; Herzyk, P.; et al. Identification of Bacterial Target Proteins for the Salicylidene Acylhydrazide Class of Virulence-Blocking Compounds. *J. Biol. Chem.* **2011**, *286* (34), 29922–29931.

(30)   Wang, F.; Sambandan, D.; Halder, R.; Wang, J.; Batt, S. M.; Weinrick, B.; Ahmad, I.; Yang, P.; Zhang, Y.; Kim, J.; et al. Identification of a Small Molecule with Activity against Drug-Resistant and Persistent Tuberculosis. *Proc. Natl. Acad. Sci. U. S. A.* **2013**, *110* (27), E2510–E2517.

(31)   Eirich, J.; Orth, R.; Sieber, S. A. Unraveling the Protein Targets of Vancomycin in Living S. Aureus and E. Faecalis Cells. *J. Am. Chem. Soc.* **2011**, *133* (31), 12144–12153.

CHAPTER 6

TARGET IDENTIFICATION OF '8882

6.1 Introduction

As discussed in chapter 3, two activities of '8882 were observed; activation of heme biosynthesis leading to intracellular accumulation of endogenous heme with concomitant activation of HssRS; and toxicity to anaerobically growing *S. aureus*.[1] At the outset of this project, I had not completed the work presented in chapter 3 and we hypothesized that '8882 had one target responsible for both activities. Therefore, the focus of early target identification experiments was on finding one target. Later experiments would focus primarily on identifying the target responsible for activation of heme biosynthesis, with toxicity pursued to a lesser extent.

A complementary genetic approach identified HemY, a rate limiting enzyme in the later stages of heme biosynthesis[2], as the target of '8882 responsible for activation of HssRS. With this knowledge, we can retrospectively examine the success and utility of the probes developed for '8882 target identification.

The photoaffinity experiments described towards the end of this chapter were part of an ongoing effort to use PALs for target identification and the general process will continue to be discussed in chapter 7. The various aspects of the experiment such as irradiation conditions, click conditions, sample preparation, etc. were continually optimized throughout the process.

6.2 Affinity purification approach to '8882 target identification

Synthesis of biotinylated '8882 probe

We initially pursued an affinity purification approach for '8882 target identification and envisioned developing a probe based on the structure of '8882 with a biotinylated linker incorporated. This could be immobilized on streptavidin beads and used to isolate putative targets from a *S. aureus* lysate. Preliminary SAR data indicated that removal of the B-ring of the naphthol moiety of '8882 resulted in a modest drop in activity. We determined that removal of the B-ring and placement of a carboxylic acid *para* to the pyrazole moiety would permit attachment of a linker.
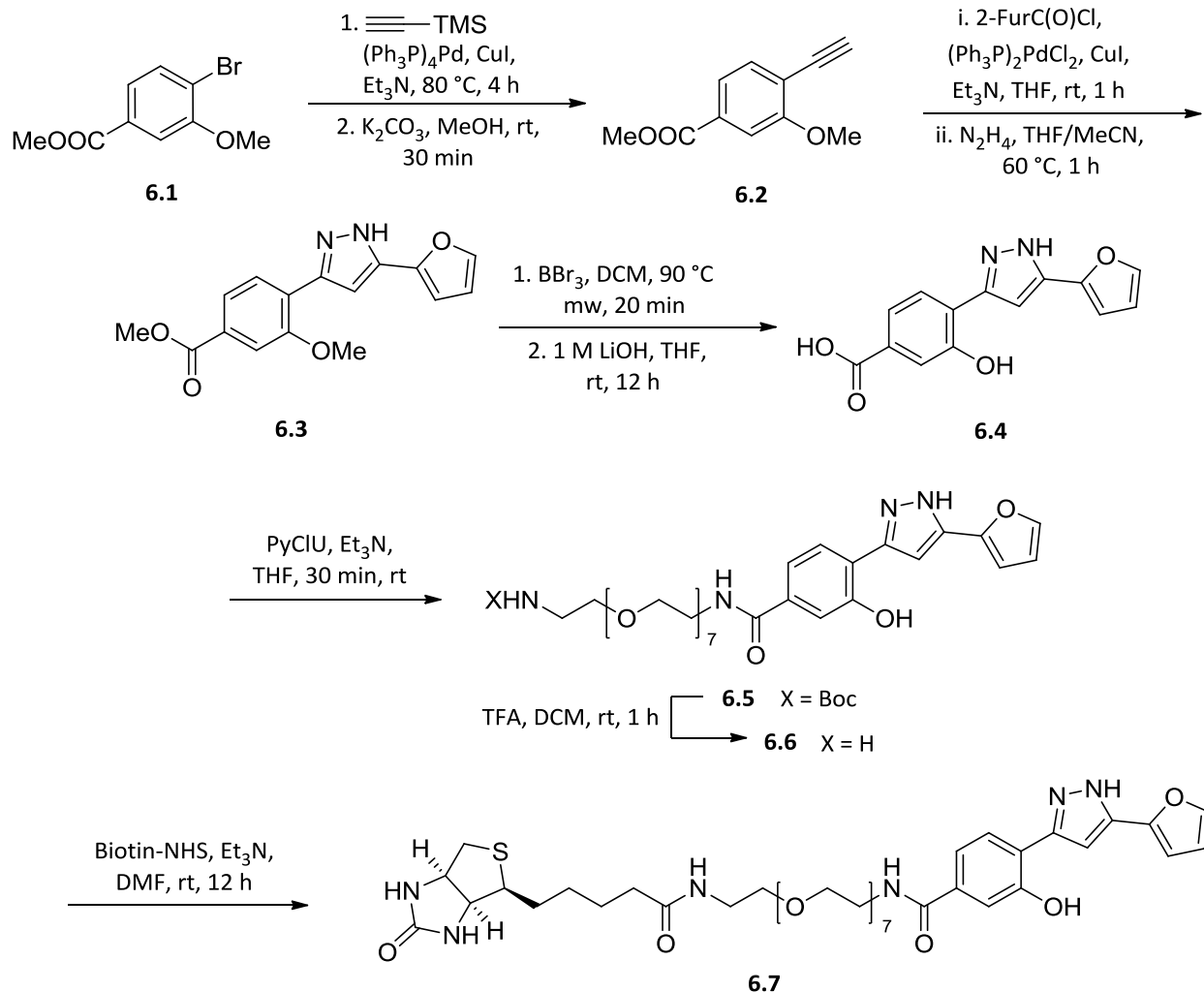
Scheme 6.1. Synthesis of affinity probe **6.7.**

Synthesis of the '8882 component of the probe (Scheme 6.1) began with Pd-mediated cross coupling of commercially available **6.1** with trimethylsilylacetylene followed by TMS removal by stirring with potassium carbonate in methanol to provide **6.2**. In one pot, **6.2** was converted to **6.3** by Pd-mediated cross coupling with 2-furoyl chloride to provide the alkynone which was then condensed with hydrazine to provide the pyrazole. **6.3** was reacted with boron tribromide in dichloromethane in a microwave reactor to cleave the methyl ether. These

conditions resulted in some hydrolysis of the methyl ester to provide a mixture of the methyl ester and **6.4**. The methyl ester was isolated during workup and saponified by treatment with lithium hydroxide in THF to convert the remainder of the material to **6.4**. The two fractions of **6.4** were combined and purified.

As previously described in chapter 5, the choice of an appropriate linker is critical for affinity purification. We chose to use a PEG-7 linker since the use of hydrophilic linkers (as opposed to long alkyl chains) deters nonspecific binding. In addition, long linker length is correlated with better target identification outcomes.[3] A mono-boc protected diamino-PEG-7 linker was purchased and the free amine coupled to **6.4** using PyClU to provide **6.5**. **6.5** was treated with trifluoroacetic acid in DCM to remove the boc group and provide **6.6** (as the TFA salt). This was stirred with biotin-NHS ester[4] and triethylamine in DMF. Once **6.6** had been consumed as determined by TLC, the product was purified by HPLC to provide biotinylated probe **6.7**.

Evaluation of HssRS activity of 6.7

The ability of **6.7**, **6.6**, and **6.4** to activate HssRS was evaluated using the XylE assay and compared to '8882 and **3.2** (Figure 6.1). Placement of a carboxylic acid *para* to the pryazole (**6.4**) resulted in considerable loss of activity compared to '8882 and **3.2**, although it did exhibit some activity compared to vehicle. However, the presence of the free amine linker and biotinylated linker resulted in complete loss of activity.
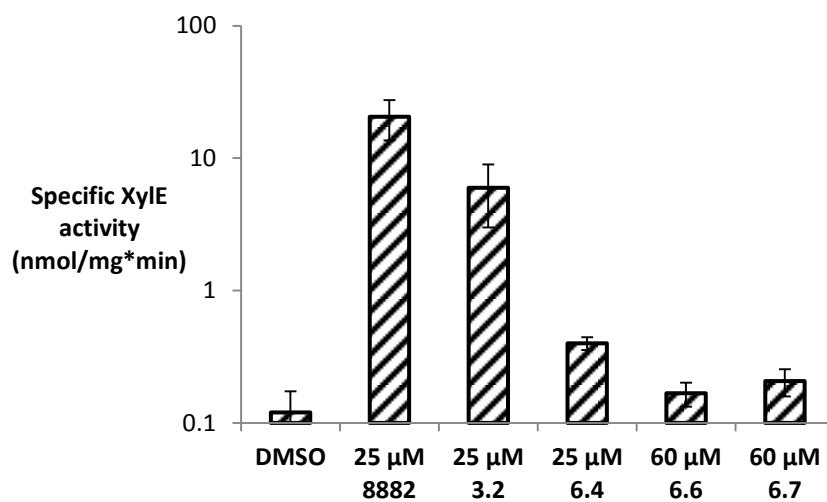
Figure 6.1. Activity of **6.7** and precursors.

There are several possibilities as to why **6.7** did not activate HssRS in the XylE assay. The presence of the linker could prevent binding to the target. In this case, **6.7** would not be useful for target identification. Another possibility is that it may be able to bind its target, but the large biotinylated linker renders the molecule unable to pass through the cell wall and/or membrane, preventing it from interacting with its target. In this case, the probe may still be able to bind the target in a lysate. We decided to proceed with target identification experiments using **6.7** hoping the latter was the case.

Affinity purification with 6.7
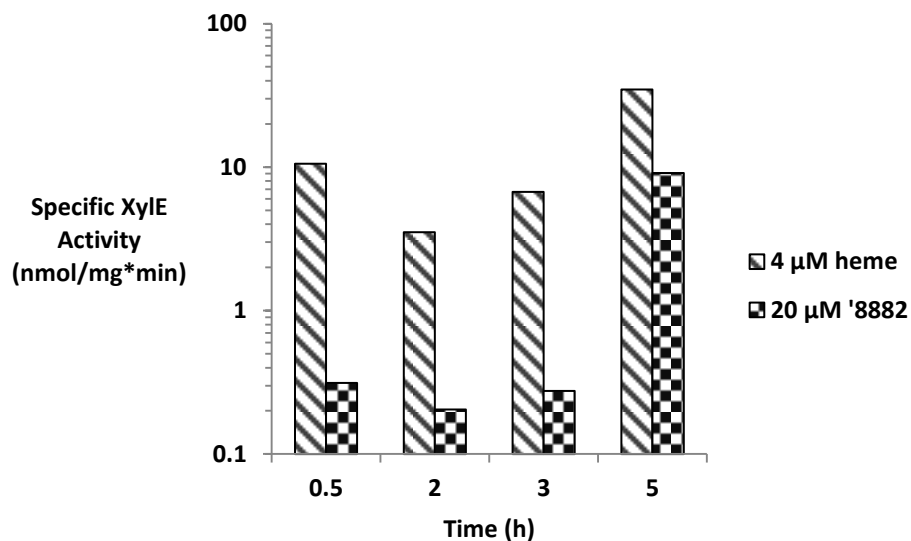
Figure 6.2. '8882 activation of HssRS at various time points.

With **6.7** in hand, we began conducting affinity purification experiments. Based on monitoring XylE activity at various time points (Figure 6.2), we hypothesized that the target was expressed in log phase so lysates were prepared after growing *S. aureus* for five hours after subculturing overnight cultures into fresh media. The lysates were split and incubated with either **6.7** or DMSO as a control. Streptavidin beads were then added to bind the probe and a series of washes with PBS were conducted followed by elution by boiling in 1X SDS-PAGE loading buffer for ten minutes. The samples were run on a gel and visualized with colloidal blue staining. A band ~26 kDa appeared to be enriched in the probe compared to control (Figure 6.3).
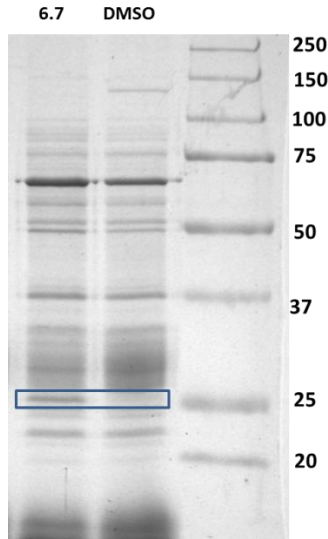
Figure 6.3. Elution lanes of affinity purification experiment with **6.7**.

We excised the band along with the adjacent section of the control lane and submitted these samples to the Vanderbilt Proteomics Core for identification and quantification using spectral counts. Between the two samples, 120 proteins were identified. Two proteins stood out because of their abundance in the sample and their enrichment in the probe vs. control lane. SufC, a protein involved in Fe-S cluster assembly[5] was the most abundant based on spectral counting and was enriched ~1.5x in the probe vs. control sample. The other protein, NWMN_0632, was unannotated and enriched ~3x in the probe vs. control sample. Follow up experiments confirmed that these proteins were pulled down by **6.7**, and in a more extensive proteomic analysis of the entre elution sample, several other components of the Suf system were identified.

Efforts towards validating these targets were primarily undertaken by Laura Mike. Validation efforts included attempts to knockout SufC and NWMN_0632, make overexpression strains, and express and purify each protein to biochemically characterize interactions with

'8882. None of these efforts were ultimately conclusive in establishing either of these candidates as definitive targets.

I attempted to optimize the affinity purification experiment by developing better controls based on the available SAR data, the use of alternate solid supports, and employing milder elution methods. However, none of these strategies gave better results than the initial experiment. Given the uncertainty regarding the activity of **6.7** the affinity purification strategy was ultimately abandoned in favor of a ligand directed approach using clickable photoaffinity probes.

I reasoned that the photoreactive groups and click handles could be incorporated into the structure of '8882 more innocuously than the biotinylated linker giving better chances that activity could be preserved. In addition, experiments could be conducted *in vivo* providing a more realistic system than proteins in a lysate.

6.3 Development of clickable photoaffinity probes

To develop an active photoaffinity probe that could be utilized for *in vivo* target identification experiments, we again relied on SAR data to determine placement of photoreactive groups and click handles. Removal of the B-ring and placement of smaller groups in the eastern ring, such as a methyl ether, *para* to the pyrazole ring was possible without significant loss of activity. However, larger group such as the biotinylated PEG linker were not tolerated suggesting that placement of smaller groups would be ideal. The furan (Western) could be replaced with various aromatic groups and still retain activity. Since a free phenol and pyrazole were required for activity, those should be unaltered in any probe.

Given these constraints, we set out to synthesize a small library of putative '8882 photoaffinity probes. We decided to place the click handle in the eastern ring *para* to the pyrazole. Two clickable functional groups were used to increase the diversity of the library; a propargyl either for CuAAC and iodine for Pd-mediated click reactions (we initially envisioned using the Sonogashira reaction for this).

Given the size and shape of benzophenones, using these in the initial probe design seemed undesirable since they would not be easy to incorporate around the parent scaffold and maintain activity based on SAR data. In contrast, the aryl azide and aryl trifluoromethyldiazirine were relatively small and could be easily incorporated in the Western aryl ring. We opted to place these in the 3- and 4-positions to increase diversity and the likelihood that an active probe would be identified.

Synthesis of components for first generation probe library

We envisioned using the same intramolecular Claisien condensation-hydrazine cyclocondensation reaction sequence outlined in Chapter 3. Components for the probe synthesis were generally prepared following literature procedures with some minor modifications. Propargyl ether **6.8** was prepared by mono-alkylation at the 4-position of 2,4-dihydroxyacetophenone with propargyl bromide and potassium carbonate in acetone. Iodoacetophenone **6.12** was prepared from 3-iodophenol by acetylation with acetic anhydride and Fries rearrangement of the acetate by heating a mixture of acetate **6.11** and aluminum(III) chloride at 140 °C.

3- and 4-azidobenzoic acids (**6.15** and **6.16**) were prepared from 3-and 4-aminobenzoic acid by diazotization and treatment with sodium azide (4-azidobenzoic acid is also commercially

available).[6] While diazirines **6.29** and **6.30** are commercially available, they are prohibitively expensive and were prepared de novo from inexpensive starting materials. Diazirines are prepared from the corresponding ketone through a sequence of activated oxime formation followed by reaction with ammonia to produce the diaziridine and subsequent oxidation to the diazirine. Typical oxidation conditions/reagents include iodine-triethylamine, tert-butyl hypochlorite-triethylamine, manganese dioxide, and silver(I) oxide.[7] Diazirines **6.29** and **6.30** were prepared from 3- and 4-bromotrifluoromethylacetophenone, respectively.[8] Oxime formation was accomplished by reaction with hydroxylamine hydrochloride and sodium acetate in ethanol at 150 °C in a microwave reactor. The oximes were tosylated by treatment with tosyl chloride and N,N-diisopropylethyamine in dichloromethane. The diaziridines were formed by dissolving the tosyloximines in liquid ammonia at -78 °C in a sealed tube and allowing the mixture to warm to room temperature. In order to install the carboxylic acid, the diaziridines were protected as the di-trimethylsilyl amide by treatment with trimethylsilyl trifluoromethanesulfonate and triethylamine at -78 °C. The protected diaziridines were treated with n-butyl lithium to effect lithium halogen exchange and the lithiates quenched by passing a stream of carbon dioxide through the reaction. Acidic workup resulted in N-deprotection to provide the diaziridine benzoic acids. The diazirines were formed by oxidation of the diaziridines with iodine-triethylamine.

Propargyl ether component
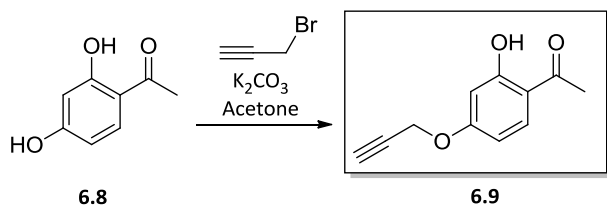
Aryl iodide component
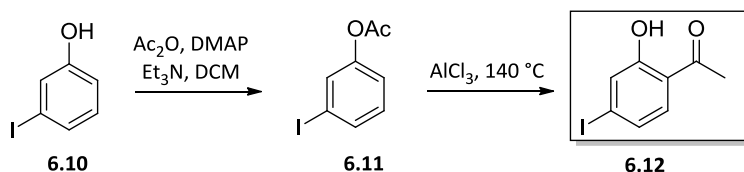
Aryl azide component
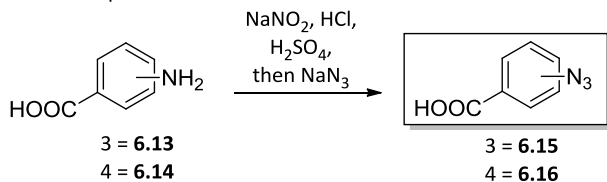
Diazirine component
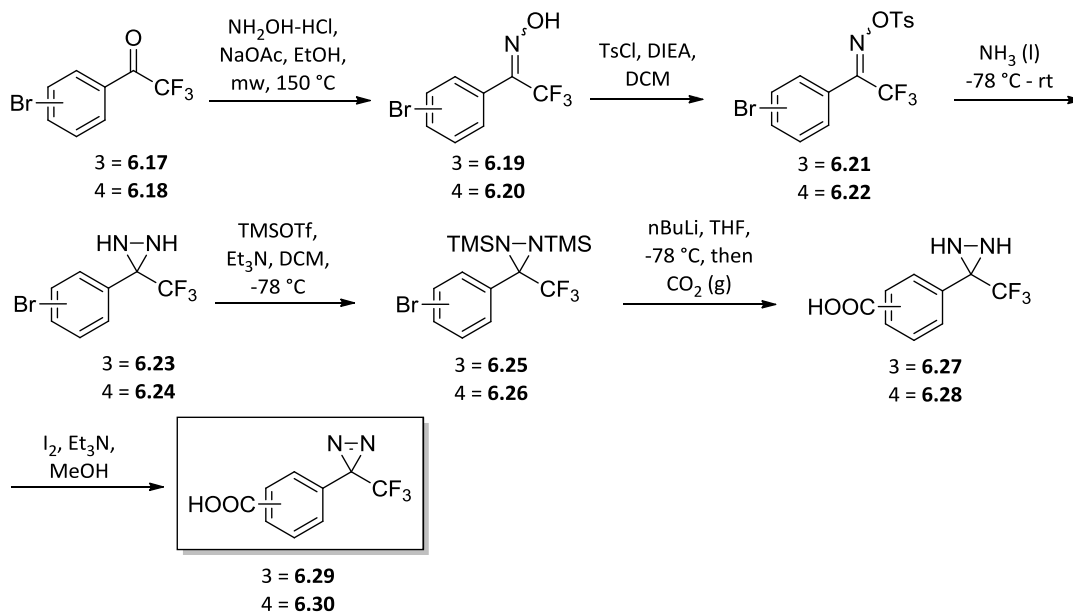
Figure 6.4. Synthesis of components for first generation probe synthesis.

Synthesis of first generation probe library

With the necessary components in hand, we began synthesis of the '8882 photoaffinity probe library (Scheme 6.2) by formation of the ester substrates from intramolecular Claisen condensation. Initial efforts to directly couple the acids to the hydroxyacetophenones using PyClU gave undesirable results as the reactions were not high yielding and required purification. To circumvent this, the acids were converted to the acid chlorides by treatment with thionyl chloride and pyridine. This reaction was quite convenient since the workup only involved filtering through a short plug of silica gel and gave products in excellent yield and purity. The acid chlorides were reacted with the corresponding hydroxyacetophenones to provide the esters in excellent yields with no need for further purification after workup.

Initial efforts to form the pyrazole from intramolecular Claisen condensation and subsequent reaction of the crude product with hydrazine were complicated and mostly unsuccessful. The chapter 3 procedure using potassium *tert*-butoxide in DMF was employed and resulted in a complex mixture of products. Since the β-diketone was typically carried through to the next reaction crude during the library synthesis in Chapter 3, the same procedure was employed here. The reaction with hydrazine was conducted at room temperature since azides and diazirines are known to be unstable at elevated temperatures. These reactions were monitored by LCMS for peaks corresponding to the mass of the product. While several reactions showed expected product masses, isolation of these peaks and subsequent characterization by NMR revealed they were not the correct structures.

Considerable optimization for this reaction sequence was carried out. Potassium bis(trimethylsilyl)amide replaced potassium *tert*-butoxide as the base for Claisen condensation

as this generally gave much cleaner reactions. Careful control of the amount of hydrazine used for the cyclocondensation step was also critical. Initially, a large excess of hydrazine was used to compensate for running the reaction in at lower temperatures. We speculated that the excess hydrazine was likely reducing the azides and diazirines leading to complicated product mixtures. Use of one equivalent proved to be sufficient for cyclization while minimizing unwanted side reactions. Ultimately, the eight iterations of probes using these six starting components were prepared.

Evaluation of the activity of probe 6.31 – 6.38

Probes **6.31 – 6.38** were screened for their ability to activate HssRS using the XylE assay. The compounds were tested at 50 µM and compared to '8882. As in Chapter 3, anything less than 5 % of the activity of '8882 was deemed inactive. We also conducted a secondary screen for toxicity towards anaerobically grown *S. aureus* by calculating IC_{50}s to determine their suitability as probes for identifying the target responsible for toxicity. The results are present in Table 6.1.

All probes with propargyl ethers were inactive with the most active compound exhibiting only ~1 % the activity of '8882. The two aryl iodide and diazirine containing probes **6.36** and **6.38** were toxic under the assay conditions so their activity could not be gauged. **6.35** with azide in the 3-position was inactive under our criteria showing 3.3 % the activity of '8882. However, **6.37** with azide in the 4-position exhibited ~20 % the activity of '8882. This result was encouraging and the results together provided insights into probe design. First, the inactivity of the propargyl ethers compared to the iodides suggests the ethers might be too large. Second, incorporation of halogens into the molecule promotes toxicity.
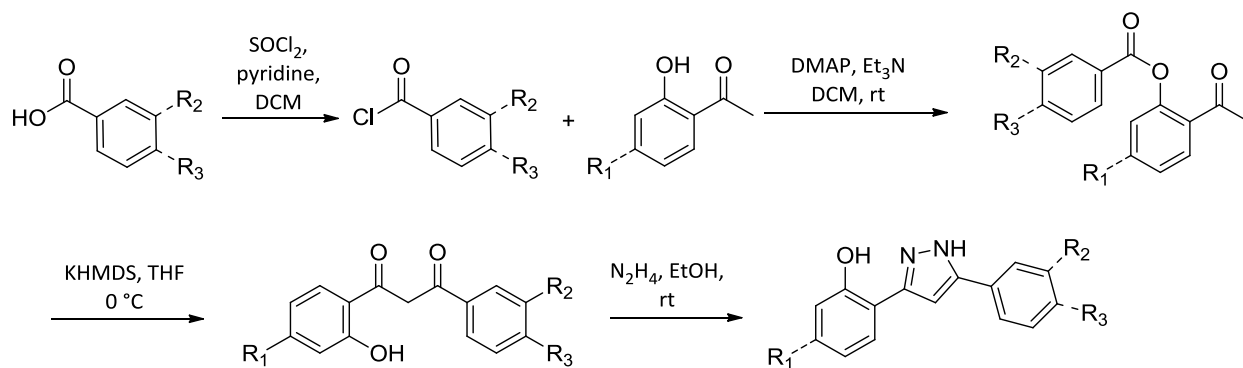
Scheme 6.2. General synthesis of first generation photoaffinity probes.

Cmpd	R_1	R_2	R_3	Relative HssRS Activity	Anaerobic IC$_{50}$ (µM)
6.31	propargyl-O	$-N_3$	$-H$	0.00934	>60
6.32	propargyl-O	N=N / CF$_3$	$-H$	0.00417	19.4
6.33	propargyl-O	$-H$	$-N_3$	0.0112	>60
6.34	propargyl-O	$-H$	N=N / CF$_3$	0.017	27.2
6.35	I	$-N_3$	$-H$	0.0328	16.9
6.36	I	N=N / CF$_3$	$-H$	Toxic	8.7
6.37	I	$-H$	$-N_3$	0.213	11.1
6.38	I	$-H$	N=N / CF$_3$	Toxic	8.8

Table 6.1. Activity of first generation photoaffinity probes. HssRS activation is presented as the fraction> of XylE activity at 50 µM compared to '8882. Anaerobic IC50 was calculated for 9 h of growth at 37 °C. >60 µM is considered nontoxic.

Synthesis and evaluation of second generation '8882 photoaffinity probes

While **6.37** is an active probe and could be used directly in target identification experiments, it does have some potential drawbacks. The iodide click handle and the Pd-mediated chemistry associated with it has not been validated as extensively as the CuAAC in biological systems. In addition, it seems the presence of the iodide contributes to toxicity which may convolute target identification efforts by interacting with off-target proteins. Since the primary goal was to identify the target of '8882 responsible for activation of heme biosynthesis, this should be avoided if possible.

We speculated that replacement of iodine with an ethynyl group would eliminate the toxicity and provide an alkyne click handle while not negatively affecting activity since it is approximately the same size as iodine. We prepared the hydroxybenzophenone precursor for this from **6.12** by Sonogashira coupling with trimethylsilylacetylene. This was carried through the established route with 4-azidobenzoic acid and the TMS group removed after pyrazole formation by treatment with potassium carbonate in methanol to provide **6.43**. We also reasoned that replacement of the azide of **6.43** with a trifluoromethyl diazirine would be active and less toxic than **6.38** since iodine was replaced. This compound was synthesized using an analogous route to provide **6.44**. Finally, due to the propensity for aryl azide photoaffinity probes to rearrange to less reactive didehydroazepines after irradiation, we envisioned synthesizing a derivative of **6.43** where the eastern ring is fluorinated since this will suppress the rearrangement. The compound (**6.45**) was prepared from **6.39** and 4-azido-2,3,5,6-tetrafluorobenzoic acid (**6.42**). **6.42** was prepared from methyl pentafluorobenzoate by refluxing with sodium azide and subsequent ester saponification.[9]
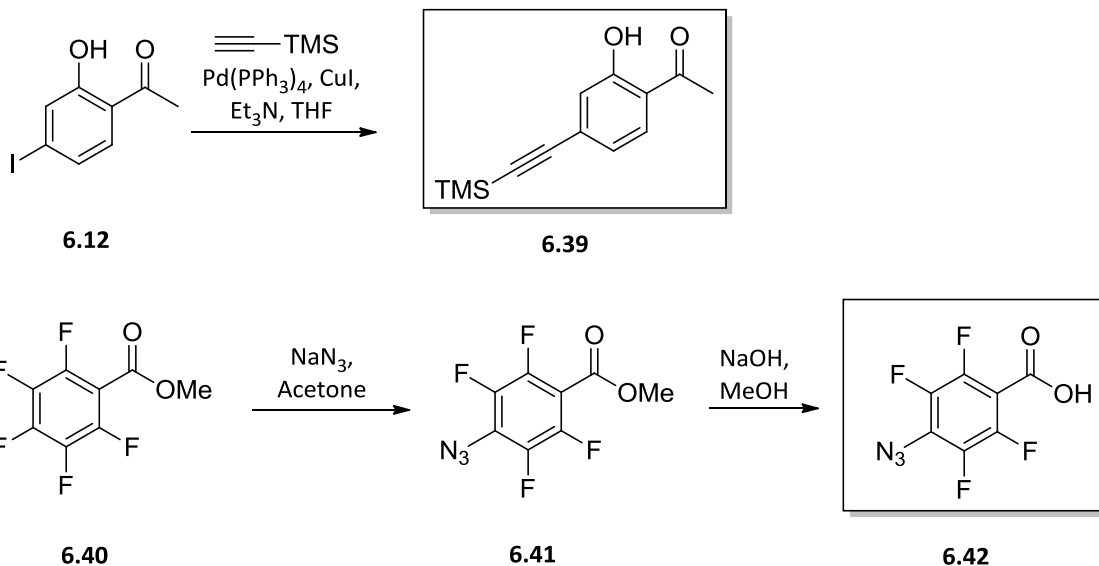
Figure 6.5. Synthesis of components for second generation probes.

6.43, R = p-C$_6$H$_4$N$_3$
6.44, R = p-C$_6$H$_4$C(N$_2$)CF$_3$
6.45, R = p-C$_6$F$_4$N$_3$
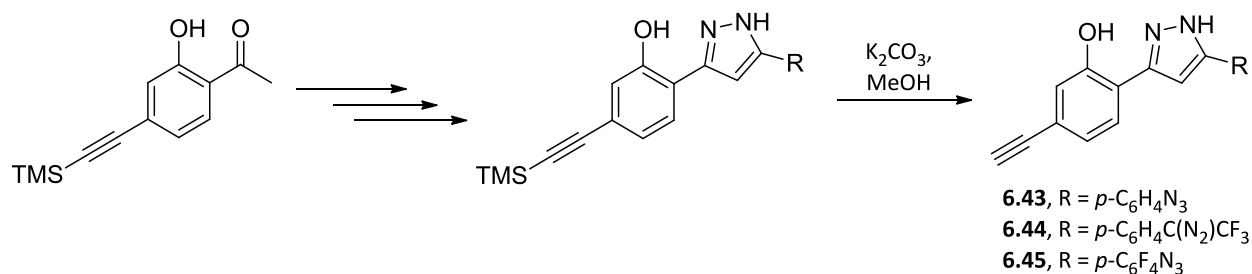
Scheme 6.3. Synthesis of second generation probes **6.43**, **6.44**, and **6.45**.

These probes were evaluated for HssRS activation using the XylE assay. **6.43** exhibited 44 % of the activity of '8882 and was nontoxic under anaerobic conditions. **6.44** was less active than **6.43**, but still showed considerable activity compared to vehicle. **6.45** was fairly toxic under the assay conditions and could only be tested at low concentrations. At 10 μM, **6.45** only exhibited ~2 % of the activity of '8882 suggesting that fluorination is deleterious to activity.

Given that di-fluoro substitution did not promote toxicity in previous '8882 derivatives (**3.19**) and fluorination of the positions *ortho* to the azide is sufficient to suppress ring expansion[10], we could potentially prepare a probe with only *ortho* fluorine substituents that may not be as toxic as **6.45** and could be tested at higher concentrations. However, we could not devise a practical route from commercially available starting materials to the necessary precursor benzoic acid and did not pursue this.
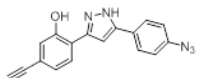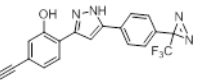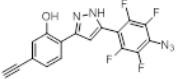
Cmpd	Structure	Fraction HssRS Activation
6.43		0.44 (40 µM)
6.44		0.0804 (50 µM)
6.45		0.0139 (10 µM)

Table 6.2. HssRS activation of second generation probes. Activity is presented as fraction of '8882 activity (concentration tested in parentheses).

Alternate '8882 photoaffinity probes

At the outset of probe development, it seemed advantageous to have an additional probe (or set of probes) with the photoreactive group in the opposite rings as the previous set of probes (Western ring). It is possible that the molecule binds its target in such a way that the eastern ring is solvent exposed. In this case, the reactive intermediate generated by irradiation would not react with the protein, and instead either be quenched by water (in the case of a carbene or triplet nitrene) or not react before diffusing away from the target (in the case of a

didehydroazepine). Incorporating the photoreactive group in different locations would increase coverage and the likelihood of successful target identification.

Since iodine and the ethynyl group in the 4-position of the Western ring were well tolerated in the previous series of probes, it was likely that a trifluoromethyl diazirine in this position would also work since they are similar in size. Diazirine containing hydroxyacetophenone **6.50** was prepared in seven steps from 3-bromoanisole (**6.46**). The bromide was converted to a trifluoromethyl ketone by lithium halogen exchange and quenching with trilfluormethylacetyl-piperidine. **6.47** was carried through the usual route for converting a ketone to diazirine.[11] The acetyl group was installed by Firiedel-Crafts acylation with acetyl chloride and aluminum(III) chloride.[12] Methyl ether deprotection was accomplished by treatment of **6.49** with boron tribromide in DCM. In this step, it was essential that fresh boron tribromide be used as older reagent did not induce demethylation.
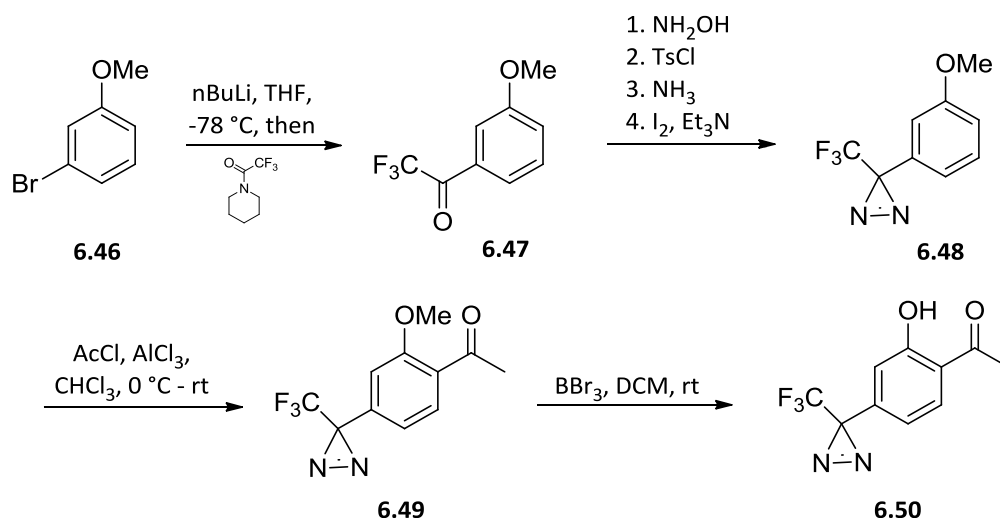
Scheme 6.4. Synthesis of photoaffinity probe component **6.50**.

Despite accessing **6.50**, only one probe was synthesized starting from this material. That probe used 5-bromofuran as the Eastern aryl group and was quite toxic in the XylE assay and did not activate HssRS at low concentrations. Efforts to replace the bromine with an ethynyl group were under way, but ultimately abandoned in favor of utilizing **6.43** and **6.44** as probes. This route was not revisited because of the identification of HemY as a target by genetic methods.

6.4 Photoaffinity experiments conducted with probe 6.43

The first probe utilized for photoaffinity experiments was **6.43**, mainly because it was the first of the second generation probes to be prepared. The experimental strategy was based partially on work with azide photoaffinity probes of oxazolidinones described in chapter 5.[13,14] In this experiment, the authors grew the bacteria to a specific OD before adding the probe primarily because of the growth inhibition induced by the molecule. Since **6.43** does not affect growth, it could be added to growth media before subculturing bacteria. For photolabeling, the authors used a Stratalinker device, which is normally used for cross linking RNA to membranes for Northern blotting. The light source provides 254 nm light and a specific amount of energy can be delivered. In the oxazolidinone work, 180 mJ was sufficient for photolabeling so this amount was used for these experiments.

I initially favored use of a fluorescent reporter since a gel could be run and immediately visualized without any transferring or staining steps. Rhodamine reporter **6.51** was prepared as described.[15] Throughout the use of this probe, I was not entirely familiar with in-gel fluorescence and the use of gel scanners for visualization. Instead, I used the AlphaImager UV-

lamp. While fluorescence is visible, this is not near the max excitation wavelength and many of the gel images are of poor quality. Despite this, the outcome of each experiment is still mostly discernible. An analogous biotin reporter was also prepared (**6.52**) to complement the fluorescent reporter.
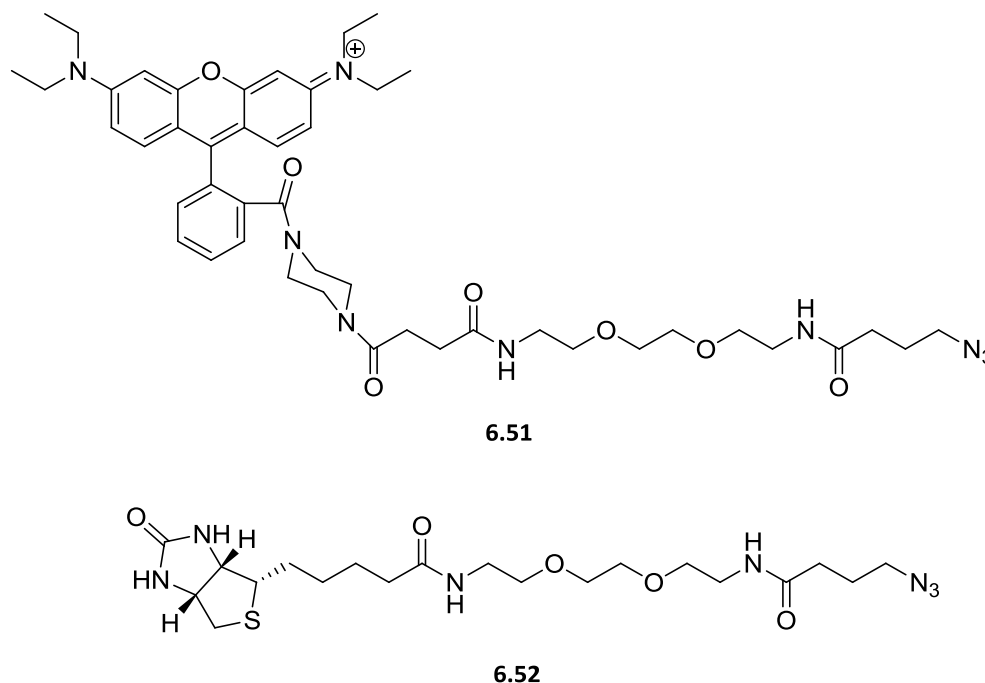
Figure 6.6. Clickable reporters used for '8882 target identification.

Initial photolabeling experiment

The first experiment with **6.43** was conducted simply to see if photolabeling followed by click chemistry attachment of rhodamine reporter **6.51** occurred and to determine a good concentration of **6.43** to use in subsequent experiments. Media was prepared with either 10, 20, or 40 µM **6.43**. Controls consisted of '8882 at the same concentrations. Bacteria were subcultured into each condition and grown for ~6 hours at 37 °C. The bacteria were then transferred to a 12 well plate and irradiated in the Stratalinker with 180 mJ of 254 nm light. The

bacteria were collected and lysed. The click conditions used were adapted from Schultz and coworkers.[16] After the click reaction, the lysates were subjected to TCA precipitation to pellet the proteins. The pellets were washed with acetone and resuspended in 1X loading buffer. Resuspension was difficult and required several rounds of heating and sonication. This led to the future use of acetone precipitations instead of TCA. The samples were run on gel and visualized with the AlphaImager UV light. Several bands were visible in the probe lanes but not the '8882 treated lanes indicating that the rhodamine reporter was specifically binding those proteins through the alkyne moiety of the probe and that the probe is adducting proteins. In addition, there does not appear to be a significant difference in the labeling between the three concentrations suggesting that future experiments could be successfully conducted with 10 µM **6.43**. Coomassie staining indicated even protein loading in all lanes.
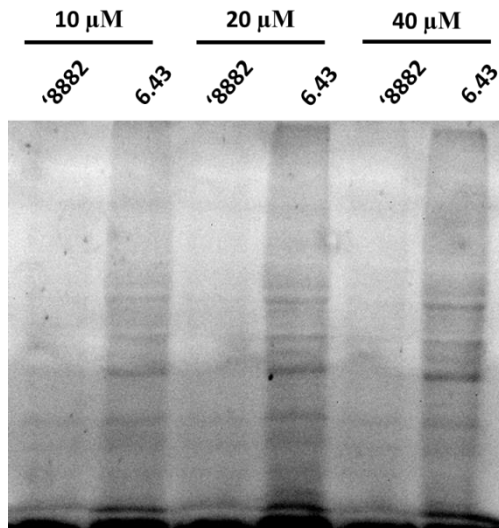
Figure 6.7. Preliminary **6.43** photolabeling experiment.

Competition experiment

The goal of the competition experiment was to add increasing concentrations of '8882 to **6.43** treated bacteria and observe any disappearance of bands in the final gel as a result of '8882 competing for specific binding to its target and preventing photolabeling by **6.43**. Despite the previous hypothesis that '8882 was acting during log phase, photolabeling experiments were also conducted in lag phase. To obtain enough bacteria for analysis, the lag phase cultures were incubated in a large volume of media containing compound. At 1.5 h, the bacteria were pelleted, media decanted and the bacteria were resuspended in the residual media. All samples were treated with 10 µM of **6.43**. The lysis, click, and sample preparation steps were the same as previously described except and acetone precipitation was used instead of TCA.
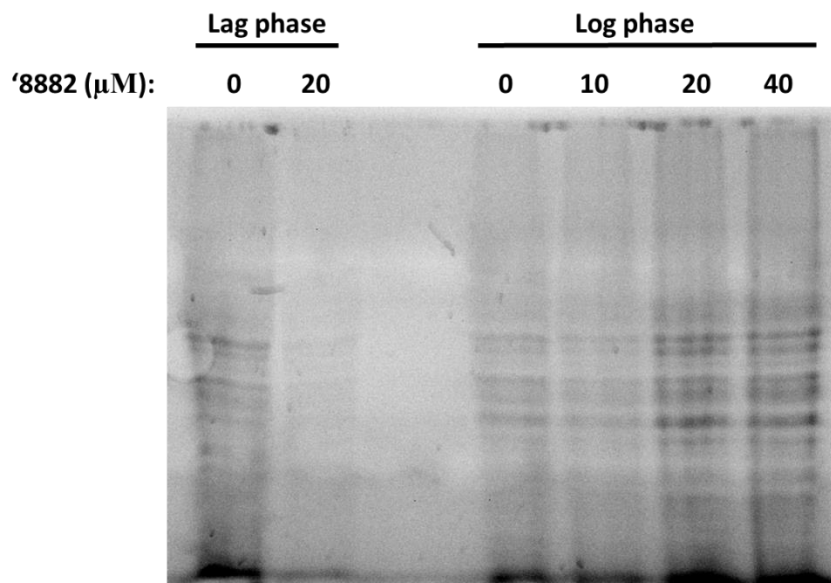
Figure 6.8. Competition experiment with **6.43**. All samples were treated with 10 µM **6.43** and varying concentrations of '8882. Lag phase bacteria were irradiated at 1.5 h after subculture. Log phase bacteria were irradiated at 5 h after subculture.

The results of this competition experiment do not clearly indicate any specific interactions were competed off with added '8882 in either growth phase. The lag phase **6.43** +

'8882 lane shows a global lack of photolabeling. The pellet from this condition was grey whereas the pellets from all other conditions are the typical golden color of *S. aureus*. One possible explanation for this is the overproduction of some metabolite as a result of '8882 treatment. This metabolite may absorb the 254 nm light preventing photoactivation of the azide. Subsequent experiments yielded similar results.

Photoaffinity experiments in lysates with 6.43

Given the lack of success with *in vivo* photoaffinity experiments, photolabeling in lysates was attempted. Since the probe was active *in vivo*, it should bind its target in a lysate assuming the protein is stable after lysis and during the subsequent photolabeling. Lysates of *S. aureus* covering various points in the growth curve were prepared. These were normalized by BCA assay and incubated with 80 μM of **6.43** alone or with 40 μM of '8882. The samples were irradiated in the Stratalinker and the rhodamine azide was clicked on. Proteins were then precipitated with acetone, resuspended in loading buffer and ran on a gel. As with *in vivo* experiments, no clear competition of specific interactions were observed. Given these results, we decided to switch to using probe **6.44** for experiments.

	Stationary PHase				Lag Phase						Log Phase	
Time (min)	0		30		60		90		120		180	
80 µM Probe	+	+	+	+	+	+	+	+	+	+	+	=
40 µM '882	-	+	-	+	-	+	-	+	-	+	-	+
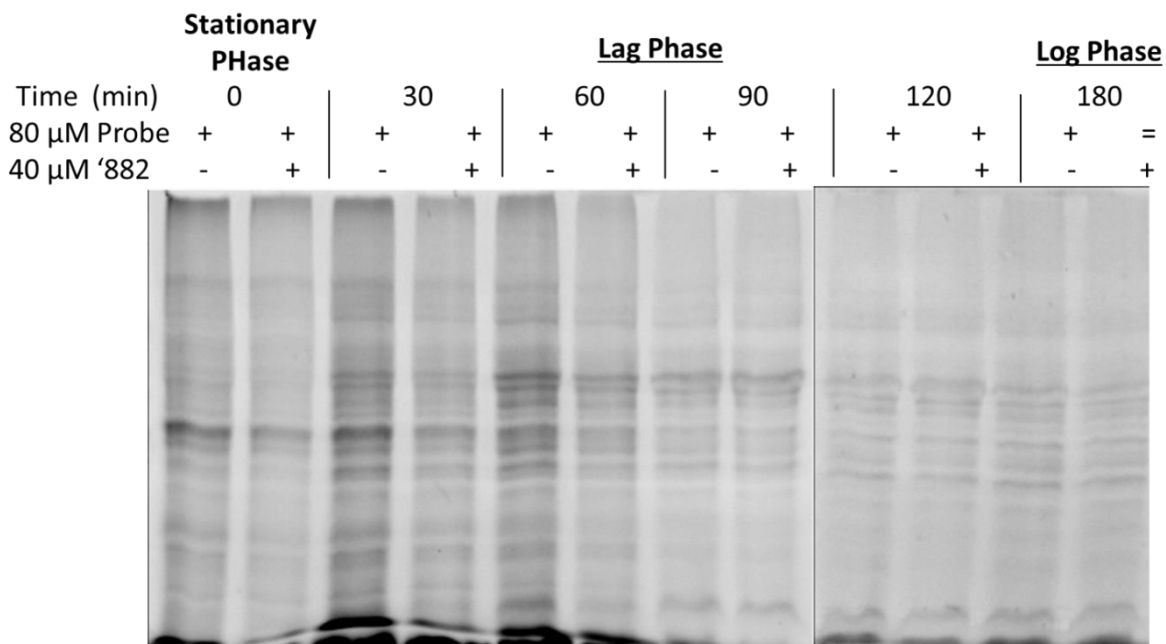
Figure 6.9. Photoaffinity experiments in lysates with **6.43**.

6.5 Photoaffinity experiments with probe 6.44

We hypothesized that the lack of results using **6.43** was primarily due to the undesirable ring expansion typical of the aryl azide after photolysis. The resulting didehydroazepine is likely not in an environment where it can be captured by nucleophilic residues. Since the aryl azide can also proceed to a triplet nitrene state and adduct proteins through radical chemistry, it is possible that the aryl azide is solvent exposed and quenched to the aniline. In either case, the environment is not ideal for protein adduction. Given this result, we further hypothesized that use of the **6.44** may overcome some of these disadvantages, particularly the former, since the carbene generated through photolysis is much more reactive than the didehydroazepine.

175

While preliminary experiments were conducted, **6.44** was not as extensively utilized for experiments as **6.43** due to the parallel discovery through genetic methods of HemY as the target of '8882 responsible for activation of heme biosynthesis.

6.6 Conclusion

Use of chemical probes for '8882 target identification gave mixed results. The affinity probe was able to identify proteins of the Suf complex, and thus Fe-S cluster assembly, as a possible target of '8882, particularly with regards to toxicity. Subsequent work to validate Suf as a target has demonstrated that '8882 inhibits *in vitro* Fe-S cluster assembly and down-regulates *in vivo* activity of certain Fe-S cluster containing proteins (unpublished data). Despite this compelling story, the genetically validated target HemY did not appear in the affinity purification results. There are several possible explanations for this. In particular, it is possible that the presence of the linker interferes with binding to HemY resulting in a weak interaction that is easily disrupted during the wash steps. This could be confirmed by evaluating the activity of **6.7** in the HemY assay. Loss of activity would likely indicate poor binding. Placement of the linker elsewhere on the '8882 scaffold might lead to better results.

Many factors may have contributed to the lack of success with photoaffinity probes. First, the most active probe was aryl azide **6.43**. Due to the photoinduced rearrangement to less reactive didehydroazepines, aryl azides may not be ideal labeling groups despite preserving activity.[17] For both probes tested, the photoreactive group was in the same position of the molecule. If this part of the molecule is solvent exposed when bound to its target, the reactive intermediate would be quenched by water and not adduct the protein. To minimize the

possibility of this affecting a successful outcome, it would have been prudent to develop and utilize another probe with the photolabel in the western ring.

Experimental Section

General Procedures: All non-aqueous reactions were performed in flame-dried flasks under an atmosphere of argon. Stainless steel syringes were used to transfer air- and moisture-sensitive liquids. Reaction temperatures were controlled using a thermocouple thermometer and analog hotplate stirrer. Reactions were conducted at room temperature (rt, approximately 23 °C) unless otherwise noted. Flash column chromatography was conducted using silica gel 230-400 mesh. Analytical thin-layer chromatography (TLC) was performed on E. Merck silica gel 60 F254 plates and visualized using UV and iodine stain.

Materials: All solvents and chemicals were purchased from Sigma-Aldrich unless otherwise noted. Dry dichloromethane was collected from an MBraun MB-SPS solvent system. N,N-dimethylformamide (DMF), tetrahydrofuran (THF), and acetonitrile (MeCN) were used as received in a bottle with a Sure/Seal. Triethylamine was distilled from calcium hydride and stored over KOH. Deuterated solvents were purchased from Cambridge Isotope Laboratories. Methyl-4-bromo-3-methoxybenzoate was purchased from Combi-Blocks. Trimethylsilylacetylene and 1-(Chloro-1-pyrrolidinylmethylene)pyrrolidinium hexafluorophosphate were purchased from Oakwood Chemicals.

Instrumentation: ^{1}H NMR spectra were recorded on Bruker 400 or 600 MHz spectrometers and are reported relative to deuterated solvent signals. Data for ^{1}H NMR spectra are reported as follows: chemical shift (δ ppm), multiplicity (s = singlet, d = doublet, t = triplet, q = quartet, p = pentet, m = multiplet, br = broad, app = apparent), coupling constants (Hz), and integration.

13C NMR spectra were recorded on Bruker 100 or 150 MHz spectrometers and are reported relative to deuterated solvent signals. Low resolution mass spectrometry (LRMS) was conducted and recorded on an Agilent Technologies 6130 Quadrupole instrument.
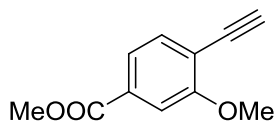
Methyl 4-ethynyl-3-methoxybenzoate (**6.2**). To a stirred solution of 2.08 g (8.49 mmol, 1.0 eq) methyl-4-bromo-3-methoxybenzoate in 25 mL of triethylamine was added 455 mg (0.394 mmol, 0.046 eq) palladium tetrakistriphenylphosphine, 160 mg (0.842 mmol, 0.099 eq) copper(I) iodide, and 2.50 mL (17.6 mmol, 2.1 eq) trimethylsilylacetylene. The reaction was refluxed for 2 h when it was judged complete by LC-MS. The reaction was diluted with ethyl acetate (50 mL), filtered through celite, washed with saturated ammonium chloride (3x) and brine (2x), dried (MgSO$_4$), and concentrated. The crude residue was dissolved in 25 mL of methanol and 1.80 g of potassium carbonate was added. The reaction was stirred for 15 min when judged complete by LC-MS. The reaction was concentrated and partitioned between 50 mL of ethyl acetate and 20 mL of brine. The organic layer was filtered through silica gel, concentrated, and the residue purified by flash chromatography to provide 1.24 g (77 %) of **S1** as a brown solid over 2 steps. ^{1}H-NMR (400 MHz, CDCl$_3$) δ 7.56 (dd, J=7.88 Hz, J=1.44 Hz, 1H), 7.51 (d, J=1.28 Hz, 1H), 7.47 (d, J=7.88 Hz, 1H), 3.92 (s, 3H), 3.89 (s, 3H), 3.43 (s, 1H); 13C-NMR (100 MHz) δ 166.4, 160.5, 134.0, 131.6, 121.7, 116.0, 111.3, 83.9, 79.4, 56.1, 52.4; LRMS calculated for C11H10O3 [M+H]$^+$ *m/z*: 191.1, measured 191.1.
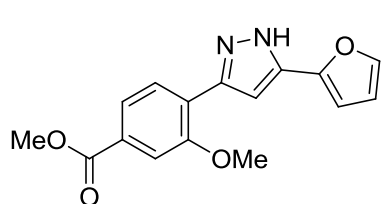
\Methyl 4-(5-(furan-2-yl)-1H-pyrazol-3-yl)-3-methoxybenzoate (**6.3**). To a stirred solution of 2.97 g (15.6 mmol, 1.0 eq) **6.2** in 50

mL of THF was added 2.18 mL (15.6 mmol, 1.0 eq) of triethylamine, 118 mg (0.167 mmol, 0.011 eq) of bis(triphenylphosine)palladium chloride, 111 mg (0.584 mmol, 0.037 eq) of copper(I) iodide, and 2.30 mL (23.3 mmol, 1.5 eq) 2-furoyl chloride. The reaction was stirred at room temperature for 1 h until it was judged complete by TLC. The reaction was diluted with 25 mL of acetonitrile, 1.50 mL (23.4 mmol, 1.5 eq) of hydrazine hydrate was added, and the mixture was heated to 60 °C for 2 h until judged complete by TLC. The reaction was filtered through celite, concentrated, and purified by flash chromatography to give 3.98 g (86 %) of **S2** as a yellow solid. 1H-NMR (600 MHz, CDCl$_3$) δ 7.76 (d, J=8.10 Hz, 1H), 7.71 (dd, J=8.04 Hz, J=1.44 Hz, 1H), 7.67 (d, J=1.26 Hz, 1H), 7.46 (d, J=1.14 Hz, 1H), 6.93 (s, 1H), 6.72 (d, J=3.28 Hz, 1H), J=3.30 Hz, J=1.74 Hz, 1H), 4.0δ2 (s, 3H), 3.94 (s, 3H); ^{13}C-NMR (150 MHz) δ 166.5, 155.8, 148.7, 142.0, 141.2, 130.8, 127.8, 122.9, 121.9, 112.7, 111.5, 106.0, 101.0, 56.2, 52.3; LRMS calculated for C$_{16}$H$_{14}$N$_2$O$_4$ [M+H]$^+$ m/z: 299.1, measured 299.1.
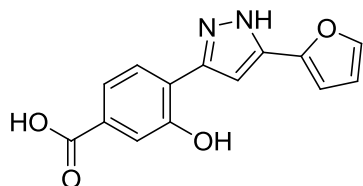
4-(5-(furan-2-yl)-1H-pyrazol-3-yl)-3-hydroxybenzoic acid (6.4). To a stirred solution of 258 mg (0.864 mmol, 1.0 eq) of **6.3** dissolved in 1 mL dichloromethane in a microwave vial was added 3.45 mL (3.45 mmol, 4.0 eq) of a 1 M solution of boron tribromide in dichloromethane. The vial was sealed and maintained at 90 °C for 20 min. The reaction was quenched in15 mL of saturated sodium bicarbonate, extracted with 30 mL of ethyl acetate (2x). The aqueous layer was acidified with 1 N HCl and extracted with 30 mL of ethyl acetate (2x) and set asside. The organic layer from the bicarbonate wash was concentrated and the residue dissolved in 2 mL THF. To the stirred THF solution was added 2.0 mL of 2 M lithium hydroxide and the resulting mixture was maintained at 50 °C for 3 h until the reaction was judged complete by TLC. The mixture was

acidified with 1 N HCl, extracted with ethyl acetate, and the organic layer combined with the organic layer from the acid wash from the previous step. The organics were concentrated and the residue purified by flash chromatography to provide 143 mg (61 %) of **S3** as a light brown solid. ^{1}H-NMR (600 MfHz, acetone-d6) δ 7.90 (br, 1H), 7.73 (br, 1H), 7.61 (br, 2H), 7.25 – 7.22 (m, 1H), 6.98 – 6.94 (m, 1H), 6.64 (br, 1H); ^{13}C-NMR (150 MHz) δ 167.3, 156.7, 145.5, 144.2, 132.0, 127.7, 121.5, 121.4, 118.7, 112.7, 108.7, 100.0; LRMS calculated for $C_{14}H_{10}N_2O_4$ [M+H]$^+$ m/z: 271.1, measured 271.1.
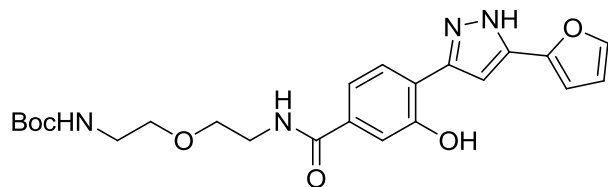
tert-butyl (1-(4-(5-(furan-2-yl)-1H-pyrazol-3-yl)-3-hydroxyphenyl)-1-oxo-5,8,11,14,17,20,23-heptaoxa-2-azapentacosan-25-yl)carbamate (**6.5**) To a stirred solution of 15.0 mg (0.555 mmol, 1.0 eq) of **6.4** in 1 mL THF was added 51.9 mg (0.111 mmol, 2.0 eq) of O-(2-Aminoethyl)-O'-[2-(Boc-amino)ethyl]hexaethylene glycol, 15.5 µL (0.111 mmol, 2.0 eq) of triethylamine, and 36.9 mg (0.111 mmol, 2.0 eq) of 1-(Chloro-1-pyrrolidinylmethylene)pyrrolidinium hexafluorophosphate. The reaction was stirred at room temperature for 1 h when it was judged complete by LC-MS. The solvent was removed, the residue was dissolved in DMSO and purified by preparative scale reverse phase HPLC (MeCN:H$_2$O mobile phase) to provide 14.9 mg (37 %) of **S4**. ^{1}H-NMR (400 MHz, CDCl$_3$) δ 10.77 (br, 1H), 7.65 (d, J=8.00 Hz, 1H), 7.50 (d, J=1.24 Hz, 1H), 7.46 – 7.40 (m, 2H), 6.98 (br, 1H), 6.76 (d, J=3.32 Hz, 1H), 6.52 (dd, J=3.24 Hz, J=1.76 Hz, 1H), 5.08 (br, 1H), 3.71 – 3.48 (m, 30H), 3.33 – 3.26 (m, 2H), 1.43 (s, 9H).
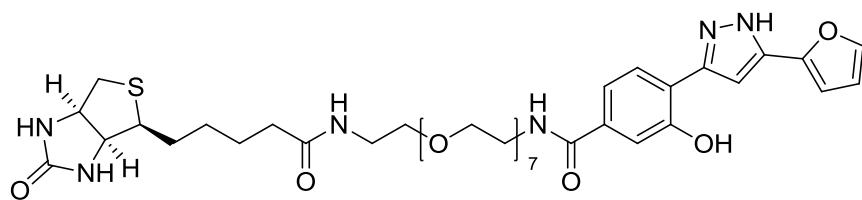
4-(5-(furan-2-yl)-1H-pyrazol-3-yl)-3-hydroxy-N-(25-oxo-29-((3aS,4S,6aR)-2-oxohexahydro-1H-thieno[3,4-d]imidazol-4-yl)-3,6,9,12,15,18,21-heptaoxa-24-azanonacosyl)benzamide (6.7) A total of 200 μL TFA was added to a solution of 14.9 mg (20.6 μmol, 1.0 eq) of **6.5** in 1 mL dichloromethane. The reaction was stirred at room temperature for 1 h when it was judged complete by TLC. The volatiles were removed *in vacuo* and the residue dissolved in 1 mL of DMF. To this stirred solution was added 8.6 μL (61.8 μmol, 3.0 eq) of triethylamine and 8.4 mg (24.4 μmol, 1.2 eq) of biotin-NHS ester. The reaction was stirred at room temperature for 1 h when it was judged complete by LCMS. The reaction was concentrated and the residue purified by preparative scale HPLC to provide 9.5 mg (48 %) of 8882 biotin probe as TFA salt. ^{1}H-NMR (600 MHz, MeOD) δ 7.80 (d, J=8.04 Hz, 1H), 7.63 (d, J=1.20 Hz, 1H), 7.44 – 7.38 (m, 2H), 7.10 (br. 1H), 6.85 (d, J=3.30 Hz, 1H), 6.58 (dd, J=3.24 Hz, J=1.74 Hz, 1H), 4.49 – 4.45 (m, 1H), 4.29 – 4.26 (m, 1H), 3.71 – 3.55 (m, 30H), 3.51 (t, J=5.43 Hz, 2H), 3.34 (t, J=5.43 Hz, 2H), 3.19 – 3.14 (m, 1H), 2.90 (dd, J=12.75 Hz, J=5.01 Hz, 1H), 2.70 (d, J=12.72 Hz, 1H), 2.20 (t, J=7.35 Hz, 2H), 1.75 – 1.54 (m, 4H), 1.44 – 1.38 (m, 2H); LRMS calculated for $C_{40}H_{58}N_6O_{12}S$ [M+H]$^+$ *m/z*: 847.4, measured 847.2.

General synthesis of acid chlorides. To a stirred solution of carboxylic acid (1.0 eq) in dichloromethane (0.2 M) was added pyridine (1.1 eq) and thionyl chloride (1.5 eq). The reaction was stirred for 1.5 h at room temperature at which point it was flash filtered through a plug of

silica gel with dichloromethane. Volatiles were removed *in vacuo* to provide acid chloride in 70 – 95 % yields.

General synthesis of esters for Claisen condensation. As described in chapter 3.

General procedure for intramolecular Claisen condensation. To a stirred solution of ester (1.0 eq) dissolved in THF and cooled to 0 °C was added 0.5 M KHMDS in toluene (2.0 eq). The reaction was maintained at 0 °C for 2 h at which point it was judged complete by TLC. The reaction was quenched by addition of 1 N HCl and the resulting mixture extracted with diethyl ether, washed with brine, dried (MgSO$_4$), and concentrated. The product was carried on crude to the next step.

General procedure for pyrazole synthesis. The crude claisen condensation product was carefully dissolved in an amount of ethanol containing 2.0 mg/mL of hydrazine containing approximately 1.0 eq of hydrazine. The reaction was maintained at room temperature until judged complete by LCMS. The product was purified by preparative scale reverse phase HPLC (except **6.43** – **6.45** which were concentrated and carried through crude to the final TMS removal step described below).

General procedure for TMS removal. To crude pyrazole (1.0 eq) dissolved in methanol (1 mL) was added a small quantity of potassium carbonate. The reaction was stirred for 30 min until judged complete by LCMS. The reaction was partitioned between water and ethyl acetate. The organic layer was washed with brine, dried (MgSO$_4$), and concentrated. The crude residue was purified by preparative scale reverse phase HPLC.
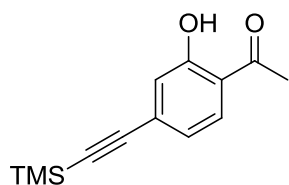
1-(2-hydroxy-4-((trimethylsilyl)ethynyl)phenyl)ethanone (6.39) To a stirred solution of **6.12** (25.0 mg, 1.0 eq) in tetrahydrofuran (1 mL) was

added triethylamine (19.2 µL, 2.0 eq), bis(triphenylphosphine)palladium dichloride (3.3 mg, 0.05 eq), copper(I) iodide (0.9 mg, 0.05 eq), and trimethylsilylacetylene (20.2 µL, 1.5 eq).   The mixture was stirred for 4 h under an atmosphere of argon until judged complete by TLC.

Affinity purification. Overnight cultures of *S. aureus* strain Newman were subcultured 1:100 into 5 mL TSB in triplicate and incubated at 37 °C for 5 h. The bacteria were combined, pelleted, washed with PBS, pelleted again, and resuspended in lysis buffer (PBS + 25 µg/ml lysotaphen and 0.1 mM PMSF). Lysates were prepared by incubating the cells at 37 °C for 20 mins and sonicating 2x for 10 s at 80 % power on ice. The lysate was split in half and to one batch was added 150 µL of 1.5 mg/mL **6.7** in DMSO and to the other was added an equal volume of DMSO. The lysates were incubated at room temperature for 30 min. NeutrAvidin beads were added to both conditions and incubated at room temperature for 1 h. The beads were washed 5x with PBS and then heated to 90 °C in 1X SDS-PAGE loading buffer for 10 min to effect elution.
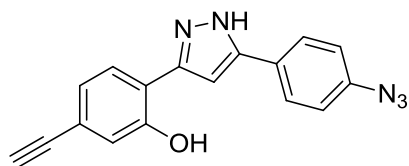
2-(3-(4-azidophenyl)-1H-pyrazol-5-yl)-5-ethynylphenol (6.43)

^{1}H-NMR (400 MHz, acetone-d6) δ 7.91 (d, J=8.52 Hz, 2H), 7.77 (d, J=8.36 Hz, 1H), 7.29 (s, 1H), 7.23 (d, J=8.48 Hz, 2H), 7.08 – 7.03 (m, 2H), 3.96 (s, 1H); LRMS calculated for $C_{17}H_{11}N_5O$ [M+H]$^+$ *m/z*: 302.1, measured 302.1.

Photoaffinity experiment. An overnight of S. aureus strain Newman was subcultured 1:100 into 500 µL of TSB containing probe or probe and competitor on a 12 well plate. The bacteria were incubated at 37 °C and irradiated in a Stratagene Stratalinker 2400 set at 180 mJ. Replicates were combined, pelleted, and the cells washed with PBS. The cells were pelleted and resuspended in lysis buffer (PBS + 25 µg/mL lysostaphen + 1X EDTA-free protease inhibitor),

incubated at 37 °C for 20 min, and sonicated 2x for 10 s at 80 % power. To the lysates were added CuSO$_4$ and TBTA to a final concentration of 200 μM, sodium ascorbate to a final concentration of 400 μM, and reporter to a final concentration of 50 μM. The lysates were rotated at room temperature in the dark for 2 h. Cold acetone was added to precipitate proteins and proteins were pelleted, the supernatant decanted, and the proteins resuspended in 1X SDS-PAGE loading buffer.

References

(1)   Mike, L. A.; Dutter, B. F.; Stauff, D. L.; Moore, J. L.; Vitko, N. P.; Aranmolate, O.; Kehl-Fie,

        T. E.; Sullivan, S.; Reid, P. R.; DuBois, J. L.; et al. Activation of Heme Biosynthesis by a

        Small Molecule That Is Toxic to Fermenting Staphylococcus Aureus. *Proc. Natl. Acad. Sci.*

        U. S. A. **2013**, *110* (20), 8206–8211.

(2)   Johansson, P.; Hederstedt, L. Organization of Genes for Tetrapyrrole Biosynthesis in

        Gram-Positive Bacteria. *Microbiology* **1999**, *145* (3), 529–538.

(3)   Sato, S.; Murata, A.; Shirakawa, T.; Uesugi, M. Biochemical Target Isolation for Novices:

        Affinity-Based Strategies. *Chem. Biol.* **2010**, *17* (6), 616–623.

(4)   Li, Y.; Zuilhof, H. Photochemical Grafting and Patterning of Organic Monolayers on

        Indium Tin Oxide Substrates. *Langmuir* **2012**, *28* (12), 5350–5359.

(5)   Py, B.; Barras, F. Building Fe-S Proteins: Bacterial Strategies. *Nat. Rev. Microbiol.* **2010**, *8*

        (6), 436–446.

(6)   Loner, C. M.; Luzzio, F. A.; Demuth, D. R. Preparation of Azidoaryl- and Azidoalkyloxazoles

        for Click Chemistry. *Tetrahedron Lett.* **2012**, *53* (42), 5641–5644.

(7)   Dubinsky, L.; Krom, B. P.; Meijler, M. M. Diazirine Based Photoaffinity Labeling. *Bioorg.*

        Med. Chem. **2012**, *20* (2), 554–570.

(8)   Bender, T.; Huss, M.; Wieczorek, H.; Grond, S.; von Zezschwitz, P. Convenient Synthesis of

        a [1-14C]Diazirinylbenzoic Acid as a Photoaffinity Label for Binding Studies of V-ATPase

        Inhibitors. *European J. Org. Chem.* **2007**, *2007* (23), 3870–3878.

(9) Mecomber, J. S.; Murthy, R. S.; Rajam, S.; Singh, P. N. D.; Gudmundsdottir, A. D.; Limbach, P. A. Photochemical Functionalization of Polymer Surfaces for Microfabricated Devices. *Langmuir* **2008**, *24* (7), 3645–3653.

(10) Karney, W. L.; Borden, W. T. Why Does O -Fluorine Substitution Raise the Barrier to Ring Expansion of Phenylnitrene? *J. Am. Chem. Soc.* **1997**, *119* (14), 3347–3350.

(11) Lawrence, E. J.; Wildgoose, G. G.; Aldous, L.; Wu, Y. A.; Warner, J. H.; Compton, R. G.; McNaughter, P. D. 3-Aryl-3-(Trifluoromethyl)diazirines as Versatile Photoactivated "Linker" Molecules for the Improved Covalent Modification of Graphitic and Carbon Nanotube Surfaces. *Chem. Mater.* **2011**, *23* (16), 3740–3751.

(12) Hashimoto, M.; Hatanaka, Y.; Nabeta, K. Effective Synthesis of a Carbon-Linked Diazirinyl Fatty Acid Derivative via Reduction of the Carbonyl Group to Methylene with Triethylsilane and Trifluoroacetic Acid. *Heterocycles* **2003**, *59* (1), 395.

(13) The Site of Action of Oxazolidinone Antibiotics in Living Bacteria and in Human Mitochondria. *Mol. Cell* **2007**, *26* (3), 393–402.

(14) Colca, J. R.; McDonald, W. G.; Waldon, D. J.; Thomasco, L. M.; Gadwood, R. C.; Lund, E. T.; Cavey, G. S.; Mathews, W. R.; Adams, L. D.; Cecil, E. T.; et al. Cross-Linking in the Living Cell Locates the Site of Action of Oxazolidinone Antibiotics. *J. Biol. Chem.* **2003**, *278* (24), 21972–21979.

(15) Nguyen, T.; Francis, M. B. Practical Synthetic Route to Functionalized Rhodamine Dyes. *Org. Lett.* **2003**, *5* (18), 3245–3248.

(16) Wang, F.; Sambandan, D.; Halder, R.; Wang, J.; Batt, S. M.; Weinrick, B.; Ahmad, I.; Yang, P.; Zhang, Y.; Kim, J.; et al. Identification of a Small Molecule with Activity against Drug-Resistant and Persistent Tuberculosis. *Proc. Natl. Acad. Sci. U. S. A.* **2013**, *110* (27), E2510–E2517.

(17) Park, K. D.; Stables, J. P.; Liu, R.; Kohn, H. Proteomic Searches Comparing Two (R)-Lacosamide Affinity Baits: An Electrophilic Arylisothiocyanate and a Photoactivated Arylazide Group. *Org. Biomol. Chem.* **2010**, *8* (12), 2803–2813.

CHAPTER 7

TARGET IDENTIFICATION OF '3981

7.1 Introduction

Previous work on '3981 and its more active derivative '7501 indicate that, unlike '8882, '3981/'7501 do not rely on heme biosynthesis or cause intracellular accumulation of heme. Therefore, a hypothesis that these small molecules activate HssRS through a pathway that overlaps with the stages of HssS activation downstream of heme seems reasonable (Figure 4.1). Since details of this signaling process is not well understood, '3981/'7501 may prove useful as chemical probes for defining the mechanism of sensing heme toxicity in S. aureus.

Efforts towards identifying the cellular target of '3981 began after much of the work with '8882 had been conducted and the strategy for '3981 was influenced by experiences with '8882. We decided against an affinity purification approach for several reasons. First, given that '8882 affinity probe **6.7** was inactive, it seemed likely that adding large groups such as biotinylated linkers to a '3981 probe would also be detrimental to HssRS activation. While this could be related to preventing passage of the molecule into the cell, it may also interfere with binding to the target. Given this inherent uncertainty, a ligand directed approach was favored at the outset since smaller groups could be incorporated into the molecule with better chances of retaining activity. Second, an affinity purification experiment would be conducted in a lysate. This introduces more uncertainty into the experiment particularly with regard to the stability of the protein in the lysate and under the purification conditions. In contrast, ligand directed target identification can be conducted *in vivo* in a context where the probe has known activity.

As with '8882, photoaffinity affinity labeling was the preferred method of adducting proteins for ligand directed '3981 target identification. This was primarily due to the uncertainty that a nonphotoactivatable group such as an electrophile would be able to adduct proteins given the environment the probe was in when bound to its target (i.e. proximity to nucleophiles). Since the aryl azide '8882 probe **6.43** was not successful, likely because of the rearrangement of the singlet nitrene to the less reactive didehydroazepine, trifluoromethyldiazirines were exclusively used for '3981 target identification.

Several other aspects of the experiment were altered from those used for '8882 target identification. First, experiments using a fluorescent reporter were imaged by a GE Healthcare Typhoon gel scanner which uses a laser more specific to rhodamine's maximum excitation wavelength than the AlphaImager used for '8882 target identification experiments. Second, many of the later experiments rely on a biotin reporter which was visualized by Western blotting with a streptavidin-680 fluorophore imaged using a LICOR Odyssey. Finally, the click conditions used for reporter attachment were altered and optimized throughout these experiments.

7.2 Development of photoaffinity probes for '3981 target identification

Given the SAR data and the previously described constraints of developing a ligand directed photoaffinity probe using trifluoromethyldiazirines as the photoreactive group, the probe development strategy focused on incorporating the diazirine in the biaryl ether system and the click handle in the 3-position of the benzyl amine component. The 3-position was chosen because SAR data demonstrated that substitution at this position promoted efficacy (in

the case of '7501) and potency **4.10** (Chapter 4). The click handles to be investigated were an ethynyl group, benzyl azide, and iodo group. 3-iodine substitution in the benzyl component has already been established as a promoter of activity. A benzyl azide or ethynyl group in the 3-position were also likely to maintain activity since they are similar in size to iodine and a methyl ether (as in '7501).

The synthetic method for producing '3981 derivatives presented in chapter 4 offered the possibility of a modular approach for development of a '3981 probe. In this strategy, benzyl amines containing the click components and aminobiaryl ethers containing the diazirine would be prepared and initially coupled to the corresponding component of '7501. That compound would then be tested for HssRS activation using the XylE assay as an indication of the components effect on activity. When components are identified as active in the hybrid molecule, they will be coupled to each other to form putative probes. This strategy was advantageous over producing and screening every iteration of probes possible because it preserved advanced material.
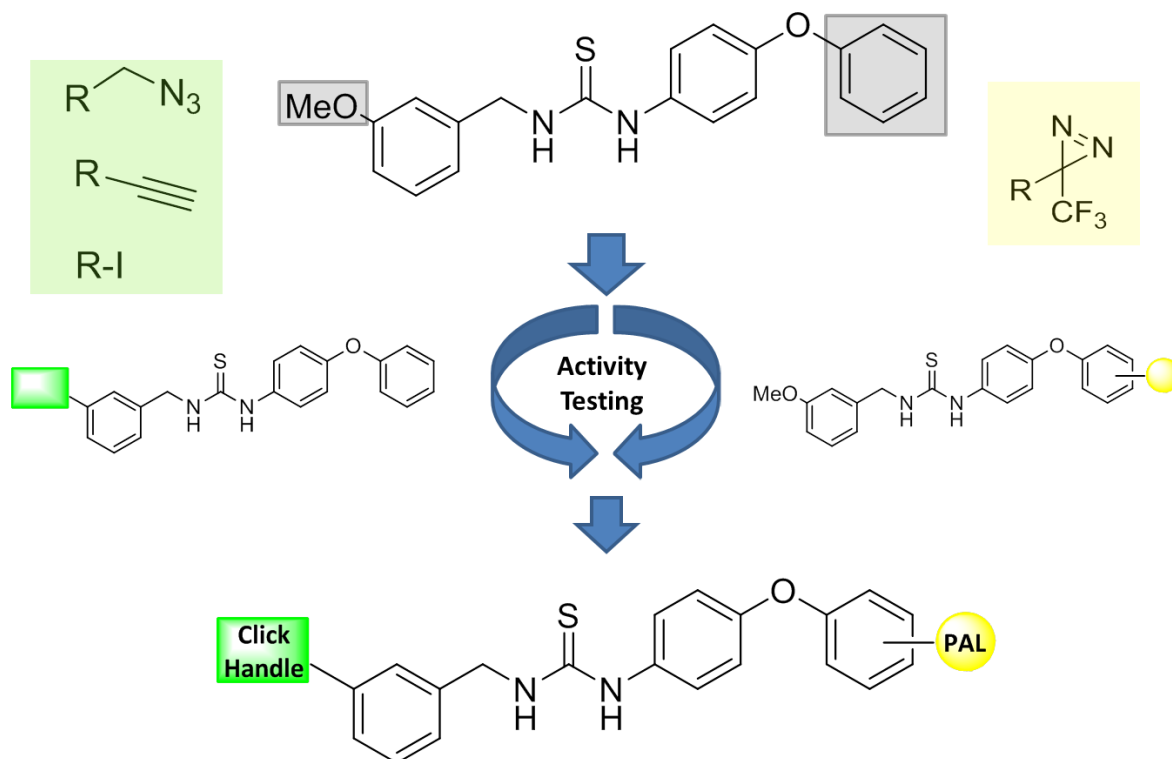
Figure 7.1. Modular strategy for probe development.

Synthesis of benzylamine components

3-iodobenzylamine is commercially available and also served as the starting material for 3-ethynylbenzylamine (**7.2**). **7.2** was prepared by Sonogashira coupling of **7.1** with trimethylsilyl acetylene followed by TMS removal with ammonia in methanol.[1]

No synthesis of benzyl azide component **7.7** had been reported. We envisioned synthesizing this compound through displacement of an activated benzyl alcohol with azide. 3-Methylaminobenzyl alcohol **7.4** was prepared by refluxing methyl 3-cyanobenzoate (**7.3**) with lithium aluminum hydride in THF to effect global reduction to the amino alcohol.[2] The amino group was selectively protected as the trifluoroacetamide with trifluoroacetic anhydride to provide **7.5**. Acetamide **7.5** was converted to the benzyl azide by treating with

diphenylphosphorylazide. Trifluoroacetamide deprotection was effected by sodium hydroxide to provide **7.7**.
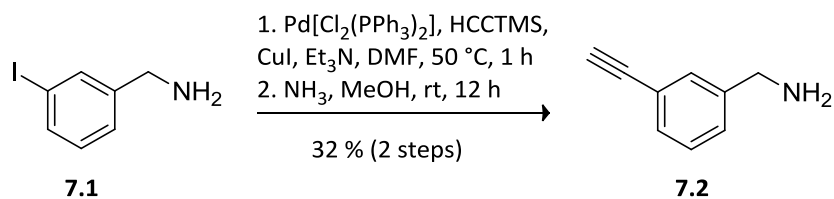
Scheme 7.1. Synthesis of **7.2**.
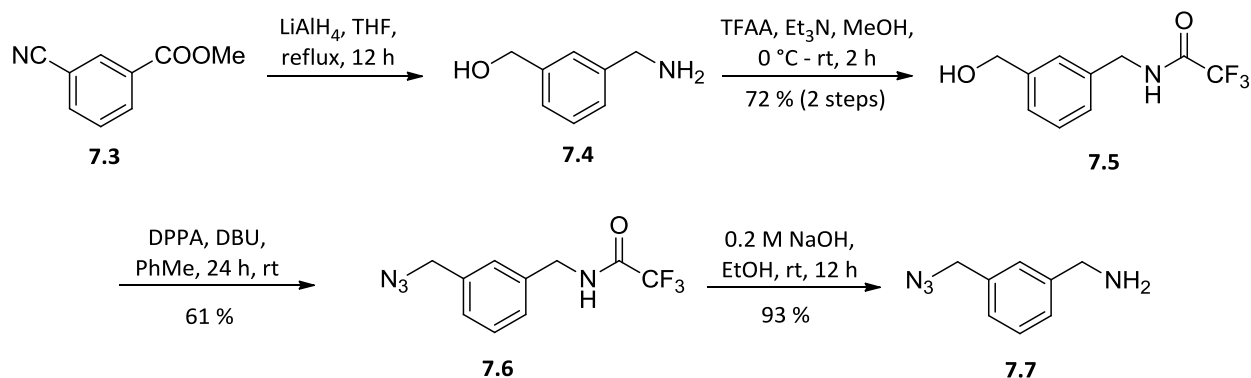
Scheme 7.2. Synthesis of **7.7**.

Synthesis of biaryl ether components

Initial efforts to synthesize a trifluoromethyldiazirine containing amino biaryl ether focused on converting 4-(4-bromophenoxy)aniline to the trifluoromethyl ketone and conversion to the diazirine through the previously described route. The planned route to the diketone started with protection of the aniline, lithium-halogen exchange by treatment with nBuLi, and quenching of the lithiate with N-trifluoroacetylpiperidine. This route was

192

problematic due to difficulties with protecting groups. These were either not stable during the lithium-halogen exchange or resulted in complex mixtures of products that could not be taken forward or could not be removed at the end.

Ultimately, this route was abandoned in favor of biaryl ether formation using S_NAr chemistry where the diazirine could be prepared as the anisole, demethylated, and coupled with a suitable electrophile. This approach would theoretically allow the synthesis of 3- and 4-substituted, though preparation of the 4-isomer would prove problematic.

Diazirine **7.9** was prepared in five steps from 3-bromoanisole and demethylated with boron tribromide as described in chapter 6.[3] **7.10** was stirred with 4-fluoronitrobenzene and potassium carbonate in DMF to form nitro biaryl ether **7.11**. The nitro group was reduced to the aniline with tin(II) chloride under acidic conditions to provide **7.12**.
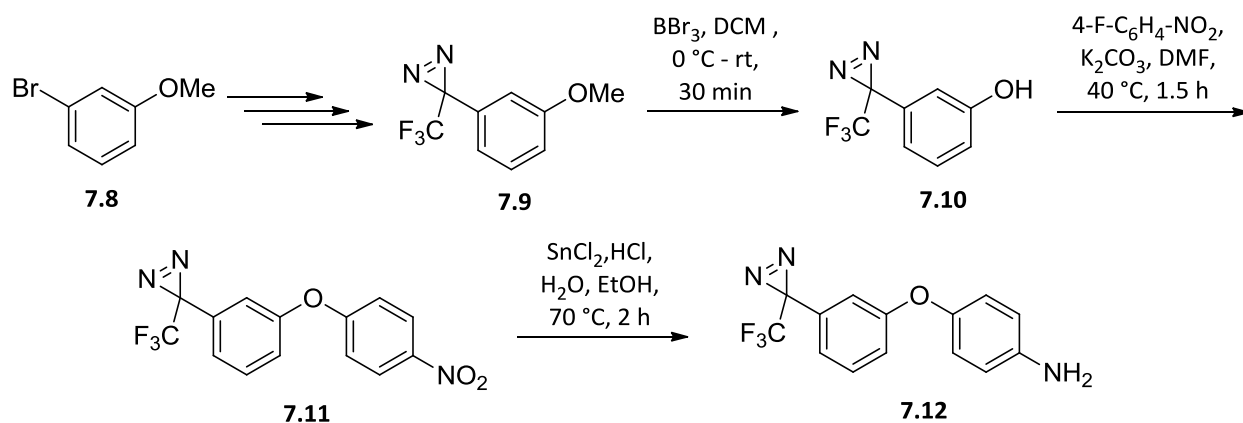
Scheme 7.3. Synthesis of probe component **7.12**.

Attempts to prepare the 4-diazirine substituted compound through a similar route were unsuccessful. **7.14** was successfully prepared from 4-iodoanisole using an analogous route as

7.9. However, demethylation with boron tribromide was problematic. TLC samples taken directly from the reaction mixture showed one spot. Unfortunately, upon workup and standing for several minutes in deuterated chloroform, a complex mixture was evident by NMR and TLC analysis. A possible explanation for this is depicted in scheme 7.4. We speculate decomposition occurs due to the electron releasing phenol located *para* to the delicate diazirine.
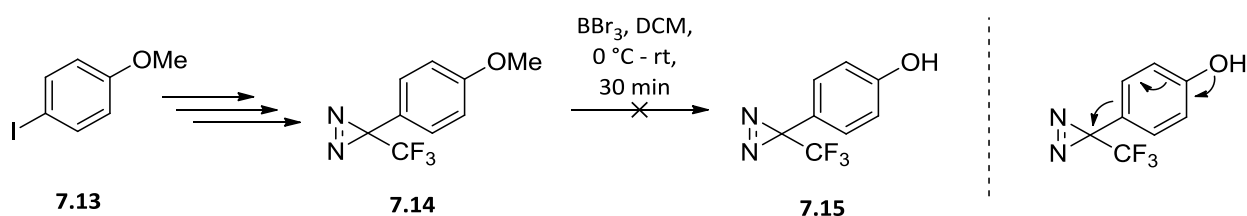
Scheme 7.4. Attempted synthesis of **7.15** for S_NAr coupling.

To overcome this, an alternate coupling strategy making use of the electron withdrawing properties of trifluoromethyl ketones was employed. The nucleophile and electrophile roles were switched to accommodate this and the biaryl ether was prepared at the ketone stage with the diazirine installed after coupling. The sequence began with boc protection of 4-aminophenol.[4] This was then reacted with 4'-fluoro-2,2,2-trifluoroacetophenone and potassium carbonate in DMF at 120 °C under microwave irradiation to provide biaryl ether **7.19** in 29 % yield. The ketone was converted to the diazirine using the previously described method to provide **7.20** in 19 % yield over three steps. While this sequence including the S_NAr coupling and diazirine formation was low yielding, it provided

enough material to move forward with activity testing. **7.20** was treated with trifluoroacetic acid in DCM to provide **7.21** as the TFA salt.
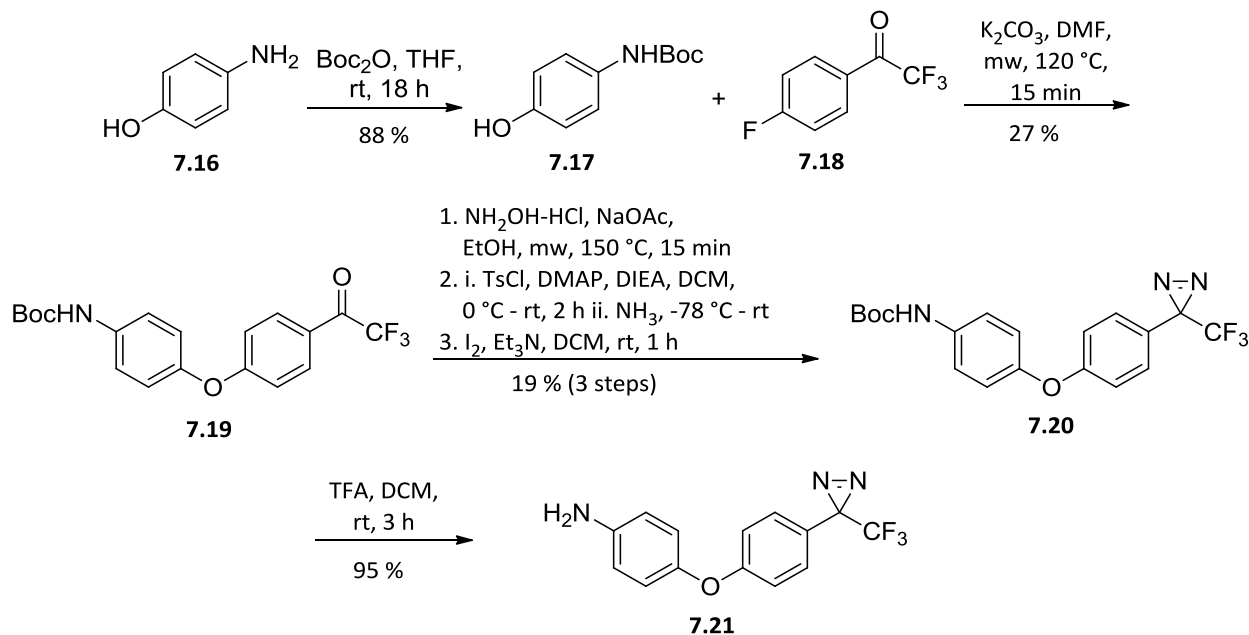
Scheme 7.5. Synthesis of component **7.21**.

Modular synthesis and evaluation of probe activity

With click components **7.2** and **7.7** and photoaffinity components **7.12** and **7.21** in hand, compounds **7.22** and **7.23** were prepared according to the modular testing scheme (Figure 7.3) using the chemistry outlined in chapter 4. Compounds were tested for activation of HssRS using the XylE assay at 10 and 40 µM and compared to '7501 at the same concentrations. The compound using click component **7.1** was not tested against '7501 in this series since its activity compared to '3981 was establish in chapter 4 and exhibited comparable activity to '7501. Therefore, it will likely not negatively affect activity if incorporated into a probe. In addition, for the same reasons outlined in chapter 6, namely the limited examples of Pd-mediated click

reactions, an iodine click handle containing probe was not preferred to a handle for CuAAC and only kept as a possibility if the other handles were not well tolerated.
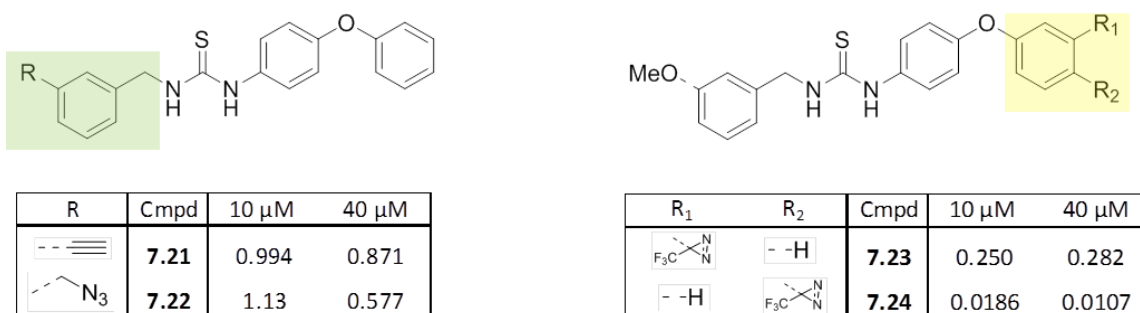
Figure 7.2. Activation of HssRS using modular probe synthesis scheme. Data are presented as the fraction of HssRS activity compared to '7501 at the same concentration.

Compounds **7.21** and **7.22** both exhibit comparable activities to '7501 at 10 μM, but a loss of activity is observed at 40 μM. This is consistent with previous observations that these thiourea molecules do not activate HssRS in the XylE assay as well at higher concentrations. Given these results, both the benzyl azide and ethynyl group appear to be appropriate click handles for a future '3981/'7501 probe.

In contrast, placement of the trifluoromethyl diazirine significantly affects the activity of the resulting molecule compared to '7501. With the diazirine in the 4-position, **7.24** only exhibits ~1 % the activity of '7501. With the diazirine in the 3-position, **7.23** activates ~25 % that of '7501 at both concentrations, indicating that this is the best position for the diazirine in a future probe.

Having identified **7.2** and **7.7** as suitable click handles and **7.12** as the photoaffinity

component for the best activity, the two possible probes from this combination, **7.25** and **7.26**

were prepared and tested for HssRS activation and compared to '7501. Probe **7.25** with ethynyl

click handle was not significantly active demonstrating ~1-2 % the activity of '7501 at both

concentrations. Probe **7.26** with benzyl azide click handle exhibited fairly good activation at 10

μM with ~40 % the activity of '7501, but appeared to be toxic at 40 μM. As a result, the activity

appeared significantly diminished at this concentration. Despite this, the activity of **7.26** at

lower concentrations indicates it will be an acceptable probe for '7501 target identification. A

concentration response curve of **7.26** was generated and an EC_{50} of 2.16 μM was determined.
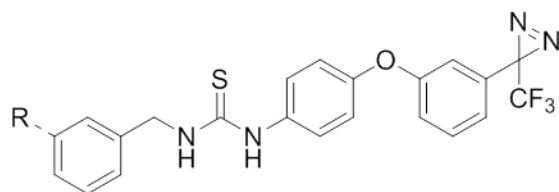
R	Cmpd	10 μM	40 μM
▬	**7.25**	0.0131	0.0176
N₃	**7.26**	0.400	0.0540

Figure 7.3. HssRS activation of putative probes **7.25** and **7.26**. Data are presented as the fraction of HssRS activity compared to '7501 at the same concentration.
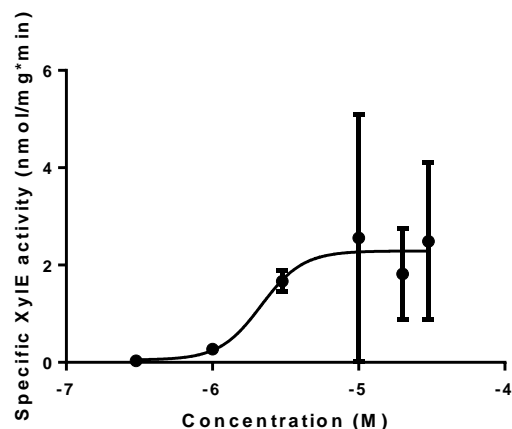
Figure 7.4. Concentration response curve of **7.26**.

7.3 Target identification experiments with 7.26

As with the strategy for '8882 target identification, the emphasis of early experiments was to identify bands on a gel that are present in a probe treated sample but diminish or disappear when co-treated with a competitor. For most experiments '7501 was used as competitor. Once bands were identified, experiments would move into a phase geared towards isolating and identifying the proteins that correspond to the bands.

General experimental details

The UV light source utilized for these experiments was a Reptisun 10.0 bulb housed in a deep dome lamp fixture generally used as a light source for indoor reptile enclosures (for this reason, the assembly will be referred to as the "lizard lamp"). The emission spectrum of this bulb exhibits a large spike around 360 nm which is the appropriate wavelength for diazirine activation. To determine an optimum irradiation time, the probe was dissolved in methanol and irradiated with the lizard lamp. The ratio of unreacted probe to the methanol adduction product of photolysis was observed. Based on this experiment, irradiation times of 6 – 10 min

seemed optimal and in general, most samples were irradiated for 8 - 10 min. Because this is a relatively long irradiation time, with the exception of the first few experiments which were conducted at room temperature, most samples were irradiated in an incubator at 37 °C with 120 rpm shaking. The purpose of this was to prevent any change in protein expression or compound binding affinity as a result of the culture cooling to room temperature during the irradiation process.

In order to accommodate the azido click handle in **7.26**, terminal alkyne-rhodamine reporters **7.28** and **7.29** were prepared**. 7.28** was prepared by reacting **7.27** (as the TFA salt) with *o*-nitrophenol carbonate-activated 5-pentynol. **7.29** was prepared by reacting **7.27** (as the TFA salt) with the succinimide ester of pentynoic acid under basic conditions. Biotin reporter **7.30** was similarly prepared. The choice of base for this reaction influenced the ease of purification by column chromatography. Use of triethylamine resulted in triethylammonium trifluoroacetate which was difficult to separate from the product on silica gel. Use of potassium carbonate instead of triethylamine eliminated this complication.

As previously mentioned, experiments using reporters **7.28** and **7.29** were imaged using a GE Healthcare Typhoon gel scanner and experiments using biotin reporter **7.30** as well as cleavable biotin probes (which will be discussed later) were visualized on a LICOR Odyssey after western blotting with streptavidin-680 or -800 fluorophores. Protein concentrations were normalized by BCA assay during the experiment to ensure equal protein concentrations across samples.
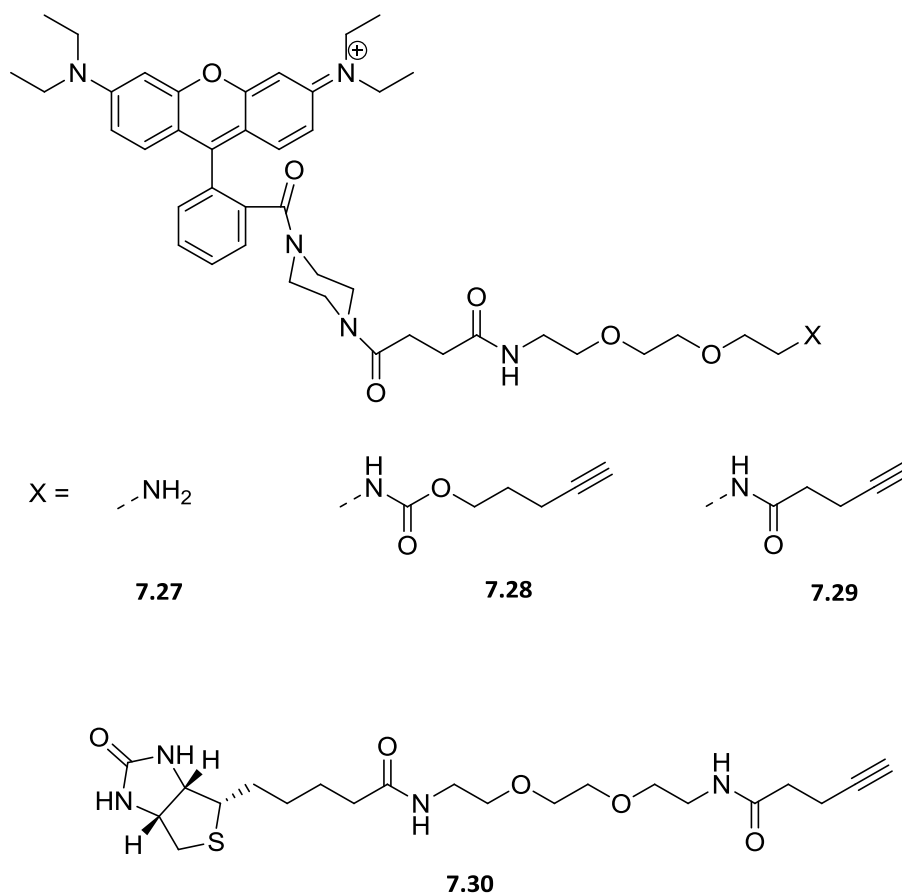
Figure 7.5. Clickable reporters used in this chapter.

Competition experiments

The first experiment conducted was a simple competition experiment. *S. aureus* was subcultured into media with 20 µM of **7.26** and either 0, 1, 10, 20, or 40 µM of '7501. The bacteria were grown for 4 h and then irradiated with the lizard lamp for 10 min. The bacteria were lysed and the lysates treated with **7.28** under the previously described click conditions.[5] Proteins were precipitated with acetone and resuspended in 1X loading buffer, separated by SDS-PAGE, and visualized with the Typhoon gel scanner (Figure 7.7). Several controls were run including a sample that was treated with 20 µM of **7.26** but no irradiation, a sample from

bacteria not grown with **7.26** but subjected to the same experimental conditions as the rest of the samples, and a **7.26** labeled sample where reporter **7.28** was excluded from the click reaction.
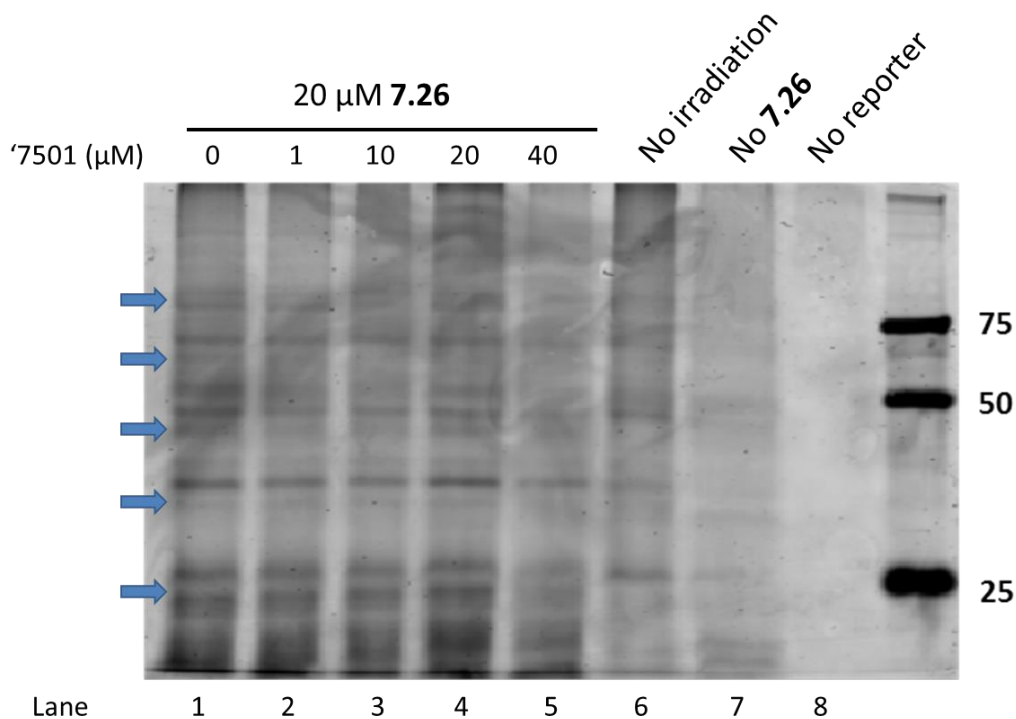
Figure 7.6. Results of competition experiment with **7.26** and **'7501** visualized with reporter **7.28**.

No fluorescently labeled bands and very little background fluorescence was observed in the sample not treated with reporter **7.28** (Figure 7.7, lane 8) indicating that any fluorescence was the result of labeling by **7.28**. The sample not treated with probe **7.26** (Figure 7.7, lane 7) exhibited some faint bands but considerable background compared to lane 8 suggesting some nonspecific labeling of proteins by **7.28** was occurring. Treatment with **7.26** without irradiation (lane 6) resulted in several distinct bands exhibiting fluorescence as well as a stronger

background than the previous controls. Several bands in lane 6 overlap with bands in lanes 1 – 5 indicating that nonphotoinduced labeling was occurring. This may be occurring through thermal activation of the diazirine or some other mode of covalent adduction by the probe, possibly through the thiourea moiety. Despite this, several bands not appearing in lane 6 were present in lanes 1 – 5 and several of these seemed to diminish or disappear with increasing concentrations of '7501 competitor (Figure 7.7, blue arrows).

This result was encouraging and further experiments were conducted to optimize the target identification scheme. Despite demonstrating that '7501 activates HssRS during log phase, a photoaffinity experiment sampling different time points along the S. aureus growth curve was conducted by incubating bacteria with 20 μM of **7.26** either alone or with 40 μM '7501 to determine any differential protein labeling between time points. Irradiation was conducted at 1 h (lag phase), 3 h (early log phase), and 5 h (mid to late log phase).
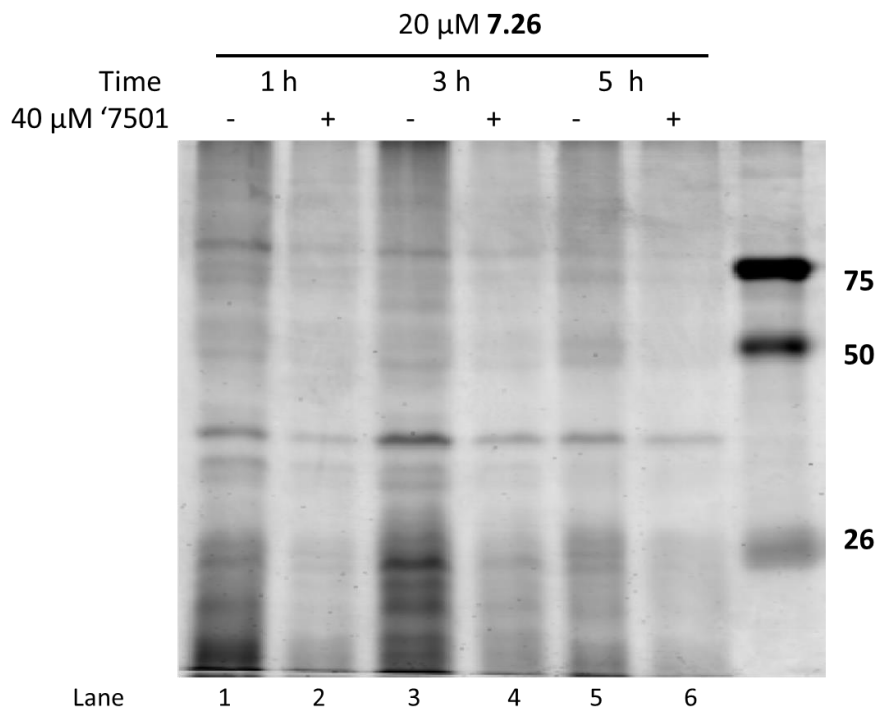
Figure 7.7. Competition experiment with **7.26** and '7501 at different time points.

Another optimization experiment examined what aspects of the experiment contributed to the nonspecific labeling seen in control samples. One possibility was that cellular nucleophiles could potentially react with the carbamate moiety of **7.28,** displacing 5-pentyn-1-ol and resulting in nonspecific protein labeling during the click reaction or further sample processing steps. To control for this, reporter **7.29** was prepared replacing the carbamate with a less reactive amide bond. Bacteria were incubated with **7.26** and either irradiated with the lizard lamp or not exposed to light to prevent photolabeling. Each sample was subjected to CuAAC conditions with either **7.28** or **7.29**. The results indicate no significant labeling differences between the two reporters in either condition. A control where a probe treated *S. aureus* lysate incubated with only reporter **7.28** and no other click reagents (Figure 7.8, lane 6)

displays some amount of labeling indicating there was nonspecific labeling of proteins by reporter **7.28** through some feature of the molecule not related to CuAAC. Given the difference in background between lane 6, and lanes 1 – 4, it seems that this is not a significant source of nonspecific labeling. A lysate of *S. aureus* not incubated with **7.26**, but treated with **7.28** under CuAAC conditions also did not exhibit the magnitude of background as lanes 1 – 4 indicating that the background fluorescence is likely due to nonspecific labeling by the probe itself and not through the linkers.
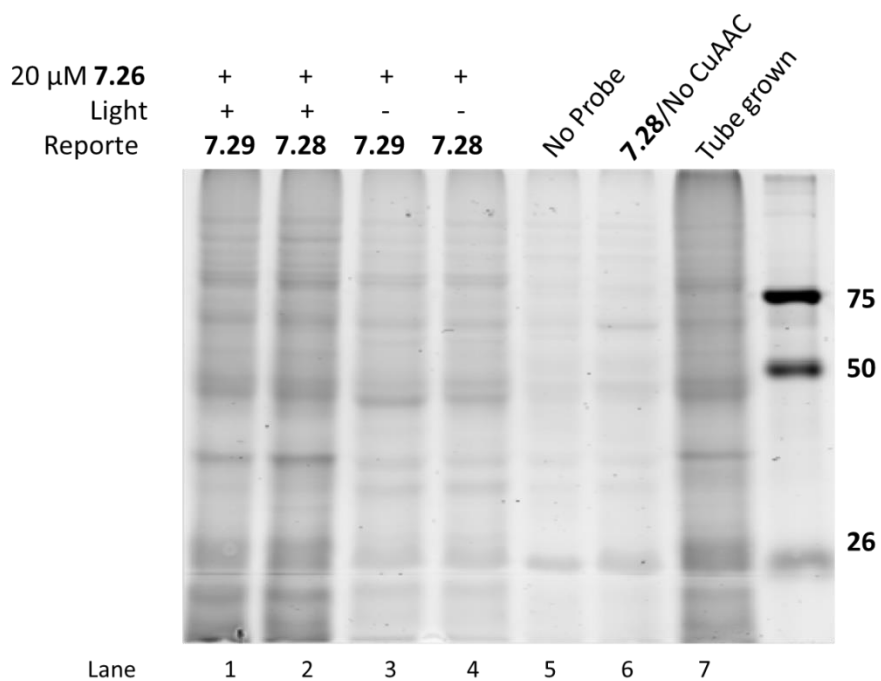
Figure 7.8. Competition experiment with probe **7.26** and reporters **7.28** and **7.29**.

These experiments have demonstrated that probe **7.26** can label proteins and this labeling can be competed off by '7501. However, considerable background labeling occurred which may have been the result of using high concentrations of probe **7.26**. Therefore, the probe concentration was lowered to 5 or 10 μM in future experiments. In addition, a significant

amount of protein labeling occurs in controls where bacteria are incubated with **7.26**, but not irradiated with the lizard lamp. This may be because of thermal activation of the diazirine or possibly through some other mode of covalent protein adduction by **7.26**.

The same experiment was conducted using 10 μM of **7.26** for the probe incubations and utilizing biotin reporter **7.30**. The purpose of using this reporter was to demonstrate that a similar result could be obtained to the results with reporter **7.28**. In addition, the Typhoon gel imager did not always give consistently clear images and results possibly because the instrument samples a plane of the gel for imaging and the three dimensional distribution of proteins can vary from gel to gel. In contrast, using reporter **7.30** required transferring to a nitrocellulose membrane which moves the proteins on to one plane.

This experiment was also conducted with an additional probe where the sulfur of **7.26** was replaced with oxygen to provide the urea. Since the urea derivative of '3981 was comparably active to '3981, it was possible that this would be the case with **7.26**. Urea probe **7.31** demonstrated comparable activity to **7.26** at 10 μM but was significantly more active at 40 μM due to its lack of toxicity at that concentration. Due to the lack of toxicity, it was likely **7.31** would bind fewer proteins nonspecifically and permit better analysis of results. If a band appeared in both the **7.26** and **7.31** lanes and diminished in competitor lanes, that band would be a strong candidate for a target.
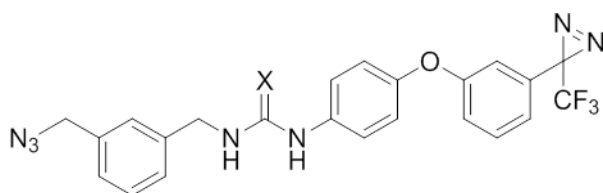
X	Cmpd	10 μM	40 μM
S	**7.26**	0.358	0.0531
O	**7.31**	0.323	0.320

Figure 7.9. Relative HssRS activation of **7.26** and **7.31** compared to '7501 at the same concentrations.
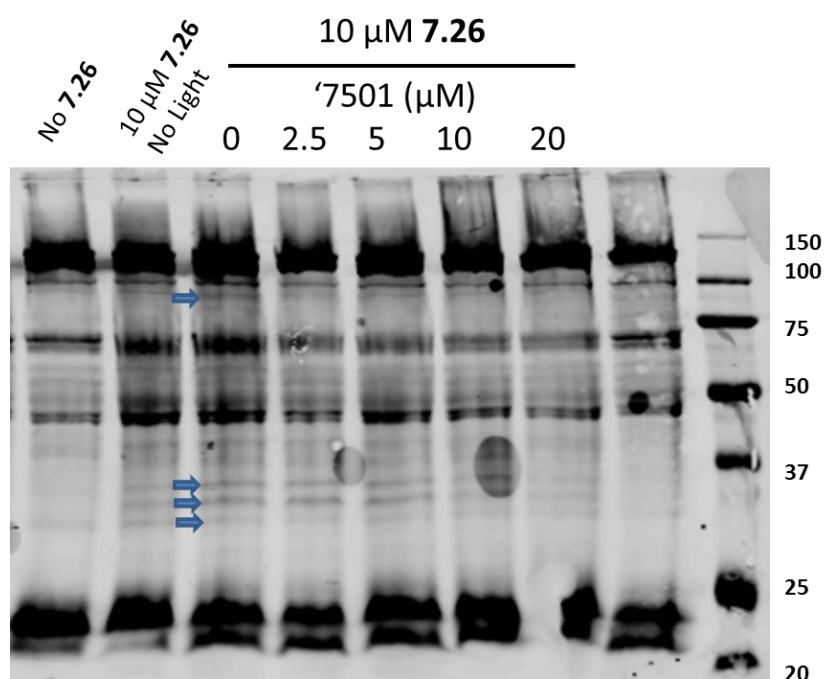
Figure 7.10. Photoaffinity experiment visualized using biotin reporter **7.30** and streptavidin-680. Arrows indicate bands that appear to diminish with '7501 competition.

The results of this experiment were mostly consistent with those visualized with **7.28** and the gel scanner. There appears to be less background in the samples in general which was likely the result of using less **7.26** in the experiment though this was not directly tested. There appear to be several bands around 30 – 37 kDa that diminish with increasing '7501 treatment

as well as a band around 100 kDa. There were similar bands in the experiments conducted with **7.28**. Unfortunately, there were no bands that appeared in the **7.31** treated lane suggesting that despite being active, this is not likely to aid in the target identification process.

7.4 Isolation of tagged proteins using cleavable linkers

These results taken together suggested that it was possible to isolate targets using a photoaffinity approach. In order to effectively identify the labeled proteins, they must be separated from the whole cell lysate. One method of accomplishing this is by exploiting the interaction between biotin and streptavidin. The lysates with biotin reporter clicked on could be incubated with streptavidin beads, thoroughly washed to remove nonspecifically bound proteins, and then eluted to release the tagged proteins for proteomic analysis. However, eluting biotinylated molecules from streptavidin typically requires harsh conditions and results in contamination of the resulting samples with nonspecifically bound proteins that were not removed during washing steps.[6]

One method to overcome this is the use of cleavable linkers as described in chapter 5. Tirrell and coworkers evaluated several cleavable linkers for their selectivity during elution. They found that a dialkoxydiphenylsilane containing linker, which is cleaved under mildly acidic conditions, was the most selective. They reported a synthesis for an azido linker. Attempts to make an alkynyl version of this linker for '7501 target identification were unsuccessful. Instead of this linker, carboxybenzophenone-based cleavable linker **7.32**, developed by the Porter and coworkers[7], was employed. This functional group can be cleaved by irradiation with 365 nm light.

With this linker in hand, photoaffinity experiments with **7.26** were conducted. The same growth and irradiation conditions as previous experiments were utilized. The samples were lysed and the cleavable linker clicked on. At this point, alternate click conditions were used consisting of 200 µM CuBR, 200 µM TBTA, and 50 µM of **7.32**. These conditions were chosen because they were used by Tirrell and coworkers in their linker evaluation paper. After the click reaction, excess **7.32** was removed by passage of the reaction through a GE Healthcare PD10 desalting column. The samples were then incubated with M280 Dynabeads for 1 h at room temperature. The beads were washed sequentially with 0.1 % SDS in PBS, 4 M urea, and 1 M NaCl, each targeting a specific protein-protein interaction, and finally the beads were washed with water to remove excess NaCl. The beads were then resuspended in PBS and irradiated for 2 h with a 365 nm UV lamp. This elution was sequestered from the beads and the beads were heated to 90 °C in 1X SDS-PAGE loading buffer to remove any residual proteins.
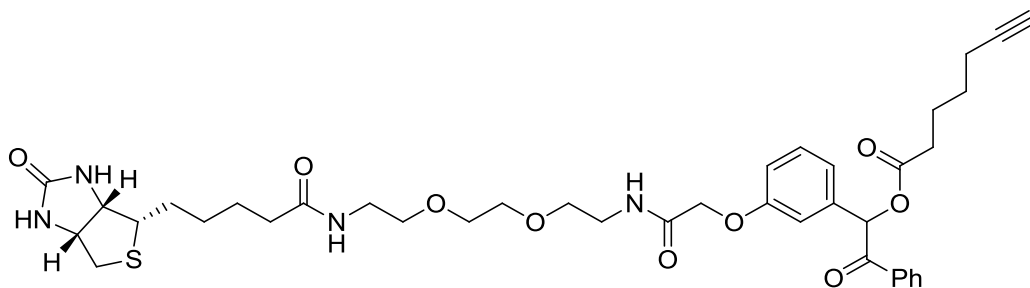
Figure 7.11. Photo cleavable linker **7.32**.
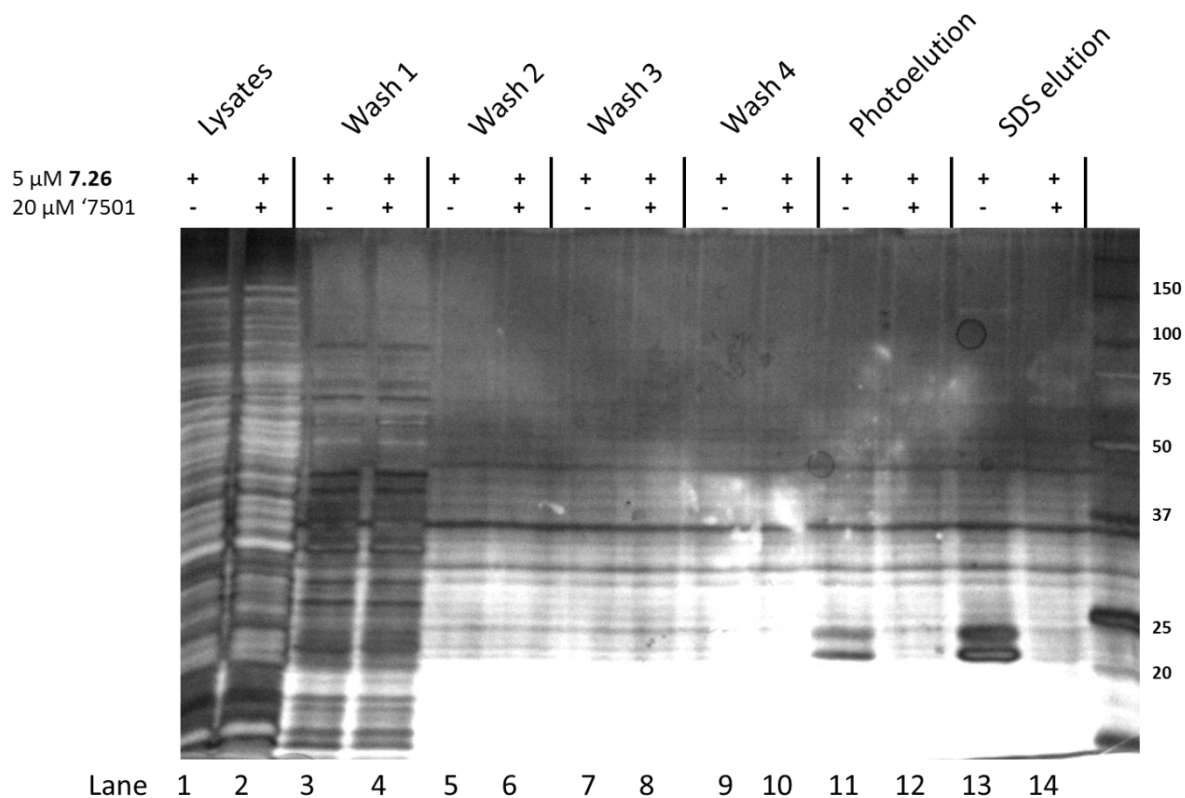
Figure 7.12. Photoaffinity probe pulldown with photocleavable linker **7.31**. Wash 1 = 0.1 % SDS in PBS, Wash 2 = 4 M urea, Wash 3 = 1 M NaCl, Wash 4 = water. Gel visualized by silver staining.

The samples from this experiment were separated by SDS-PAGE and visualized by silver staining. The gel required a fairly long developing time to visualize bands in the photoelution lanes resulting in a high background in other lanes. Several bands appear enriched in the **7.26** treated lane (lane 11) compared to the **7.26** cotreated with '7501 lane (lane 12). However, none of the bands between 30 – 37 kDa that appeared in the previous competition experiments appeared in this lane.

The elution samples were submitted to the proteomics core for identification and relative quantitation by spectral counting. Not surprisingly, the top hits were endogenously

biotinylated proteins, pyruvate kinase and acetyl-CoA carboxylase. In addition to being the most abundant, in the sample, there was also an enrichment in probe vs. competitor suggesting that they could be real targets.

A refined list of proteins identified in this experiment is presented in Table 7.1. In order to validate these hits, the NARSA transposon mutant library was utilized.ref) Seven of the 11 hits had transposon mutants in the NARSA library. If protein expression was knocked down because of transposon insertion into a gene, '7501 should not be active. Using the same assay described in chapter 3, these transposon mutants were tested for their ability to be preadapted to heme toxicity by '7501. If one of these genes were the target, '7501 should not be able to preadapt that strain to heme toxicity. All of the mutants were able to sense '7501 and adapt to heme toxicity. In addition, an IsaA knockout in S. aureus strain SH1000 was obtained courtesy of the Boles lab.(ref) This strain was also tested for its ability to preadapt to heme toxicity by '7501 and was successful. These data indicate that none of the proteins pulled down are likely the target.

Protein name	MW (kDA)	Newman gene	USA300 gene	NARSA	Pathway
Pyruvate carboxylase	129	pycA	pyc	Yes	Central metabolism
Acetyl-CoA carboxylase, biotin carboxyl carrier protein	17	accB	accC	Yes	Fatty acid biosynthesis
Probable transglycosylase	24	isaA		No	Cell wall biosynthesis
Inosine-5'-monophosphate dehydrogenase	53	guaB		No	Nucleotide biosynthesis
Putative uncharacterized protein	12	NWMN_1673		Yes	
Serine protease	87	htrA	htrA	Yes	
Glycerol kinase	56	glpK	glpK	Yes	Fatty acid biosynthesis
Hyaluronate lyase	92	hysA		Yes	Cell wall biosynthesis
Phage transcriptional activator	16	NWMN_1013		No	
2-succinylbenzoate--CoA ligase	55	menE		No	Menaquinone biosynthesis
Putative uncharacterized protein	68	NWMN_2339		Yes	

Table 7.1. Refined list of proteins identified by proteomics from photoaffinity pulldown experiment.

These results indicate certain problems with the overall experimental design. First, the abundance of endogenously biotinylated proteins is problematic since the photoelution step should not result in their release from the beads and they should only elute when heated in 1X loading buffer. It is possible that these proteins are nonspecifically released from the beads during this step. Since they were the most abundant proteins in the samples, it also suggests

that the beads were oversaturated with endogenously biotinylated proteins. This means that any proteins tagged by **7.26** and **7.32** did not bind the beads and were washed away. Another concerning result is the larger amount of endogenously biotinylated proteins in the probe sample compared to control. Pyruvate kinase was six times more abundant in the probe sample than control and no peptides from acetyl-CoA carboxylase were found in the control sample. It is unlikely this result is due to differences in protein concentration since the proteins concentration of each sample was normalized by BCA assay. Sample handling could have been a source of error since the probe and control samples were handled separately, but the same procedures were carefully applied to both of them. One explanation for the discrepancy is that '7501 decreases the abundance of endogenously biotinylated proteins. While the premise of this experiment requires that **7.26** and '7501 have the same target and same effects on the cell, '7501 exhibits greater efficacy than **7.26** and is present in higher concentrations in the control sample. This difference in concentration and efficacy may lead to differential protein expression between the probe and control samples. This problem is not easily fixed as the previous competition experiments indicate a high concentration of '7501 is needed to effectively compete with **7.26**.

To address the possibility that endogenously biotinylated proteins were oversaturating the streptavidin beads during the binding step, an experiment was conducted where a lysate from *S. aureus* was treated with **7.26** was incubated with varying amounts of M280 Dynabeads, then treated with **7.32** under CuAAC conditions, and each sample desalted. A sample from each condition was visualized with streptavidin-680 fluorophore after separation by SDS-PAGE and transferring to nitrocellulose. Endogenously biotinylated samples were still visible in the highest

concentration of beads used indicating that they are likely being oversaturated and any **7.26/7.31** tagged proteins are not binding as a result of competition. A similar experiment was conducted using higher capacity GE Healthcare Streptavidin Sepharose beads. The results are displayed in Figure 7.12. Pretreatment with the higher capacity beads seems better able to remove endogenously biotinylated proteins from samples. While the lower bands are cut off, the band corresponding to pyruvate carboxylase at 127 kDa is visible and clearly diminishes, though not completely, with increased amount of streptavidin beads used.
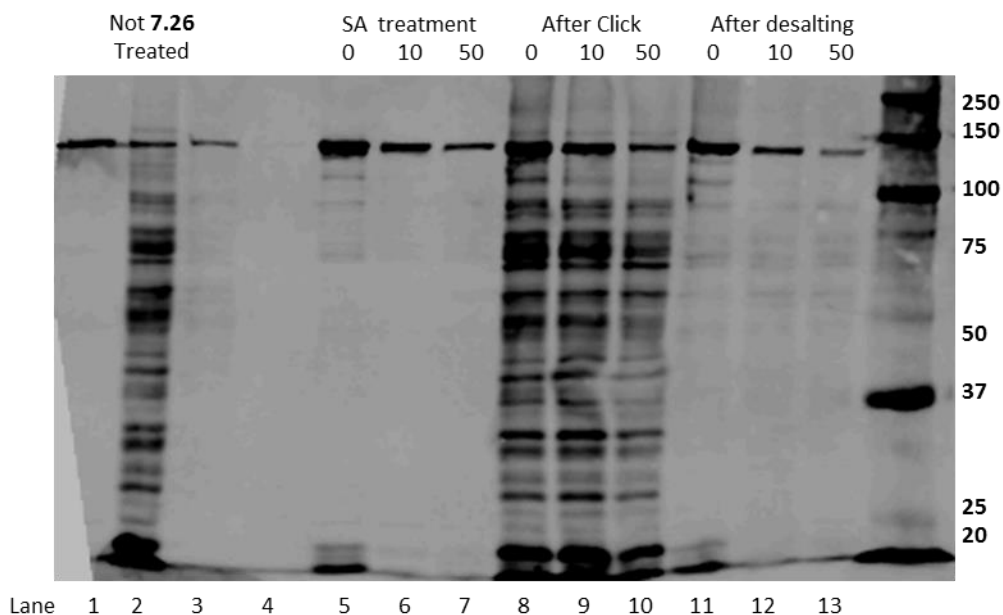
Figure 7.13. Streptavidin pretreatment results. Lane 1 – 3 was from a lysate of bacteria not treated with probe. 1 = sampled immediately after pretreatment with 50 µL SA beads, 2 = sampled after click reaction, 3 = sampled after desalting. Lanes 5 – 13 were lysates from bacteria treated with 10 µM **7.26**. Numbers above lanes indicate amount (µL) SA beads used for pretreatment. Lanes 5 – 7 = sampled after SA pretreatment, lanes 8-10 = sampled after click reaction, and lane 11 – 13 = sampled after desalting step.

This experiment also indicated two other potential issues with the photoaffinity pulldown. The heavy labeling observed in the lanes corresponding to samples taken

immediately after the click reaction (lanes 2, 8, 9, and 10) was indicative of nonspecific labeling by reporter **7.32.** Furthermore, the samples taken after desalting (lanes 3, 11, 12, and 13) do not exhibit this labeling indicating the nonspecific labeling is likely occurring through direct interaction of **7.32** with proteins. It is not clear how this is occurring. These samples were prepared by directly sampling the reaction mixture, adding 1X loading buffer, and heating at 90 °C for 10 min to denature proteins. These harsh conditions likely led to the considerable nonspecific labeling observed in this experiment. While this would not be an issue during the pulldown experiment due to the desalting step removing excess **7.32**, several optimization experiments were conducted where the samples were prepared in this manner and may have provided misleading results. Furthermore, acetone precipitation of proteins after the click reaction, which should theoretically remove excess **7.32**, does not consistently prevent nonspecific labeling.

Another issue indicated by this experiment was that very little specific labeling appeared to be occurring since desalted probe treated lanes 11 – 13 did not differ significantly in appearance from control lane 3. This could be the result of the new click conditions (CuBr, TBTA) not being as efficient as the previous conditions (CuSO$_4$, sodium ascorbate, TBTA), However, an experiment was conducted directly comparing the two conditions and they did not appear to differ. Another possibility was that the large acetophenone group prevents the alkyne from accessing the azide. These experiments were conducted in lysates with proteins retaining their native conformation and it is possible **7.26** binds somewhere other than the surface of its target. **7.28 – 7.30** are all fairly linear while **7.32** has quite a bit of steric bulk due to the photocleavable moiety. This may prevent the linker from penetrating to the binding site

and reacting with the azide. To test this, labelling of lysates from **7.26** treated S. aureus using standard conditions with native proteins was compared to tagging in a lysate subjected to acetone precipitation. The acetone precipitation samples showed several extra bands compared to the native proteins. This suggested that denaturation of proteins before the click reaction with **7.32** was advantageous.

An experiment was conducted taking into account all of these factors. *S. aureus* was incubated with 5 µM of **7.26** or 5 µM **7.26** and 20 µM of '7501 as competitor for 3 h at which point they were irradiated with the lizard lamp. Bacteria were collected and run through the standard experimental procedure. Samples were taken at each point to confirm click labeling and streptavidin binding. GE high capacity streptavidin sepharose was used for the pulldown. Samples were evaluated by Western blotting to determine the presence of biotinylated proteins and samples from the pulldown washes and elutions were visualized by silver staining.
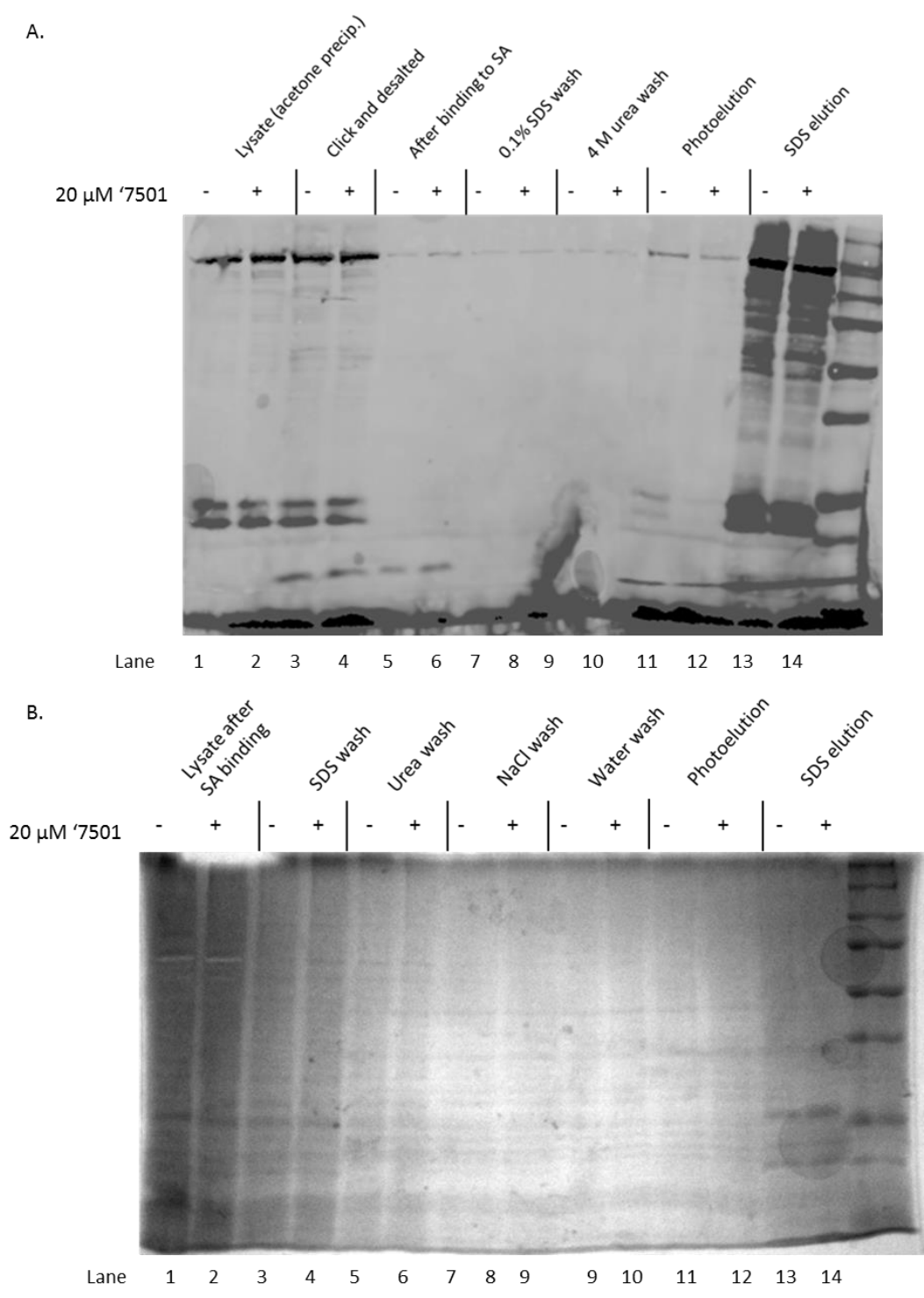
Figure 7.14. Pulldown experiment with photocleavable linker. A. Western blot visualized using streptavidin-680 fluorophore. B. SDS-PAGE gel visualized by silver staining.

This experiment demonstrated that the streptavidin binding step binds most of the biotinylated proteins, either endogenous or labeled with **7.32**. There are several bands that appear in lanes 3 and 4 (Figure 7.14.A) that disappear after treatment with streptavidin beads (lanes 5 and 6). The endogenously biotinylated proteins are completely absorbed, except for a small amount of pyruvate carboxylase. In addition, some of these proteins reappear in the photoelution samples indicating that these proteins may nonspecifically dissociate from the bead during this step. Several bands corresponding 7.32 labelled proteins are apparent in lanes 3 and 4, particularly around 50 kDa and a strong band around 10 kDa. 50 kDa proteins appear to bind the beads completely while there is some residual 10 kDa protein in the sample.

Unfortunately, there did not seem to be any enrichment of **7.32** labelled proteins in probe samples compared to competitor samples. Furthermore, no bands were clearly visible in the photoelution lanes (besides background) when the samples were separated by SDS-PAGE and visualized by silver staining.

Given these results, the decision was made to forgo analysis of samples by Western blotting and SDS-PAGE and instead, submit samples directly to the proteomics core for analysis. While it would have been ideal to observe enrichment of proteins in a probe treated sample over a sample cotreated with competitor this may not be realistic. A final experiment was conducted using the same conditions and procedures as the previous pulldown and including a sample treated with **7.31**. These samples were submitted directly to the proteomics core. The list of proteins is fairly long and is presented in the appendix to this chapter. The current focus of experiments is to narrow this list down by using more controls.

7.5 Conclusions

Using SAR data and a modular approach to probe design, probe **7.26** was prepared. Several experiments were conducted to preliminarily establish the ability of **7.26** to specifically label proteins and for '7501 to be able compete with this specific labeling and appeared to be successful. However, efforts to isolate these proteins from a whole cell lysate have been unsuccessful so far. A variety of optimization experiments have been conducted and these have led to a fairly refined experimental protocol. Despite this, the most recent proteomics results do not conclusively point to any particular targets. Future experiments should include more than one control to help narrow down candidate target proteins.

Experimental Section

General Procedure: All non-aqueous reactions were performed in flame-dried flasks under an atmosphere of argon. Stainless steel syringes were used to transfer air- and moisture-sensitive liquids. Reaction temperatures were controlled using a thermocouple thermometer and analog hotplate stirrer. Reactions were conducted at room temperature (rt, approximately 23 °C) unless otherwise noted. Flash column chromatography was conducted using silica gel 230-400 mesh. Analytical thin-layer chromatography (TLC) was performed on E. Merck silica gel 60 F254 plates and visualized using UV and iodine stain.

Materials: All solvents and chemicals were purchased from Sigma-Aldrich. Dry dichloromethane was collected from an MBraun MB-SPS solvent system. Triethylamine, N,N-dimethylformamide (DMF) and dimethyl sulfoxide were used as received in a bottle with a Sure/Seal. N,N-diisopropylethylamine was distilled from calcium hydride and stored over KOH. Deuterated solvents were purchased from Cambridge Isotope Laboratories.

Instrumentation: ^{1}H NMR spectra were recorded on Bruker 400, 500, or 600 MHz spectrometers and are reported relative to deuterated solvent signals. Data for ^{1}H NMR spectra are reported as follows: chemical shift (δ ppm), multiplicity (s = singlet, d = doublet, t = triplet, q = quartet, p = pentet, m = multiplet, br = broad, app = apparent), coupling constants (Hz), and integration. ^{13}C NMR spectra were recorded on Bruker 100, 125, or 150 MHz spectrometers and are reported relative to deuterated solvent signals. Low resolution mass spectrometry (LRMS) was conducted and recorded on an Agilent Technologies 6130 Quadrupole instrument.

N-(3-(azidomethyl)benzyl)-2,2,2-trifluoroacetamide (7.6) To a stirred suspension of **7.5** (131.4 mg, 0.563 mmol) in toluene (5 mL)

was added diphenylphosphorylazide (145 μL, 0.676 mmol) and the resulting mixture was cooled

to 0 °C. To this cooled reaction was added DBU (102 μL, 0.676 mmol). The reaction was allowed

to warm to room temperature and stirred for 3 d. The reaction was concentrated and the

residue was purified by column chromatography to afford 88.8 mg (61 %) of **7.6**. ^{1}H-NMR (400

MHz, CDCl$_3$) δ 7.48 – 7.41 (m, 1H), 7.36 – 7.27 (m, 3H), 4.57 (d, J=5.96 Hz, 2H), 4.40 (s, 2H); [13]C-

NMR (100 MHz, CDCl$_3$) δ 136.9, 136.3., 129.5, 128.0, 127.9, 127.7, 54.5, 43.6.
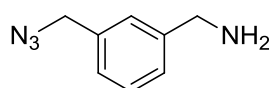
(3-(azidomethyl)phenyl)methanamine (7.7) To a stirred solution of **7.6**

(88.8 mg, 0.344 mmol) in ethanol (5.0 mL) was added 0.2 N NaOH (1.0

mL) and the resulting solution was stirred overnight at room temperature. The reaction was

diluted with ethyl acetate, washed with brine 10 % NaOH (2x), brine (1x), dried (MgSO$_4$),

filtered, and concentrated to afford 52.0 mg (93 % of **7.7**. ^{1}H-NMR (400 MHz, CDCl$_3$) δ 7.39 –

7.32 (m, 3H), 7.32 – 7.27 (m, 1H), 4.30 (s, 2H), 3.96 (s, 2H).
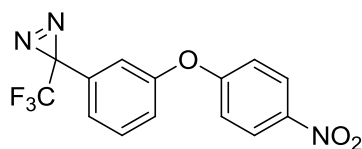
3-(3-(4-nitrophenoxy)phenyl)-3-(trifluoromethyl)-3H-diazirine

(7.11) To a stirred solution of **7.10** (30 mg, 0.148 mmol) in DMF

(1.0 mL) was added 4-fluoronitroaniline (20.8 mg, 0.148 mmol)

and potassium carbonate (61.4 mg, 0.444 mmol). The mixture was heated to 40 °C and stirred

for 2 h at which point it was judged complete by TLC. The reaction was partitioned between

water and diethyl ether, the organic layer washed with brine, dried (MgSO$_4$), filtered, and

concentrated to provide 37.0 mg (77 %) of **7.11**. ^{1}H-NMR (400 MHz, CDCl$_3$) δ 8.25 – 8.20 (m,

2H), 7.47 (t, J=8.06 Hz, 1H), 7.13 (dd, J=8.16 Hz, J=2.20 Hz, 1H), 7.07 (d, J=8.20 Hz, 1H), 7.04 –

6.99 (m, 2H), 6.93 (s, 1H); ^{19}F-NMR (376 MHz) δ 68.2.
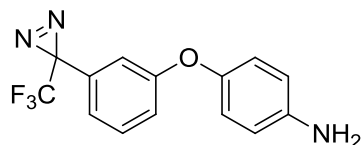
4-(3-(3-(trifluoromethyl)-3H-diazirin-3-yl)phenoxy)aniline (7.12)

To a stirred solution of **7.11** (37.0 mg, 0.114 mmol) in EtOH (8 mL) was added a solution of tin(II) chloride dihydrate (102 mg, 0.456 mmol) dissolved in concentrated HCl (2.0 mL). The resulting mixture was maintained at 70 °C for 1 h when it was judged complete by TLC. The reaction was neutralized with saturated sodium bicarbonate, extracted with ethyl acetate, the organic layer washed with brine, dried (MgSO$_4$), filtered, concentrated and the residue purified by column chromatography to provide 9.5 mg (28 %) of **7.12**.

Thiourea synthesis. As described in Chapter 4. Compounds purified by preparative scale reverse phase HPLC.
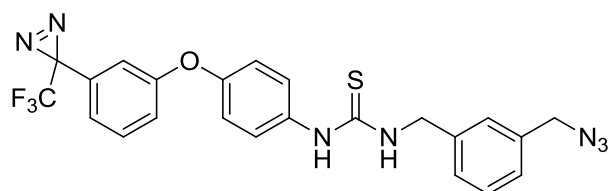
1-(3-(azidomethyl)benzyl)-3-(4-(3-(3-(trifluoromethyl)-3H-diazirin-3-yl)phenoxy)phenyl)thiourea (7.26) ^{1}H-NMR (400 MHz, acetone-d6) δ 9.06 (br s, 1H), 7.74 (br s, 1H), 7.57 − 7.48 (m, 3H), 7.41 − 7.33 (m, 3H), 7.30 − 7.25 (app d, 1H), 7.10 (dd, J=8.32 Hz, J=2.32 Hz, 1H), 7.07 − 7.01 (m, 3H), 6.88 (s, 1H), 4.92 (d, J=5.64 Hz, 2H), 4.43 (s, 2H).

Photoaffinity competition experiment. An overnight of S. aureus strain Newman was subcultured 1:100 into 500 μL of TSB containing probe or probe and competitor on a 12 well plate. The bacteria were incubated at 37 °C and irradiated with the lizard lamp for 8 min. Replicates were combined, pelleted, and the cells washed with PBS. The cells were pelleted and resuspended in lysis buffer (PBS + 25 μg/mL lysostaphen + 1X EDTA-free protease inhibitor), incubated at 37 °C for 20 min, and sonicated 2x for 10 s at 80 % power. To the lysates were

added CuSO$_4$ and TBTA to a final concentration of 200 μM, sodium ascorbate to a final concentration of 400 μM, and reporter to a final concentration of 50 μM. The lysates were rotated at room temperature in the dark for 2 h. Cold acetone was added to precipitate proteins and proteins were pelleted, the supernatant decanted, and the proteins resuspended in 1X SDS-PAGE loading buffer.

Pulldown with photocleavable linker. Photolabeling and lysate preparation were conducted as described for the competition experiment. To the prepared lysate was added TBTA to a final concentration of 200 μM, CuBr to a final concentration of 200 μM, and cleavable linker **7.32** to a final concentration of 50 μM. The reaction was incubated at room temperature on a sample rotisserie in the dark for 2 h. The lysate was passed through a GE Healthcare PD10 desalting column. To the desalted lysate was added streptavidin beads and the reaction was rotated at room temperature in the dark for 1 h. The beads were washed with 0.1 % SDS in PBS, 4 M urea, 1 M NaCl, and H$_2$O. The beads were suspended in PBS and irradiated for 2 h with a 365 nm UV-lamp. The supernatant was collected and concentrated in a 3K centrifuge filter. The streptavidin beads were suspended in 1X SDS-PAGE loading buffer and heated at 90 °C for 10 min.

References

(1)   Minakawa, N.; Ono, Y.; Matsuda, A. A Versatile Modification of on-Column Oligodeoxynucleotides Using a Copper-Catalyzed Oxidative Acetylenic Coupling Reaction. *J. Am. Chem. Soc.* **2003**, *125* (38), 11545–11552.

(2)   Pignataro, L.; Carboni, S.; Civera, M.; Colombo, R.; Piarulli, U.; Gennari, C. PhthalaPhos: Chiral Supramolecular Ligands for Enantioselective Rhodium-Catalyzed Hydrogenation Reactions. *Angew. Chem. Int. Ed. Engl.* **2010**, *49* (37), 6633–6637.

(3)   Lawrence, E. J.; Wildgoose, G. G.; Aldous, L.; Wu, Y. A.; Warner, J. H.; Compton, R. G.; McNaughter, P. D. 3-Aryl-3-(Trifluoromethyl)diazirines as Versatile Photoactivated "Linker" Molecules for the Improved Covalent Modification of Graphitic and Carbon Nanotube Surfaces. *Chem. Mater.* **2011**, *23* (16), 3740–3751.

(4)   Burgy, G.; Tahtouh, T.; Durieu, E.; Foll-Josselin, B.; Limanton, E.; Meijer, L.; Carreaux, F.; Bazureau, J.-P. Chemical Synthesis and Biological Validation of Immobilized Protein Kinase Inhibitory Leucettines. *Eur. J. Med. Chem.* **2013**, *62*, 728–737.

(5)   Wang, F.; Sambandan, D.; Halder, R.; Wang, J.; Batt, S. M.; Weinrick, B.; Ahmad, I.; Yang, P.; Zhang, Y.; Kim, J.; et al. Identification of a Small Molecule with Activity against Drug-Resistant and Persistent Tuberculosis. *Proc. Natl. Acad. Sci. U. S. A.* **2013**, *110* (27), E2510–E2517.

(6)   Szychowski, J.; Mahdavi, A.; Hodas, J. J. L.; Bagert, J. D.; Ngo, J. T.; Landgraf, P.; Dieterich, D. C.; Schuman, E. M.; Tirrell, D. A. Cleavable Biotin Probes for Labeling of Biomolecules

via Azide-Alkyne Cycloaddition. *J. Am. Chem. Soc.* **2010**, *132* (51), 18351–18360.

(7)   Kim, H.-Y. H.; Tallman, K. A.; Liebler, D. C.; Porter, N. A. An Azido-Biotin Reagent for Use in the Isolation of Protein Adducts of Lipid-Derived Electrophiles by Streptavidin Catch and Photorelease. *Mol. Cell. Proteomics* **2009**, *8* (9), 2080–2089.

Appendix to Chapter 7

Table A7.1. Protein hit from last photocleavable pulldown experiment. Values are spectral counts.

#	Identified Proteins (150)	Molecular Weight	10 µM **7.26** + 20 µM 7501	10 µM **7.26**	10 µM **7.31**
6	DNA-directed RNA polymerase subunit beta' OS=Staphylococcus aureus (strain Newman) GN=rpoC PE=3 SV=1	135 kDa	2	33	15
7	Pyruvate carboxylase OS=Staphylococcus aureus (strain Newman) GN=pycA PE=4 SV=1	129 kDa	11	20	16
8	DNA-directed RNA polymerase subunit beta OS=Staphylococcus aureus (strain Newman) GN=rpoB PE=3 SV=1	133 kDa	2	38	9
9	Elongation factor G OS=Staphylococcus aureus (strain Newman) GN=fusA PE=3 SV=1	77 kDa	5	28	10
10	Elongation factor Tu OS=Staphylococcus aureus (strain Newman) GN=tuf PE=3 SV=1	43 kDa	2	22	15
11	Pyruvate kinase OS=Staphylococcus aureus (strain Newman) GN=pykA PE=3 SV=1	63 kDa	2	20	11
12	Putative uncharacterized protein OS=Staphylococcus aureus (strain Newman) GN=NWMN_0811 PE=4 SV=1	44 kDa	2	16	6
14	Probable malate:quinone oxidoreductase 2 OS=Staphylococcus aureus (strain Newman) GN=mqo2 PE=3 SV=1	56 kDa	0	13	7

15	Dehydrogenase family protein OS=Staphylococcus aureus (strain Newman) GN=NWMN_2201 PE=4 SV=1	41 kDa	2	11	7
17	Glycine--tRNA ligase OS=Staphylococcus aureus (strain Newman) GN=glyQS PE=3 SV=1	54 kDa	2	13	4
18	Glutamine synthetase OS=Staphylococcus aureus (strain Newman) GN=glnA PE=3 SV=1	51 kDa	0	15	3
19	Phosphoenolpyruvate-protein phosphotransferase OS=Staphylococcus aureus (strain Newman) GN=NWMN_0950 PE=3 SV=1	63 kDa	0	18	1
21	Leucine--tRNA ligase OS=Staphylococcus aureus (strain Newman) GN=leuS PE=3 SV=1	92 kDa	0	11	6
22	Dihydrolipoamide acetyltransferase component of pyruvate dehydrogenase complex OS=Staphylococcus aureus (strain Newman) GN=pdhC PE=3 SV=1	46 kDa	1	9	5
23	Glucosamine-fructose-6-phosphate aminotransferase, isomerizing OS=Staphylococcus aureus (strain Newman) GN=glmS PE=3 SV=1	66 kDa	0	13	3
24	FeS assembly protein SufB OS=Staphylococcus aureus (strain Newman) GN=sufB PE=4 SV=1	53 kDa	2	8	3
26	Dihydrolipoyl dehydrogenase OS=Staphylococcus aureus (strain Newman) GN=pdhD PE=3 SV=1	49 kDa	0	8	5
27	30S ribosomal protein S3 OS=Staphylococcus aureus (strain Newman) GN=rpsC PE=3 SV=1	24 kDa	1	6	5

28	Oligoendopeptidase F OS=Staphylococcus aureus (strain Newman) GN=NWMN_0870 PE=4 SV=1	70 kDa	0	9	3
29	Phosphoglycerate kinase OS=Staphylococcus aureus (strain Newman) GN=pgk PE=3 SV=1	43 kDa	2	7	2
30	30S ribosomal protein S2 OS=Staphylococcus aureus (strain Newman) GN=rpsB PE=3 SV=1	29 kDa	1	6	3
31	6-phosphogluconate dehydrogenase, decarboxylating OS=Staphylococcus aureus (strain Newman) GN=gnd PE=3 SV=1	52 kDa	1	9	1
32	ATP-dependent Clp protease, ATP-binding subunit ClpC OS=Staphylococcus aureus (strain Newman) GN=clpC PE=3 SV=1	91 kDa	0	7	5
33	Glyceraldehyde 3-phosphate dehydrogenase 1 OS=Staphylococcus aureus (strain Newman) GN=gapA PE=3 SV=1	36 kDa	1	6	4
34	Protein translocase subunit SecA 1 OS=Staphylococcus aureus (strain Newman) GN=secA1 PE=3 SV=1	96 kDa	0	7	1
35	Carbamoyl-phosphate synthase large chain OS=Staphylococcus aureus (strain Newman) GN=carB PE=3 SV=1	117 kDa	1	11	1
36	Ribonucleoside-diphosphate reductase OS=Staphylococcus aureus (strain Newman) GN=nrdE PE=3 SV=1	82 kDa	0	5	5
37	Isoleucine--tRNA ligase OS=Staphylococcus aureus (strain Newman) GN=ileS PE=3 SV=1	105 kDa	0	10	1

38	Glutamyl-tRNA(Gln) amidotransferase subunit A OS=Staphylococcus aureus (strain Newman) GN=gatA PE=3 SV=1	53 kDa	0	6	4
39	GMP synthase [glutamine-hydrolyzing] OS=Staphylococcus aureus (strain Newman) GN=guaA PE=3 SV=1	58 kDa	0	8	2
40	Aconitate hydratase OS=Staphylococcus aureus (strain Newman) GN=NWMN_1263 PE=4 SV=1	99 kDa	1	8	0
41	Adenylosuccinate lyase OS=Staphylococcus aureus (strain Newman) GN=purB PE=4 SV=1	50 kDa	0	6	5
42	ABC transporter ATP-binding protein OS=Staphylococcus aureus (strain Newman) GN=NWMN_1303 PE=4 SV=1	60 kDa	0	8	3
43	Acetate kinase OS=Staphylococcus aureus (strain Newman) GN=ackA PE=3 SV=1	44 kDa	1	8	2
44	ATP-dependent helicase/nuclease subunit A OS=Staphylococcus aureus (strain Newman) GN=addA PE=3 SV=1	141 kDa	1	3	0
46	Transketolase OS=Staphylococcus aureus (strain Newman) GN=tkt PE=3 SV=1	72 kDa	0	8	1
48	Inosine-5'-monophosphate dehydrogenase OS=Staphylococcus aureus (strain Newman) GN=guaB PE=3 SV=1	53 kDa	0	7	1
49	Chaperone protein DnaK OS=Staphylococcus aureus (strain Newman) GN=dnaK PE=3 SV=1	66 kDa	0	6	3

50	Naphthoate synthase OS=Staphylococcus aureus (strain Newman) GN=memB PE=4 SV=1	30 kDa	0	7	2
51	Putative uncharacterized protein OS=Staphylococcus aureus (strain Newman) GN=NWMN_0677 PE=4 SV=1	16 kDa	0	5	1
52	Acetyl-CoA carboxylase, biotin carboxyl carrier protein OS=Staphylococcus aureus (strain Newman) GN=accB PE=4 SV=1	17 kDa	2	1	1
53	Aspartyl/glutamyl-tRNA(Asn/Gln) amidotransferase subunit B OS=Staphylococcus aureus (strain Newman) GN=gatB PE=3 SV=1	54 kDa	0	6	2
54	Asparagine--tRNA ligase OS=Staphylococcus aureus (strain Newman) GN=asnS PE=3 SV=1	49 kDa	0	6	2
55	6-phosphofructokinase OS=Staphylococcus aureus (strain Newman) GN=pfkA PE=3 SV=1	35 kDa	1	5	2
56	Molecular chaperone Hsp31 and glyoxalase 3 OS=Staphylococcus aureus (strain Newman) GN=hchA PE=3 SV=1	32 kDa	1	3	2
57	RNA-metabolising metallo-beta-lactamase OS=Staphylococcus aureus (strain Newman) GN=NWMN_1184 PE=4 SV=1	63 kDa	0	3	3
58	Aspartate--tRNA ligase OS=Staphylococcus aureus (strain Newman) GN=aspS PE=3 SV=1	67 kDa	0	4	2
59	Small GTP-binding protein domain:GTP-binding protein TypA OS=Staphylococcus aureus (strain Newman) GN=NWMN_0974 PE=4 SV=1	69 kDa	0	4	2

229

60	Glucose-6-phosphate isomerase OS=Staphylococcus aureus (strain Newman) GN=pgi PE=3 SV=1	50 kDa	0	7	0
61	Putative uncharacterized protein OS=Staphylococcus aureus (strain Newman) GN=NWMN_0956 PE=4 SV=1	63 kDa	1	2	1
62	Aldehyde dehydrogenase family protein OS=Staphylococcus aureus (strain Newman) GN=NWMN_2026 PE=3 SV=1	52 kDa	1	2	0
63	Catalase OS=Staphylococcus aureus (strain Newman) GN=katA PE=3 SV=1	59 kDa	0	5	1
64	Aerobic glycerol-3-phosphate dehydrogenase OS=Staphylococcus aureus (strain Newman) GN=glpD PE=3 SV=1	64 kDa	0	3	2
65	DNA-directed RNA polymerase subunit alpha OS=Staphylococcus aureus (strain Newman) GN=rpoA PE=3 SV=1	35 kDa	0	4	2
66	Dak phosphatase OS=Staphylococcus aureus (strain Newman) GN=NWMN_1136 PE=4 SV=1	61 kDa	0	4	2
67	ATP synthase subunit alpha OS=Staphylococcus aureus (strain Newman) GN=atpA PE=3 SV=1	55 kDa	0	3	1
68	30S ribosomal protein S5 OS=Staphylococcus aureus (strain Newman) GN=rpsE PE=3 SV=1	17 kDa	0	6	1
69	4-amino-4-deoxychorismate lyase OS=Staphylococcus aureus (strain Newman) GN=pabC PE=4 SV=1	24 kDa	0	2	1

70	Polyribonucleotide nucleotidyltransferase OS=Staphylococcus aureus (strain Newman) GN=pnp PE=3 SV=1	77 kDa	0	5	0
72	Elongation factor 4 OS=Staphylococcus aureus (strain Newman) GN=lepA PE=3 SV=1	68 kDa	0	3	1
74	DNA polymerase III subunit beta OS=Staphylococcus aureus (strain Newman) GN=dnaN PE=3 SV=1	42 kDa	0	3	2
75	CTP synthase OS=Staphylococcus aureus (strain Newman) GN=pyrG PE=3 SV=1	60 kDa	0	2	2
76	Pyruvate dehydrogenase E1 component, beta subunit OS=Staphylococcus aureus (strain Newman) GN=phdB PE=4 SV=1	35 kDa	0	4	2
77	S-adenosylmethionine synthase OS=Staphylococcus aureus (strain Newman) GN=metK PE=3 SV=1	44 kDa	0	3	2
78	ATP-dependent Clp protease, ATP-binding subunit ClpC OS=Staphylococcus aureus (strain Newman) GN=clpC PE=4 SV=1	78 kDa	0	3	1
79	Pyruvate oxidase OS=Staphylococcus aureus (strain Newman) GN=poxB PE=3 SV=1	64 kDa	0	4	1
80	Ribose-phosphate pyrophosphokinase OS=Staphylococcus aureus (strain Newman) GN=prs PE=3 SV=1	35 kDa	0	4	1
81	Alkyl hydroperoxide reductase subunit C OS=Staphylococcus aureus (strain Newman) GN=ahpC PE=4 SV=1	21 kDa	0	3	1

82	Proline--tRNA ligase OS=Staphylococcus aureus (strain Newman) GN=proS PE=3 SV=1	64 kDa	0	3	1
83	ATP-dependent DNA helicase OS=Staphylococcus aureus (strain Newman) GN=pcrA PE=4 SV=1	84 kDa	0	4	0
84	D-alanine--poly(phosphoribitol) ligase subunit 1 OS=Staphylococcus aureus (strain Newman) GN=dltA PE=3 SV=1	55 kDa	0	3	0
85	Cell division protein ftsA OS=Staphylococcus aureus (strain Newman) GN=ftsA PE=3 SV=1	53 kDa	0	4	0
86	Putative uncharacterized protein OS=Staphylococcus aureus (strain Newman) GN=NWMN_1739 PE=4 SV=1	18 kDa	1	3	1
87	30S ribosomal protein S10 OS=Staphylococcus aureus (strain Newman) GN=rpsJ PE=3 SV=1	12 kDa	1	1	3
88	50S ribosomal protein L21 OS=Staphylococcus aureus (strain Newman) GN=rplU PE=3 SV=1	11 kDa	1	1	2
89	Putative uncharacterized protein OS=Staphylococcus aureus (strain Newman) GN=NWMN_0600 PE=4 SV=1	76 kDa	0	0	2
90	50S ribosomal protein L5 OS=Staphylococcus aureus (strain Newman) GN=rplE PE=3 SV=1	20 kDa	0	2	1
91	Nicotinate phosphoribosyltransferase OS=Staphylococcus aureus (strain Newman) GN=nadC PE=3 SV=1	56 kDa	0	2	0

92	MarR family regulatory protein OS=Staphylococcus aureus (strain Newman) GN=NWMN_0655 PE=4 SV=1	17 kDa	0	3	2
93	Bifunctional purine biosynthesis protein PurH OS=Staphylococcus aureus (strain Newman) GN=purH PE=3 SV=1	54 kDa	0	2	1
94	Arginine--tRNA ligase OS=Staphylococcus aureus (strain Newman) GN=argS PE=3 SV=1	62 kDa	0	2	1
96	ATP-dependent Clp protease proteolytic subunit OS=Staphylococcus aureus (strain Newman) GN=clpP PE=3 SV=1	22 kDa	0	4	1
97	UPF0447 protein NWMN_0550 OS=Staphylococcus aureus (strain Newman) GN=NWMN_0550 PE=3 SV=1	29 kDa	0	4	1
98	Phosphoribosylformylglycinamidine synthase 2 OS=Staphylococcus aureus (strain Newman) GN=purL PE=3 SV=1	80 kDa	0	3	0
99	Phenylalanine--tRNA ligase beta subunit OS=Staphylococcus aureus (strain Newman) GN=pheT PE=3 SV=1	89 kDa	0	5	0
100	UDP-N-acetylglucosamine 1-carboxyvinyltransferase 1 OS=Staphylococcus aureus (strain Newman) GN=murA PE=3 SV=1	45 kDa	0	5	0
103	Uridylate kinase OS=Staphylococcus aureus (strain Newman) GN=pyrH PE=3 SV=2	26 kDa	1	0	2
104	50S ribosomal protein L4 OS=Staphylococcus aureus (strain Newman) GN=rplD PE=3 SV=1	22 kDa	0	2	1

105	Aspartate carbamoyltransferase OS=Staphylococcus aureus (strain Newman) GN=pyrB PE=3 SV=1	33 kDa	0	2	2
106	3-hydroxy-3-methylglutaryl coenzyme A synthase OS=Staphylococcus aureus (strain Newman) GN=mvaS PE=4 SV=1	43 kDa	0	2	2
107	Hydrolase OS=Staphylococcus aureus (strain Newman) GN=NWMN_2480 PE=4 SV=1	31 kDa	0	2	1
108	DNA mismatch repair protein MutS OS=Staphylococcus aureus (strain Newman) GN=mutS PE=3 SV=1	100 kDa	1	3	0
109	Transcriptional regulator sarA OS=Staphylococcus aureus (strain Newman) GN=sarA PE=1 SV=1	15 kDa	0	3	1
110	DNA gyrase subunit B OS=Staphylococcus aureus (strain Newman) GN=gyrB PE=3 SV=1	73 kDa	0	2	1
111	50S ribosomal protein L14 OS=Staphylococcus aureus (strain Newman) GN=rplN PE=3 SV=1	13 kDa	0	2	2
112	50S ribosomal protein L22 OS=Staphylococcus aureus (strain Newman) GN=rplV PE=3 SV=1	13 kDa	0	1	3
113	Pyruvate dehydrogenase E1 component, alpha subunit OS=Staphylococcus aureus (strain Newman) GN=phdA PE=4 SV=1	41 kDa	0	2	2
114	3-oxoacyl-[acyl-carrier protein] reductase OS=Staphylococcus aureus (strain Newman) GN=fabG PE=3 SV=1	26 kDa	0	1	2

115	Alkaline shock protein 23 OS=Staphylococcus aureus (strain Newman) GN=NWMN_2086 PE=4 SV=1	19 kDa	0	3	0
116	Glycerol kinase OS=Staphylococcus aureus (strain Newman) GN=glpK PE=3 SV=1	56 kDa	0	4	0
117	Fumarylacetoacetate hydrolase family protein OS=Staphylococcus aureus (strain Newman) GN=NWMN_0839 PE=4 SV=1	33 kDa	0	4	0
118	UDP-N-acetylglucosamine 1-carboxyvinyltransferase 2 OS=Staphylococcus aureus (strain Newman) GN=murZ PE=3 SV=1	45 kDa	0	4	0
119	UDP-N-acetylglucosamine--N-acetylmuramyl-(pentapeptide) pyrophosphoryl-undecaprenol N-acetylglucosamine transferase OS=Staphylococcus aureus (strain Newman) GN=murG PE=3 SV=1	40 kDa	3	0	0
120	Coenzyme A disulfide reductase OS=Staphylococcus aureus (strain Newman) GN=cdr PE=3 SV=1	49 kDa	0	2	0
121	RNA polymerase sigma factor OS=Staphylococcus aureus (strain Newman) GN=sigA PE=3 SV=1	42 kDa	1	2	0
122	Sigma factor sigB regulation protein OS=Staphylococcus aureus (strain Newman) GN=rsbU PE=4 SV=1	38 kDa	1	2	0
123	(3R)-hydroxymyristoyl-[acyl-carrier-protein] dehydratase OS=Staphylococcus aureus (strain Newman) GN=fabZ PE=3 SV=1	16 kDa	0	2	1
124	Putative uncharacterized protein OS=Staphylococcus aureus (strain Newman) GN=NWMN_0355 PE=4 SV=1	41 kDa	0	2	0

125	Enolase OS=Staphylococcus aureus (strain Newman) GN=eno PE=3 SV=1	47 kDa	0	1	2
126	30S ribosomal protein S4 OS=Staphylococcus aureus (strain Newman) GN=rpsD PE=3 SV=1	23 kDa	0	1	2
127	DNA polymerase III gamma subunit OS=Staphylococcus aureus (strain Newman) GN=dnaX PE=4 SV=1	63 kDa	2	1	0
129	DNA topoisomerase OS=Staphylococcus aureus (strain Newman) GN=topA PE=3 SV=1	79 kDa	0	2	0
130	DNA polymerase III polC-type OS=Staphylococcus aureus (strain Newman) GN=polC PE=3 SV=1	163 kDa	0	2	0
131	Cysteine synthase OS=Staphylococcus aureus (strain Newman) GN=NWMN_0475 PE=3 SV=1	33 kDa	0	3	0
132	Probable manganese-dependent inorganic pyrophosphatase OS=Staphylococcus aureus (strain Newman) GN=ppaC PE=3 SV=1	34 kDa	0	3	0
133	D-alanine--D-alanine ligase OS=Staphylococcus aureus (strain Newman) GN=ddl PE=3 SV=1	40 kDa	0	2	0
134	Putative uncharacterized protein OS=Staphylococcus aureus (strain Newman) GN=NWMN_2045 PE=4 SV=1	53 kDa	0	2	0
135	DNA gyrase subunit A OS=Staphylococcus aureus (strain Newman) GN=gyrA PE=3 SV=1	100 kDa	0	2	0

136	Oligoendopeptidase F OS=Staphylococcus aureus (strain Newman) GN=pepF PE=4 SV=1	69 kDa	0	2	0
138	Zinc-containing alcohol dehydrogenase superfamily protein OS=Staphylococcus aureus (strain Newman) GN=NWMN_2272 PE=4 SV=1	37 kDa	0	3	0
141	Pyridoxal biosynthesis lyase pdxS OS=Staphylococcus aureus (strain Newman) GN=pdxS PE=3 SV=1	32 kDa	0	0	2
142	Glutamate racemase OS=Staphylococcus aureus (strain Newman) GN=murI PE=3 SV=1	30 kDa	0	2	0
143	Alanine--tRNA ligase OS=Staphylococcus aureus (strain Newman) GN=alaS PE=3 SV=1	99 kDa	0	2	0
144	Methionyl-tRNA synthetase OS=Staphylococcus aureus (strain Newman) GN=metS PE=3 SV=1	75 kDa	0	2	0
145	ATP-dependent zinc metalloprotease FtsH OS=Staphylococcus aureus (strain Newman) GN=ftsH PE=3 SV=1	78 kDa	0	2	0
146	Transcription termination-antitermination factor OS=Staphylococcus aureus (strain Newman) GN=nusA PE=4 SV=1	44 kDa	0	2	0
147	Glucokinase OS=Staphylococcus aureus (strain Newman) GN=glk PE=4 SV=1	35 kDa	0	2	0
148	General stress protein-like protein OS=Staphylococcus aureus (strain Newman) GN=NWMN_1632 PE=4 SV=1	18 kDa	0	2	0

149	Glutamyl-aminopeptidase OS=Staphylococcus aureus (strain Newman) GN=NWMN_1638 PE=4 SV=1	40 kDa	0	2	0
150	Ferritin OS=Staphylococcus aureus (strain Newman) GN=NWMN_1831 PE=4 SV=1	20 kDa	0	2	0

CHAPTER 8

CONCLUSIONS AND FUTURE DIRECTIONS

8.1 Summary

The work presented in this dissertation has focused on the chemical synthesis and application of small molecule probes for the study of bacterial metal acquisition and homeostasis. This has encompassed two main projects; 1) the total synthesis of the natural product siderophore coelichelin and 2) structure-activity relationship and target identification studies of two small molecule activators of the heme stress response in *Staphyloccocus aureus*. The following is a general summary of the results and elaboration on the future directions for these projects.

8.2 Progress towards the total synthesis of coelichelin

Studies towards the total synthesis of coelichelin have focused on developing a convergent route beginning from readily available starting materials and utilizing orthogonal protecting groups. Reaction sequences have been optimized to provide gram-scale quantities of the advanced intermediate coupling components **8.1**, **8.2**, and **8.3** (Figure 8.1). The coupling strategy outlined in Chapter 2 employing preparation of a central dipeptide followed by *N*-deprotection and bis-acylation to provide the fully protected tetrapeptide has been partially elaborated. Conditions for the first coupling to prepare central dipeptide **8.4** have been developed. However, yields of this critical first coupling step are not high typically giving 50 – 60 % of the protected dipeptide. In addition, Boc group removal proceeds with considerable

decomposition requiring the product to be further purified by HPLC. Conditions for the coupling-deprotection sequence require further optimization in order to maximize material throughput.

Several attempts at the second key bis-amide coupling were encouraging but not conclusive. Preliminary spectral analysis of the coupling product indicated the reaction proceeded but requires further optimization and complete characterization of the product. This step will likely require screening of several reactions to identify optimal coupling conditions. With the protected tetrapeptide in hand, removal of protecting groups to afford coelichelin should proceed in two steps, the order of which may or may not be important. Removal of the Boc protecting groups requires acidic conditions. While this deprotection step should not be complicated, we do anticipate some product decomposition as observed in the preceding Boc deprotection. Finally, the four benzyl protecting groups need to be removed by hydrogenoloysis, a reaction well precedented in related siderophore syntheses.[1,2] We anticipate the benzyl ester will also be removed to provide the acid under these reaction conditions.

With the compound in hand, the biological activity of the synthesized natural product can then be evaluated. We originally intended to study the effects of coelichelin treatment on S. aureus, though these experiments can be extended to other organisms. IC_{50} curves for *S. aureus* treated with coelichelin will be generated to determine concentrations that inhibit growth. A similar experiment with added Fe^{3+} and Zn^{2+} will be conducted to determine their ability to reverse coelichelin induced growth inhibition. Using a strain of *S. aureus* bearing a

luciferase reporter under the control of Fur, the ability of coelichelin to activate an iron-stress response will be evaluated at several concentrations.

A potentially useful application building off of this route to coelichelin would be the development of a photoactivatable coelichelin derivative. Photoreactive groups such as *o*-nitrobenzyl compounds, which are commonly used for photocaging applications[3], could be introduced by replacing the *O*-benzyl ethers with *o*-nitrobenzyl ethers as protecting groups for the hydroxylamine moieties. The molecule, which almost certainly would not chelate iron in the caged form, could be activated at any point during bacterial growth by irradiation with the appropriate wavelength of light. The activation wavelength can be red-shifted by various substitutions on the phenyl ring[4] to avoid using UV light for activation which would likely damage the biological system under study. The growth media could be inoculated with the photocaged siderophore at the beginning of the experiment and, at any desired time point, irradiated to activate the siderophore and induce iron sequestration. Such a molecule could facilitate the study of the response to iron depletion in bacteria (and other organisms) by allowing greater temporal control over iron concentrations.
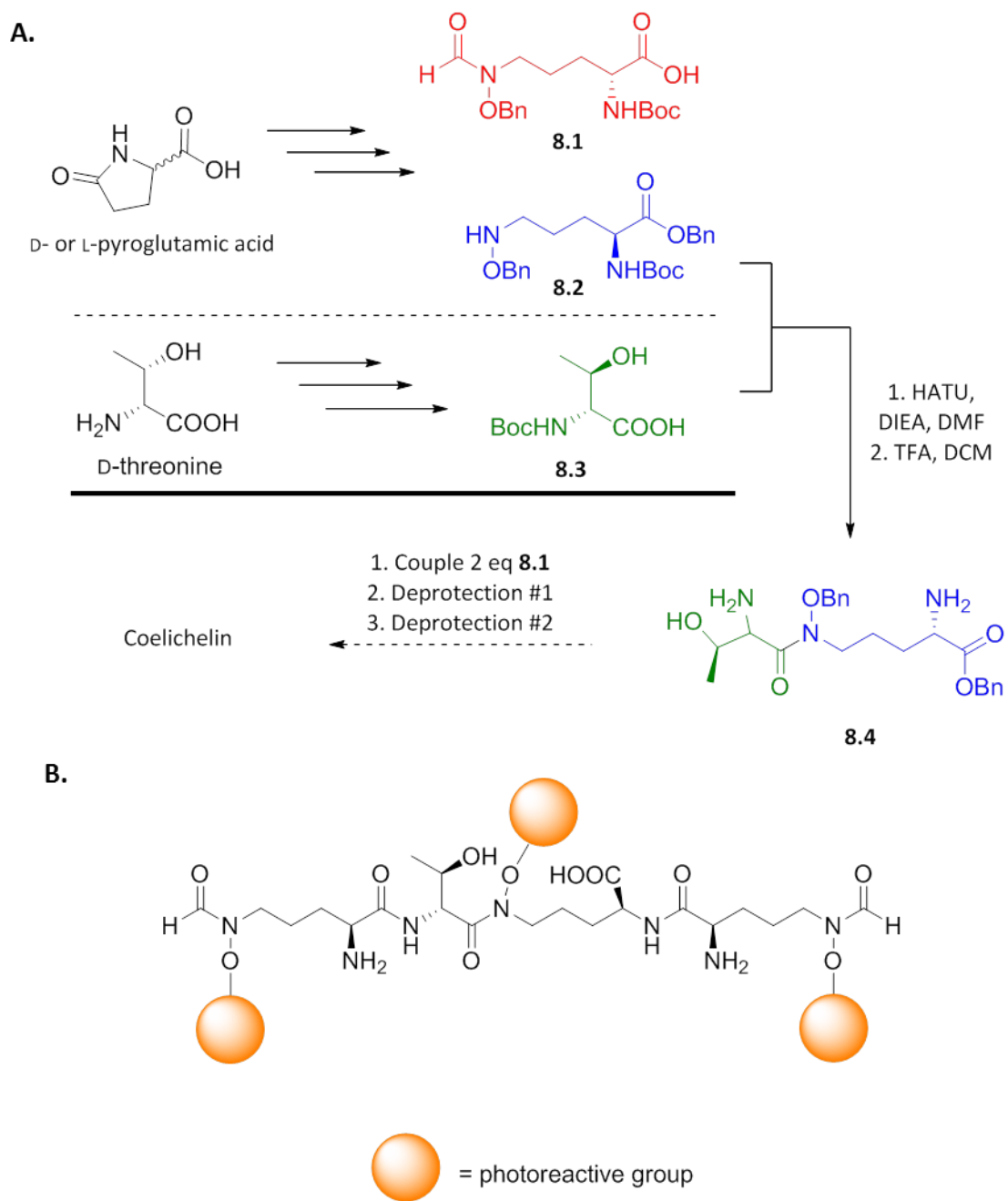
Figure 8.1. Summary of coelichelin project. A. Progress towards the total synthesis of coelichelin. B. Proposed photoactivatable coelichelin.

8.3 Small molecule activators of the heme stress response in *S. aureus*

Chapters 3 and 4 focus on studying the structure-activity relationships of '8882 and '3981, molecules identified as activators of HssRS in *S. aureus*. The information gained was applied to the development of chemical probes for target identification and this work was presented in Chapters 6 and 7.
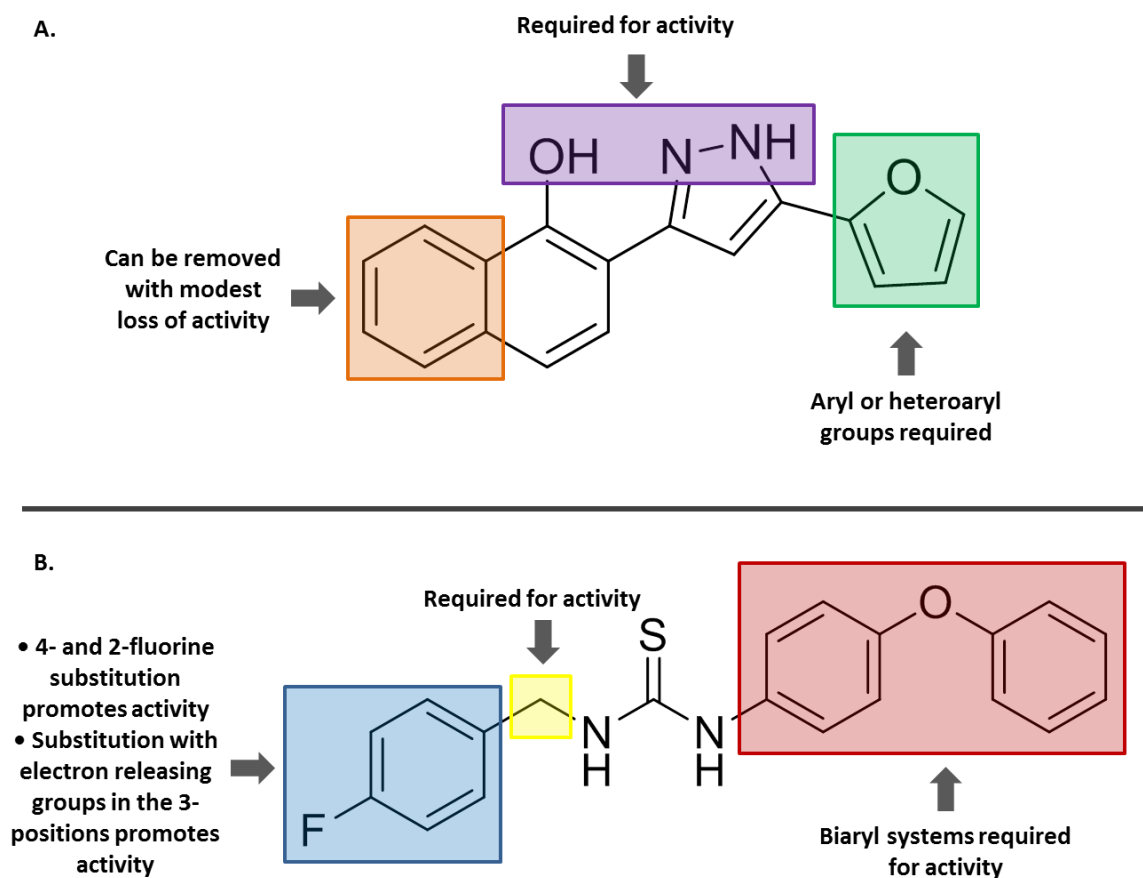

Figure 8.2. Summary of structure-activity relationship studies of '8882 (A) and '3981 (B). (Note: Summary of '8882 activity is for HssRS activation.

SAR studies of '8882

The preliminary studies on structure-activity relationships of '8882 presented in Chapter 3 featured the synthesis and activity testing of 31 derivatives focused on understanding SAR

around four regions of the molecule (Figure 8.2). While the information gained from this work has been useful for understanding basic SAR and applying that to probe design, more extensive SAR studies should be conducted. This includes expansion of the library to include more derivatives to focus on the areas of the molecule not thoroughly covered by the work presented in Chapter 3. In particular, modification of the western ring was not extensively studied and alternate substituents such as indazoles, fluorinated phenyl rings, and nitrogen containing rings should be prepared and tested. In addition, the central pyrazole core should be replaced by alternate heterocycles.

New derivatives should be screened for HssRS (*in vivo*) and HemY (*in vitro*) activation. Given the discrepancy between these two activities as discussed in Chapter 3, it is worth exploring the reason for this disparity, particularly in the context of developing therapeutics as both activities would need to be optimized.

SAR studies of '3981

The SAR around '3981 has been extensively studied as presented in Chapter 4. It is clear that inductive effects are important for activity and substitution on the benzyl ring controls activity. Derivatives that should be prepared to further study SAR include introducing chirality at the benzylic carbon (by substitution with methyl or other groups), placement of electron withdrawing or releasing groups into the phenoxy ether ring of the biaryl ether, and cyclization to aminobenzothiazole derivatives.

Several molecules were identified from the initial SAR studies of '3981 that exhibited greater efficacy and reduced potency compared to the parent molecule. Given that '3981 and '7501 do not require heme to activate HssRS, these molecules may be valuble probes for

244

studying heme toxicity in *S. aureus*. It would be interesting to compare RNAseq data between heme and '7501 treated samples. There would most likely be overlap between certain RNAs that may help define heme toxicity.
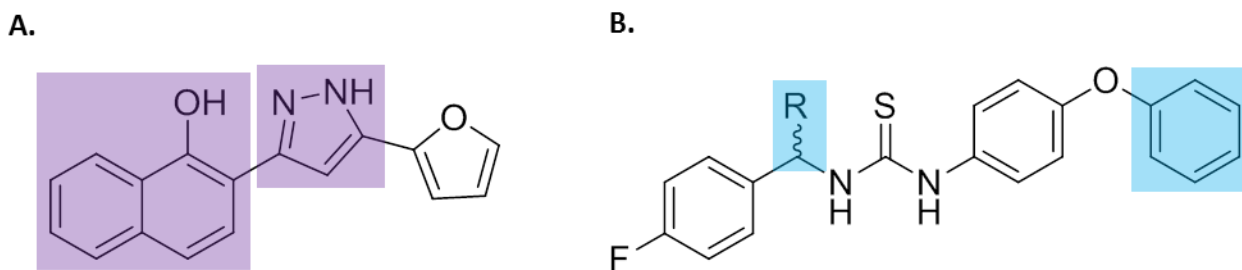

Figure 8.3. Areas of '8882 (A) and '3981 (B) to explore SAR in future studies.

'8882 target identification

As presented in Chapter 6, several clickable photoaffinity probes based on '8882 SAR were prepared and are able to activate HssRS. Presumably, this activation is through interaction with HemY though the probes have not been directly tested in the HemY assay and should be evaluated and compared to the other derivatives. While **8.6** was extensively used for target identification experiments, no samples were ever submitted for proteomic analysis. A pulldown experiment using **8.6, 8.7** and suitable controls should be conducted to generate a list of putative target proteins. This could serve to further confirm HemY and SufC as targets as well as identify potential undiscovered targets. In addition, these probes can be used to confirm *in vivo* target (HemY or SufC) engagement.

'3981 target Identification

A clickable photoaffinity probe developed based on '3981 SAR was prepared as detailed in Chapter 7. Several experiments were conducted. The first round of experiments focused on identifying bands that appear in a probe treated sample and diminish or disappear in a control sample. Controls were generally treated with free compound to compete off specific interactions. These experiments did not consistently identify candidate targets. The focus was then shifted towards utilizing proteomics data to identify candidate targets. To facilitate this, a photocleavable linker was utilized to minimize nonspecific binding proteins appearing in proteomics samples. Several experiments were conducted using this linker and, after much optimization, the final experiment generated a fairly long list of candidate target proteins. It is clear additional controls will be necessary in future experiments. These could include using a "just beads' control where a sample excluding the photocleavable linker is prepared to control for proteins that stick to the beads. In theory, these proteins should not appear in the photoelution samples but this may not be the case. Another potential control would be the use of an alternate cleavable linker.
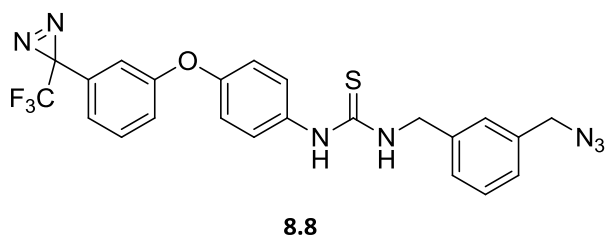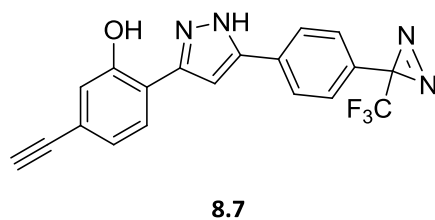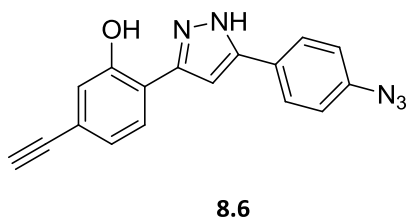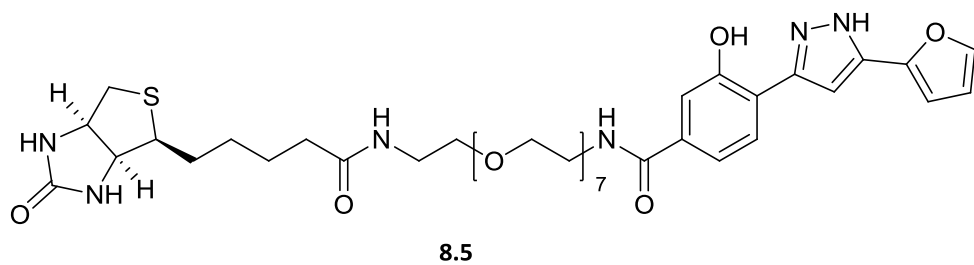
Figure 8.4. Summary of probes developed for target identification for '8882 (**8.5 – 8.7**) and '3981 (**8.8**).

References

(1) Miller, M. J. Syntheses and Therapeutic Potential of Hydroxamic Acid Based Siderophores and Analogs. *Chem. Rev.* **1989**, *89* (7), 1563–1579.

(2) Mashiach, R.; Meijler, M. M. Total Synthesis of Pyoverdin D. *Org. Lett.* **2013**, *15* (7), 1702–1705.

(3) Deiters, A. Principles and Applications of the Photochemical Control of Cellular Processes. *ChemBioChem* **2009**, *11* (1), 47–53.

(4) Hansen, M. J.; Velema, W. A.; Lerch, M. M.; Szymanski, W.; Feringa, B. L. Wavelength-Selective Cleavage of Photoprotecting Groups: Strategies and Applications in Dynamic Systems. *Chem. Soc. Rev.* **2015**, *44* (11), 3358–3377.